Turkish Journal of
Analytical Chemistry

www.turkjac.org

Turkish Journal of

Analytical Chemistry

TurkJAC

Prof. Mehmet Yaman	Fırat University, Faculty of Sciences, Department of Chemistry
Prof. Halit Kantekin	Karadeniz Technical University, Faculty of Sciences, Department of Chemistry
Prof. Esin Canel	Ankara University, Faculty of Sciences, Department of Chemistry
Prof. Dilek Ak	Anadolu University, Faculty of Pharmacy, Department of Basic Pharmaceutical Sciences
Prof. Mustafa Küçükislamoğlu	Sakarya University, Faculty of Science and Literature, Department of Chemistry
Prof. Salih Zeki Yildiz	Sakarya University, Faculty of Science and Literature, Department of Chemistry
Prof. Recai İnam	Gazi University, Faculty of Sciences, Department of Chemistry
Prof. Dr. Durişehvar Ünal	İstanbul University, Faculty of Pharmacy, Department of Basic Pharmaceutical Sciences
Prof. Mehmet Tüfekçi	Avrasya University, Faculty of Science and Literature, Department of Biochemistry
Prof. Hüseyin Kara	Selçuk University, Faculty of Sciences, Department of Chemistry
Prof. Sezgin Bakirdere	Yıldız Technical University, Faculty of Science and Literature, Department of Chemistry
Prof. Hasan Basri Şentürk	Karadeniz Technical University, Faculty of Sciences, Department of Chemistry
Prof. Yusuf Atalay	Sakarya University, Faculty of Science and Literature, Department of Physics
Prof. Salih Zeki Yildiz	Sakarya University, Faculty of Science and Literature, Department of Chemistry

Authorship, Originality, and Plagiarism: The authors accept that the work is completely original and that the works of others have been appropriately cited or quoted in the text with the necessary permissions. The authors should avoid plagiarism. It is recommended that they check the article using appropriate software such as Ithenticate and CrossCheck. The responsibility for this matter rests entirely with the authors. All authors will be notified when the manuscript is submitted. If a change of author is needed, the reason for the change should be indicated. Once the manuscript is accepted, no author changes can be made.

Aims and Scope

"Turkish Journal of Analytical Chemistry" publishes original full-text research articles and reviews covering a variety of topics in analytical chemistry. Original research articles may be improved versions of known analytical methods. However, studies involving new and innovative methods are preferred. Topics covered include:

- Analytical materials
- Atomic methods
- Biochemical methods
- Chromatographic methods
- Electrochemical methods
- Environmental analysis
- Food analysis
- Forensic analysis
- Optical methods
- Pharmaceutical analysis
- Plant analysis
- Theoretical calculations
- Nanostructures for analytical purposes
- Chemometric methods
- Energy

ETHICAL GUIDELINES

TurkJAC follows ethical tasks and responsibilities are defined by the Committee on Publication Ethics (COPE) in publication procedure. Based on this guide, the rules regarding publication ethics are presented in the following sections.

Ethical Approval

Ethics committee approval must be obtained for studies on clinical and experimental regarding human and animals that require an ethical committee decision, this approval must be stated in the article and documented in the submission. In such articles, the statement that research and publication ethics are complied with should include. Information about the approval such as committee name, date, and number should be included in the method section and also on the first/last page of the article.

Editors

1. In the preliminary evaluation of a submission, the editor of the journal evaluates the article's suitability for the purpose and scope of the journal, whether it is similar to other articles in the literature, and whether it meets the expectations regarding the language of writing. When it meets the mentioned criteria, the scientific evaluation process is started by assigning a section editor if necessary.
2. A peer-reviewed publication policy is employed in all original studies, taking into full account of possible problems due to related or conflicting interests.

3. Section editors work on the articles with a specific subject and their suggestion is effective in the journal editor's decision about acceptance or rejection of the article.
4. No section editor contacts anyone except the authors, reviewers, and the journal editor about articles in the continued evaluation process.
5. In the journal editor's decision to accept or reject an article, in the addition of section editor's suggestion in consequence of scientific reviewing, the importance of the article, clarity and originality are decisive. The final decision, in this case, belongs to the journal editor.

Authors
1. The authors should actively contribute to the design and execution of the work. Authorship should not be given to a person who does not have at least one specific task in the study.
2. Normally all authors are responsible for the content of the article. However, in interdisciplinary studies with many authors, the part that each author is responsible for should be explained in the cover letter.
3. Before the start of the study, it would be better to determine the authors, contributors, and who will be acknowledged in order to avoid conflict in academic credits.
4. The corresponding author is one of the authors of the article submitted to the journal for publication. All communications will be conducted with this person until the publication of the article. The copyright form will be signed by the corresponding author on all the authors' behalf.
5. It is unacceptable to submit an article that has already been published entirely or partly in other publication media. In such situation, the responsibility lies with all authors. It is also unacceptable that the same article has been sent to TurkJAC and another journal simultaneously for publication. Authors should pay attention to this situation in terms of publication ethics.
6. Plagiarism from others' publications or their own publications and slicing of the same study is not acceptable.
7. All authors agree that the data presented in the article are real and original. In case of an error in the data presented, the authors have to be involved in the withdraw and correction process.
8. All authors must contribute to the peer-reviewed procedure.

Reviewers
1. Peer reviewers worked voluntarily are external experts assigned by editors to improve the submitted article.
2. It is extremely important that the referee performs the review on time so that the process does not prolong. Therefore, when the invitation is agreed upon, the reviewer is expected to do this on time. Also, the reviewer agrees that there are no conflicts of interest regarding the research, the authors, and/or the research funders.
3. Reviewers are expected not to share the articles reviewed with other people. The review process should be done securely.
4. Reviewers are scored according to criteria such as responding to the invitations, whether their evaluations are comprehensive and acting in accordance with deadlines, and the article submissions that they can make to TurkJAC are handled with priority.

Contents

*Author of correspondence:

Turkish Journal of

Analytical Chemistry

www.turkjac.org
2019

Determination of cytotoxic, anti-acetylcholinesterase and antioxidant activity of some medicinal *Artemisia* spp.

Zehra Can¹* [iD] , Elif Ayazoglu Demir² [iD] , Zeynep Akar³ [iD] , Yakup Kara⁴ [iD] , Betul Gidik⁵ [iD]

¹ Bayburt University, Faculty of Applied Sciences, Department of Emergency Aid and Disaster Management, 69000, Bayburt, Türkiye
² Karadeniz Technical University, Maçka Vocational School, Department of Chemistry and Chemical Processing Technologies, 61750, Trabzon, Türkiye
³ Gümüşhane University, Department of Genetics and Bioengineering, Faculty of Engineering and Natural Sciences, 29000, Gümüşhane, Türkiye
⁴ Karadeniz Technical University, Faculty of Science, Department of Chemistry, 61080 Trabzon, Türkiye
⁵ Bayburt University, Faculty of Applied Sciences, Department of Organic Farming Management, 69000, Bayburt, Türkiye

Abstract

The study aims to investigate the antioxidant activities, phenolic compounds, acetylcholinesterase enzyme inhibition and cytotoxic effects of two different *Artemisia* spp. (*Artemisia dracunculus* L. and *Artemisia dracunculoides* Pursh) cultivated in Türkiye organically, for the first time. The total phenolic and total flavonoid contents of the plants were determined spectrophotometrically while antioxidant activity DPPH•, CUPRAC, and FRAP was determined using the colorimetric method. And also, acetylcholinesterase *in vitro* enzyme inhibition activity and anti-cancer activity against human melanoma (VMM917, CRL-3232), lung carcinoma (A549, CCL-185), and normal human fibroblast (hGF, PCS-201-018) cells were studied. Total phenolic (225-324 µg GAE/mL extract) and total flavonoid contents (0.066–0.085 µg QE/mL extract), antioxidant activity Color Scavenging Concentration 50% (DPPH• (CSC_{50}: 1.371–1.655 mg/mL), CUPRAC (0.246–0.344 µM CTEAC) and FRAP (462.133–726.661 µM CTEAC)). *A. dracunculus* and *A. dracunculoides* extracts inhibited 40.09 ± 0.65%, and 39.48 ± 3.68% of acetylcholinesterase activity. It was determined that demonstrated the selective effect of *A. dracunculus* and *A. dracunculoides* on the cytotoxicity of A549 and hGF cells. According to our results, both tarragon plant species, it may be said that it is not only consumed as food but also used for therapeutic purposes will be beneficial for health.

Keywords: *Artemisia dracunculus*, *Artemisia dracunculoides*, acetylcholinesterase, lung carcinoma, human melanoma

1. Introduction

In recent years, there has been a remarkable increase in the amount of pharmacological and chemical studies on members of *Artemisia* L. (Asteraceae) because of their medicinal properties [1–3]. Among the species, *Artemisia dracunculus* L. which is an important medicinal and aromatic plant has been used in the treatment of various diseases such as malaria, liver disease, neoplasms, inflammatory diseases, and infections.

Tarragon or dragon's-wort (*Artemisia dracunculus* and *Artemisia dracunculoides* Pursh), known as "tarhun"in Anatolia are plants of the Asteraceae family. *Artemisia dracunculus* (tarragon) is an edible spice plant as both fresh (leaves) and dried (herb). Most of these plant species are edible and used as a flavoring in food in many traditional recipes. It is also used for medicinal purposes [4]. The essential fatty acids [5–7] phenolic compounds, flavonoids [8] carotenoids [9], tannins [10],

and mineral compounds [11] in the tarragon plant were suitably used for therapeutic purposes.

Cancer is one of the diseases with the highest mortality rate following cardiovascular diseases worldwide. Among cancer types, lung cancer having the second highest mortality rate in both sexes is the most common type behind prostate cancer in men and breast cancer in women [12]. In addition, skin cancer is one of the most common types of cancer among all cancer types. There are many methods in the treatment of cancer diseases such as chemotherapy, radiation therapy, surgery and immunotherapy including utilization [13]. However, these methods are known to damage healthy cells during cancer treatment [14]. In order to reduce these side effects, researchers are increasing their interest in the application of alternative medicines and natural and herbal compounds. It was

determined that the activity of AChE increased in the cortex and hippocampus in brains with AD; therefore, the amount and activation of ACh decreased. Nowadays, acetylcholinesterase inhibitors (AChE) are the most widely used AD treatment with drugs. Most of the inhibitors are plant origins. In recent years, studies on the treatment of AD have been planned according to strategies aimed at the discovery and development of new AChE's that are more effective and have fewer side effects and may also have protective properties as well as therapeutic effects.

In this study, it was investigated whether or not tarragon's could be a natural inhibitor of the acetylcholinesterase enzyme. While antioxidant activity was determined by the colorimetric method with dropping on TLC plate in the study and phenolic compounds of tarragon plants were analyzed in PDA-HPLC. To the best of our knowledge, in this study is the first investigation of tarragon on lung carcinoma (A549, CCL-185), human melanoma (VMM917, CRL-3232) and human normal fibroblast (hGF, PCS-201-018) cells.

2. Material and Methods

2.1. Chemicals and reagents

HPLC- grade methanol, absolute ethanol, acetonitrile solutions, all phenolic compounds standards and all chemicals used for antioxidant testing were purchased from Sigma-Aldrich (Munich, Germany). Electric eel acetylcholinesterase (EC 3.1.1.7, type-VI-S), acetylthiocholine iodide, and 5,5′-dithiobis-(2-nitrobenzoic acid) (DTNB) and donepezil were purchased from the Sigma (St. Louis, MO). Dimethyl sulfoxide (DMSO, D2650), 3-(4,5-dimethylthiazol-2-yl)-2,5-diphenyltetrazolium bromide (MTT, M2128) and cisplatin (P4394) were purchased from Sigma-Aldrich (St. Louis, MO, USA). All chemicals and solutions used in the cell culture studies were purchased from American Type Culture Collection (ATCC, Manassas, VA, USA), Gibco (NY, USA) and Sigma-Aldrich (St. Louis, MO, USA).

2.2. Providing of plant material and extract preparation

Tarragon is one of the important medicinal and aromatic plants which had significant expansions in its usage areas recently. The best-known species of tarragon are *Artemisia dracunculus* and *Artemisia dracunculoides* [15]. The species are grown as culture plants in Türkiye. In this study, *Artemisia dracunculus* and *Artemisia dracunculoides* were grown in ecological conditions, and organic production conditions in the Bayburt Province

of Türkiye. Random Blocks Trial Design was used in the field experiment, which was prepared in three replications with a distance of 40 x 40 cm between rows. Since the plants are not flowering plants, they were harvested in June 2020 when they reached maturity.

After plants samples were at dried room temperature in a cool place, it was ground to a powder a using blender. 3.5 g of the powdered was weighed for each plant samples and 35 ml of ethanol was added, and then extracted by shaking vigorously Heidolph MR HEI-Standard, Schwabach, Germany for 24 hours. At the end of the time, the extracts were filtered with filter paper and then a syringe filter (Whatman, NY 0.45 μm) respectively. The extracts were divided into 4 parts (cytotoxic activity, antioxidant activity, phenolic compounds, and enzyme inhibition). Then, extracts were stored in the dark and at room temperature till analysis time.

2.3. Antioxidant Activity

2.3.1. Spectrophotometric Total Phenolic Content (TPC) and Total Flavonoid Content (TFC)

The total phenolic content of tarragon plant extracts was evaluated using the Folin-Ciocalteu reagent [16]. In this method, 50 μL of sample solution was diluted with 2.5 mL of pure water. 250 μL, 0.2 N Folin-Ciocalteu reagent was added. Then 750 μL Na_2CO_3 (7.5%) was added to the vortexed. After 2 hours of incubation at room temperature, absorbance values were measured at 760 nm.

Gallic acid antioxidant standard, which was prepared at five different concentrations (500–250–125–62.5–31.25 μg/mL), was used for the calibration graph. The amount of phenolic substance was expressed in microgram gallic acid equivalent per milliliter extract (μg GAE /mL extract).

Flavonoids in the tarragon plants were determined with the method which was developed by Fukumoto and Mazza [17]. The study was carried out in three parallels. Initially, an equal volume (250 μL) of the sample was pipetted into the tubes and 2.1 mL of methanol was added. Finally, 50 μL of 1M ammonium acetate (CH_3COONH_4) and 10% aluminum nitrate nonahydrate ($Al(NO_3)_3.9H_2O$) were added respectively, except for the sample blank. The mixtures were mixed with a vortex. After 40 minutes, absorbance values were read at 415 nm. Quercetin was preferred as standard. It was prepared at six different concentrations (0.25 mg/mL). A graph was drawn with the absorbance values corresponding to the concentration. According to the drawn graph, the total flavonoid substance amount of

the extracts was determined as microgram quercetin equivalent per milliliter extract (µg QE /mL).

2.3.2. Colorimetric DPPH• Radical Scavenging Activity, FRAP and CUPRAC Antioxidant Activity Test

In the study, the DPPH• antioxidant activity method [18] which is commonly used in the literature was carried as colorimetric [19] instead of spectrophotometric. Preliminary tests were applied for tarragon plant extracts with 2000 µM freshly prepared DPPH• solution. Then initial concentrations of each sample were determined. Plant extracts and antioxidant standard (Trolox®) were studied at 5 different concentrations. Measurements of samples, reagent blanks and sample blanks were performed in triplicate. DPPH• solution was transferred at equal volumes onto the solutions. The mixtures in the tubes were mixed with vortex and incubated for 60 minutes at room temperature. At the end of the incubation, the mixtures were dropped onto a TLC plate (Merck Silica gel 60) as triplicates (15 µL). After 5 min incubation, the formed colors on TLC plates were scanned via scanner and transferred to the computer. Images were shown as Jpeg files. The color result of each spot-on TLC plates was determined with Image J software. The color values were plotted against sample concentrations for the calculation of Color Scavenging Concentration 50% (CSC_{50}) values. CSC_{50} is the concentration of the sample which increases the color value (intensity of color) to half of its maximum at complete DPPH• reduction. When calculating the CSC_{50} values of the samples, their 1st degree derivative was taken.

The FRAP reagent was prepared freshly in the colorimetric method [20] as in the spectrophotometric method [21]. In the study, the Trolox antioxidant standard was studied at 5 different concentrations (1000, 500, 250, 125, 62.5 µM) to draw the standard calibration graph. Samples, reagent blanks and sample blanks were measured in triplicate. Pipetting of all samples was carried out as in the spectrophotometric method [21]. First, 50 µL of the extract was transferred to the test tubes and 1.5 mL FRAP reagent was added. The solutions were vortexed and kept for 20 minutes. Then the mixtures were dripped onto a TLC plate (Merck silica gel 60) as triplicates (15 µL). Also, the same amount of reagent blank and sample blank was dropped onto the TLC plate. It was left to dry at room temperature for 7 minutes. Then, it was transferred with the scanner device to the computer and saved as a JPEG file. The color values of the images were analyzed with the Image J program. graphs of the color values and concentrations were drawn using Microsoft Excel. µM Color TEAC (CTEAC) values were calculated for each sample with equality of the standard antioxidant Trolox plot [20].

As in the other tests, the CUPRAC antioxidant activity test was performed in triplicate. Trolox as a standard antioxidant was studied at 6 different concentrations (1000–500–250–125–62.5–31.25 µM). In this method, the tubes were added equal volume of Cu (II) chloride solution, neocuproin solution, ammonium acetate buffer (pH=7) and analysis solutions, respectively. The final solution volume was completed to 1.03 mL with distilled water. The tubes were stored at room temperature for 30 minutes [22]. At the end of the waiting period, 15 µL of the mixtures in the tubes were dropped onto the TLC plate in triplicate for all the samples. Because of pure water in the CUPRAC reagent, the TLC plates were left for 10 minutes and thus it was dried. Then the plates were scanned via a scanner, transferred to the computer and saved as JPEG files. Image J program was used in the determination of color values. Graphs were drawn based on average color values. The µM Color TEAC (CTEAC) values of each extract were calculated [23].

2.4. Phenolic and Flavonoid Compounds Analysis by RP-HPLC-PDA

The phenolic and flavonoid contents of tarragon plants were determined by RP-HPLC-PDA. The HPLC analyses were conducted on a Shimadzu Liquid Corporation LC 20AT HPLC system equipped with a PDA detector, C_{18} column (250 mm × 4.6 mm, 5 µm; GL Sciences). The mobile phases include acetic acid (2%) in water (A), acetonitrile (30%) in water (B), and the flow rate was selected as 1mL/min, injection volume of 20 µL, a column at 30ºC, were used and the detection range from 250, 280, 320 and 360 nm. The gradient was as follows: 0 min, 95% solvent A; 8 min, 15% solvent A; 10 min, 21% solvent A; 20 min 52% solvent A; 35 min 67% solvent A; 50 min 90% solvent A; 60 min 5% solvent A [24]. In order to confirm the phenolic compounds of the samples and to determine the concentrations, the retention times were compared with the real standards and ultraviolet absorption spectrum data. Samples were passed through a 0.45 µm filter before were given to the device.

2.5. Acetylcholinesterase Enzyme Inhibition

The extracts prepared for cell culture and antioxidant activity were also used for enzyme inhibition. Ellman method was modified with minor modification and applied [25,26]. Briefly, 50 µL of plant extract in various concentrations, 50 µL acetylcholinesterase (0.22 U/mL) enzyme, and 3 mL 0.1M phosphate buffer (pH = 8) 30 by mixing after minutes incubated. After 100 µL of 0.01 M 5.5'-dithiobis (2-nitrobenzoic acid) (DTNB) to the tube, adding 50 µL of 0.75 mM acetylthiocholine iodide the reaction was initiated.

The absorbance of the yellow compound [5-thio-2-nitrobenzoate dianion (TNB)] formed as a result of the reaction of thiocholine with chromogenic DTNB, which is released due to hydrolysis of acetylthiocholine, was measured in a spectrophotometer at 412 nm. Donepezil and ethanol were used as positive control and negative control respectively.

2.6. Cell Culture

Lung carcinoma (A549, CCL-185), human melanoma (VMM917, CRL-3232) and human normal fibroblast (hGF, PCS-201-018) cells were purchased from ATCC (Manassas, VA, USA). Both cells were cultured in Rosewell Park Memorial Institute-1640 Medium (RPMI-1640) with 10% heat inactivated fetal bovine serum (FBS) and 1% penicillin/streptomycin. Cells were incubated at 37°C supplied with 5% CO_2 [27].

2.6.1. Drug Preparation and Treatment

Extracts of *A. dracunculus* and *A. dracunculoides* and cisplatin were prepared in ethanol. All of the extracts and cisplatin concentrations were diluted with their solvents for cytotoxicity studies. Cisplatin was preferred as a positive control in this work [28]. Final solvent concentrations were adjusted to a maximum of 0.5 % for the medium.

2.6.2. Measurement of Cell Viability

Cell viability was evaluated using a colorimetric MTT [3-(4,5-d i m e t h y l t h i a z o l -2- y l) - 2,5-d i p h e n y l t e t r a z o l i u m b r o m i d e] assay [29]. Briefly, 5×10^3 cells A549, VMM917 and hGF cells were seeded into the well of sterile 96-well cell culture plates. After overnight incubation, the media on the plates were replaced with fresh media for A549, VMM917 and hGF. Then the plates were treated with various concentrations of the plant extracts (0.9–125 µg/mL) in A549, VMM917

and hGF for 72 h. Cisplatin was treated at different concentrations (0.25–32 µM) on both A549, VMM917 and hGF cell lines for 72h. Subsequently, 10 µL of MTT dye (0.25 mg/mL) was added to each well for 2 h. At the end of the time, the dye was removed and 200 µL of DMSO was added to each well to dissolve the formazan crystals. Absorbance values were read at 570 nm in a microplate reader (Molecular Devices Versamax, CA, USA) [28]. Optical densities were used to evaluate the percentage of viabilities in treated cells compared to untreated control cells. A logarithmic plot of log concentrations against cell viability was drawn to determine the IC50 value. The IC50 values of *A. dracunculus* and *A. dracunculoides* extracts in both cell lines were used to calculate the selectivity index with the following formula [27].

$$Selectivity\ Index = hGF\ cells\ IC_{50}/\ Cancer\ cells\ IC_{50}$$

2.7. Statistical Analysis

All experiments were conducted as three repeats and the results were given as arithmetic mean and ± standard deviation. Statistical analyzes were carried out using SPSS (Statistics Program for Social and Science) software (Version13.0.1). One-Way ANOVA test and post-hoc Tukey test were used in the study. p value less than 0.05 was considered as statistically significant.

3. Results and Discussion

3.1. Antioxidant Activity

In our study, total phenolic and total flavonoid were determined spectrophotometrically, while antioxidant activity was determined colorimetrically. The results of the antioxidant activity test were given in Table 1. The results showed that the *A. dracunculus* sample has the lower total phenolic and flavonoid contents than *A.*

Table 1. Colorimetric and Spectrophotometric Antioxidant Activity, Test Results of the Plant Extracts

Samples	Colorimetric Antioxidant Activity Tests			Spectrophotometric Antioxidant Activity Tests	
	DPPH (mg/mL) CSC50	FRAP (µM CTEAC)	CUPRAC (µM CTEAC)	Total Phenolic Substance µg GAE /mL extract	Total Flavonoid Substance µg QE /mL extract
Artemisia dracunculus L.	1.371 ± 0.120	462.133 ± 0.201	0.246 ± 0.060	225 ± 0.090	0.066 ± 0.010
Artemisia dracunculoides Pursh	1.165 ± 0.100	726.661 ± 0.270	0.304 ± 0.080	324 ± 0.110	0.085 ± 0.020
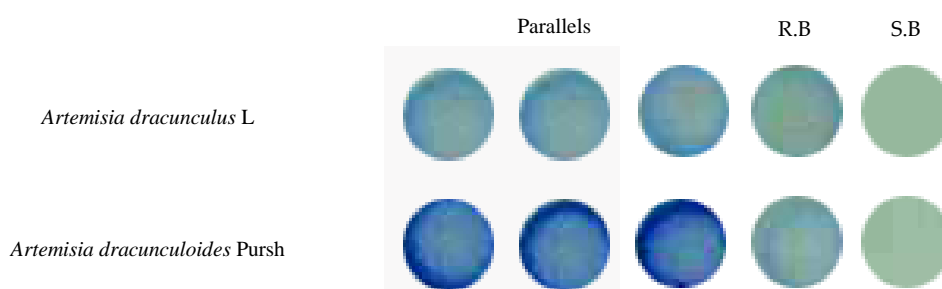
Three-parallel, reagent blank (R.B) and sample blank (S.B) images of the samples in the colorimetric FRAP antioxidant activity test

dracunculoides. The total phenol and flavonoid content values were determined at 324 μg GAE/mL extract and 0.085 μg QE/mL extract in *A. dracunculoides* while the values were measured at 225 μg GAE/mL extract and 0.066 μg QE/mL extract in *A. dracunculus*, respectively. In addition, DPPH, FRAP, and CUPRAC antioxidant activity assays were performed as colorimetric for the plant samples. The highest activity values of DPPH, FRAP and CUPRAC tests were founded in *A. dracunculoides*. The extracts of *A. dracunculoides* exhibited inhibition of DPPH activity than the *A. dracunculus* and CSC_{50} inhibition was measured as 1.371 and 1.162 mg/mL extract, respectively. Values of FRAP and CUPRAC tests in extracts of *A. dracunculoides* were determined as 726.661 and 0.304 respectively. However, the values were measured as 462.133 and 0.246 μM CTEAC for *A. dracunculus*.

Artemisia L. genus having small shrubs and herbs, belongs to the family of Asteraceae, is a traditional medicinal plant and is used in the treatment of many diseases [30]. There are many studies in the literature about members of *Artemisia*. One of the aims of the current study is to reveal the phytochemical properties of two species (*A. dracunculus* and *A. dracunculoides*) of the *Artemisia* genus. The relevance of polyphenols rests in their potential properties as an antioxidant, anti-inflammatory, anti-microbial, and anti-tumoral [31–33].

Contents of phenolic and flavonoid of the *A. dracunculus* and *A. dracunculoides* were compared based on spectrophotometric measurements (Table 1). The total phenolic content was evaluated based on the Folin-Ciocalteu colorimetric method using gallic acid as standard [16]. Mumivand et al. [34] reported the total phenolic content of tarragons (*A. dracunculus*) obtained from 12 different parts of Iran as 40.9–96.52 mg GAE/g. In another study, Ismail et al. [35] determined that total phenol and flavonoids in *A. dracunculus* as 28.5 and 1.54mg/g respectively. These results are higher than those our present. Because, there are many factors (e.g., different developmental stages of plants, genetic diversity, differences between different plant parts) that affect the chemical composition of plants. One of them is environmental factors due to location [36].

There are different methods to determine the antioxidant activity of the plants. In this study, the colorimetric dropping method was preferred. Because, it was cheaper cost due to using reagents and solvents less than the spectrophotometric method. In addition, there is no need for a costly spectrophotometer device. DPPH, FRAP and CUPRAC antioxidant tests were applied to plant extracts. The antioxidant activity values in all the methods were measured higher for *A. Dracunculoides* than *A. dracunculus*. Behbahani et al. [37] found that the IC_{50} value of *A. dracunculus* was 0.065 mg/ml in essential

Table 2. Phenolic Compounds

Standards	*Artemisia dracunculus* L. μg phenolic / g sample	*Artemisia dracunculoides* Pursh μg phenolic / g sample
Gallic Acid	n.d.	n.d.
Protocatechuic Acid	n.d.	n.d.
Chlorogenic Acid	**281.938**	**365.523**
p-OH Benzoic Acid	15.294	n.d.
Epicatechin	n.d.	n.d.
Caffeic Acid	n.d.	331.381
Syringic Acid	n.d.	40.586
m-OH Benzoic Acid	n.d.	n.d.
Rutin	n.d.	n.d.
Ellagic Acid	n.d.	n.d.
p-Coumaric Acid	n.d.	44.519
Ferulic Acid	**407.751**	**399.833**
Myricetin	n.d.	n.d.
Resveratrol	n.d.	n.d.
Daidzein	n.d.	n.d.
Luteolin	n.d.	n.d.
Quercetin	n.d.	n.d.
t-Cinnamc Acid	n.d.	n.d.
Apigenin	n.d.	n.d.
Hesperidin	n.d.	n.d.
Rhamnetin	n.d.	n.d.
Chrysin	n.d.	n.d.
Pinocembrin	n.d.	n.d.
CAPE	n.d.	n.d.
Curcumin	n.d.	n.d.

*n.d.: not detected

oil extracts. In another study was reported that DPPH values of *A. dracunculus* were determined as 94.2 μg/mL in essential oil extracts [38].

Carvalho et al. [39] reported that total phenolic contents of six different *Artemisia* species varied from 0.22 to 0.39 mg of GAE g^{-1}.

3.2. Phenolic Compounds by RP-HPLC-PDA

HPLC-PDA analysis was performed to determine the phenolic profiles in the leaves of *A. dracunculus* and *A. dracunculoides*. Twenty-five standards (gallic acid, protocatechuic acid, chlorogenic acid, *p*-OH benzoic acid, epicatechin, caffeic acid, syringic acid, *m*-OH benzoic acid, rutin, ellagic acid, *p*-coumaric acid, ferulic acid, myricetin, resveratrol, daidzein, luteolin, quercetin, *t*-cinnamc acid, apigenin, hesperidin, rhamnetin, chrysin, pinocembrin, caffeic acid phenyl ester (CAPE), curcumin) were identified and quantified (Table 2). It was identified ferulic acid (407.751μg/g sample), chlorogenic acid (281.938 μg/g sample) and *p*-OH benzoic acid (15.294 μg/g sample) in the *A. dracunculus* while chlorogenic acid (365.523μg/g), ferulic acid (399.833 μg/g sample) and caffeic acid (331.381μg/g sample) in the *A. dracunculoides* as a major compound.

Table 3. Acetylcholinesterase Enzyme Inhibition

Sample	Inhibition of AChE activity %	
Artemisia dracunculus L.	1.35 (mg/mL)	40.09 ± 0.65
Artemisia dracunculoides Pursh	1.16 (mg/mL)	39.48 ± 3.68
Donepezil	62.5 (µg/mL)	79.50 ± 0.20

In addition, syringic acid (40.586 µg/g) and *p*-coumaric acid (44.519 µg/g sample) were also detected in the A. *dracunculoides*.

Hydroxybenzoic acid, hydroxycinnamic acid and flavonols compounds found in plants can be considered therapeutic agents because they have protective effects against many diseases such as certain cancers, cardiovascular diseases and aging [40]. However, environmental factors and growing conditions can be affecting the chemical composition of plants; especially secondary metabolites [41]. In the present study, the phenolic composition of the *Artemisia* species was identified using RP-HPLC-PDA analysis.

The most important classes of bioactive substances of the tarragon plant are phenolic acid derivatives, flavonoids, essential oil, coumarins and alkamides [42–44]. The major phenolic compound in the extract of *A. dracunculus* was ferulic acid with 407.751 µg/g. It was followed by chlorogenic acid with 281.938 µg/g sample and *p*-OH benzoic acid with 15.294 µg/g sample. As in *A. dracunculus,* ferulic acid was determined as a major compound in the extract of *A. dracunculoides* with 399.833 µg/g. Other dominant compounds were chlorogenic acid (365. 523 µg/g sample), caffeic acid (331.381 µg/g sample) and syringic acid (40.586 µg/g sample). Ferulic acid was detected as the predominant component in both species. Lee et al. [45] reported that ferulic acid detected a lower value of 53.55 µg/g in *Artemisia absinthium* L. This may

be associated with the species and environmental differences. In another study, it was reported that chlorogenic acid (0.44 mg/g) was detected in the methanol extract of leaves of *A. vulgaris* collected from Serbia in similar amounts as in the present study [46]. Chlorogenic acid, one of the hydroxycinnamic acid derivatives, is associated with a reduced risk of developing Alzheimer's disease, a common neurodegenerative disorder [47].

3.3. Acetylcholinesterase Enzyme Inhibition

One of the changes that happen in Alzheimer's disease is the rise in the activity of acetylcholinesterase (AChE), the enzyme responsible for the hydrolysis of acetylcholine from both cholinergic and non-cholinergic neurons of the brain [48] The AChE inhibition effects of samples are given in Table 3. Respectively, *A. dracunculus* and *A. dracunculoides* extracts inhibited 40.09 ± 0.65%, and 39.48 ± 3.68% of acetylcholinesterase activity at a concentration of about 1 mg/mL. The samples showed acetylcholinesterase inhibitory activities less than 50% although it has been shown to be effective against lung and melanoma cells.

Alzheimer's disease is the most common type of dementia. The treatment of Alzheimer's disease, which is multifactorial, requires multiple therapeutic approaches. By blocking the degradation of ACh using acetylcholinesterase inhibitors, it forms the most important therapeutic strategy by controlling the level of acetylcholine (ACh) as a neurotransmitter in cholinergic synapses [49]. To date, some *Artemisia* species have been determined by AChE inhibition effects. However, it has not been studied in *A. dracunculus* and *A. dracunculoides.* The inhibitory activity of these ethanolic samples was determined against the AChE enzyme at 1.35 and 1.16 mg/mL in vitro. As shown in Table 3, the highest

Figure 1. The cytotoxic effect of *A. dracunculus* on A549, VMM917, hGF cells for 72h. Cell viabilities (%) are shown in each cell after treatment with *A. dracunculus*, at various concentrations. Error bars are representative of the standard deviation of at least three independent experiments. * *p < 0.05.*

Table 4. IC$_{50}$ values (μM) and selectivity index values calculated for, *A. dracunculus*, *A. dracunculoides*, cisplatin on A549, VMM917 and hGF cell lines (n=3)

Test compound/Cell Lines	A549	VMM917	hGF
Artemisia drancunculus L.	53.17 ± 1.09	> 125	> 125
Artemisia dracunculoides Pursh	46.66 ± 0.49	76.90 ± 1.63	> 125
Cisplatin	0.77 ± 0.06	6.86 ± 1.02	13.5 ± 0.71

Table 5. Selectivity index values calculated for *A. dracunculus*, *A. dracunculoides* and cisplatin on A549, VMM917 and hGF cell lines (n=3)

Cell Lines/Test compound	*Artemisia dracunculus*	*Artemisia dracunculoides* Pursh	Cisplatin
A549	> 2.35	> 2.68	17.50
VMM917	> 1	> 1.63	1.97

AChE inhibition was observed for *A. dracucunlus* with 40% inhibition at 1.35mg/mL concentration while it was measured for *A. dracunculoides* with 39.48% inhibition at 1.16 mg/mL concentration. Ferrante et al. [50] reported that among methanol, ethyl acetate, water and essential oil extracts of *Artemisia santonicum* L. was determined highest acetylcholinesterase inhibition effect in essential oil extract as IC$_{50}$ 2.26 mg/mL.

3.4. Cytotoxicity Effect

This study revealed the effects of *A. dracunculus* and *A. dracunculoides* extracts on cell viabilities in A549, VMM917 and hGF cells. *A. dracunculus* and *A. dracunculoides* induced cytotoxicity in all cells in a dose-dependent manner (Table 4, Fig. 1, Fig. 2) (*p < 0.05*). In all of the cytotoxicity studies, cisplatin, an anticancer drug known as a positive control, was used [28,48]. The cytotoxicity studies of cisplatin on A549, VMM917 and hGF cells and the IC$_{50}$ values explained by all cells are given in Table 4. Demonstrated the selective effect of *A. drancunculus* and *A. dracunculoides* on the cytotoxicity of A549 and hGF cells. The selective index of the plant extracts was calculated using Formula 1, (Table 5).

Skin and lung cancer has increased in the last 20 years. The number of these cancers is increasing every year [51,52]. New methods and research are being tried in order to treat cancer and prevent the rapid increase in deaths due to cancer types every year [53–56]. There is a range of therapeutic approaches in the treatment of melanoma and lung cancer such as chemotherapy, photodynamic therapy, immunotherapy, targeted therapy and enzyme inhibition therapy. Conventional chemotherapy has been frequently used particularly in the of improved melanoma and nonsmall cell lung cancer (NSCLC), however, increased resistance to chemotherapeutic drugs and/or possible mutagenic effect of chemotherapeutics on healthy cells may reduce the success rate of treatment [53–56]. The side effects of chemotherapeutic drugs used in cancer treatment lead constantly researchers to the discovery of new drugs. Therefore, studies have increased on endemic, rare plant species and plants grown in extreme environments in recent years. Among them, species belonging to the genus *Artemisia* L. attracted the attention of researchers [3]. In a study on *A. dracunculus* L., it was associated with diabetes and was reported that increase insulin secretion
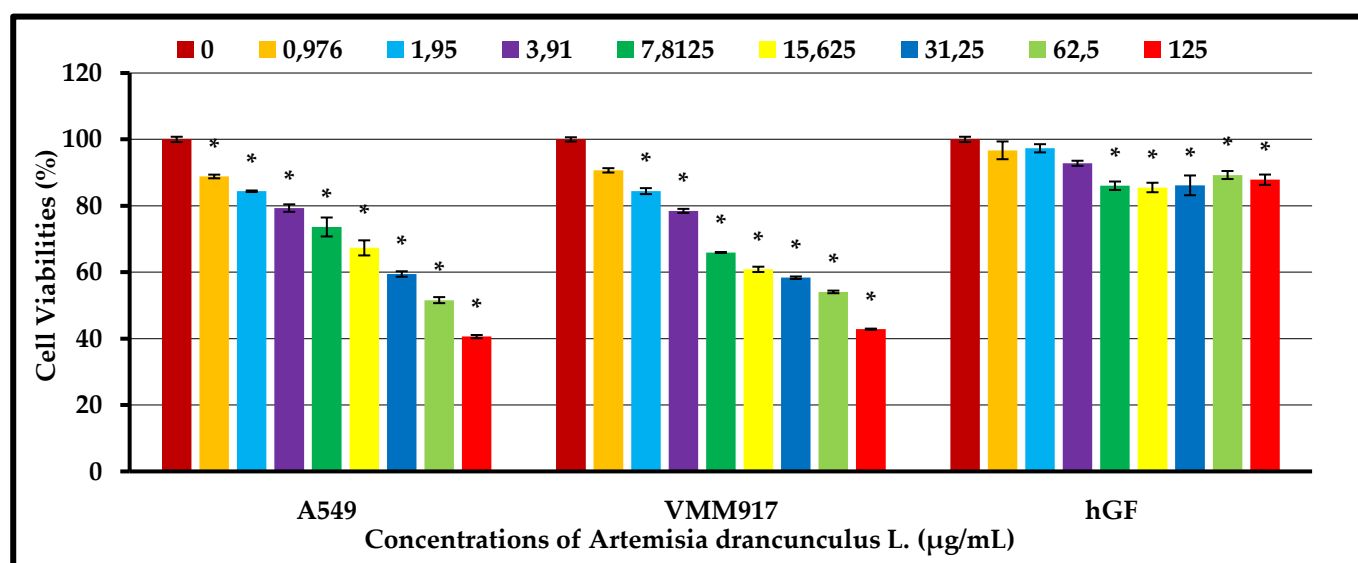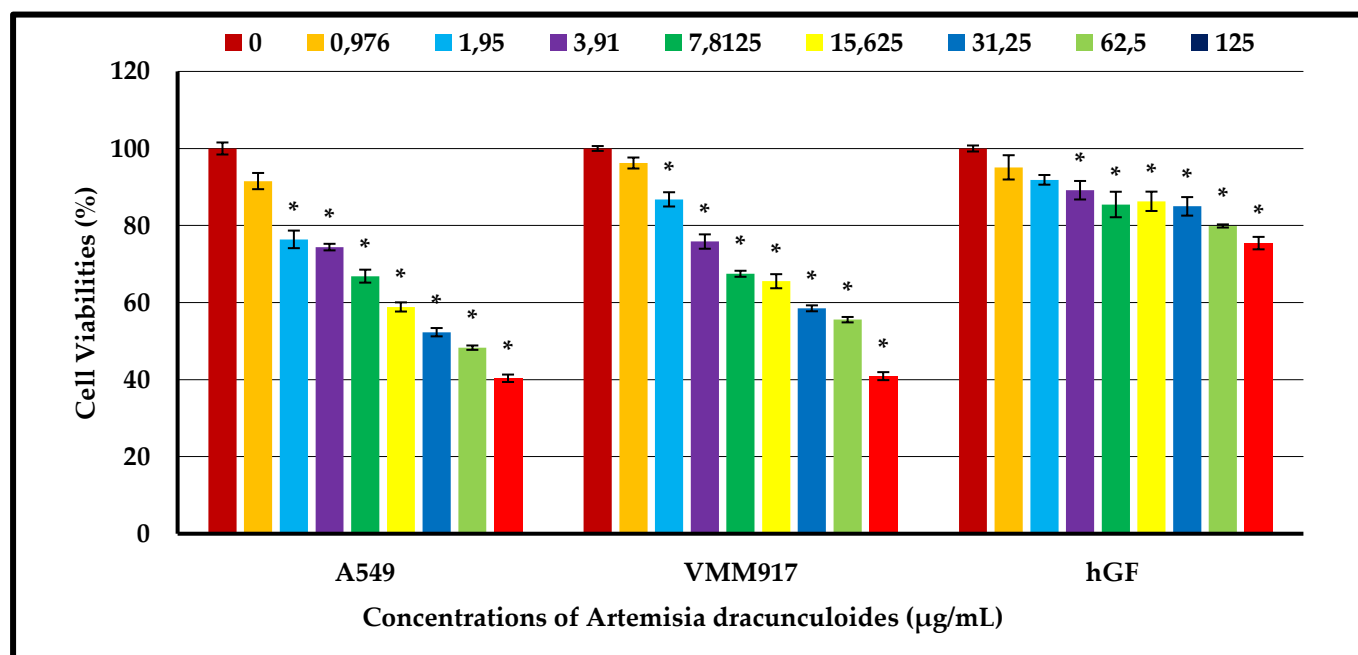

Figure 2. The cytotoxic effect of *A. dracunculoides* on A549, VMM917, hGF cells for 72h. Cell viabilities (%) are shown in each cell after treatment with *A. dracunculoides* at various concentrations. Error bars are representative of the standard deviation of at least three independent experiments. * *p < 0.05*.

and protect β cell number. In addition, it suppressed LPS/INFy-induced inflammation [57]. In another study on the same species of *Artemisia*, an MTT test was performed on cell viability at concentrations between 7–500 μg/mL on MCF-7, T-47D, MDA-MB-231, MCF-10 cancer and Hu-02 fibroblast cells. Although IC$_{50}$ values are not calculated, the extract has been shown to cause a reduction in cancer cells at a concentration of 500 μg/mL compared to control cells [58]. In addition to in vitro studies, in vivo studies on *Artemisia dracunculus* were also carried out, it has been shown that *Artemisia dracunculus* causes a decrease in cytokines through IL-17 and IL-23, which are known as inflammatory parameters in an experimental rat model [59].

4. Conclusion

In this study, it was determined that, total phenolic and flavonoid contents, antioxidant activity, phenolic compounds, acetylcholinesterase enzyme inhibition, and cytotoxic effect of two species of *Artemisia*. Total polyphenols, flavonoids, FRAP, CUPRAC and the antioxidant activities and polyphenol contents of the plants were found to be very close. DPPH antioxidant capacities, were investigated in plant extracts. It is clearly seen that plant extracts have at a certain level efficient inhibition properties on AChE, so these plants can be considered for drug design in the treatment of Alzheimer's disease. There are a number of drugs developed chemically or biotechnologically. It is clearly seen that there is no study on VMM917 and A549 cancer cells associated with *A. dracunculus* and *A. dracunculoides* in the literature. In this respect, the results of the study suggest that the use of extracts at certain doses will be a pioneer in evaluating its potential novel chemotherapeutic drug.

Funding:

Conflicts of Interest:

The authors declare no conflict of interest.

Author Contributions

ZC: Planning of the study, formal analyses, writing-editing article.

EAD: cytotoxic activity analyses.

ZA: Colorimetric Antioxidant activity analysis.

YK: HPLC studies.

BG: Cultivation of the plant used in the study.

References

[1] M. Willcox, Artemisia species: from traditional medicines to modern antimalarials-and back again J Altern Complem Med, 15, 2009, 101–109.

[2] B. Koul, P, Taak, The Artemisia genus: a review on traditional uses, phytochemical constituents, pharmacological properties and germplasm conservation. JGL. 7(1):1000142. 2017.

[3] H. Ekiert, J. Swiatkowska, E. Knut, P. Klin, A. Rzepiela, M. Tomczyk, A. Szopa, Artemisia dracunculus (Tarragon): A Review of Its Traditional Uses, Phytochemistry and Pharmacology. Frontiers in Pharacol, 14. 2021.

[4] R. Phillips, N. Foy, Herbs. Pan Books Ltd., London, pp. 1990, 171–178.

[5] G. Haghi, F. Ghasian, J. Safaei-Ghomi, Determination of the essential oil from root and aerial parts of Artemisia dracunculus L. cultivated in central Iran, J Essential Oil Res, 22, 2010, 294–296.

[6] E.M. Suleimenov, A.V. Tkachev, S.M. Adekenov, Essential oil from Kazakhstan Artemisia species. Chem, Nat Compd, 46(1), 2010, 135–139.

[7] I. Tak, D. Mohiuddin, B.A. Ganai, M.Z. Chishti, F. Ahmad, J.S. Dar, Phytochemical studies on the extract and essential oils of Artemisia dracunculus L. (tarragon), Afr J Plant Sci, 8(10), 2014, 72–75.

[8] S. Weinoehrl, B. Feistel, I. Pischel, B. Kopp, V. Butterweck, Comparative evaluation of two different Artemisia dracunculus L. cultivars for blood sugar lowering effects in rats, Phytother Res, 26, 2012, 625–629.

[9] T. Daly, M.A. Jiwan, N.M. O'Brien, S.A. Aherne, Carotenoid content of commonly consumed herbs and assessment of their bioaccessibility using an in vitro digestion model, Plant Food Hum Nutr, 65, 2010, 164–169.

[10] D. Obolskiy, I. Pischel, B. Feistel, N. Glotov, M. Heinrich, Artemisia dracunculus L. (tarragon): A critical review of its traditional use, chemical composition, pharmacology, and safety, J Agric Food Chem, 59, 2011, 11367–11384.

[11] G. ZawiĞlak, K. Dzida, Composition of essentials oils and content of macronutrients in herbage of tarragon (Artemisia dracunculus L.) grown in south-eastern Poland, J Elementol, 4, 2012, 721–729.

[12] A. Jemal, R. Siegel, E. Ward, Y. Hao, J. Xu, T. Murray, M.J. Thun, Cancer Statistics, CA Cancer J Clin, 58(2), 2008, 71–96.

[13] R.T. Skeel, Handbook of cancer chemotherapy. Lippincott Williams and Wilkins, Philadelphia, 2003.

[14] S. Duangmano, P. Sae-Lim, A. Suksamrarn, F.E. Domann, P. Patmasiriwat, B. Cucurbitacin, Inhibits human breast cancer cell proliferation through disruption of microtubule polymerization and nucleophosmin/B23 translocation, BMC Complement Medicine Ther, 12, 2012,185.

[15] A. Trendafilova, L.M. Moujir, P.M.C. Sousa, A.M.L. Seca, Research advances on health effects of edible Artemisia species and some sesquiterpene lactones constituents, Foods, 10(1),2021,65.

[16] K. Slinkard, V.L. Singleton, Total phenol analysis: Automation and comparison with manual methods, Am J Enol Vitic, 28, 1997,49–55.

[17] L.R. Fukumoto, G. Mazza, Assessing antioxidant and prooxidant activities of phenolic compounds, J Agric Food Chem, 48, 2000, 3597–3604.

[18] W. Brand-Williams, M.E. Cuvelier, C. Berset, Use of a free radical method to evaluate antioxidant activity, LWT-Food Sci Technol, 28,1995,25–30.

[19] Z. Akar, M. Kucuk, H. Doğan, A new colorimetric DPPH• scavenging activity method with no need for a spectrophotometer

applied on synthetic and natural antioxidants and medicinal herbs, J Enzyme Inhib Med Chem, 32 (1), 2017, 640–47.

[20] Z. Iskefiyeli, PhD. Thesis, Karadeniz Technical University, The Graduate School of Natural and Applied Sciences, Chemistry Graduate Program, Trabzon, Türkiye. 2014.

[21] I.F.F. Benzie, J.J. Strain, The ferric reducing ability of plasma (FRAP) as a measure of ''antioxidant power'': The FRAP assay, Anal Biochem, 239, 1996,70–6.

[22] R. Apak, K. Guclu, M. Ozyurek, S.E. Karademir, Novel total antioxidant capacity index for dietary polyphenols and vitamins C and E, using their cupric ion reducing capability in the presence of neocuproine: CUPRAC method, J Agric Food Chem, 52, 2004,7970–81.

[23] Z. Akar, Chemical compositions by using LC–MS/MS and GC–MS and antioxidant activities of methanolic extracts from leaf and flower parts of Scabiosa columbaria subsp. columbaria var. columbaria L., Saudi J Biol Sci, 28(11), 2021, 6639–6644.

[24] Z. Can, N. Baltas, Bioactivity and enzyme inhibition properties of Stevia rebaudiana, Current Enzyme Inhib, 12(2), 2016, 188–194.

[25] G.L. Ellman, K.D. Courtney, JrV. Andres, R.M. Featherstone. A new and rapid colorimetric determination of acetylcholinesterase activity, Biochem Pharmacol, 7(2), 1961, 88–95.

[26] N. Baltas, O. Yildiz, S. Kolayli, Inhibition properties of propolis extracts to some clinically important enzymes, J Enzyme Inhib Med Chem, 31(sup1), 2016, 52–55.

[27] E. Demir-Ayazoğlu, S. Demir, Y. Aliyazicioğlu, In vitro Cytotoxic Effect of Ethanol and Dimethyl Sulfoxide on Various. Human Cell Lines, KSU J Agric Natur, 23(5): p. 2020, 1119–1124.

[28] E. Demir-Ayazoğlu, A. Colak, S. Celik-Uzuner, O. Bekircan, 2021. Cytotoxic effect of a 3-(4-chlorophenyl)-5-(4-methoxybenzyl)-4H-1,2,4-triazole derivative compound in human melanoma cells, Inter J Biol Chem, 14, (1), 2021, 139–48.

[29] T. Mosmann, Rapid colorimetric assay for cellular growth and survival: application to proliferation and cytotoxicity assays, J Immunol Methods, 65(1–2), 1983, 55–63.

[30] M.J. Abad, L.M. Bedoya, L. Apaza, P. Bermejo, The Artemisia L. genus: a review of bioactive essential oils, Molecules, 17(3), 2012, 2542–2566.

[31] T.S. Cid-Pérez, R. Ávila-Sosa, C.E. Ochoa-Velasco, B.E. RiveraChavira, G.V. Nevárez-Moorillón, Antioxidant and antimicrobial activity of mexican oregano (Poliomintha longiflora) essential oil, hydrosol and extracts fromwaste solid residues, Plants 8 (1),2019.

[32] J. Arias, J. Mejía, Y. Córdoba, J.R. Martínez, E. Stashenko, J.M. del Valle, Optimization of flavonoids extraction from Lippia graveolens and Lippia origanoides chemotypes with ethanol-modified supercritical CO2 after steam distillation, Ind Crops Prod, 146, 2020, 112170.

[33] I. Bautista-Hernández, C.N. Aguilar, G.C. Martínez-Ávila, A. Ilina, C. Torres-León, D.K. Verma, M.L. Chávez-González, Phenolic compounds and antioxidant activity of Lippia graveolens Kunth residual leaves fermented by two filamentous fungal strains in solid-state process, Food Bioprod Process, 136, 2022, 24–35.

[34] H. Mumivand, M. Babalar, L. Tabrizi, L.E. Craker, M. Shokrpour, J. Hadian, Antioxidant properties and principal phenolic phytochemicals of Iranian tarragon (Artemisia dracunculus L.) accessions, Hortic Environ Biote, 58(4), 2017,414–422.

[35] A. Ismail, E.S. Abdalla, F.A. Khalil, E.M. El-Hadidy, Effect of Tarragon (Artemisia dracunculus L.) and its ethanolic extracts on chronic liver disease in male albino rats. Inter J Food Sci, 4(2), 2021, 46–59.

[36] Z. Akar, N.A. Burnaz, A new colorimetric method for CUPRAC assay with using of TLC plate, LWT - Food Sci Technol, 112,2019, 108212.

[37] B.A. Behbahani, F. Shahidi, F.T. Yazdi, S.A. Mortazavi, M. Mohebbi, Antioxidant activity and antimicrobial effect of tarragon (Artemisia dracunculus) extract and chemical

[38] N. Sahakyan, P. Andreoletti, M. Cherkaoui-Malki, M. Petrosyan, A. Trchounian, Artemisia dracunculus L. essential oil phytochemical components trigger the activity of cellular antioxidant enzymes, J Food Biochem, 45(4) 2021, e13691.

[39] I.S. Carvalho, T. Cavaco, M. Brodelius, Phenolic composition and antioxidant capacity of six Artemisia species, Ind Crop Prod, 33(2), 2011, 382–388.

[40] J.A. Ross, C.M. Kasum, Dietary flavonoids: Bioavailability, metabolic effects, and safety, Annu Rev Nutr, 22, 2002,19–34.

[41] B. Deng, S. Fang, X. Shang, X. Fu, W.Yang, Influence of genotypes and environmental factors on leaf triterpenoid content and growth of Cyclocarya paliurus, J Forest Res, 30 (3), 2019, 789–798.

[42] S. Logendra, D.M. Ribnicky, H. Yang, A. Poulev, Ma J. E.J. Kennelly, I. Raskın, Bioassay-guided isolation of aldose reductase inhibitors from Artemisia dracunculus, Phytochem, 67(14), 2006, 1539–1546.

[43] D. Govorko, S. Logendra, Y. Wang, D. Esposito, S. Komarnytsky, D. Ribnicky, A. Poulev, Z. Wang, T.C. William, I. Raskin, Polyphenolic compounds fromArtemisia dracunculus L.inhibit PEPCK gene expression and gluconeogenesis in an H4IIE hepatoma cell line, Am J Physiol Endocrinol, 293 (6), 2007, E1503–E1510.

[44] L.Z. Lin, J.M. Harnly, LC-PDA-ESI/MS Identification of the phenolic components of three compositae spices: Chamomile, tarragon, and mexican arnica, Nat Prod Commun, 7(6), 2012,749–752.

[45] Y.J. Lee, M. Thiruvengadam, I.M. Chung, P. Nagella, Polyphenol composition and antioxidant activity from the vegetable plant Artemisia absinthium L, Aust J Crop Sci, 7(12), 2013,1921–1926.

[46] D. Melguizo, E. Diaz-de-Cerio, R. Quirantes-Piné, J. Švarc-Gajić, A. Segura-Carretero, The potential of Artemisia vulgaris leaves as a source of antioxidant phenolic compounds, J Funct Foods, 2014,192–200.

[47] A. Farah, M. Monteiro, C.M. Donangelo, S. Lafay, Chlorogenic Acids from Green Coffee Extract are Highly Bioavailable in Humans, J Nutr, 138(12), 2008, 2309–2315.

[48] C.A. Curcio, T. Kemper, Nucleus rape dorsalis in dementia of the Alzheimer type: Neurofibrillary changes and neuronal packing density, J Neuropathol Exp, 43 (4),1984, 359–368.

[49] G. Orhan, I. Orhan, B. Sener, Recent developments in natural and synthetic drug research for Alzheimer's disease, Lett Drug Des Discov, 3(4), 2006, 268–274.

[50] C. Ferrante, G. Zengin, L. Menghini, A. Diuzheva, J. Jekő, Z. Cziáky, L. Recinella, A. Chiavaroli, S. Leone, L. Brunetti, D. Lobine, I. Senkardes, M.F. Mohomoodally, Qualitative Fingerprint Analysis and Multidirectional Assessment of Different Crude Extracts and Essential Oil from Wild Artemisia santonicum L., Process, 7, 2019, 522.

[51] R.T. Greenlee, T. Murray, S. Bolden, P.A. Wingo, Cancer statistics, CA CA: A Cancer J Clin, 50(1): 2000, p. 7–33.

[52] R.L. Siegel, K.D. Miller, H.E. Fuchs, A. Jemal, Cancer Statistics, 2021, CA: A Cancer J Clin, 71(1), 2021,7–33.

[53] B. Domingues, J.M. Lopes, P. Soares, H. Populo, Melanoma treatment in review, Immuno Targets Ther, 7, 2018, p. 35–49.

[54] A.R. Rao, H.N. Sindhuja, S.M. Dharmesh, K.U. Sankar, R. Sarada, G.A. Ravishankar,. Effective inhibition of skin cancer, tyrosinase, and antioxidative properties by astaxanthin and astaxanthin esters from the green alga Haematococcus pluvialis, J Agric Food Chem, 61(16), 2013, 3842–51.

[55] J. Ferlay, E. Steliarova-Foucher, J. Lortet-Tieulent, S. Rosso, J.W. Coebergh, H. Comber, D. Forman, F. Bray, Cancer incidence and mortality patterns in Europe: estimates for 40 countries in 2012, Eur J Cancer, 49(6), 2013, p. 1374–403.

[56] H. Hardardottir, S. Jonsson, O. Gunnarsson, B. Hilmarsdottir, J. Asmundsson, I. Gudmundsdottir, V.Y. Saevarsdottir, S. Hansdottir, P. Hannesson, T. Gudbjartsson, Advances in lung

cancer diagnosis and treatment- a review, Laeknabladid, 108 (1), 2022, 17–29.

[57] S. Aggarwal, G. Shailendra, D.M. Ribnicky, D. Burk, N. Karki, M.S.Q.X. Wang, An extract of Artemisia dracunculus L. stimulates insulin secretion from beta cells, activates AMPK and suppresses inflammation, J Ethnopharmacol, 170, 2015, 98–105.

[58] K. Safinejad, A. Mohebifar, H. Tolouei, P. Monfared, A. Razmjou, Comparative study on the toxicity of mentha piperita L. and Artemisia dracunculus L. hydroalcoholic extracts on human breast cancer cell lines, Int J Biology Biotechnol, 18(2), 2021, 253–261.

[59] H. Safari, G. Anani-Sarab, M. Naseri, Artemisia dracunculus L. modulates the immune system in a multiple sclerosis mouse model, Nutr Neurosci, 24(11), 2021, 843–849.

Turkish Journal of Analytical Chemistry

www.turkjac.org
2019

The use of honey as a green solvent in the extraction of raw propolis

Sevgi Kolaylı (iD)

Karadeniz Technical University, Faculty of Science, Department of Chemistry, 61080 Trabzon, Türkiye

Abstract

Propolis is a resinous natural mixture taken by scraping beehives. It is used as a food supplement due to its high biological active properties. After extracting crude propolis with various solvents, it is used as propolis extracts. The best propolis extraction is obtained with 70% ethanol, while green solvents are preferred because of some side effects of alcohol. Recently, green solvents have attracted interest in the extraction of propolis. In this study, the solubility of raw propolis in honey was investigated. The results were evaluated as total phenolic content and total antioxidant activity. In the study carried out with honey:water mixtures in different ratios, it was determined that the most ideal ratio was 1:20 (0.333 ± 0.033 mg GAE/mL). As a result, the production of such solvents from beehive products further encourages diversification of bee products and the discovery of new applications using environmentally friendly solutions.

1. Introduction

Honey is a sweet, viscous food substance produced by bees. Bees produce honey by collecting nectar from flowers and processing it in their digestive system, regurgitating and storing it in honeycombs. The process of creating honey involves enzymatic activity, evaporation, and the addition of enzymes from the bees. Honey has been used as a food, medicine, and sweetener for thousands of years. It has a long history of use in traditional medicine for its antibacterial and wound-healing properties. Honey is also rich in antioxidants and has been associated with a range of health benefits, including reducing inflammation and improving heart health [1,2]. Honey can vary in color and flavor depending on the type of flower nectar collected by the bees. Some common types of honey include clover, orange blossom, and manuka honey. Manuka honey, which is produced in New Zealand and Australia, has gained popularity for its high antibacterial properties and is used in wound care and other medical applications. While honey is generally considered safe for consumption, it should not be given to infants under one year of age due to the risk of botulism. Honey may also cause allergic reactions in some people [3,4].

Propolis is a natural resinous substance collected by honeybees from various plants and trees. Bees use

propolis to seal small gaps and cracks in their hives, as well as to protect against infections and other threats. Propolis is a complex mixture of plant resins, beeswax, essential oils, and various organic compounds [5]. Propolis has been used in traditional medicine for centuries, particularly for its antimicrobial and anti-inflammatory properties. Research has also shown that propolis has antioxidant, immunomodulatory, and anticancer effects [6]. There are several types of propolis, which can vary in color and chemical composition depending on the location and plant sources used by the bees. Some of the most common types include Brazilian propolis, European propolis, and Chinese propolis. Propolis can be taken as a supplement or used topically as a natural remedy for various health conditions. Some of the most common uses of propolis include treating sore throat, colds and flu, dental infections, and skin problems. While propolis is generally considered safe, it may cause allergic reactions in some people. It may also interact with certain medications, so it is important to talk to a healthcare provider before using propolis supplements [7].

The escalating utilization of non-renewable substances has prompted researchers to seek alternatives that are renewable and pose lesser risks. Green

---

chemistry plays a crucial role in this context. Extensive research has been conducted to explore less toxic or bio-based solvents known as green solvents. Water, solvents derived from biological sources, ionic liquids (ILs), deep eutectic solvents (DESs), green synthetic organic solvents, and supercritical liquids (SCF) stand out as prominent classifications within the realm of green solvents.

Propolis is a complex mixture of plant resins, waxes, essential oils, and other biologically active compounds. The choice of solvent used in propolis extraction can have a significant impact on the chemical composition and bioactivity of the resulting extract. Here are some of the solvents that have been used for propolis extraction along with their advantages and disadvantages:

Ethanol: Ethanol is a commonly used solvent for propolis extraction. It is relatively inexpensive and readily available and has been shown to extract a wide range of bioactive compounds from propolis. However, high concentrations of ethanol can cause degradation of some of the more sensitive components of propolis [8-10].

Methanol: Methanol is another solvent that has been used for propolis extraction. It has similar advantages and disadvantages to ethanol but is generally less effective at extracting certain bioactive compounds [11, 14].

Water: Water is a safe and environmentally friendly solvent for propolis extraction. However, it is generally not as effective as organic solvents at extracting lipophilic compounds and may require the use of additional solvents or extraction techniques to obtain a high-quality propolis extract [12]. Freitas et al. compared the efficiency of honey brandy and mead in propolis extraction with ethanol and water in a study they conducted in 2022 with the hypothesis of environmentally friendly solvent [13]. When we look at the studies on environmentally friendly solvents or green solvents, it is seen that there is an open field for research. It has been observed that there are almost no studies on the effectiveness of the use of honey-water mixture as a solvent in propolis extraction under different extraction conditions.

In this context, it is aimed to determine the ratio of honey-water mixture as green solvent for propolis

Table 1. The effectiveness of the ethanolic propolis residue in the honey-water mixture

BP1	Honey + 70% EtOH
BP2	Residue + 70% EtOH
BP3	Honey + Residue + 70% EtOH
BP4	Honey-Water Solution
BP5	Residue + Water
BP6	Residue + Honey-Water Solution

extraction and the best propolis-solvent ratio with this honey-water mixture. In addition, the antioxidant efficiencies of propolis evaporated after alcoholic extraction in honey, water and honey-water mixture were investigated.

2. Material and methods

2.1. Sample extraction
In the study, Anatolian propolis obtained from various beekeepers and flower honey obtained from the Black Sea region were used. Until the time of analysis, propolis was stored at -20 °C and honey was stored under dark and room conditions. Honey and propolis samples used were extracted in methanol and 70% ethanol at a ratio of 1:10 (24 hours, 200 rpm, room temperature), respectively [10]. Antioxidant properties and phenolic components of propolis and honey samples used in the study were determined. Propolis:honey-water extraction efficiency studies were performed on these two samples. This study was planned in three stages.

-The ratio of the honey-water mixture to be used was determined (at a fixed amount of propolis).

-The ideal propolis-solvent ratio was determined in the solvent at the determined honey-water ratio.

-The effectiveness of the ethanolic propolis residue in the honey-water mixture was investigated.

Firstly, honey-water solutions were prepared at 1:1, 1:2, 1:3, 1:4, 1:5, 1:10, 1:20 and 1:40 (propolis-solvent) ratios to determine the ratio of honey-water mixture to be used in propolis extraction (200 rpm, 24 h, rt). Secondly, different amounts of propolis (0.25, 0.5, 0.75, 1, 2, 3 and 4 g in 10 ml solvent) were extracted in the determined honey-water ratio solution. Finally, after the propolis extract extracted with 70% ethanol was evaporated, the residue was dissolved in 2 ml of 70% ethanol. The following experiments were carried out with this residue (Table 1). In the experiments, 1 g of honey, 500 microliters of propolis residue and 10 mL of solvent (70% EtOH, HW and water) were used. The total phenolic (TP) values of the extracts were analyzed, and the results are given as mg GAE/mL extract. Since the main theme of our study was honey-water mixture, firstly, the extraction efficiency of crude propolis was examined. Then, the efficiency of ethanolic propolis residue in the honey-water mixture was tried to be determined.

2.2. Antioxidant capacity
The method described by Slinkard and Singleton (1977) was used to determine the total phenolic content [15]. Initially, 20 μL of the sample was mixed with 680 μL of distilled water. Subsequently, 400 μL of 1:10 diluted Folin-Ciocalteu reagent added to the mixture and

incubated for 4 min. Then, 400 µL of 10% Na_2CO_3 solution was added, and the resulting mixture was allowed to incubate at room temperature for 120 min. Spectrophotometric measurement was performed at 760 nm, and the total amount of phenolic substance present in the sample was determined. The results were expressed as mg gallic acid equivalent (mg GAE/g) using gallic acid as a standard.

To determine the total flavonoid substances, the method outlined by Fukumoto and Mazza (2000) with slight modifications was utilized [16]. First, 2150 µL of methanol was added to 250 µL of the sample, followed by the addition of 50 µL of 10% $Al(NO_3)_3$ and 50 µL of 1 M NH_4CH_3COO solution. After incubation for 40 min, the absorbance of the resulting colored product formed because of the redox reaction between flavonoids and aluminum (III) was measured at a wavelength of 415 nm. The amount of flavonoid substance present was calculated using quercetin as a standard, and the results were expressed as mg quercetin equivalent (mg QUE/g).

2.3. Antioxidant activity

The antioxidant activity was determined using the widely used 2,2-diphenyl-1-picryl hydrazyl (DPPH) test. The DPPH• radical, which has a maximum absorbance at 517 nm, was used as a synthetic radical for this test. The method proposed by Molyneux (2004) was used to assess the scavenging of DPPH radicals with antioxidants present in the sample [17]. A 100 µM methanolic DPPH• solution was employed. In this assay, sample solutions of equal volume were added to the constant DPPH• radical concentration in the medium after being serially diluted. Trolox was utilized as a standard, and the results were expressed as the SC50 value (mg/ml).

The Ferric reducing/antioxidant power (FRAP) assay was used to determine antioxidant activity based on the reduction of Fe(III)-TPTZ-2,4,6-tris(2-pyridyl)-S-triazine complex in the presence of antioxidants [18]. Fresh FRAP reagent was prepared by mixing pH:3.6 acetate buffer, TPTZ , and FeCl$_3$ solution in a ratio of 10:1:1. A volume of 50 µL of the sample was added to 1500 µL of FRAP reagent, and the absorbance was read at 593 nm after 4 min. A standard curve was constructed using different concentrations of $FeSO_4.7H_2O$, and the results were reported as µmol $FeSO_4.7H_2O$/g [10].

2.4. Phenolic component

The HPLC-PDA analysis of the samples for phenolic content specified by Kara et al. involved preparation and subsequent injection into the device [19]. The analysis was performed using a Shimadzu Corporation LC 20AT HPLC system with a mobile phase consisting of a gradient of 70-30% acetonitrile-ultrapure water and 2% acetic acid-ultrapure water. The sample injection volume was 20 µL, the mobile flow rate was 1.0 mL/min, and the column oven temperature was maintained at 30 °C. Analysis of the phenolic content was done using 25 standard substances. The results were expressed in µg of standard phenolic substance per gram of sample.

3. Results and discussion

Antioxidant and phenolic analysis results of propolis and honey samples used in the experiment are given in Table 2. According to research, the total phenolic content in propolis varies depending on the source and solvent used. One study by Cottica et al. (2011) found the range to be between 31-299 mg of GAE/g of ethanolic extract [21]. Another study by Stoia et al. (2015) analyzed 10 propolis samples and reported an average of 9.71 ± 0.80 mg GAE/g for extracts [20]. In our study, the TP value of the propolis used was 28.847 ± 0.221 mg GAE/g, highlighting the variability in obtaining a propolis extract rich in polyphenolic components. Research has demonstrated a correlation between the antioxidant capacity of honey and its polyphenol content [22]. Chestnut honey, heather honey, and oak honey possess

Table 2. Antioxidant and phenolic component analysis results of honey and propolis

Analysis	Sample	
	Honey	Propolis
TP (mg GAE/ g sample)	0.141 ± 0.013	28.847 ± 0.221
TF (mg QE/ g sample)	0.035 ± 0.002	1.119 ± 0.072
FRAP (µmol Fe₂SO₄.7H₂O/g sample)	3.320 ± 0.041	317.347 ± 2.573
DPPH SC₅₀ (mg/ml)	20.400 ± 0.085	0.135 ± 0.003
Gallic acid	—	47.596
Protocatechuic acid	—	—
Chlorogenic acid	—	—
p-OH benzoic acid	1.726	—
Epicatechin	—	—
Caffeic acid	—	231.544
Syringic acid	—	—
m-OH benzoic acid	—	—
Rutin	—	84.681
Ellagic acid	—	996.589
p- coumaric acid	2.162	270.568
Ferulic acid	—	401.705
Myricetin	—	—
Resveratrol	—	—
Daidzein	—	—
Luteolin	—	24.957
Quercetin	—	57.726
t-cinnamic acid	1.587	41.521
Apigenin	—	93.093
Hesperetin	1.964	—
Rhamnetin	—	—
Chrysin	8.548	775.017
Pinocembrin	5.672	662.761
CAPE	—	—
Curcumin	—	—

(Row group label, rotated: µg phenolic /g sample)

Table 3. The ratio of the honey-water mixture for propolis extraction

Ratio	TP (mg GAE/mL extract)
1:1	0.228 ± 0.031
1:2	0.138 ± 0.021
1:3	0.180 ± 0.020
1:4	0.216 ± 0.009
1:5	0.154 ± 0.008
1:10	0.189 ± 0.010
1:20	0.333 ± 0.033
1:40	0.326 ± 0.012

a total polyphenol content of around 1 mg GAE/g. In addition, other types of flower honeys have lower values and as a result, its antioxidant properties are lower. In our study, we determined that the TP value of the flower honey sample used was 0.141 ± 0.013 mg GAE/g.

The TP value of the extracts obtained to determine the honey-water mixture to be used in propolis extraction is given in Table 3. The TP value of the extract was calculated by subtracting the antioxidant value of the honey sample. Although there is no clear order in the total TP content obtained in the extracts at the ratios of 1:1 to 1:4, it is seen that the TP value of the extract prepared at the ratio of 1:20 is the highest. It can be thought that the 1:20 ratio of honey-water mixture has the highest ionic and molecular level interactions with the phenolic compounds in propolis. In the following steps, it was decided to use a 1:20 honey-water mixture.

To determine the ideal propolis-solvent ratio, the TP value of the solvent used in the extractions was also calculated. Extraction was performed by adding different amounts of propolis to equal solvent volumes and the TP values of the obtained extract were calculated (Table 4). When we look at the results obtained, it is seen that the TP values per unit volume of the extract increase with the increasing amount of propolis. However, it is also seen that this increase is not directly proportional to the increase in the amount of propolis used in extraction. As a result, the amount of propolis used in the extraction

can be increased to obtain higher antioxidant activity, but it should not be ignored that the yield to be obtained from the gram amount of propolis will decrease.

The TP values of the samples after processing were calculated to look at the agonistic or antagonistic activity of ethanolic propolis residue and honey in ethanol and HW mixture (Table 5). When the findings were examined, it was observed that the extract, in which honey and propolis residues were used together (1.313 ± 0.013), was higher than the sum of the TP values of honey and propolis residue prepared separately in ethanol (0.036 ± 0.001 and 1.141 ± 0.006, respectively). Nonetheless, in the extracts prepared using HW mixture and water, it was noted that the TP value of the extract (0.202 ± 0.004), in which the propolis residue was prepared in HW mixture, remained lower compared to the extract (0.279 ± 0.005) where the propolis residue was prepared solely in water. As a result of removing the alcohol from the ethanolic propolis extract and re-dissolving it only in HW mixture, a higher TP value could not be obtained as desired in terms of TP value. In addition, an upward trend was observed in the TP value with the mixing of honey and propolis residue in ethanolic solvent. Based on this information, new and different extraction conditions can be obtained by adding different components or ambient conditions (such as temperature) while preparing the honey-water mixture.

Table 4. The ideal propolis-solvent (1:20 HW mixture) ratio for propolis extraction

g propolis in 10 ml 1:20 HW mixture	TP (mg GAE/mL extract)
0	0.023 ± 0.005
0,25	0.163 ± 0.006
0,5	0.237 ± 0.006
0,75	0.285 ± 0.013
1	0.368 ± 0.015
2	0.532 ± 0.008
3	0.755 ± 0.019
4	0.897 ± 0.004

*HW: Honey-Water

Table 5. The effectiveness of the ethanolic propolis residue in the honey-water mixture

Extract	TP (mg GAE/mL extract)
BP1	0.036 ± 0.001
BP2	1.141 ± 0.006
BP3	1.313 ± 0.013
BP4	0.028 ± 0.002
BP5	0.256 ± 0.005
BP6	0.230 ± 0.004

In the literature, there are different propolis extraction methods in which maceration, ultrasound assisted, and microwave assisted extraction, Soxhlet, supercritical CO_2 extraction, high pressure methods and different solvents are applied [8]. Although researchers generally agree that the best solvent is ethanol-water mixtures, they are trying to obtain high efficiency propolis extraction with non-alcoholic and green solvents. Researchers studying the effectiveness of honey brandy and mead on propolis extraction state that extracts prepared with these two solvents have a non-negligible antioxidant and antibacterial effect (26.6 ± 2.8% and 6.5 ± 1.0%, respectively)[13]. As an alternative to ethanolic solvents used in propolis extraction, Natural Deep Eutectic Solvents (NADES) has started to come to the fore. In a study conducted to provide equivalent antioxidant content and efficacy, it was stated that the extracts obtained with NADES solvents made from choline chloride-propylene glycol or lactic acid at 50 °C could be equivalent to that with 70% EtOH. Again, in this study, they stated that NADES, aqueous L-Lysine and honey solutions can replace ethanol or water [23]. In another study, the antioxidant properties of aqueous (AqEP), polyethylene glycol-aqueous (Pg-AqEP) and ethanolic (EEP) propolis extracts were compared. As a result of the data they obtained, they stated that phenolic acids and aldehydes constituted 40-42% of all compounds extracted and identified in AqEP and Pg-AqEP and 16% in EEP. As a result of their cell culture study, they reported that they showed similar antioxidant activity, but Pg-AqEP and EEP had better mitochondrial superoxide effect [24]. Researchers, on the other hand, reported that aqueous extracts of propolis have stimulatory activity on cell proliferation in vitro [25]. Considering all these studies it is seen that green solvent studies to replace ethanolic propolis extracts have gained importance in recent years. However, in the extractions made with only water, the lack of efficiency at the level of the ethanolic extract leads to experimenting and using aqueous solvent mixtures. It has been reported that the use of honey, which is also a bee product and its products, has small or large effects on the effectiveness of propolis extracts.

4. Conclusions

The consumption of propolis, which is a valuable natural product with various biological activities among bee products, is increasing day by day. This pushes the researchers to optimize the extraction of this product. Recently, studies have been carried out especially on NADES and water-based extract preparation methods. For this reason, the effect of honey-water mixture as a water-based solvent on the antioxidant efficiency of propolis extract was investigated in our study. When we look at the first step results of our study, a significant increase in antioxidant activity was observed with propolis extraction using 1:20 HW mixture. Higher antioxidant activity can be obtained by improving the extraction conditions. However, the amount of propolis to be extracted in the determined HW mixture is also important. While the high amount of propolis increases the antioxidant activity to a certain extent, there is a decrease in the extraction efficiency after a certain point. Finally, after evaporation of the ethanolic propolis, after the residue was dissolved in HW and EtOH, it was seen that there was no significant difference in antioxidant activity between these two cases. The extract prepared with HW mixture did not provide high antioxidant as expected. Of course, more work is needed to find the best way to extract bioactive compounds from different types of propolis on a green solvent basis.

Acknowledgments

References

[1] O. O. Erejuwa, S. A. Sulaiman, M. S. Ab Wahab, Honey: a novel antioxidant, Molecules, 17(4), 2012, 4400-4423.

[2] J. M Alvarez-Suarez, F. Giampieri, M. Battino, Honey as a source of dietary antioxidants: structures, bioavailability, and evidence of protective effects against human chronic diseases, Curr Med Chem, 20(5), 2013, 621-638.

[3] R. Cooper, Honey for wound care in the 21st century, J Wound Care, 25(9), 2016, 544-552.

[4] K. Brudzynski, C. Sjaarda, Honey glycoproteins containing antimicrobial peptides, Jelleins of the Major Royal Jelly Protein 1, are responsible for the cell wall lytic and bactericidal activities of honey, Plos One, 10(4), 2015, e0120238.

[5] V. Bankova, Chemical diversity of propolis and the problem of standardization, J Ethnopharmacol, 100(1-2), 2005, 114-117.

[6] W. Krol, S. Scheller, J. Shani, G. Pietsz, Z. Czuba, Synergistic effect of ethanolic extract of propolis and antibiotics on the growth of staphylococcus aureus, Arznei-Forschung, 43(5), 1993, 607-609.

[7] J. M. Sforcin, V. Bankova, Propolis: is there a potential for the development of new drugs?, J Ethnopharmacol, 133(2), 2011, 253-260.

[8] V. Bankova, B. Trusheva, M. Popova, Propolis extraction methods: a review, J Apicult Res, 60:5, 2021, 734-743.

[9] M. Jug, O. Karas, I. Kosalec, The influence of extraction parameters on antimicrobial activity of propolis extracts, Nat Prod Commun, 12(1), 2017, 1934578X1701200113

[10] Y. Kara, Z. Can, S. Kolaylı, What should be the ideal solvent percentage and solvent-Propolis ratio in the preparation of Ethanolic Propolis extract?, Food Anal Method, , 15(6), 2022, 1707-1719.

[11] B. Lawal, O. K. Shittu, A. N. Abubakar, I. A. Olalekan, A. M. Jimoh, A. K. Abdulazeez, Drug leads agents from methanol extract of Nigerian bee (Apis mellifera) propolis, J Intercultural Ethnopharmacol, 5(1), 2016, 43.

[12] M. Sambou, J. Jean-François, F. J. Ndongou Moutombi, J. A. Doiron, M. P. Hébert, A. P. Joy, M. Touaibia, Extraction, antioxidant capacity, 5-lipoxygenase inhibition, and phytochemical composition of propolis from Eastern Canada, Molecules, 25(10), 2020, 2397.

[13] A. S. Freitas, A. Cunha, P. Parpot, S. M. Cardoso, R. Oliveira, C. Almeida-Aguiar, Propolis efficacy: the quest for eco-friendly solvents, Molecules, 27(21), 2022, 7531.

[14] S. Ma, H. Ma, Z. Pan, L. Luo, L. Weng, Antioxidant activities of propolis's extracts by different solvents in vitro, Journal of Chinese Institute of Food Science and Technology, 16(8), 2016, 53–58. [in Chinese] (abstract in English available at: https://www.researchgate.net/publication/308363945_Antioxidant_activities_of_propolis%27s_extracts_by_different_solvents_in_vitro, 11.05.2023)

[15] K. Slinkard, V. L. Singleton, Total phenol analysis: automation and comparison with manual methods, Am J Enol Viticult, 28(1), 1977, 49-55.

[16] L. R. Fukumoto, G. Mazza, Assessing antioxidant and prooxidant activities of phenolic compounds, J Agr Food Chem, 48(8), 2000, 3597-3604.

[17] P. Molyneux, The use of the stable free radical diphenylpicrylhydrazyl (DPPH) for estimating antioxidant activity, Songklanakarin J. sci. technol, 26(2), 2004, 211-219.

[18] I. F. Benzie, J. J. Strain, [2] Ferric reducing/antioxidant power assay: direct measure of total antioxidant activity of biological fluids and modified version for simultaneous measurement of total antioxidant power and ascorbic acid concentration. In Methods in enzymology, 299, 1999, 15-27.

[19] Y. Kara, Z. Can, S. Kolaylı, Applicability of Phenolic Profile Analysis Method Developed with RP-HPLC-PDA to some Bee Product, Braz Arch Biol Techn, 65, 2022.

[20] M. Stoia, A. Cotınghıu, F. Budın, S. Oancea, Total phenolics content of Romanian propolis and bee pollen, Victoria, 2, 2015, 20.

[21] S. M. Cottica, A. C. Sawaya, M. N. Eberlin, S. L. Franco, L. M. Zeoula, J. V. Visentainer, Antioxidant activity and composition of propolis obtained by different methods of extraction, J Brazil Chem Soc, 22, 2011, 929-935.

[22] Z. Can, O. Yildiz, H. Sahin, E. A. Turumtay, S. Silici, S. Kolayli, An investigation of Turkish honeys: their physico-chemical properties, antioxidant capacities and phenolic profiles, Food Chem, 180, 2015, 133-141.

[23] C. S. Funari, A. T. Sutton, R. L. Carneiro, K. Fraige, A. J. Cavalheiro, V. da Silva Bolzani, R. D. Arrua, Natural deep eutectic solvents and aqueous solutions as an alternative extraction media for propolis, Food Res Int, 125, 2019, 108559.

[24] L. Kubiliene, A. Jekabsone, M. Zilius, S. Trumbeckaite, D. Simanaviciute, R. Gerbutaviciene, D. Majiene, Comparison of aqueous, polyethylene glycol-aqueous and ethanolic propolis extracts: antioxidant and mitochondria modulating properties, BMC Complem Altern M, 18, 2018, 1-10.

[25] A. K. Kuropatnicki, E. Szliszka, M. Kłósek, W. Król, The beginnings of modern research on propolis in Poland, Evid-Based Compl Alt, 2013.

Turkish Journal of Analytical Chemistry

www.turkjac.org
2019
TurkJAC

The use of honey as a green solvent in the extraction of raw propolis

Sevgi Kolaylı (iD)

Karadeniz Technical University, Faculty of Science, Department of Chemistry, 61080 Trabzon, Türkiye

Abstract

Propolis is a resinous natural mixture taken by scraping beehives. It is used as a food supplement due to its high biological active properties. After extracting crude propolis with various solvents, it is used as propolis extracts. The best propolis extraction is obtained with 70% ethanol, while green solvents are preferred because of some side effects of alcohol. Recently, green solvents have attracted interest in the extraction of propolis. In this study, the solubility of raw propolis in honey was investigated. The results were evaluated as total phenolic content and total antioxidant activity. In the study carried out with honey:water mixtures in different ratios, it was determined that the most ideal ratio was 1:20 (0.333 ± 0.033 mg GAE/mL). As a result, the production of such solvents from beehive products further encourages diversification of bee products and the discovery of new applications using environmentally friendly solutions.

Keywords: Solvent, honey-water, propolis, extract

1. Introduction

Honey is a sweet, viscous food substance produced by bees. Bees produce honey by collecting nectar from flowers and processing it in their digestive system, regurgitating and storing it in honeycombs. The process of creating honey involves enzymatic activity, evaporation, and the addition of enzymes from the bees. Honey has been used as a food, medicine, and sweetener for thousands of years. It has a long history of use in traditional medicine for its antibacterial and wound-healing properties. Honey is also rich in antioxidants and has been associated with a range of health benefits, including reducing inflammation and improving heart health [1,2]. Honey can vary in color and flavor depending on the type of flower nectar collected by the bees. Some common types of honey include clover, orange blossom, and manuka honey. Manuka honey, which is produced in New Zealand and Australia, has gained popularity for its high antibacterial properties and is used in wound care and other medical applications. While honey is generally considered safe for consumption, it should not be given to infants under one year of age due to the risk of botulism. Honey may also cause allergic reactions in some people [3,4].

Propolis is a natural resinous substance collected by honeybees from various plants and trees. Bees use propolis to seal small gaps and cracks in their hives, as well as to protect against infections and other threats. Propolis is a complex mixture of plant resins, beeswax, essential oils, and various organic compounds [5]. Propolis has been used in traditional medicine for centuries, particularly for its antimicrobial and anti-inflammatory properties. Research has also shown that propolis has antioxidant, immunomodulatory, and anticancer effects [6]. There are several types of propolis, which can vary in color and chemical composition depending on the location and plant sources used by the bees. Some of the most common types include Brazilian propolis, European propolis, and Chinese propolis. Propolis can be taken as a supplement or used topically as a natural remedy for various health conditions. Some of the most common uses of propolis include treating sore throat, colds and flu, dental infections, and skin problems. While propolis is generally considered safe, it may cause allergic reactions in some people. It may also interact with certain medications, so it is important to talk to a healthcare provider before using propolis supplements [7].

The escalating utilization of non-renewable substances has prompted researchers to seek alternatives that are renewable and pose lesser risks. Green

chemistry plays a crucial role in this context. Extensive research has been conducted to explore less toxic or bio-based solvents known as green solvents. Water, solvents derived from biological sources, ionic liquids (ILs), deep eutectic solvents (DESs), green synthetic organic solvents, and supercritical liquids (SCF) stand out as prominent classifications within the realm of green solvents.

Propolis is a complex mixture of plant resins, waxes, essential oils, and other biologically active compounds. The choice of solvent used in propolis extraction can have a significant impact on the chemical composition and bioactivity of the resulting extract. Here are some of the solvents that have been used for propolis extraction along with their advantages and disadvantages:

Ethanol: Ethanol is a commonly used solvent for propolis extraction. It is relatively inexpensive and readily available and has been shown to extract a wide range of bioactive compounds from propolis. However, high concentrations of ethanol can cause degradation of some of the more sensitive components of propolis [8-10].

Methanol: Methanol is another solvent that has been used for propolis extraction. It has similar advantages and disadvantages to ethanol but is generally less effective at extracting certain bioactive compounds [11, 14].

Water: Water is a safe and environmentally friendly solvent for propolis extraction. However, it is generally not as effective as organic solvents at extracting lipophilic compounds and may require the use of additional solvents or extraction techniques to obtain a high-quality propolis extract [12]. Freitas et al. compared the efficiency of honey brandy and mead in propolis extraction with ethanol and water in a study they conducted in 2022 with the hypothesis of environmentally friendly solvent [13]. When we look at the studies on environmentally friendly solvents or green solvents, it is seen that there is an open field for research. It has been observed that there are almost no studies on the effectiveness of the use of honey-water mixture as a solvent in propolis extraction under different extraction conditions.

In this context, it is aimed to determine the ratio of honey-water mixture as green solvent for propolis

Table 1. The effectiveness of the ethanolic propolis residue in the honey-water mixture

BP1	Honey + 70% EtOH
BP2	Residue + 70% EtOH
BP3	Honey + Residue + 70% EtOH
BP4	Honey-Water Solution
BP5	Residue + Water
BP6	Residue + Honey-Water Solution

extraction and the best propolis-solvent ratio with this honey-water mixture. In addition, the antioxidant efficiencies of propolis evaporated after alcoholic extraction in honey, water and honey-water mixture were investigated.

2. Material and methods

2.1. Sample extraction
In the study, Anatolian propolis obtained from various beekeepers and flower honey obtained from the Black Sea region were used. Until the time of analysis, propolis was stored at -20 °C and honey was stored under dark and room conditions. Honey and propolis samples used were extracted in methanol and 70% ethanol at a ratio of 1:10 (24 hours, 200 rpm, room temperature), respectively [10]. Antioxidant properties and phenolic components of propolis and honey samples used in the study were determined. Propolis:honey-water extraction efficiency studies were performed on these two samples. This study was planned in three stages.

-The ratio of the honey-water mixture to be used was determined (at a fixed amount of propolis).

-The ideal propolis-solvent ratio was determined in the solvent at the determined honey-water ratio.

-The effectiveness of the ethanolic propolis residue in the honey-water mixture was investigated.

Firstly, honey-water solutions were prepared at 1:1, 1:2, 1:3, 1:4, 1:5, 1:10, 1:20 and 1:40 (propolis-solvent) ratios to determine the ratio of honey-water mixture to be used in propolis extraction (200 rpm, 24 h, rt). Secondly, different amounts of propolis (0.25, 0.5, 0.75, 1, 2, 3 and 4 g in 10 ml solvent) were extracted in the determined honey-water ratio solution. Finally, after the propolis extract extracted with 70% ethanol was evaporated, the residue was dissolved in 2 ml of 70% ethanol. The following experiments were carried out with this residue (Table 1). In the experiments, 1 g of honey, 500 microliters of propolis residue and 10 mL of solvent (70% EtOH, HW and water) were used. The total phenolic (TP) values of the extracts were analyzed, and the results are given as mg GAE/mL extract. Since the main theme of our study was honey-water mixture, firstly, the extraction efficiency of crude propolis was examined. Then, the efficiency of ethanolic propolis residue in the honey-water mixture was tried to be determined.

2.2. Antioxidant capacity
The method described by Slinkard and Singleton (1977) was used to determine the total phenolic content [15]. Initially, 20 μL of the sample was mixed with 680 μL of distilled water. Subsequently, 400 μL of 1:10 diluted Folin-Ciocalteu reagent added to the mixture and

incubated for 4 min. Then, 400 μL of 10% Na₂CO₃ solution was added, and the resulting mixture was allowed to incubate at room temperature for 120 min. Spectrophotometric measurement was performed at 760 nm, and the total amount of phenolic substance present in the sample was determined. The results were expressed as mg gallic acid equivalent (mg GAE/g) using gallic acid as a standard.

To determine the total flavonoid substances, the method outlined by Fukumoto and Mazza (2000) with slight modifications was utilized [16]. First, 2150 μL of methanol was added to 250 μL of the sample, followed by the addition of 50 μL of 10% Al(NO₃)₃ and 50 μL of 1 M NH₄CH₃COO solution. After incubation for 40 min, the absorbance of the resulting colored product formed because of the redox reaction between flavonoids and aluminum (III) was measured at a wavelength of 415 nm. The amount of flavonoid substance present was calculated using quercetin as a standard, and the results were expressed as mg quercetin equivalent (mg QUE/g).

2.3. Antioxidant activity

The antioxidant activity was determined using the widely used 2,2-diphenyl-1-picryl hydrazyl (DPPH) test. The DPPH• radical, which has a maximum absorbance at 517 nm, was used as a synthetic radical for this test. The method proposed by Molyneux (2004) was used to assess the scavenging of DPPH radicals with antioxidants present in the sample [17]. A 100 μM methanolic DPPH• solution was employed. In this assay, sample solutions of equal volume were added to the constant DPPH• radical concentration in the medium after being serially diluted. Trolox was utilized as a standard, and the results were expressed as the SC50 value (mg/ml).

The Ferric reducing/antioxidant power (FRAP) assay was used to determine antioxidant activity based on the reduction of Fe(III)-TPTZ-2,4,6-tris(2-pyridyl)-S-triazine complex in the presence of antioxidants [18]. Fresh FRAP reagent was prepared by mixing pH:3.6 acetate buffer, TPTZ , and FeCl₃ solution in a ratio of 10:1:1. A volume of 50 μL of the sample was added to 1500 μL of FRAP reagent, and the absorbance was read at 593 nm after 4 min. A standard curve was constructed using different concentrations of FeSO₄.7H₂O, and the results were reported as μmol FeSO₄.7H₂O/g [10].

2.4. Phenolic component

The HPLC-PDA analysis of the samples for phenolic content specified by Kara et al. involved preparation and subsequent injection into the device [19]. The analysis was performed using a Shimadzu Corporation LC 20AT HPLC system with a mobile phase consisting of a gradient of 70-30% acetonitrile-ultrapure water and 2% acetic acid-ultrapure water. The sample injection volume was 20 μL, the mobile flow rate was 1.0 mL/min, and the column oven temperature was maintained at 30 °C. Analysis of the phenolic content was done using 25 standard substances. The results were expressed in μg of standard phenolic substance per gram of sample.

3. Results and discussion

Antioxidant and phenolic analysis results of propolis and honey samples used in the experiment are given in Table 2. According to research, the total phenolic content in propolis varies depending on the source and solvent used. One study by Cottica et al. (2011) found the range to be between 31-299 mg of GAE/g of ethanolic extract [21]. Another study by Stoia et al. (2015) analyzed 10 propolis samples and reported an average of 9.71 ± 0.80 mg GAE/g for extracts [20]. In our study, the TP value of the propolis used was 28.847 ± 0.221 mg GAE/g, highlighting the variability in obtaining a propolis extract rich in polyphenolic components. Research has demonstrated a correlation between the antioxidant capacity of honey and its polyphenol content [22]. Chestnut honey, heather honey, and oak honey possess

Table 2. Antioxidant and phenolic component analysis results of honey and propolis

Analysis	Sample	
	Honey	Propolis
TP (mg GAE/ g sample)	0.141 ± 0.013	28.847 ± 0.221
TF (mg QE/ g sample)	0.035 ± 0.002	1.119 ± 0.072
FRAP (μmol Fe₂SO₄.7H₂O/g sample)	3.320 ± 0.041	317.347 ± 2.573
DPPH SC₅₀ (mg/ml)	20.400 ± 0.085	0.135 ± 0.003
Gallic acid	—	47.596
Protocatechuic acid	—	—
Chlorogenic acid	—	—
p-OH benzoic acid	1.726	—
Epicatechin	—	—
Caffeic acid	—	231.544
Syringic acid	—	—
m-OH benzoic acid	—	—
Rutin	—	84.681
Ellagic acid	—	996.589
p- coumaric acid	2.162	270.568
Ferulic acid	—	401.705
Myricetin	—	—
Resveratrol	—	—
Daidzein	—	—
Luteolin	—	24.957
Quercetin	—	57.726
t-cinnamic acid	1.587	41.521
Apigenin	—	93.093
Hesperetin	1.964	—
Rhamnetin	—	—
Chrysin	8.548	775.017
Pinocembrin	5.672	662.761
CAPE	—	—
Curcumin	—	—

(μg phenolic /g sample)

Table 3. The ratio of the honey-water mixture for propolis extraction

Ratio	TP (mg GAE/mL extract)
1:1	0.228 ± 0.031
1:2	0.138 ± 0.021
1:3	0.180 ± 0.020
1:4	0.216 ± 0.009
1:5	0.154 ± 0.008
1:10	0.189 ± 0.010
1:20	0.333 ± 0.033
1:40	0.326 ± 0.012

a total polyphenol content of around 1 mg GAE/g. In addition, other types of flower honeys have lower values and as a result, its antioxidant properties are lower. In our study, we determined that the TP value of the flower honey sample used was 0.141 ± 0.013 mg GAE/g.

The TP value of the extracts obtained to determine the honey-water mixture to be used in propolis extraction is given in Table 3. The TP value of the extract was calculated by subtracting the antioxidant value of the honey sample. Although there is no clear order in the total TP content obtained in the extracts at the ratios of 1:1 to 1:4, it is seen that the TP value of the extract prepared at the ratio of 1:20 is the highest. It can be thought that the 1:20 ratio of honey-water mixture has the highest ionic and molecular level interactions with the phenolic compounds in propolis. In the following steps, it was decided to use a 1:20 honey-water mixture.

To determine the ideal propolis-solvent ratio, the TP value of the solvent used in the extractions was also calculated. Extraction was performed by adding different amounts of propolis to equal solvent volumes and the TP values of the obtained extract were calculated (Table 4). When we look at the results obtained, it is seen that the TP values per unit volume of the extract increase with the increasing amount of propolis. However, it is also seen that this increase is not directly proportional to the increase in the amount of propolis used in extraction. As a result, the amount of propolis used in the extraction

can be increased to obtain higher antioxidant activity, but it should not be ignored that the yield to be obtained from the gram amount of propolis will decrease.

The TP values of the samples after processing were calculated to look at the agonistic or antagonistic activity of ethanolic propolis residue and honey in ethanol and HW mixture (Table 5). When the findings were examined, it was observed that the extract, in which honey and propolis residues were used together (1.313 ± 0.013), was higher than the sum of the TP values of honey and propolis residue prepared separately in ethanol (0.036 ± 0.001 and 1.141 ± 0.006, respectively). Nonetheless, in the extracts prepared using HW mixture and water, it was noted that the TP value of the extract (0.202 ± 0.004), in which the propolis residue was prepared in HW mixture, remained lower compared to the extract (0.279 ± 0.005) where the propolis residue was prepared solely in water. As a result of removing the alcohol from the ethanolic propolis extract and re-dissolving it only in HW mixture, a higher TP value could not be obtained as desired in terms of TP value. In addition, an upward trend was observed in the TP value with the mixing of honey and propolis residue in ethanolic solvent. Based on this information, new and different extraction conditions can be obtained by adding different components or ambient conditions (such as temperature) while preparing the honey-water mixture.

Table 4. The ideal propolis-solvent (1:20 HW mixture) ratio for propolis extraction

g propolis in 10 ml 1:20 HW mixture	TP (mg GAE/mL extract)
0	0.023 ± 0.005
0,25	0.163 ± 0.006
0,5	0.237 ± 0.006
0,75	0.285 ± 0.013
1	0.368 ± 0.015
2	0.532 ± 0.008
3	0.755 ± 0.019
4	0.897 ± 0.004

*HW: Honey-Water

Table 5. The effectiveness of the ethanolic propolis residue in the honey-water mixture

Extract	TP (mg GAE/mL extract)
BP1	0.036 ± 0.001
BP2	1.141 ± 0.006
BP3	1.313 ± 0.013
BP4	0.028 ± 0.002
BP5	0.256 ± 0.005
BP6	0.230 ± 0.004

In the literature, there are different propolis extraction methods in which maceration, ultrasound assisted, and microwave assisted extraction, Soxhlet, supercritical CO_2 extraction, high pressure methods and different solvents are applied [8]. Although researchers generally agree that the best solvent is ethanol-water mixtures, they are trying to obtain high efficiency propolis extraction with non-alcoholic and green solvents. Researchers studying the effectiveness of honey brandy and mead on propolis extraction state that extracts prepared with these two solvents have a non-negligible antioxidant and antibacterial effect (26.6 ± 2.8% and 6.5 ± 1.0%, respectively)[13]. As an alternative to ethanolic solvents used in propolis extraction, Natural Deep Eutectic Solvents (NADES) has started to come to the fore. In a study conducted to provide equivalent antioxidant content and efficacy, it was stated that the extracts obtained with NADES solvents made from choline chloride-propylene glycol or lactic acid at 50 °C could be equivalent to that with 70% EtOH. Again, in this study, they stated that NADES, aqueous L-Lysine and honey solutions can replace ethanol or water [23]. In another study, the antioxidant properties of aqueous (AqEP), polyethylene glycol-aqueous (Pg-AqEP) and ethanolic (EEP) propolis extracts were compared. As a result of the data they obtained, they stated that phenolic acids and aldehydes constituted 40-42% of all compounds extracted and identified in AqEP and Pg-AqEP and 16% in EEP. As a result of their cell culture study, they reported that they showed similar antioxidant activity, but Pg-AqEP and EEP had better mitochondrial superoxide effect [24]. Researchers, on the other hand, reported that aqueous extracts of propolis have stimulatory activity on cell proliferation in vitro [25]. Considering all these studies it is seen that green solvent studies to replace ethanolic propolis extracts have gained importance in recent years. However, in the extractions made with only water, the lack of efficiency at the level of the ethanolic extract leads to experimenting and using aqueous solvent mixtures. It has been reported that the use of honey, which is also a bee product and its products, has small or large effects on the effectiveness of propolis extracts.

4. Conclusions

The consumption of propolis, which is a valuable natural product with various biological activities among bee products, is increasing day by day. This pushes the researchers to optimize the extraction of this product. Recently, studies have been carried out especially on NADES and water-based extract preparation methods. For this reason, the effect of honey-water mixture as a water-based solvent on the antioxidant efficiency of propolis extract was investigated in our study. When we look at the first step results of our study, a significant increase in antioxidant activity was observed with propolis extraction using 1:20 HW mixture. Higher antioxidant activity can be obtained by improving the extraction conditions. However, the amount of propolis to be extracted in the determined HW mixture is also important. While the high amount of propolis increases the antioxidant activity to a certain extent, there is a decrease in the extraction efficiency after a certain point. Finally, after evaporation of the ethanolic propolis, after the residue was dissolved in HW and EtOH, it was seen that there was no significant difference in antioxidant activity between these two cases. The extract prepared with HW mixture did not provide high antioxidant as expected. Of course, more work is needed to find the best way to extract bioactive compounds from different types of propolis on a green solvent basis.

Acknowledgments

References

[1] O. O. Erejuwa, S. A. Sulaiman, M. S. Ab Wahab, Honey: a novel antioxidant, Molecules, 17(4), 2012, 4400-4423.

[2] J. M Alvarez-Suarez, F. Giampieri, M. Battino, Honey as a source of dietary antioxidants: structures, bioavailability, and evidence of protective effects against human chronic diseases, Curr Med Chem, 20(5), 2013, 621-638.

[3] R. Cooper, Honey for wound care in the 21st century, J Wound Care, 25(9), 2016, 544-552.

[4]   K. Brudzynski, C. Sjaarda, Honey glycoproteins containing antimicrobial peptides, Jelleins of the Major Royal Jelly Protein 1, are responsible for the cell wall lytic and bactericidal activities of honey, Plos One, 10(4), 2015, e0120238.

[5]   V. Bankova, Chemical diversity of propolis and the problem of standardization, J Ethnopharmacol, 100(1-2), 2005, 114-117.

[6]   W. Krol, S. Scheller, J. Shani, G. Pietsz, Z. Czuba, Synergistic effect of ethanolic extract of propolis and antibiotics on the growth of staphylococcus aureus, Arznei-Forschung, 43(5), 1993, 607-609.

[7]   J. M. Sforcin, V. Bankova, Propolis: is there a potential for the development of new drugs?, J Ethnopharmacol, 133(2), 2011, 253-260.

[8]   V. Bankova, B. Trusheva, M. Popova, Propolis extraction methods: a review, J Apicult Res, 60:5, 2021, 734-743.

[9]   M. Jug, O. Karas, I. Kosalec, The influence of extraction parameters on antimicrobial activity of propolis extracts, Nat Prod Commun, 12(1), 2017, 1934578X1701200113

[10] Y. Kara, Z. Can, S. Kolaylı, What should be the ideal solvent percentage and solvent-Propolis ratio in the preparation of Ethanolic Propolis extract?, Food Anal Method, , 15(6), 2022, 1707-1719.

[11] B. Lawal, O. K. Shittu, A. N. Abubakar, I. A. Olalekan, A. M. Jimoh, A. K. Abdulazeez, Drug leads agents from methanol extract of Nigerian bee (Apis mellifera) propolis, J Intercultural Ethnopharmacol, 5(1), 2016, 43.

[12] M. Sambou, J. Jean-François, F. J. Ndongou Moutombi, J. A. Doiron, M. P. Hébert, A. P. Joy, M. Touaibia, Extraction, antioxidant capacity, 5-lipoxygenase inhibition, and phytochemical composition of propolis from Eastern Canada, Molecules, 25(10), 2020, 2397.

[13] A. S. Freitas, A. Cunha, P. Parpot, S. M. Cardoso, R. Oliveira, C. Almeida-Aguiar, Propolis efficacy: the quest for eco-friendly solvents, Molecules, 27(21), 2022, 7531.

[14] S. Ma, H. Ma, Z. Pan, L. Luo, L. Weng, Antioxidant activities of propolis's extracts by different solvents in vitro, Journal of Chinese Institute of Food Science and Technology, 16(8), 2016, 53–58. [in Chinese] (abstract in English available at: https://www.researchgate.net/publication/308363945_Antioxidant_activities_of_propolis%27s_extracts_by_different_solvents_in_vitro, 11.05.2023)

[15] K. Slinkard, V. L. Singleton, Total phenol analysis: automation and comparison with manual methods, Am J Enol Viticult, 28(1), 1977, 49-55.

[16] L. R. Fukumoto, G. Mazza, Assessing antioxidant and prooxidant activities of phenolic compounds, J Agr Food Chem, 48(8), 2000, 3597-3604.

[17] P. Molyneux, The use of the stable free radical diphenylpicrylhydrazyl (DPPH) for estimating antioxidant activity, Songklanakarin J. sci. technol, 26(2), 2004, 211-219.

[18] I. F. Benzie, J. J. Strain, [2] Ferric reducing/antioxidant power assay: direct measure of total antioxidant activity of biological fluids and modified version for simultaneous measurement of total antioxidant power and ascorbic acid concentration. In Methods in enzymology, 299, 1999, 15-27.

[19] Y. Kara, Z. Can, S. Kolaylı, Applicability of Phenolic Profile Analysis Method Developed with RP-HPLC-PDA to some Bee Product, Braz Arch Biol Techn, 65, 2022.

[20] M. Stoia, A. Cotınghıu, F. Budın, S. Oancea, Total phenolics content of Romanian propolis and bee pollen, Victoria, 2, 2015, 20.

[21] S. M. Cottica, A. C. Sawaya, M. N. Eberlin, S. L. Franco, L. M. Zeoula, J. V. Visentainer, Antioxidant activity and composition of propolis obtained by different methods of extraction, J Brazil Chem Soc, 22, 2011, 929-935.

[22] Z. Can, O. Yildiz, H. Sahin, E. A. Turumtay, S. Silici, S. Kolayli, An investigation of Turkish honeys: their physico-chemical properties, antioxidant capacities and phenolic profiles, Food Chem, 180, 2015, 133-141.

[23] C. S. Funari, A. T. Sutton, R. L. Carneiro, K. Fraige, A. J. Cavalheiro, V. da Silva Bolzani, R. D. Arrua, Natural deep eutectic solvents and aqueous solutions as an alternative extraction media for propolis, Food Res Int, 125, 2019, 108559.

[24] L. Kubiliene, A. Jekabsone, M. Zilius, S. Trumbeckaite, D. Simanaviciute, R. Gerbutaviciene, D. Majiene, Comparison of aqueous, polyethylene glycol-aqueous and ethanolic propolis extracts: antioxidant and mitochondria modulating properties, BMC Complem Altern M, 18, 2018, 1-10.

[25] A. K. Kuropatnicki, E. Szliszka, M. Kłósek, W. Król, The beginnings of modern research on propolis in Poland, Evid-Based Compl Alt, 2013.

Turkish Journal of
Analytical Chemistry
www.turkjac.org
2019

TurkJAC

Assessment of some element content and potential health risks in infant formulas available in Turkish markets

Kubra Ozturk[1] (iD), Cigdem Er Caliskan[2]* (iD), Zehra Akinci[3] (iD), Harun Ciftci[4,5] (iD)

[1] Kırşehir Ahi Evran University, Project Coordinator, 40100, Kırşehir, Türkiye
[2] Kırşehir Ahi Evran University, Faculty of Agriculture, Department of Field Crops, 40100, Kırşehir, Türkiye
[3] Fırat University, Faculty of Engineering, Department of Bioengineering, 23119, Elazığ, Türkiye
[4] Kırşehir Ahi Evran University, Faculty of Medicine, Department of Medical Biochemistry, 40100, Kırşehir, Türkiye
[5] Çankırı Karatekin University Rectorate, 18100, Çankırı, Türkiye

Abstract

Accurately determining the composition of essential and toxic elements in commercial infant formulas is critical to ensuring safe nutrition for infants. In this study, the concentrations of essential and toxic elements (Pb, Ni, Cd, Al, Cr, Cu, Fe, Mn, Zn, Co) in infant formulas were determined using high-resolution continuum-source flame atomic absorption spectrometry (HR-CS FAAS) and have been evaluated for health risk. The measured values for concentrations from lowest to highest were (in mg/kg): 36.38–77.45 (Zn), 6.28–12.88 (Al), 2.37–4.91 (Cu), 22.01–51.64 (Fe), and 0.55–2.06 (Mn). The highest concentrations of Ni and Cd were 0.18 and 0.09 mg/kg, respectively, while the lowest concentrations for these metals were below the detection limit. The Cr, Co and Pb levels were below the detection limits in all samples. According to the risk assessment conducted for infants aged 0–24 months, which involved calculating the estimated daily intake (EDI), the estimated weekly intake (EWI), the target hazard quotient (THQ), and the hazard index (HI), it was found that the THQ values range from 0.00 to 0.06 for Ni, from 0.00 to 0.69 for Cd, and from 0.17 to 0.22 for Al. However, since the HI for all age groups is less than 1, it can be concluded that there is no health concern for the elements Ni, Cr, Cd, Pb, Al, and Co.

1. Introduction

Nowadays, the intense involvement of women in business life is increasing the demand for commercial infant formulas. Thanks to the development of food technology, this high demand has increased production and consumption, as well as an increase in the quality and variety of infant formulas [1]. According to the 2018 data from the Turkey Demographic and Health Survey, infant formula consumption is 59% for infants aged 0–1 months and 45% for infants aged 2–3 months, but this rate decreases rapidly with age, falling to 14% for infants aged 4–5 months [2]. In addition to environmental contaminants, agrochemical residues and natural toxins, contaminants introduced during food processing, packaging and storage pose safety concerns for infant formula [3]. This has also become a matter of growing concern within society.

Providing a growing baby with an appropriate diet is critical for healthy growth and development. Low intake or reduced bioavailability of nutrients can lead to deficiencies and impaired body functions [4]. Recent clinical research has shown that certain metals and metalloids, such as iron, copper, zinc, and selenium, which are essential micronutrients, play a crucial role in various biochemical functions in all living organisms, including infants. These functions include bone mineralization, enzymatic reactions, redox reactions, hormone secretion, as well as protection of cells and lipids in biological membranes [5]. However, excessive exposure to these metals can cause toxicity and lead to adverse health effects, such as neurotoxicity, developmental delays, and impaired immune function in infants. Therefore, it is essential to understand the

*Author of correspondence: cigdemer86@gmail.com,
cigdem.ercaliskan@ahievran.edu.tr
Tel: +90 (386) 280 58 50
Fax: +90 (386) 280 48 15

balance between the benefits and risks of these metals in infant formulas to ensure optimal infant health [6].

Improper nutrition during infancy can directly affect infant growth, as well as lead to long-term adverse health effects on organ development and function. Several studies have shown that formula feeding is associated with several health risks. These include immune system disorders, food allergies, obesity, diabetes, and coronary heart disease later in life [7]. Parents are becoming more conscious about the healthy nutrition of their children and are demanding more information about the contents of commercial baby foods [8]. In recent years, numerous studies have been conducted on the mineral profile of infant formula samples [9]. Most of these studies have focused on comparing breast milk with cow's milk-based formula substitutes [8]. A review of the literature shows that studies on infant feeding are available in both developing and industrialized countries [4,10–13]. Chajduk et al. (2018) analyzed the basic contents of 16 formulas for infants aged 0 to 8 months in Poland [8]. Mohamed et al. (2021) determined the concentrations of seventeen elements (Al, Br, Ca, Cl, Co, Cu, Fe, I, K, Mg, Mn, Na, Rb, Sb, Sc, Se, and Zn) in infant formulas of 34 different brands collected from pharmacies and local markets in Egypt [14]. Kazi et al. (2010) conducted studies on a total of eight different infant formula products in Pakistan [15], while Basaran (2022) determined the levels of toxic metals in 36 infant formula samples in Turkey [10]. It has been observed that research on trace element analysis of commercially available baby foods is limited in our country.

The most widely published techniques for elemental analysis of infant formula are inductively coupled plasma optical emission spectrometry (ICP/OES) [16], electrothermal atomic absorption spectrometer (ETAAS) [17], flame and graphite furnace atomic absorption spectrometry (GF-AAS) [18,19], and inductively coupled plasma mass spectrometry (ICP-MS) [10,20,21]. Furthermore, elemental levels in milk powder formulations for infants and cereals have been successfully determined by energy dispersive X-ray fluorescence (EDXRF), and wavelength dispersive X-ray fluorescence (WDXRF) [22,23]. The main advantages of plasma techniques are high sensitivity and the ability to determine multiple elements. However, these techniques can be expensive, and high organic matrix content, particularly in the case of ICP-MS, can affect results through spectral and/or non-spectral interferences. [24]. High-resolution continuum source flame atomic absorption spectrometry (HR-CS FAAS) offers several advantages over other techniques, including low cost of analysis, a high resolution monochromator, and the ability to determine multiple

elements using a single light source (xenon arc) [25,26]. In addition, HR-CS FAAS allows the analysis of a wide range of elements, enabling consistent methodology across different application areas. HR-CS FAAS was therefore selected as the method of choice for this study.

The nutritional values, mineral, and vitamin content of ready-to-eat infant formulas may not have enough data on their labeling. Toxic elements could be present due to raw materials used in the preparation of infant formulas and foods, contamination, or food processing. Finding micronutrients is important to know if infants are getting the right nutrients during this critical developmental period. This study aims to determine the levels of some essential and toxic elements in commercial infant formulas and their contribution to the dietary intake of infants. Additionally, the risk of toxic elements, estimated daily intake (EDI), target hazard quotient (THQ), and hazard index (HI) were calculated for infants (0 to 24 months), and estimated weekly intake (EWI) values were compared with provisional tolerated weekly intake (PTWI) values.

2. Materials and Method

2.1. Sample Collection
In this study, a total of 36 samples, 2 product from each brand with different production dates (6 different brands × 3 different age groups × 2 different production date), were purchased from supermarkets and pharmacies in the province of Kırşehir, Turkey, in 2022. The samples were analyzed before their expiration date.

2.2. Chemicals
During the process of determining the levels of essential and toxic elements in infant formulas aged 0–24 months, it was ensured that all chemicals used were of analytical reagent quality. Concentrated nitric acid (65% HNO_3) and hydrogen peroxide (30% H_2O_2) were purchased from Merck Co. (Darmstadt, Germany). Additionally, ultrapure deionized water (18.3 MΩ cm, Millipore, Corporation, MA, USA) was used to prepare the standards and sample solutions.

2.3. Preparation of Samples
For infant food samples (0.25–0.30 g), 100 mL containers made of polytetrafluoroethylene (PTFE) containers with screw caps resistant to microwave oven pressure and temperature were used. To each sample placed in the PTFE containers, 5 mL of 65% HNO_3 (w/w) was added, followed by 1 mL of 30% H_2O_2 (w/w) solution. The mixture was incubated for 30 min at room temperature. The sealed lids of the PTFE containers were closed and solubilized in a microwave oven using 3 different programs. The digestion program was applied

Table 1. HR-CS FAAS device variables and limit of detection

Variables	Pb	Ni	Cd	Al	Cr	Cu	Fe	Mn	Zn	Co
Wavelength, nm	217.00	232.00	228.80	396.15	359.34	324.75	248.32	279.48	213.85	240.72
N_2O-C_2H_2 flow rate, L/h	0	0	0	215	0	0	0	0	0	0
C_2H_2-air flow rate L/h	65	55	50	55	100	55	60	80	60	60
Burner height, mm	8	7	6	7	7	6	5	8	8	6
Evaluation Pixels, pm	3	3	3	3	3	3	3	3	3	3
*LOD (µg/L)	5	1.2	0.4	22	5	1	1	1	1	2

* 3σ, 11 repetitions

as 250 W for 5 min; 450 W for 5 min and 800 W for 10 min. After the PTFE containers were cooled to room temperature, their lids were carefully opened in a fume hood and the volume of the obtained clear mixture (undigested samples had the microwave digestion process applied again) was made up to 10 mL with 0.1 M HNO_3 solution. The same procedures were applied to the blank solution, which did not contain the food sample [27]. Analysis of the samples was carried out by making three parallel readings. In the study, the HR-CS FAAS device model Analytik Jena ContrAA 300 (GLE, Berlin, Germany) was used for the metal detection. The detection limits for the elements studied (Catalog Analytikjena, 2008) are given in Table 1. Additionally, an air-acetylene flame was used for the determination of Pb, Ni, Cd, Cr, Cu, Fe, Mn, Zn, and Co and a nitrous oxide-acetylene flame for Al under optimized conditions as specified in Table 1.

2.4. Human Health Risk Assessment
The risk of toxic elements for infants (0 to 24 months) was assessed by calculating EDI, THQ, and the HI. The EDI was calculated according to Equation 1 [28].

$$EDI = \frac{M_c \; x \; DI}{BW} \qquad (1)$$

Where EDI is the estimated daily intake (mg/kg/day), M_c is the elemental content of infant formula (mg/kg dry weight), and DI is the daily infant formula intake (kg); 120 g/day for (0–6 months) infants, 160 g/day for (6–12 months) infants, and 200 g/day for (12–24 months) infants [11]. Where BW is the reference body weight (kg); 5.9 kg for (0–6 months) infants, 9.3 kg for (6–12 months) infants, and 12.2 kg for (12–24 months) infants [11].

The THQ value was used to assess the non-carcinogenic risk (Equation 2);

$$THQ = \frac{EDI}{RfD} \qquad (2)$$

The reference dose (RfD) values for metals are given in Table 2 [29,30]. The value given as Total THQ (T THQ) or HI, is calculated as the total THQ values of all elements investigated. A TTHQ greater than 1 indicates non-carcinogenic health risks to the consumer [31]. When consuming food, people are exposed not only to one metal but also to multiple metals contained in that food. Therefore, the HI was calculated by summing the THQ values of each metal in the study (Equation 3). HI < 1 indicates no health risk concern, while HI ≥ 1 indicates a potential health concern.

$$\sum THQ (HI) \; = (THQ_1 \; + \; THQ_2 + \ldots\ldots + THQ_n) \qquad (3)$$

Table 2. Reference dose (RfD) values of metals

Metal	RfD (mg/kg/day)
Pb	0.004
Ni	0.02
Cd	0.001
Al	1.00
Cr	1.5
Cu	0.04
Fe	0.7
Mn	0.14
Zn	0.3

3. Results and Discussion

As infant formula is often the primary source of nutrition for infants and children, it is essential that the quality and nutritional content of these foods are appropriate for their health due to their low body weight in the face of high nutrient needs, infants are particularly vulnerable to exposure to nutritional products with the wrong ingredients [32]. Metals such as Pd, Cd, Hg and As are considered toxic and cause adverse effects even at low levels. To demonstrate the adequacy of infant formula products, it is important to determine whether the macro- and micro-element content of these products is within the range of reliable reference values.

The measured values for concentrations from lowest to highest were (in mg/kg): 36.38–77.45 (Zn), 6.28–12.88 (Al), 2.37–4.91 (Cu), 22.01–51.64 (Fe), and 0.55–2.06 (Mn). The highest concentrations of Ni and Cd were 0.18 and 0.09 mg/kg, respectively, while the lowest concentrations for these metals were below the detection limit. The concentrations of Cr, Co and Pb were below the limit of detection in all samples (Table 3). The

accuracy of the method was determined using the standard addition method. The recoveries were calculated above 90%. EDI and EWI of various metals for infants are shown in Table 4. PTWI is the maximum amount of heavy metals in the weekly and daily diet that does not pose a risk to human health. Therefore, according to the FAO/WHO (2004) recommendation, the heavy metal data in infant formulas were compared with the PTWI. This was performed to determine the safe level for weekly consumption of infant formul.

Zinc (Zn) is an essential part of the activity of more than 200 enzymes involved in digestion, metabolism, reproduction and wound healing [33]. Zinc deficiency leads to deterioration of the immune system and cognitive disorders. However, high zinc intake can cause toxicity and acute zinc poisoning has been associated with non-specific gastrointestinal symptoms such as abdominal pain, diarrhea, nausea and vomiting [34]. In this study, the mean Zn levels of infant formula samples Nos. 1, 2 and 3 were 57.47 ± 2.87, 56.23 ± 2.34 and 62.15 ± 2.33 mg/kg, respectively. In all infant formula samples, the mean Zn level was approximately 58.62 (36.38–77.45) mg/kg (Table 3). In the literature studies, Zn levels in infant formula and follow-on formula were determined to be 1.61–2.02 mg/kg [11], 4.69–11.34 mg/kg [35], 27.88–71.55 mg/kg [36], 32.53–42.98 mg/kg [37], 6.82–17.19 mg/kg [38], 36.2–52.3 mg/kg [39], 0.92–37.2 mg /kg [19],

and 23.6–53.9 mg/kg [32]. The PTWI for Zn was been determined by FAO/WHO as 7000 µg/kg body weight/week [40]. When the EWI values given in Table 4 were compared with the PTWI value, it was observed that the EWI values were above the limit value in infant formulas number 1 and 3.

Although nickel (Ni) is an essential micronutrient source for the organism at low concentrations, it is a toxic element at high concentrations. It is known to act as a cofactor in the activation of certain enzymes involved in the breakdown or usage of glucose. Nickel may aid in the production of prolactin and therefore may be involved in human breast milk production [41]. It has been shown that acute exposure of the human body to nickel can cause various health problems such as liver, kidney, spleen, brain tissue damage, vesicular eczema and lung [42]. In this study, the mean Ni levels in infant formula samples Nos. 2, and 3 were 0.068 ± 0.002 and 0.065 ± 0.003 mg/kg, respectively (Table 3). The highest Ni concentration was found in infant formula number 3 (Brand 4). In literature studies, commercial infant formulas in the Egyptian market did not contain detectable amounts of Ni [6], while in another study, the Ni levels in infant formula and follow-on formula were determined to be 0.219–2.23 mg/kg [11]. The PTWI for Ni was been determined by the FAO/WHO as 35 µg/kg body weight/week [40]. When the EWI values given in

Table 3. Macro and microelement concentrations of infant foods (mg/kg)

Mark	N	Zn	Ni	Cr	Cd	Pb	Al	Co	Cu	Fe	Mn
Number 1											
Brand 1*	2	36.38 ± 1.82	BDL	[b]BDL	BDL	BDL	7.28 ± 0.36	BDL	2.37 ± 0.17	37.15 ± 1.86	0.88 ± 0.04
Brand 2*	2	75.85 ± 3.79	BDL	BDL	BDL	BDL	12.88 ± 0.99	BDL	3.00 ± 0.15	43.45 ± 2.17	0.88 ± 0.04
Brand 3*	2	52.83 ± 2.64	BDL	BDL	BDL	BDL	11.55 ± 0.68	BDL	3.73 ± 0.19	22.01 ± 1.10	1.56 ± 0.08
Brand 4*	2	59.77 ± 2.99	BDL	BDL	BDL	BDL	11.71 ± 0.69	BDL	3.34 ± 0.17	41.84 ± 2.09	0.55 ± 0.03
Brand 5*	2	66.08 ± 3.30	BDL	BDL	BDL	BDL	11.83 ± 0.69	BDL	4.61 ± 0.23	44.18 ± 2.21	0.80 ± 0.04
Brand 6*	2	53.89 ± 2.69	BDL	BDL	BDL	BDL	9.16 ± 0.46	BDL	3.87 ± 0.19	42.62 ± 2.13	0.60 ± 0.03
Number 2											
Brand 1**	2	42.12 ± 1.45	BDL	BDL	BDL	BDL	6.28 ± 0.53	BDL	4.37 ± 0.18	39.15 ± 1.28	0.95 ± 0.06
Brand 2**	2	75.36 ± 3.16	BDL	BDL	0.030 ± 0.002	BDL	11.25 ± 1.02	BDL	3.25 ± 0.12	40.25 ± 1.29	0.96 ± 0.05
Brand 3**	2	49.23 ± 2.25	0.12 ± 0.02	BDL	0.040 ± 0.002	BDL	12.23 ± 1.56	BDL	4.53 ± 0.19	36.03 ± 1.02	1.96 ± 0.18
Brand 4**	2	55.18 ± 2.23	0.17 ± 0.02	BDL	BDL	BDL	11.31 ± 1.62	BDL	3.63 ± 0.17	51.64 ± 2.06	0.63 ± 0.04
Brand 5**	2	65.01 ± 2.88	0.12 ± 0.01	BDL	BDL	BDL	10.20 ± 1.09	BDL	4.83 ± 0.24	48.16 ± 2.02	0.90 ± 0.06
Brand 6**	2	50.52 ± 2.10	BDL	BDL	BDL	BDL	10.16 ± 0.96	BDL	3.57 ± 0.15	42.62 ± 2.13	0.72 ± 0.04
Number 3											
Brand 1***	2	52.20 ± 1.65	BDL	BDL	0.03 ± 0.01	BDL	6.58 ± 0.90	BDL	4.37 ± 0.20	40.55 ± 2.01	0.89 ± 0.03
Brand 2***	2	77.45 ± 2.63	BDL	BDL	0.03 ± 0.01	BDL	12.72 ± 1.08	BDL	3.15 ± 0.15	43.35 ± 2.10	0.96 ± 0.05
Brand 3***	2	62.83 ± 2.25	0.11 ± 0.02	BDL	0.070 ± 0.003	BDL	11.55 ± 1.23	BDL	2.93 ± 0.14	23.56 ± 1.63	2.06 ± 0.08
Brand 4***	2	58.70 ± 2.62	0.18 ± 0.02	BDL	0.090 ± 0.001	BDL	10.22 ± 1.02	BDL	3.56 ± 0.16	43.84 ± 1.62	0.61 ± 0.03
Brand 5***	2	65.35 ± 2.54	0.10 ± 0.02	BDL	BDL	BDL	10.60 ± 1.50	BDL	4.91 ± 0.21	45.08 ± 2.26	0.87 ± 0.04
Brand 6***	2	56.38 ± 2.28	BDL	BDL	BDL	BDL	9.23 ± 1.00	BDL	4.07 ± 0.18	43.15 ± 1.56	0.73 ± 0.03

x ± SD (Mean ± Standard deviation), (N=3)
*: 0–6 months, **: 6–12 months, ***: 12–24 months
[b]BDL: Below the Limit of Detection
N: Number of samples (in powder form)

Table 4 were compared with the PTWI value, it was observed that it was lower than the limit value.

Chromium (Cr) mainly appears in two forms: trivalent Cr (Cr^{3+}) and hexavalent Cr (Cr^{6+}). Cr^{6+} is reported to be toxic, mutagenic, carcinogenic and death of apoptotic cells, oxidative stress, changed gene expression and can induce DNA damage. On the other hand, Cr^{3+} is included among essential trace elements for the maintenance of effective glucose, lipid, and protein metabolism in living things [43]. In this study, Cr concentrations in all analyzed samples were below the detectable values of the device. In literature studies, Cr levels in infant formula and follow-on formula were determined to be <0.007–0.053 mg/kg [32], 2.51–83.80 µg/kg) [27], 100–1450 µg/kg [18], and <LOD–6.29 × 10^{-2} mg/kg [11]. The PTWI for chromium was determined as 23.3 µg/kg body weight/week by FAO/WHO [40].

High levels of exposure to toxic pollutants such as Cd found in foods can accumulate in the kidney and liver due to its long biological half-life, leading to kidney toxicity, cancer, kidney stone formation, neurological effects, and serious damage to calcium metabolism [6]. The highest Cd concentration was found in infant formula number 3 (0.090 ± 0.001). Some values found were above the Cd limits (0.005–0.02 mg/kg) set by the European Commission for infant formula and follow-on formula [44]. The FAO/WHO and the Joint Expert Committee on Food Additives (JECFA) have determined the PTWI for cadmium as 7 µg/kg body weight/week [40]. When the EWI values given in Table 4 were compared with the PTWI values, it was determined that the Cd values of all infant formulas analyzed were low. In the literature studies, Cd levels in infant and follow-on formulas were determined to be 0.13–3.58 µg/kg [27], <0.000–0.015 mg/kg [45], 0.038–0.476 mg/kg [28], 0.01 mg/kg [46], 0.012 mg/kg [47], and 0.005–0.017 mg/kg [6], and < LOD–1.64 × 10^{-2} mg/kg [11].

Lead (Pb) is a potent neurotoxin in its alkyl form, and ingestion with milk increases its absorption. Lead exposure in infants affects the nervous system and normal development of the brain, causing learning difficulties and anemia [48]. In this study, Pb concentrations in all analyzed samples were below the detectable values of the device. The allowable limit for lead in infant formula has been determined by the Codex Alimentarius Commission (CAC) as 10 µg/kg [49] and by the European Union as 50 µg/kg [50]. In studies conducted in infant and follow-on formulas in different countries in the literature, the Pb range was determined to be (0.36–5.57 µg/kg) in China [27], <LOD–0.01 mg/kg in Iran [11], (31.0–1040 µg/kg) in Lebanon [28], (25.7–45.5 µg/kg) in Spain [51],[36] (16.0–103 µg/kg) in Ethiopia, [35] (0.14–2.46 µg/kg), and [52] (0.55–24.9 µg/kg) in Turkey. The PTWI for lead was been determined by the FAO/WHO as 25 µg/kg body weight/week [40].

The presence of Al, a toxic element, in infant formula is a matter of great public health importance and should be treated with caution. There are epidemiological data that aluminum causes Alzheimer's disease. These data also raise doubts that exposure to aluminum may have neurological, skeletal, hematopoietic, immunological, and other adverse health effects [53]. The US Food and Drug Administration (FDA) has reported that this metal can accumulate in the central nervous system in the case of higher than 4–5 µg/ kg/day of aluminum in premature infants with impaired kidney function [54]. In this study, the mean Al levels in infant formula samples Nos. 1, 2 and 3 were 10.74 ± 0.65, 10.23 ± 1.13 and 10.15 ± 1.12 mg/kg, respectively, and the mean Al level in all infant formula samples was approximately 10.37 (6.28–12.88) mg/kg (Table 3). The highest Al concentration was found in infant formula number 1 (Brand 2). In literature studies, Al levels in infant formula and follow-on formula were determined to be 189–653 µg/kg [55], 1.3–17.1 mg/kg [56], and 718–6987 µg/ kg [10]. As a joint decision, FAO/WHO/JECFA determined the PTWI value for Al as 2 mg/kg bw [57]. On the other hand, the European Food Safety Authority (EFSA) has set a TWI (Tolerable Weekly Intake) of 1 mg/kg bw for Al in all food sources [58]. The Committee observed that the PTWI may be exceeded in some demographics, particularly in children who regularly consume foods containing Al-based additives or ingredients [59]. When the EWI values given in Table 4 were compared with the PTWI value, it was observed that all infant formulas were below the limit value.

Cobalt (Co) is an essential metal found in the active site of vitamin B-12 and is central to the biochemical reactions of life. Overexposure has caused various adverse health effects in animals and humans, such as vasodilation, flushing, and cardiomyopathy [60]. In this study, Co concentrations in all analyzed samples were below the detectable values of the device. In the literature studies, Co levels in infant formula and follow-on formula were determined to be 0.018–0.036 mg/kg [32], and 9.00 × 10^{-4}–4.90 × 10^{-3} mg/kg [11].

Copper (Cu) deficiency can decrease leukocytes, anemia, and osteoporosis in infants and children. In addition, excessive copper intake can cause acute poisoning, transient gastrointestinal disturbances with symptoms such as vomiting, nausea, and abdominal pain, and even liver toxicity resulting in death [61]. The mean Cu levels in infant formula samples Nos.1, 2 and 3 were 3.49 ± 0.18, 4.03 ± 0.17 and 3.83 ± 0.17 mg/kg, respectively, and the mean Cu level in all infant formula samples was approximately 3.78 (2.37 – 4.91) mg/kg (Table 3).

Table 4. Estimates of daily intake (EDI) and weekly intake (EWI) of various metals

	Month	Element									
		Zn	Ni	Cr	Cd	Pb	Al	Co	Cu	Fe	Mn
EDI (mg/kg bw/day)	0–6 month[a]	1.17	0.00	0.00	0.00	0.00	0.22	0.00	0.07	0.78	0.02
	6–12 month[b]	0.97	0.00	0.00	0.00	0.00	0.18	0.00	0.07	0.74	0.02
	12–24 month[c]	1.02	0.00	0.00	0.00	0.00	0.17	0.00	0.06	0.65	0.02
EWI (mg/kg bw/week)	0–6* month	8.18	0.00	0.00	0.00	0.00	1.53	0.00	0.50	5.49	0.13
	6–12** month	6.77	0.01	0.00	0.00	0.00	1.23	0.00	0.49	5.17	0.12
	12–24*** month	7.13	0.01	0.00	0.00	0.00	1.16	0.00	0.44	4.58	0.12

[a]Mean bw: 5.9 kg *: Number 1
[b]Mean bw: 9.3 kg **:Number 2
[c]Mean bw: 12.2 kg ***:Number 3

The highest copper concentration was determined in the number 3 (Brand 5) infant formula. In the literature studies, Cu levels in infant and follow-on formulas were determined to be 0.11–2.37 mg/kg [35], 0.41–6.35mg/kg [32], and $1.24 \times 10^{-3} - 1.87 \times 10^{-2}$ mg/kg [11]. For copper, PTWI was been determined as 3500 μg/kg /week by FAO/WHO [40]. When the EWI values given in Table 4 were compared with the PTWI value. It was determined that copper, which is considered a critical cofactor in the effective use of many elements, especially iron [62], was lower than the standard value.

Iron is involved in various metabolic processes in living organisms, such as electron transfer, substrate oxidation-reduction, hormone synthesis, oxygen transport and storage, DNA replication-repair and cell cycle control, nitrogen fixation, and protection from reactive oxygen species [63,64]. The decrease in the concentration of this element, which is important in terms of metabolism, increases cadmium absorption in the body [64]. Therefore, sufficient iron must be taken to reduce cadmium absorption. In this study, the mean Fe levels in infant formula samples Nos. 1, 2, and 3 were 38.54 ± 1.93, 42.97 ± 1.63 and 39.92 ± 1.86 mg/kg, respectively. The mean Fe level in all infant formula samples was approximately 40.476 (22.01–51.64) mg/kg (Table 3). The highest iron concentration was found in infant formula number 2 (Brand 4). In the literature studies, Fe levels in infant formula and follow-on formula were determined to be 1.33–7.54 mg/kg [35], 3.6–77.8 mg/kg [32], and 1.49–3.01 mg/kg [11]. For iron, PTWI has been determined as 5600 μg/kg body weight/week by FAO/WHO [40]. When the EWI values given in Table 4 were compared with the PTWI value, it was observed that it was lower than the limit value.

Manganese (Mn)is a vital element and cofactor of many key enzymes and acts as a component of metalloenzymes such as manganese superoxide dismutase (MnSOD), which is mainly responsible for scavenging Reactive Oxygen Species (ROS) in mitochondrial oxidative stress. However, excessive exposure to manganese causes toxicity in the central nervous, heart, respiratory, and reproductive systems [61,65]. In this study, the mean manganese levels in infant formula samples Nos. 1, 2 and 3 were 0.88 ± 0.26, 1.02 ± 0.07 and 1.02 ± 0.04 mg/kg, respectively. The mean Mn content in all infant formula samples was approximately 0.97 (0.55–2.06) mg/kg (Table 3). The highest manganese concentration was determined in an infant formula suitable for use number 3 (Brand 3). When the results were compared with other studies, Mn levels in infant and follow-on formulas were determined to be 0.01–0.07 mg/kg [35], 0.157–0.796 mg/kg [32], and 0.0426–0.0803 mg/kg [11]. The PTWI for manganese has been determined by the FAO/WHO as 980 μg/kg body weight/week [66]. When the EWI values given in Table 4 were compared with the PTWI value, it was found that it was lower than the limit value.

The THQ and HI (ΣTHQ) values calculated for each heavy metal are given in Table 5. The THQ values ranged from 0.00 to 0.06 for Ni, from 0.00 to 0.69 for Cd, and from 0.17 to 0.22 for Al. HI <1 was found for all age groups. Because of the evaluations, it can be said that there are no health concerns for the elements of Ni, Cr, Cd, Pb, Al, and Co.

4. Conclusions

Foods used for the healthy development of infants must have sufficient and appropriate content. Contaminated raw materials and/or contaminated equipment during the manufacturing process may result in toxic metal contamination of infant formula. Limited data on metal contamination in infant formula, especially considering the toxic effects of metals on this sensitive population, prompted the need for our study. The levels of the elements Zn, Ni, Cr, Cd, Pb, Al, Co, Cu, Fe, and Mn in infant formula sold on the market in our country were determined and their THQ values were calculated. Because of the evaluations, it was found that the levels of carcinogenic elements in the infant formula samples

Table 5. THQ and HI values of heavy metals in infants due to consumption of infant formula

Age groups	THQ						HI
	Ni	Cr	Cd	Pb	Al	Co	
0–6 months	0.00	0.00	0.00	0.00	0.22	0.00	0.22
6–12 months	0.06	0.00	0.69	0.00	0.18	0.00	0.92
12–24 months	0.05	0.00	0.66	0.00	0.17	0.00	0.88

studied were relatively low and the THQ and HI values were < 1. These results are consistent with similar studies reported in the literature and further support the safety of these products. It is important to emphasize that although the levels of heavy metals in the infant formulas studied were found to be safe, minimizing heavy metal exposure should remain a priority. Overall, this study contributes to the existing literature by providing significant data on the levels of various elements in infant formulas in our country and confirming their safety. The findings support the importance of ongoing monitoring and quality control efforts to ensure the healthy development of infants and to minimize potential risks associated with heavy metal exposure.

References

[1] WHO, WHO recommendations on postnatal care of the mother and newborn 2014, World Health Organization, Geneva.

[2] TDHS, 2018 Türkiye Demographic and Health Survey, Ankara, Türkiye, 2019.

[3] Ş. Saçmacı, M. Saçmacı, Determination of Arsenic (III) and Total Arsenic at Trace Levels in Baby Food Samples via a New Functionalized Magnetic Graphane Oxide Nanocomposite, Biol Trace Elem Res, 199, 2021, 4856–4866.

[4] N. Zand, B.Z. Chowdhry, F.B. Zotor, D.S. Wray, P. Amuna, F.S. Pullen, Essential and trace elements content of commercial infant foods in the UK, Food Chem, 128, 2011, 123–128.

[5] L.J. Taylor, M. Gallagher, F.S. McCullough, The role of parental influence and additional factors in the determination of food choices for pre-school children, Int J Consumer Stud, 28, 2004, 337–346.

[6] M.M. Ghuniem, M.A. Khorshed, M.M. Khalil, Determination of some essential and toxic elements composition of commercial infant formula in the Egyptian market and their contribution to dietary intake of infants, Int J Environ Anal Chem, 100, 2020, 525–548.

[7] A. Barclay, L. Weaver, Feeding the normal infant, child and adolescent, Medicine, 34, 2006, 551–556.

[8] E. Chajduk, M. Pyszynska, H. Polkowska-Motrenko, Determination of trace elements in infant formulas available on polish market, Biol Trace Elem Res, 186, 2018, 589–596.

[9] L. Herreros-Chavez, A. Morales-Rubio, M. Cervera, Green methodology for quality control of elemental content of infant milk powder, LWT, 111, 2019, 484–489.

[10] B. Başaran, An assessment of heavy metal level in infant formula on the market in Turkey and the hazard index, J Food Compos Anal, 105, 2022, 104258.

[11] A. Kiani, M. Arabameri, M. Moazzen, N. Shariatifar, S. Aeenehvand, G.J. Khaniki, M. Abdel-Wahhab, S. Shahsavari, Probabilistic health risk assessment of trace elements in baby food and milk powder using ICP-OES method, Biol Trace Elem Res, 200, 2022, 2486–2497.

[12] V. Sirot, T. Traore, T. Guérin, L. Noël, M. Bachelot, J.-P. Cravedi, A. Mazur, P. Glorennec, P. Vasseur, J. Jean, French infant total diet study: exposure to selected trace elements and associated health risks, Food Chem Toxicol, 120, 2018, 625–633.

[13] C. Vella, E. Attard, Consumption of minerals, toxic metals and hydroxymethylfurfural: Analysis of infant foods and formulae, Toxics, 7, 2019, 33.

[14] G.Y. Mohamed, M. Soliman, S.A. Issa, N.M. Mohamed, M. Al-Abyad, Trace elements assessment and natural radioactivity

[15] levels of infant formulas consumed in Egypt, J Radioanal Nucl Chem, 330, 2021, 1127–1136.

[15] T.G. Kazi, N. Jalbani, J.A. Baig, M.B. Arain, H.I. Afridi, M.K. Jamali, A.Q. Shah, A.N. Memon, Evaluation of toxic elements in baby foods commercially available in Pakistan, Food Chem, 119, 2010, 1313–1317.

[16] S. Bağdat, E. Köse Baran, F. Tokay, Element fractionation analysis for infant formula and food additives by inductively coupled plasma optical emission spectrometry, Int J Food Sci Technol, 49, 2014, 392–398.

[17] T.G. Kazi, N. Jalbani, J.A. Baig, H.I. Afridi, G.A. Kandhro, M.B. Arain, M.K. Jamali, A.Q. Shah, Determination of toxic elements in infant formulae by using electrothermal atomic absorption spectrometer, Food Chem Toxicol, 47, 2009, 1425–1429.

[18] F. Salah, I. Esmat, A. Mohamed, Heavy metals residues and trace elements in milk powder marketed in Dakahlia Governorate, International Food Research Journal, 20, 2013, 1807–1812.

[19] S. Saracoglu, K.O. Saygi, O.D. Uluozlu, M. Tuzen, M. Soylak, Determination of trace element contents of baby foods from Turkey, Food Chem, 105, 2007, 280–285.

[20] K. Ljung, B. Palm, M. Grandér, M. Vahter, High concentrations of essential and toxic elements in infant formula and infant foods–A matter of concern, Food Chem, 127, 2011, 943–951.

[21] H. Chen, Y. Yao, C. Zhang, J. Ping, Determination of Heavy Metal Ions in Infant Milk Powder Using a Nanoporous Carbon Modified Disposable Sensor, Foods, 12, 2023, 730.

[22] T. Gunicheva, Advisability of X-ray fluorescence analysis of dry residue of cow milk applied to monitor environment, X-Ray Spectrometry: An International Journal, 39, 2010, 22–27.

[23] L. Perring, J. Blanc, Faster measurement of minerals in milk powders: comparison of a high power wavelength dispersive XRF system with ICP-AES and potentiometry reference methods, Food Anal Method, 1, 2008, 205–213.

[24] L. Balcaen, L. Moens, F. Vanhaecke, Determination of isotope ratios of metals (and metalloids) by means of inductively coupled plasma-mass spectrometry for provenancing purposes—A review, Spectrochim. Acta B: At. Spectrosc., 65, 2010, 769–786.

[25] B. Welz, High-resolution continuum source AAS: the better way to perform atomic absorption spectrometry, Anal Bioanal Chem, 381, 2005, 69–71.

[26] R.R. Gamela, E.G. Barrera, Á.T. Duarte, W. Boschetti, M.M. da Silva, M.G.R. Vale, M.B. Dessuy, Fast sequential determination of Zn, Fe, Mg, Ca, Na, and K in infant formulas by high-resolution continuum source flame atomic absorption spectrometry using ultrasound-assisted extraction, Food Analytical Methods, 12, 2019, 1420–1428.

[27] C. Su, N. Zheng, Y. Gao, S. Huang, X. Yang, Z. Wang, H. Yang, J. Wang, Content and dietary exposure assessment of toxic elements in infant formulas from the Chinese market, Foods, 9, 2020, 1839.

[28] J. Elaridi, H. Dimassi, O. Al Yamani, M. Estephan, H.F. Hassan, Determination of lead, cadmium and arsenic in infant formula in the Lebanese market, Food Control, 123, 2021, 107750.

[29] EPA, Regional Screening Level (RSL) Summary Table 2011.

[30] EPA, Integrated Risk Information System 2016.

[31] EPA, Regional screening levels (RSLs) equations.

[32] M. Sager, C. McCulloch, D. Schoder, Heavy metal content and element analysis of infant formula and milk powder samples purchased on the Tanzanian market: International branded versus black market products, Food Chem, 255, 2018, 365–371.

[33] M. Aliasgharpour, Zn Status in gastroenteritis children under five years old, Int J Med Investig, 4, 2015, 180–182.

[34] M.J. Kwon, M.I. Boyanov, J.-S. Yang, S. Lee, Y.H. Hwang, J.Y. Lee, B. Mishra, K.M. Kemner, Transformation of zinc-concentrate in surface and subsurface environments: Implications for assessing zinc mobility/toxicity and choosing an optimal remediation strategy, Environ Pollut, 226, 2017, 346–355.

[35] G. Lutfullah, A.A. Khan, A.Y. Amjad, S. Perveen, Comparative study of heavy metals in dried and fluid milk in Peshawar by

atomic absorption spectrophotometry, Sci World J, 2014, 2014, 1–5.

[36] T. Eticha, M. Afrasa, G. Kahsay, H. Gebretsadik, Infant exposure to metals through consumption of formula feeding in Mekelle, Ethiopia, Int J Anal Chem, 2018, 2018, 1–5.

[37] A. Alemu, Levels of Essential and Toxic Metals in Commercial Powdered Infant Formulas, Addis Ababa University, 2008.

[38] O. Aguzue, S. Kakulu, S. Thomas, Flame atomic absorption spectrophotometric determination of heavy metals in selected infant formula in the Nigerian Market, Arch Appl Sci Res, 6, 2014, 128–132.

[39] M. Pandelova, W.L. Lopez, B. Michalke, K.-W. Schramm, Ca, Cd, Cu, Fe, Hg, Mn, Ni, Pb, Se, and Zn contents in baby foods from the EU market: Comparison of assessed infant intakes with the present safety limits for minerals and trace elements, J Food Compos Anal, 27, 2012, 120–127.

[40] FAO/WHO, Summary of Evaluations Performed by the Joint FAO/WHO Expert Committee on Food Additives (JECFA) 1956–2003 (First through Sixty-First Meetings), FAO and WHO, 2004.

[41] A. Singh, R.S. Kumar, Role of Nickel in animal performance: A review, The Pharma Innovation Journal, SP 10, 2021, 643–646.

[42] A. Mehri, Trace elements in human nutrition (II)–an update, I J Preven Medic, 11, 2020, 1–17.

[43] M. Shahid, S. Shamshad, M. Rafiq, S. Khalid, I. Bibi, N.K. Niazi, C. Dumat, M.I. Rashid, Chromium speciation, bioavailability, uptake, toxicity and detoxification in soil-plant system: A review, Chemosphere, 178, 2017, 513–533.

[44] EFSA, Statement on tolerable weekly intake for cadmium, 2011.

[45] B. Başaran, An assessment of heavy metal level in infant formula on the market in Turkey and the hazard index, Journal of Food Composition and Analysis, 105, 2022, 104258.

[46] A. Domínguez, S. Paz, C. Rubio, A. Gutiérrez, D. González-Weller, C. Revert, A. Hardisson, Essential and toxic metals in infant formula from the European Community, Open Access J. Toxicol, 2, 2017, 555585.

[47] M. Mania, M. Wojciechowska-Mazurek, K. Starska, M. Rebeniak, T. Szynal, A. Strzelecka, J. Postupolski, Toxic Elements in Commercial Infant Food, Estimated Dietary Intake, and Risk Assessment in Poland, Polish Journal of Environmental Studies, 24, 2015, 2525–2536.

[48] K. Schümann, The toxicological estimation of the heavy metal content (Cd, Hg, Pb) in food for infants and small children, Z Ernahrungswiss, 29, 1990, 54–73.

[49] CAC, General Standard for Contaminants and Toxins in Food and Feed. CXS193-1995 amended in 2019., 2019.

[50] EU, Commission Regulation (EU) 2015/1005 of 25 June 2015 Amending Regulation (EC) No 1881/2006 As Regards Maximum Levels of Lead in Certain Foodstuffs 2015.

[51] R. Moreno-Rojas, P. Sánchez-Segarra, C. Cañal-Ruiz, M. Amaro-López, G. Zurera-Cosano, Lead content in Spanish market infant formulas and toxicological contribution, Food Addit Contam, 19, 2002, 241–245.

[52] H. Sipahi, A. Eken, A. Aydın, G. Şahin, T. Baydar, Safety assessment of essential and toxic metals in infant formulas, Turkish J Pedıatr, 56, 2014, 385–391.

[53] S.C. Bondy, Low levels of aluminum can lead to behavioral and morphological changes associated with Alzheimer's disease and age-related neurodegeneration, Neurotoxicology, 52, 2016, 222–229.

[54] G.L. Klein, A.M. Leichtner, M.B. Heyman, Aluminum in large and small volume parenterals used in total parenteral nutrition: response to the Food and Drug Administration notice of proposed rule by the North American Society for Pediatric Gastroenterology and Nutrition, J Pediatr Gastr Nutr, 27, 1998, 457–460.

[55] R. Chekri, E. Le Calvez, J. Zinck, J.-C. Leblanc, V. Sirot, M. Hulin, L. Noël, T. Guérin, Trace element contents in foods from the first French total diet study on infants and toddlers, J Food Compos Anal, 78, 2019, 108–120.

[56] A.O. de Souza, C.C. Pereira, A.I. Heling, E.Q. Oreste, S. Cadore, A.S. Ribeiro, M.A. Vieira, Determination of total concentration and bioaccessible fraction of metals in infant cereals by MIP OES, J Food Compos Anal, 77, 2019, 60–65.

[57] FAO/WHO, Evaluation of certain food additives and contaminants: seventy-fourth report of the Joint FAO/WHO Expert Committee on Food Additives, 2011, pp. 136–136.

[58] F. Aguilar, H. Autrup, S. Barlow, L. Castle, R. Crebelli, W. Dekant, K. Engel, N. Gontard, D. Gott, S. Grilli, Safety of aluminium from dietary intake scientific opinion of the panel on food additives, flavourings, processing aids and food contact materials (AFC), EFSA J, 754, 2008, 1–34.

[59] C. Ibrahim, Z. Kammouni, M. Barake, M. Kassir, A. Al-Jawaldeh, J. Matta, Y. Sacre, L. Hanna-Wakim, J. Haddad, M. Hoteit, Pediatric Health Risk Assessment for Exposure to Aluminum from Infant Formulas and Children under the Age of Five's Food Products among Arab Infants: Experience from Lebanon, Foods, 11, 2022, 2503.

[60] C.H. Watanabe, A.S.C. Monteiro, E.S.J. Gontijo, V.S. Lira, C. de Castro Bueno, N.T. Kumar, R. Fracácio, A.H. Rosa, Toxicity assessment of arsenic and cobalt in the presence of aquatic humic substances of different molecular sizes, Ecotox Envıron Safe, 139, 2017, 1–8.

[61] S.C. Izah, N. Chakrabarty, A.L. Srivastav, A review on heavy metal concentration in potable water sources in Nigeria: human health effects and mitigating measures, Expos Health, 8, 2016, 285–304.

[62] M.A. Khan, Nutritional adequacy of commercial infant milk formulas, Ecol Food Nutr, 47, 2008, 188–204.

[63] M.M. Ghuniem, M.A. Khorshed, M. Reda, S.M. Mahmoud, G. Hammad, Assessment of the potential health risk of heavy metal exposure from the consumption of herbal, black and green tea, Biomed J Sci & Tech Res, 16, 2019, 11810–11817.

[64] C. Verma, K. Tapadia, A.B. Soni, Determination of iron (III) in food, biological and environmental samples, Food Chem, 221, 2017, 1415–1420.

[65] V.A. Lemos, C.G. Novaes, M.A. Bezerra, An automated preconcentration system for the determination of manganese in food samples, J Food Compos Anal, 22, 2009, 337–342.

[66] EPA, Manganese compounds 2014.

Electroanalytical characterization of chloroquinoline substituted redox-active phthalocyanines

Asiye Nas[1] iD , Gülsev Dilber[1]* iD , Zekeriya Biyiklioglu[2] iD

[1] Karadeniz Technical University, Maçka Vocational School, 61750, Maçka, Trabzon, Türkiye
[2] Karadeniz Technical University, Faculty of Science, Department of Chemistry, 61080 Trabzon, Türkiye

Abstract

In the first part of this study, the synthesis and characterization of organosoluble 5-chloroquinolin-8-yloxy substituted iron(II) (2) and oxo-titanium (IV) phthalocyanines (3) are reported for the first time. These compounds have been characterized by elemental analysis, Fourier transform infrared, electronic spectroscopy, and mass spectra. Electrochemical behaviors of metal-free and cobalt phthalocyanines and further new types of iron and oxo-titanium phthalocyanines were investigated using electroanalytical methods, such as cyclic (CV) and square wave voltammetry (SWV). According to the electrochemical results, phthalocyanines by and large showed one-electron metal- and/or ligand-based reversible or quasi-reversible reduction and oxidation processes.
All in all, this study's results inevitably create a useful way to use them in possible future studies, which will particularly attempt to use the compound investigated in potential areas of use.

Keywords: Iron, titanium, electrochemistry, redox-active, chloroquinoline

1. Introduction

Phthalocyanines (Pcs) are planar heteroatomic molecular systems constituted by four isoindole units linked with nitrogen atoms. Of several well-known properties; the most significant ones are thermal stability, chemical resistance, optical properties, and liquid or crystal properties. More than seventy different elements have so far been used in phthalocyanine rings as central atoms to date. Phthalocyanines have been of great interest to researchers and hence the subject of extensive research in the past few decades. Some of the critical subjects studied so far are lithium batteries, optical data storage, solar energy conversion, catalysis, etc. [1–10]. In addition to the potential of their use in pure material science, phthalocyanines are known to be rather fascinating and thought-provoking compounds in terms of their electroanalytical properties [11–13]. Many studies in the literature examine the electroanalytical and spectroelectroanalytic properties of phthalocyanines [14–16].

A neutral formula can summarize the electroanalytical behavior of phthalocyanines, which is presented as a dianion, Pc^{-2} that can be reduced or

oxidized sequentially. The electrochemical activity of the metal-free Pcs is attributed to the boundary orbitals of the molecular structure, where the oxidation is the removal of the electron (s) from the HOMO (a_{1u}). On the other hand, the reduction is the addition of electrons (s) to LUMO (e_g). While two electrons are being removed from the HOMO yielding Pc^{-1} and Pc^{-2}, four electrons are added to the doubly degenerate e_g orbitals of the LUMO yielding Pc^{-3}, Pc^{-4}, Pc^{-5} and Pc^{-6}. Besides, metallated Pcs containing electroactive central metals exhibit electroactivity, commonly associated with the central metals located at the core of the ring [17]. While the common examples of electroactive metals include iron, cobalt, manganese, and titanium, electrochemically inactive metals include nickel, zinc, and magnesium. A plurality of species can thus be formed by subsequent oxidation or reducing the phthalocyanine ring and/or the central metal ion. Each oxidation or reduction product is of a different spectrum to be used for characterization. In addition to the nature and oxidation state of the central metal and the substituents' nature in

the Pc ring, the nature of any axial ligand and solvents play a crucial role in the characterization [17].

In some of our previous papers, we reported the synthesis and electroanalytical characterization of a large number of tetra-substituted metal-free and metallophthalocyanines [18–20]. In literature, it can be seen that the aromatic methyl-substituted quinoline ring increases the conjugation effect thereby improving GCE's performance (Glassy carbon electrode) to detect nitrites [21]. In this regard, the synthesis and characterization of the 5-chloroquinolin-8-yloxy group substituted novel phthalocyanines (FePc (**2**), oxo-TiPc (**3**) were performed in this study. In addition to synthesis, electrochemistry of 5-chloroquinolin-8-yloxy group substituted novel phthalocyanines (FePc (**2**), oxo-TiPc (**3**)) and H₂Pc (**4**), CoPc (**5**) previously synthesized by our working group [22] were determined and characterized by electroanalytical methods such as example cyclic (CV) and square wave voltammetry (SWV). In the examination of the electrochemical properties of phthalocyanines, redox-active (Mn, Fe, Co, and Ti) centers and redox-inactive (Ni, Cu, and Zn) centers can be preferred. The first oxidation and first reduction processes occur at the metallic center of the MPc. For redox-inactive derivatives, redox processes arise only on the Pc ring. The reason why Co, Fe and Ti central metals are chosen in this study is that they yield the redox-active center in metallophthalocyanine complexes.

2. Experimental

2.1. Materials and Methods
All reagents and solvents were dried and purified as described in Perrin and Armarego [23]. 5-chloroquinolin-8-ol (**1**) was obtained from commercial supplier. 4-nitro phthalonitrile [24], 4-(5-chloroquinolin-8-yloxy)phthalonitrile (**1**) [22], unmetallated phthalocyanine (**4**) [3] and 2,9(10), 16(17), 23(24)-tetrakis-[(5-chloroquinolin-8-yloxy)phthalocyanato] cobalt (II) (**5**) [3] were prepared according to the reported procedures.

All electrochemical measurements were carried out with Gamry Interface 1000 potentiostat/galvanostat utilizing a three-electrode configuration at 25°C. The working electrode was a Pt disc with a surface area of 0.071 cm². A Pt wire was served as the counter electrode and saturated calomel electrode (SCE) was employed as the reference electrode and separated from the bulk of the solution by a double bridge. Electrochemical grade tetrabuthylammonium perchlorate (TBAP) in extra pure dichloromethane (DCM) was employed as the supporting electrolyte at a concentration of 0.10 mol dm⁻³.

2.2. Synthesis

2.2.1. 2, 9(10), 16(17), 23(24) -Tetrakis-[5-chloroquinolin-8-yloxy] phthalocyaninato iron (II) (**2**)
After 4-(5-chloroquinolin-8-yloxy)phthalonitrile (**3**) (0.20 g, 0.65 mmol) was dissolved in 1 mL dry n-pentanol in a sealed tube, anhydrous Fe(CH₃COO)₂ (57 mg, 0.33 mmol) and three drops of 1,8-diazabicyclo[5.4.0]undec-7-ene were added to the reaction medium. The mixture was stirred under a nitrogen atmosphere at 160 °C for 18 hours. Next, the reaction mixture was cooled to room temperature, n-hexane (20 mL) was added, and the crude product was filtered off. Purification of this new compound was carried out by silica gel column chromatography using chloroform-methanol (83:17) solvent system as an eluent.

Yield: 127 mg (61 %), M.p.: > 300 °C (decomposition). FT-IR ν_{max}/cm⁻¹: 3058 (Ar-H), 1606, 1459, 1383, 1226, 1121, 1077, 929, 816, 783, 746. MALDI-TOF, m/z: Calc.: 1278,74 for C₆₈H₃₂N₁₂Cl₄O₄Fe, Found: 1278,40 [M]⁺. UV/vis (Chloroform, 1x10⁻⁵ M): λ, nm (log ε): 363 (5.00), 594 (4.49), 690 (5.04). Anal. Calc. for C₆₈H₃₂N₁₂Cl₄O₄Fe: C, 63.87; H, 2.52; N, 13.14 %, Found: C, 61.93; H, 2.58; N, 13.09 %.

2.2.2. 2, 9(10), 16(17), 23(24) –Tetrakis-[5-chloroquinolin-8-yloxy] phthalocyaninato oxotitanium (IV) (**3**)
The synthesis method of compound **2** was used to synthesize compound **3** except that titanium (IV) butoxide salt was used instead of Fe (CH₃COO)₂ salt. The amounts of the reagents were; 4-(5-chloroquinolin-8-yloxy)phthalonitrile (**1**) (0.20 g, 0.65 mmol), anhydrous Ti(OBu)₄ (0,23 mL, 0.65 mmol). The obtained product was purified by washing with different solvents.

Yield: 87 mg (41 %), M.p.: >300 °C (decomposition). FT-IR ν_{max}/cm⁻¹: 3058 (Ar-H), 1715, 1586, 1460, 1296, 1228, 1036, 931, 822, 784, 747. MALDI-TOF, m/z: Calc.: 1286,77 for C₆₈H₃₂N₁₂Cl₄O₅Ti, Found: 1286,20 [M]⁺. UV/vis (Chloroform, 1x10⁻⁵ M): λ, nm (log ε): 342 (4.97), 398 (4.57), 630 (4.63), 664 (4.76), 700 (5.27). Anal. Calc. for C₆₀H₃₆N₂₀O₄Zn: C, 63.47; H, 2.51; N, 13.06 %, Found: C, 63.54; H, 2.46; N, 13.10 %.

3. Results and Discussion

3.1. Synthesis and characterization
The phthalonitrile **1**, metal-free phthalocyanine **4** and Co(II) phthalocyanine compounds **5** were obtained according to the procedure expressed in a previously published article [22]. The complete method used in all synthesized compounds is set out in Scheme 1 in detail.

The structure of new compounds was illuminated using FT-IR, UV-Vis, MALDI-TOF mass spectroscopic techniques and elemental analyses.
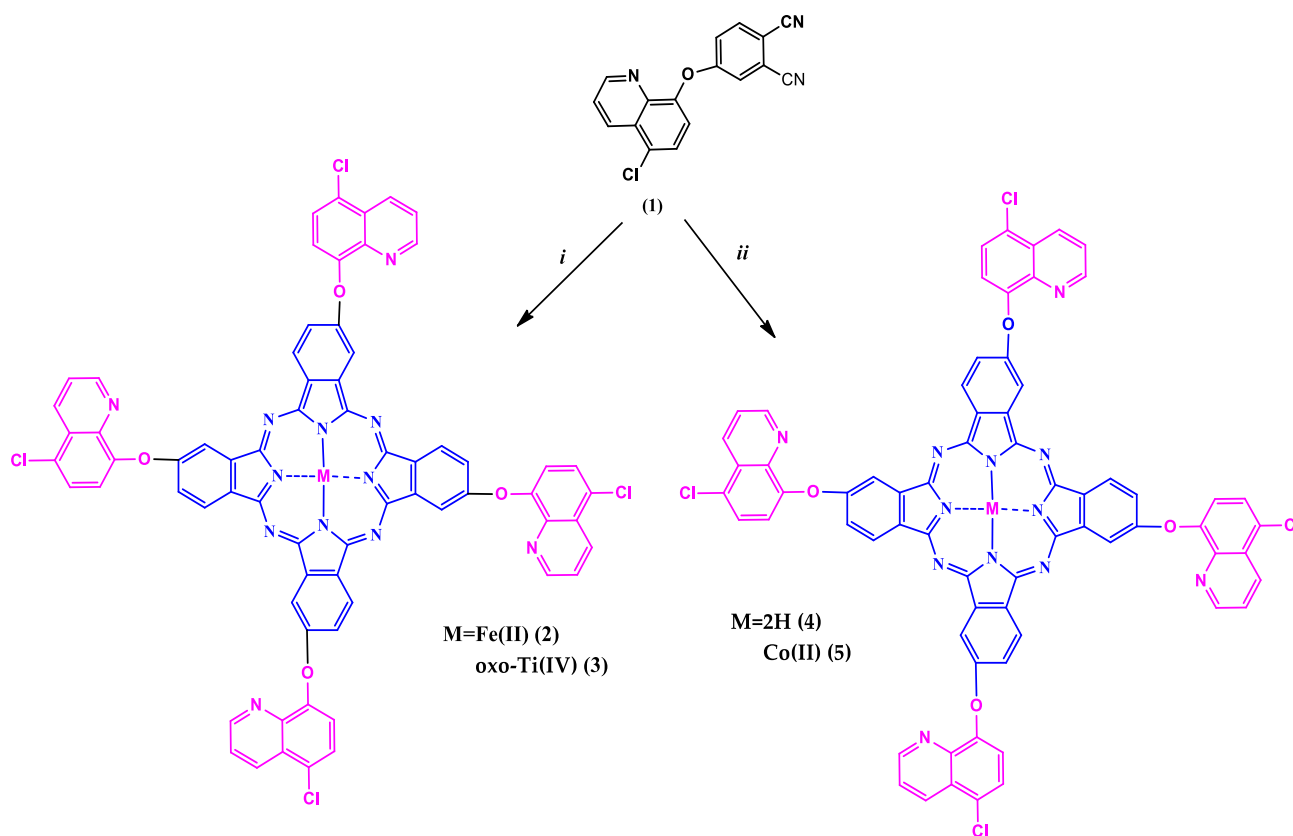
Scheme 1. Synthesis of novel phthalocyanines (**2-3**), reaction conditions: *i*: *n*-pentanol, 1,8-diazabicyclo[5.4.0]undec-7-ene and related metal salts (Fe(ac)$_2$, titanyum (IV) butoxide) at 160 °C. *ii:* [22]

Synthesis of novel iron (II) and titanium (IV) phthalocyanine compounds (**2** and **3**) were achieved by the treatment of phthalonitrile **1** in the presence of related anhydrous metal salts (Fe(CH$_3$COO)$_2$ and Ti(OBu)$_4$). The yields of the reactions carried out in dried *n*-pentanol at 160 °C were determined as 61% and 41%, respectively. Iron (II) phthalocyanine was purified using column chromatography, while titanium (IV) phthalocyanine was washed with different solvents to remove impurities.

In the FT-IR spectra of phthalocyanines **2** and **3**, the loss of peak belonging to the C≡N vibration observed at 2233 cm^{-1} of 4-(5-chloroquinolin-8-yloxy)phthalonitrile

(**3**) is a shred of strong evidence that the compounds **2** and **3** were formed by cyclotetramerization of the dinitrile compound. Besides, upon the cyclotetramerization, there were no further significant changes available in the IR spectra of these compounds. Mass spectra of phthalocyanine compounds **2** and **3** reasonably supported the expected structures when observing molecular ion peaks at 1278,40 as [M]$^+$ for **2** and 1286,20 as [M]$^+$ for **3** (Fig. 1 and Fig. 2), respectively.

3.2. UV-Vis absorption spectra

The UV-vis spectroscopy for characterization of the phthalocyanine compounds is a mean, which is known to be one of the best available approaches.
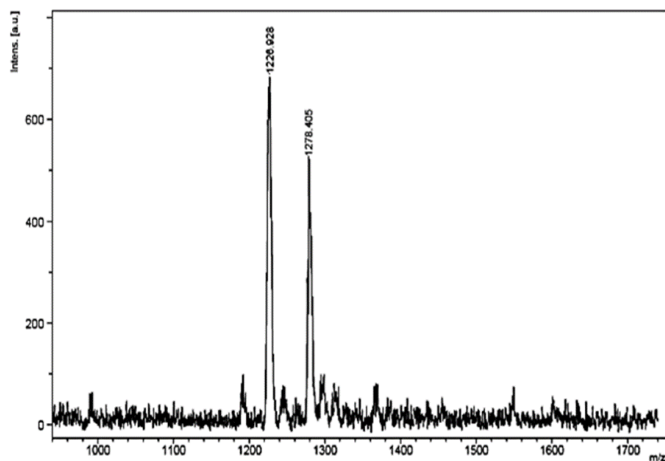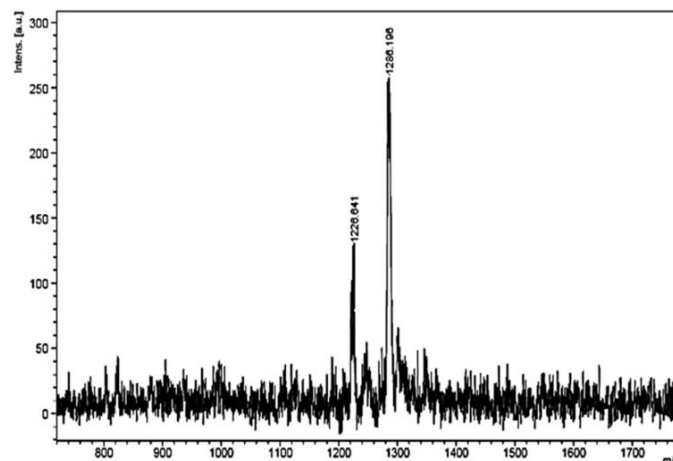

Figure 1. Mass spectrum of compound **2**

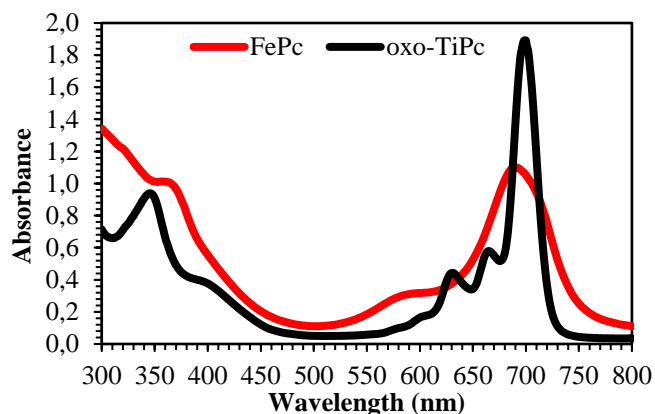**Figure 2.** Mass spectrum of compound **3**

Figure 3. Absorption spectra of novel synthesized compounds in chloroform at 1.10^{-5}M

In the UV-vis spectrum of metallophtalocyanines, two characteristic peaks called **Q** and **B** bands emerging from $\pi \rightarrow \pi^*$ electronic transitions are observed [17]. In our case, the Q band appeared at about 600–750 nm, while the B band arised at about 300–450 nm.

Oxotitanium phthalocyanine compounds displayed remarkable absorption property and photosensitivity in the near-infrared region was characterized by the sharp absorption Q band with two small peaks as shoulders [25,26].

In the UV-Vis spectrum of the newly synthesized oxotitanium phthalocyanine **3**, the intense Q-band was recorded at 700 nm. Two shoulders appeared at 664, 630 nm, and the B-band at 342 nm as expected. FePc **2**, another novel phthalocyanine, yielded Q band at 690 nm with shoulders at 594 and B band at 363 nm in the UV region set out in Fig. 3 and Table 1.

It is well-known fact that the absorption of the Q-band of the phthalocyanine compounds in the UV-vis spectrum is more or less influenced by several factors: namely, due to the existence of metal ion in the central ring, ligand-bound in the axial position, the binding position of the substituent and aggregation in solvents [17]. The Q band of oxotitanium phthalocyanine **3** exhibited red-shifted approximately 10 nm compared to that of the iron phthalocyanine, because **3** consists of oxygen atom as an axial ligand [27].

3.3. Electrochemical Studies

The definitions of the redox couples and electrochemical data, including the half-wave peak potentials ($E_{1/2}$), peak-to-peak potential separations (ΔE_p), and the difference between the first oxidation and reduction potentials ($\Delta E_{1/2}$) are listed in Table 2.

Table 1. Absorption spectral data for the substituted **2** and **3** in chloroform in 20 ^{0}C

Compound	λmax, nm (logε)	
	B band	Q band
2	363 (5.00)	594 (4.49), 690 (5.04)
3	342 (4.97), 398 (4.57)	630 (4.63), 664 (4.76), 700 (5.27)

Table 2. Voltammetric data of the phthalocyanines. All voltammetric data were given versus SCE

Phthalocyanines	Label	$^{a}E_{1/2}$	$^{b}\Delta E_P$ (mV)	$^{c}\Delta E_{1/2}$
2	R1	–0.61	153	
	R2	–0.98	144	
	R3	–1.25	234	1.47
	O1	0.86	86	
	O2	1.26	151	
3	R1	–0.55	130	
	R2	–0.72	141	
	R3	–0.89	125	1.56
	R4	–1.04	148	
	O1	1.01	245	
4	R1	–0.70	158	
	R2	–1.19	149	
	O1	0.68	162	1.87
	O2	1.17	220	
5	R1	–0.21	96	
	R2	–0.51	138	
	R3	–1.44	89	0.89
	O1	0.68	130	

Fig. 4 shows the cyclic and square-wave voltammograms of **4** in DCM. **4** gives ring-based, quasi-reversible, two one-electron reductions (R1 = –0.70 V, R2 = –1.19 V) and two oxidation (O1 = 0.68 V, O2 = 1.17 V) processes.
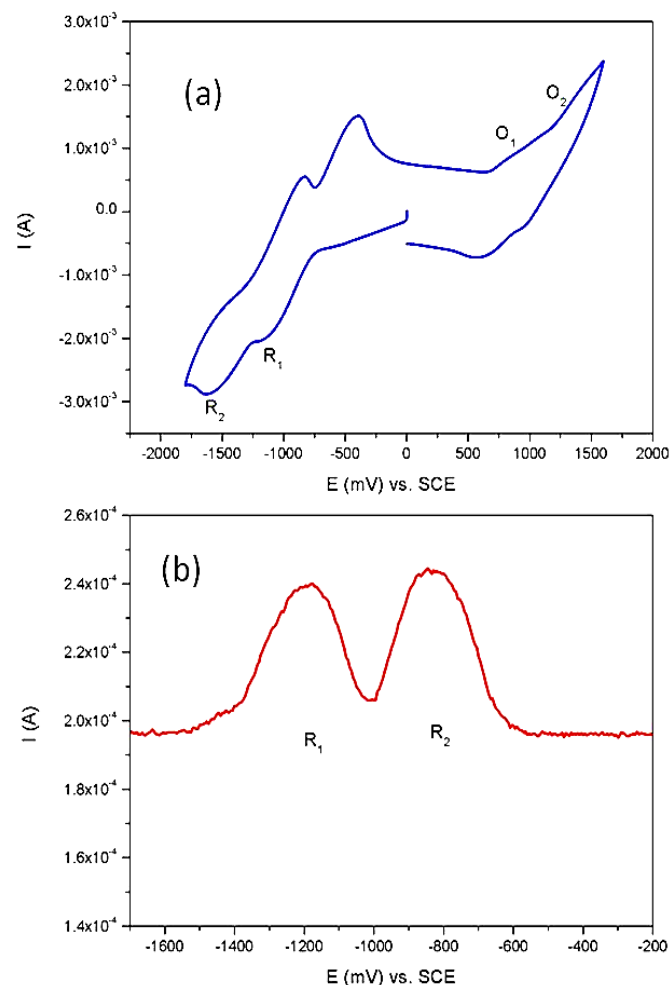

Figure 4. (**a**) Cyclic voltamogram of **4** on Pt in CH2Cl2/TBAP electrolyte. (**b**) Square wave voltamogram of **4** on Pt in CH2Cl2/TBAP electrolyte, step size = 5 mV; pulse size = 100 mV; Frequency = 25Hz

Figure 5. (a) Cyclic voltamogram of **5** on Pt in CH₂Cl₂/TBAP electrolyte

The general redox character of the **4** was found to be consistent with the known **4** behavior available in the literature [28]. As is shown in Table 2, the involvement of Co(II), Fe(II), and Ti(IV) in the center instead of 2H increased the redox richness of the phthalocyanines with an extra electron transfer process. Fig. 5 shows the CV response of **5**. Compound **5** signifying three reduction process labeled as R₁ (E₁/₂= −0.21 V, reversible), R₂ (E₁/₂= −0.51 V, quasi-reversible), R₃ (E₁/₂= −1.44 V, reversible) and one quasi-reversible oxidation reaction process labeled as O₁ (E₁/₂= 0.68 V), respectively. R₁ is a metal-based reduction process, R₂ and R₃ are ring based reduction processes. Fig. 6 shows CV and SWV responses of **2** in DCM/TBAP electrolyte. Compound **2** gave three quasi-reversible reduction processes and two oxidation processes. On the one hand, the process R₁ of the **2** was in a metal-based character. On the other hand, second and third reduction reactions (R₂ and R₃) were determined as probable ring-based processes. Fig. 7 shows CV and SWV responses of **3** in DCM/TBAP electrolyte on a Pt working electrode. **3** gave four reductions, R₁ at −0.55 V (ΔE_P= 130 mV), R₂ at −0.72 V (ΔE_P= 141 mV), R₃ at −0.89 V (ΔE_P= 125 mV), R₄ at −1.04 V (ΔE_P= 148 mV) and one oxidation reaction O₁ at 1.01 V (ΔE_P= 245 mV) within the potential window of DCM/TBAP electrolyte system. R₁, R₂, R₃ R₄ reduction processes are attributed to metal-ring-based electron transfer processes [29]. According to the ΔE_P values of reduction and oxidation, **3** gave four quasi-reversible (R₁, R₂, R₃ R₄) reduction and one irreversible oxidation (O₁) reactions. HOMO–LUMO gaps of **4** (ΔE₁/₂=1.87), **5** (ΔE₁/₂=0.89), **2** (ΔE₁/₂=1.47), **3** (ΔE₁/₂=1.56) were found to be rather consistent with those of the phthalocyanines early reported in the literature [30–32].
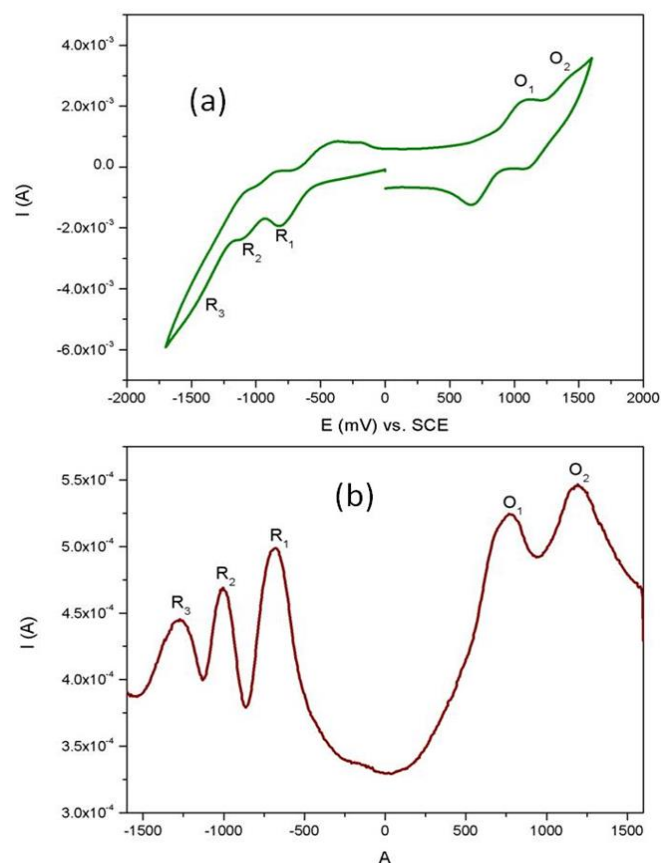
Figure 6. (a) Cyclic voltamogram of **2** on Pt in CH₂Cl₂/TBAP electrolyte. **(b)** Square wave voltamogram of **2** on Pt in CH₂Cl₂/TBAP electrolyte, step size = 5 mV; pulse size = 100 mV; Frequency = 25Hz
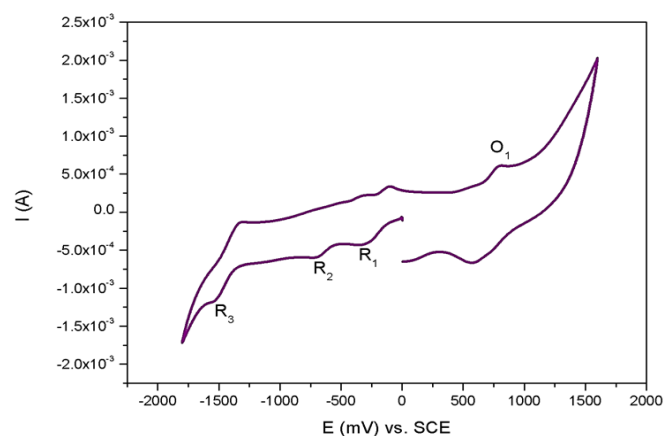

Figure 7. (a) Cyclic voltamogram of **3** on Pt in CH₂Cl₂/TBAP electrolyte. **(b)** Square wave voltamogram of **3** on Pt in CH₂Cl₂/TBAP electrolyte, step size = 5 mV; pulse size = 100 mV; Frequency = 25Hz

4. Conclusion

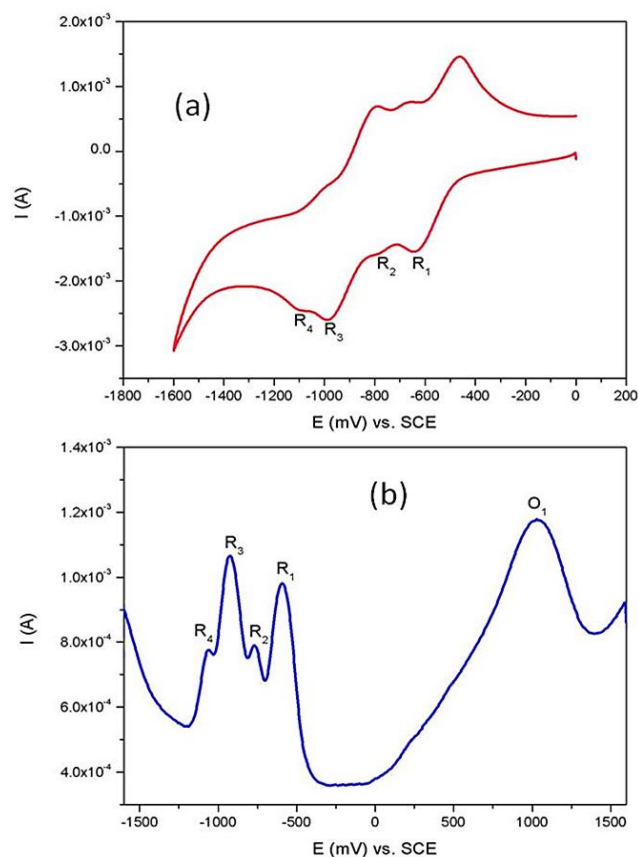In this study, the synthesis of novel peripherally chloroquinoline substituted **2,** and **3** compounds were determined and characterized using different spectroscopic techniques (e.g. FT-IR, elemental analysis, mass spectroscopy, UV/Vis spectral data) for the first time. Voltammetric analysis of 5-chloroquinolin-8-yloxy group substituted phthalocyanines were studied in solution with voltammetric measurements. While metal-free phthalocyanine **4** gave Pc ring based redox processes, metallophthalocyanines (Fe²⁺, Co²⁺, Ti⁴⁺) gave metal-based electron transfer reactions in addition to the Pc based redox reactions, which enriched the possible usage of the complex in various electrochemical technologies such as electrocatalytic and electrochromic applications.

Acknowledgment

References

[1] A. Suzuki, H. Okumura, Y. Yamasaki, T. Oku, Fabrication and characterization of perovskite type solar cells using phthalocyanine complexes, Appl Surf Sci, 488, 2019, 586–596.

[2] J. Xu, W. Yang, R. Chen, The photovoltaic performance of highly asymmetric phthalocyanine-sensitized brookite-based solar cells, Optik, 200, 2020, 163413.

[3] B. Yıldız, E. Güzel, D. Akyüz, B.S. Arslan, A. Koca, M.K. Şener, Unsymmetrically pyrazole-3-carboxylic acid substituted phthalocyanine-based photoanodes for use in water splitting photoelectrochemical and dye-sensitized solar cells, Sol Energy, 191, 2019, 654–662.

[4] S. Kong, X. Wang, L. Bai, Y. Song, F. Meng, Multi-arm ionic liquid crystals formed by pyridine-mesophase and copper phthalocyanine, J Mol Liq, 288, 2019, 111012.

[5] J.A. Jiménez-Tejada, A. Romero, J. González, N.B. Chaure, A.N. Cammidge, I. Chambrier, A.K. Ray, M.J. Deen, Evolutionary Computation for Parameter Extraction of Organic Thin-Film Transistors Using Newly Synthesized Liquid Crystalline Nickel Phthalocyanine, Micromachines, 10, 2019, 683.

[6] E.M. Bauer, T. De Caro, P. Tagliatesta, M. Carbone, Unraveling The Real pigment composition of tattoo inks: the case of bi-components phthalocyanine based greens, Dyes Pigments, 167, 2019, 225–235.

[7] Y. Zhao, J. W. Ying, Q. Sun, M. R. Ke, B. Y. Zheng, J. D. Huang, A novel silicon(IV) phthalocyanine-oligopeptide conjugate as a highly efficient photosensitizer for photodynamic antimicrobial therapy, Dyes Pigments, 172, 2020, 107834.

[8] Q. Li, Z. Sun, Q. Liang, M. Zhou, D. Sun, Novel tetrasubstituted zinc phthalocyanine-attapulgite composites for efficient catalytic oxidation of styrene with tert-butyl hydroperoxide as oxidant, Solid State Sci, 97, 2019, 106010.

[9] R. Bahluli, S. Keshipour, Microcrystalline cellulose modified with Fe(II)- and Ni(II)-phthalocyanines: Syntheses, characterizations, and catalytic applications, Polyhedron, 169, 2019, 176–182.

[10] H.S. Majumdar, A. Bandyopadhyay, A.J. Pal, Data-storage devices based on layer-by-layer self-assembled films of a phthalocyanine derivative, Org Electron, 4, 2003, 39.

[11] M.P. Malathesh, N.Y.P. Kumara, B.S. Jilani, K.R.V. Reddy, Synthesis and Characterization of Tetra-Ganciclovir Cobalt (II) Phthalocyanine for Electroanalytical Applications of AA/DA/UA, Heliyon, 5, 2019, e01946.

[12] L.F. de Holanda, F.W.P. Ribeiro, C.P. Sousa, P.N. da S. Casciano, A.N. Correia, Multi-walled carbon nanotubes–cobalt phthalocyanine modified electrode for electroanalytical determination of acetaminophen, J Electroanal Chem, 772, 2016, 9–16.

[13] L.F. de Lima, C.C. Maciel, A.L. Ferreira, J.C. de Almeida, M. Ferreira, 2020. Nickel (II) phthalocyanine-tetrasulfonic-Au nanoparticles nanocomposite film for tartrazine electrochemical sensing, Mater Lett, 262, 127186.

[14] E.O. Moiseeva, Y.B. Platonova, D.V. Konev, S.A. Trashin, L.G. Tomilova, Electrochemical and spectroelectrochemical properties of tetra-tert-butylphthalocyanine indium(III), Mendeleev Commun, 29, 2019, 212–214.

[15] F. Demir, H.Y. Yenilmez, A. Koca, Z.A. Bayır, Metallo-phthalocyanines containing thiazole moieties: Synthesis, characterization, electrochemical and spectroelectrochemical properties and sensor applications, J Electroanal Chem, 832, 2019, 254–265.

[16] S.G. Feridun, E.B. Orman, Ü. Salan, A.R. Özkaya, M. Bulut, Synthesis, characterization, and electrochemical and in-situ spectroelectrochemical properties of novel peripherally and non-peripherally 7-oxy-3-(3,4-dimethoxyphenyl) coumarin substituted phthalocyanines, Dyes Pigments, 160, 2019, 315–327.

[17] T. Nyokong, Electronic spectral and electrochemical behaviour of near infrared absorbing metallophthalocyanines". In: Structure and Bonding: Functional Phthalocyanine Molecular Materials, Editors: D.M.P Mingos, 2010, Germany, Springer.

[18] A. Nas, H. Kantekin, A. Koca, Electrochemical and Spectroelectrochemical Analysis of 4-(4-(5-Phenyl-1,3,4-oxadiazole-2-yl)phenoxy)-Substituted Cobalt(II), Lead(II) and Metal-Free Phthalocyanines, Electroanal, 27, 2015, 1602–1609.

[19] A. Nas, Z. Biyiklioglu, S. Fandaklı, G. Sarkı, H. Yalazan, H. Kantekin, Tetra(3-(1,5-diphenyl-4,5-dihydro-1H-pyrazol-3-yl) phenoxy) substituted cobalt, iron and manganese phthalocyanines: Synthesis and electrochemical analysis, Inorg Chim Acta, 466, 2017, 86–92.

[20] Ç.C. Koçak, A. Nas, H. Kantekin, Z. Dursun, Simultaneous determination of theophylline and caffeine on novel [Tetra-(5-chloroquinolin-8-yloxy) phthalocyanato] manganese(III)-Carbon nanotubes composite electrode, Talanta. 184, 2018, 452–460.

[21] B.S. Jilani, M.P. Malathesh, C.D. Mruthyunjayachari, K.R.V. Reddy, Cobalt (II) tetra methyl-quinoline oxy bridged phthalocyanine carbon nano particles modified glassy carbon electrode for sensing nitrite: A voltammetric study, Mater Chem Phys, 239, 2020, 121920.

[22] A. Nas, Ü. Demirbaş, M. Pişkin, M. Durmuş, H. Kantekin, The photophysical and photochemical properties of new unmetallated and metallated phthalocyanines bearing four 5-chloroquinolin-8-yloxy substituents on peripheral sites, J Lumin, 145, 2014, 635–642.

[23] Perrin DD, Armarego WLF, Purification of laboratory chemicals, Oxford, 1989, New York, Pergamon.

[24] J.G. Young, W. Onyebuagu, Synthesis and characterization of di-disubstituted phthalocyanines, J Org Chem, 55, 1990, 2155–2159.

[25] D. Liang , W. Peng , Y. Wang, Solvent-Stabilized Y-Type Oxotitanium Phthalocyanine Photoconductive Nanoparticles: Preparation and Application in Single-Layered Photoreceptors, Adv Mater, 24, 2012, 5249–5253.

[26] H. Zhu, H. Song, W. Zhao, Z. Peng, D. Liu, B. Di, L. Xing, H. Chen, Z. Huang, Y. Wang, K. Wu, Precursor Structures for Polymorphic Titanyl Phthalocyanine Crystal Phases on Au(111): A High-Resolution STM Study, J Phys Chem C, 123, 2019, 17390–17396.

[27] İ. Yalçın, H. Yanık, H.T. Akçay, İ. Değirmencioğlu, M. Durmuş, Photophysical and photochemical study on the tetra 4-isopropylbenzyloxy substituted phthalocyanines, J Lumin, 192, 2017, 739–744.

[28] İ. Ömeroğlu, Z. Bıyıklıoğlu, Synthesis and electrochemistry of phthalocyanines bearing [(3,4-dimethoxybenzyl)oxy] groups, Turk J Chem, 39, 2015, 347–358.

[29] D. Akyuz, T. Keleş, Z. Bıyıklıoğlu, A. Koca, Metallophthalocyanines Bearing Polymerizable {[5-({(1E)-[4-(Diethylamino)phenyl]methylene}amino)-1-naphthy1]oxy} Groups as Electrochemical Pesticide Sensor Electroanal, 29, 2017, 2913–2924.

[30] A. Aktaş, İ. Acar, Z. Bıyıklıoğlu, E.T. Saka, H. Kantekin, Synthesis, electrochemistry of metal-free, copper, titanium phthalocyanines and investigation of catalytic activity of cobalt, iron phthalocyanines on benzyl alcohol oxidation bearing 4-{2-[3-trifluoromethyl)phenoxy]ethoxy} groups, Synthetic Metals, 198, 2014, 212–220.

[31] Ö. Koyun. S. Gördük, B. Keskin, A. Çetinkaya, A. Koca, U. Avcıata, Microwave-assisted synthesis, electrochemistry and spectroelectrochemistry of phthalocyanines bearing tetra terminal-alkynyl functionalities and click approach, Polyhedron, 113, 2016, 35–49.

[32] Ü. Demirbaş, D. Akyüz, A. Mermer, H.T. Akçay, N. Demirbaş, A. Koca, H. Kantekin, The electrochemical and spectroelectrochemical properties of metal free and metallophthalocyanines containing triazole/piperazine units, Spectrochim Acta Part:A Mol Biomol Spect, 153, 2016, 478–487.

Turkish Journal of

Analytical Chemistry

www.turkjac.org
2019

TurkJAC

Natural and H₂SO₄ modified plane sawdust as a low-cost adsorbent: removal of anionic and cationic dyes from aqueous solutions

Duygu Ozdes[1] (iD), Celal Duran[2]* (iD), Sengul Tugba Ozeken[2] (iD), Ozgun Kalkisim[3] (iD), Yener Top[1] (iD)

[1] Gümüşhane University, Gümüşhane Vocational School, 29100, Gümüşhane, Türkiye
[2] Karadeniz Technical University, Faculty of Sciences, Department of Chemistry, 61080, Trabzon, Türkiye
[3] Recep Tayyip Erdoğan University, Faculty of Agriculture, Department of Horticulture, 53100, Rize, Türkiye

Abstract

Natural and H₂SO₄-modified plane (*Platanus orientalis* L.) sawdust were used for the adsorptive removal of cationic methylene blue (MB) and anionic indigo carmine (IC) dyes from aqueous media to suggest a new and cost-effective method for wastewater treatment applications. The influences of initial pH values, concentrations of MB and IC, period of contact, dosages of the natural and modified plane sawdust, and the presence of foreign ions on the adsorption of dyes were investigated in the experimental studies to describe the best conditions of the most efficient adsorption processes. Initial pH values were optimized to be between 6.0–8.0 for MB and 2.0 for IC. Optimum contact time to reach the equilibrium were determined as 120 and 240 min for the adsorption of MB onto NPS and MPS, respectively while IC adsorption onto both adsorbents reached the equilibrium in 240 min. By using the Langmuir isotherm model maximum MB adsorption capacities of NPS and MPS were calculated as 55.56 and 38.46 mg/g, respectively and the maximum IC adsorption capacities were 58.82 and 55.55 mg/g for NPS and MPS, respectively. Results showed that the natural and H₂SO₄-modified plane sawdust serve as low-cost and efficient materials in the adsorptive removal of MB and IC dyes for industrial wastewater treatment applications.

Keywords: Adsorption, dye, modification, plane sawdust (*Platanus orientalis* L.), isotherm

1. Introduction

The positive acceleration in technological development and the rapid increase in the world population led to the emergence of the problem of environmental pollution, which threatens human life and nature. Industrial dyestuffs, among the pollutants of organic origin, which exist in the wastewater of most industries release to the environment majorly from the textile, painting, leather, food, plastic, coating, and paper industries [1,2].

The complex organic structures of dyes make it time-consuming and difficult to remove them from industrial wastewater. Various techniques such as coagulation [3], flocculation [4], membrane filtration [5], photocatalytic degradation [6] and adsorption [2] are used to remove dyes from wastewater. Among these techniques, adsorption is one of the most-effective and low-capital investment-requiring methods. The adsorption method is based on the principle that solid substances called adsorbents retain the pollutants from the aqueous solutions by chemical or physical bonding [7]. In recent years, various adsorbents such as activated carbon,

natural minerals, graphene oxide, and metal-organic frameworks used in dye removal are economically valuable materials [8]. Activated carbon is a popular adsorbent with a high adsorption capacity, used to remove many organic and inorganic pollutants from aqueous or gaseous media. However, the fact that commercial activated carbon is quite expensive makes the quest for low-cost adsorbents for the adsorption processes. For this reason, wood sawdust, which is cheap, effective, and modifiable in different ways to increase its capacity, is considered an adsorbent alternative to activated carbon. Such wastes are lignocellulosic materials containing three main structural components: hemicellulose, cellulose, and lignin. Sawdust attracts more interest from environmentalists since these materials are eco-friendly, abundant, accessible, cheap, and easily applicable in wastewater treatment. Pine, oak, fir, and hornbeam sawdust modified with cetyl trimethyl ammonium bromide (CTAB) [9], orange wood sawdust modified by

sodium hydroxide (NaOH) [10], sugarcane pulp modified with formaldehyde [11], kail (*Pinus wallichiana*) sawdust [12], camphor (*Cinnamomum camphora*) sawdust [13], red pine sawdust [14], acacia sawdust [15], and many other types of sawdust wasted by the forest and agriculture industries that have no economic value, are found in the literature examining the potential of removing various dyes from aqueous solutions.

This study aimed to remove cationic methylene blue (MB) and anionic indigo carmine (IC) dyes from aqueous media through an adsorption process, using natural and H_2SO_4-modified plane sawdust as adsorbent materials. According to our literature research, although there are many studies [3,16] on MB removal from water since it is a widely used industrial dye and a model dye, there are limited studies on IC removal, which is also widely used. In the literature, there are studies in which different types of H_2SO_4-modified wastes are used for pollutant removal. Mahmood-ul-Hassan et al have used H_2SO_4-modified banana stalks, corn cob, and sunflower achene for the adsorption of Cd(II), Cr(III) and Pb(II) ions [17]. Mohebali et al have modified celery residue with H_2SO_4 to use as a low-cost adsorbent for elimination of MB from aqueous solution in batch adsorption process [18]. Djama et al have treated *Acorus calamus* firstly with H_2SO_4 and then activated by $KMnO_4$ to prepare an adsorbent for MB removal [19]. Zeydouni et al have used H_2SO_4-modified Aloe vera leaf shells for the removal of *P*-chlorophenol and MB from aqueous environment [20]. On the other hand, H_2SO_4-modified plane sawdust was used as an adsorbent for the first time in the adsorption of MB and IC in the present study. There are various modification agents to improve the adsorptive specifications of an adsorbent in the literature, yet H_2SO_4 was preferred as a chemical agent to modify the natural plane sawdust material due to the advantages of being inexpensive and simply applicable [21]. In order to obtain the optimum retention conditions, the influences of significant experimental parameters, including initial solution pH, initial dye and adsorbent concentration, and contact time on the process were evaluated. The adsorption isotherms were utilized to calculate the MB and IC adsorption capacity of NPS and MPS and to interpret the adsorption mechanism.

2. Materials and Method

2.1. Preparation of natural and modified adsorbents
Natural plane sawdust was ground without any physical or chemical pretreatments and sifted to obtain particles smaller than 150 μm for the experiments. To obtain H_2SO_4-modified plane sawdust, 20 g of plane sawdust was stirred well with 20 mL of concentrated H_2SO_4 on a hot plate at 200°C for 24 hours, and then

washed with distilled water to remove acidic residues. After washing, the sample was soaked in aqueous $NaHCO_3$ at 1% (w/v) concentration for 24 hours to neutralize the acidic residues, then washed with distilled water and dried in the oven at 105°C for 24 hours [21] and ground and sifted to separate the particles smaller than 150 μm for the experimental studies.

2.2. Chemicals and apparatus
Methylene blue ($C_{16}H_{18}ClN_3S$), indigo carmine ($C_{16}H_8N_2Na_2O_8S_2$), H_2SO_4, HNO_3, NaOH, $NaHCO_3$, Na_2CO_3, and HCl were analytical grade chemicals used in this study and purchased from Fluka (Buch, Switzerland) and Merck (Darmstadt, Germany) companies. Distilled water was used in all experimental stages. Perkin Elmer 1600 FT-IR model spectrophotometer was utilized for the FTIR analysis of the surface functional groups. Santen SE 125 model furnace was used for moisture analysis. Perkin Elmer Lambda 25 model UV-Vis spectrophotometer was used to determine the concentration of dyes remaining in the aqueous solutions. BOECO PSU-15i model mechanical shaker was used for shaking the samples in the adsorption stage. BOECO S-8 model centrifuge device was used to separate the solid and liquid phases from each other. Hanna pH-2221 model desktop digital pH meter was used to adjust the initial pH of the dye solutions. All samples were weighed by Sartorius BP1106 model analytical balance and stirred by IKA RCT Basic model magnetic stirrer.

2.3. Batch experiments
Adsorption experiments were utilized through the batch method in polypropylene centrifuge tubes. The initial pH of the MB and IC solutions was adjusted by diluted HNO_3 or NaOH solutions. Ten milliliters of MB or IC in the concentration range between 50 and 1000 mg/L was added to each sample of adsorbent (NPS or MPS) weighed (0.01–0.20 g) in the centrifuge tubes, and the samples were shaken on a mechanical shaker at 350 rpm for various contact times ranging between 1–360 min. After the adsorption process, the solid and liquid phases were separated from each other in the stage of centrifuging at 3500 rpm for 5 min, and the remaining concentrations of dyes in the supernatant solutions were measured by a UV-Vis spectrophotometer at 663 and 609 nm wavelengths for MB and IC, respectively. The amounts of adsorbed MB or IC dyes onto 1 g of NPS or MPS adsorbent (mg/g) and the percentage of adsorption (%) were calculated by using Eq.1 and Eq.2, respectively.

$$q_e = \frac{(C_o - C_e) \times V}{m} \qquad (1)$$

$$Adsorption \; (\%) = \frac{C_o - C_e}{C_o} \times 100 \qquad (2)$$

q_e (mg/g) is the amount of adsorbed dye onto 1 g of NPS or MPS, C_o (mg/L) is the initial concentration of MB or IC, C_e (mg/L) is the concentration of the unadsorbed MB or IC at the equilibrium, V (L) is the volume of the dye solution, and m (g) is the dry mass of the NPS or MPS.

3. Results and Discussion

3.1. Characterization of NPS and MPS
Characterizations of NPS and MPS were evaluated by FTIR, moisture content and pH_{pzc} analysis, and Boehm titration method. Functional groups on the surface of NPS and MPS were determined by FTIR analysis, as represented in Fig. 1 (a) and (b), respectively. Most of the functional groups on NPS were kept the same in the modified adsorbent since the modification process was utilized in low temperatures. The broad peak at 3396 cm^{-1} can be attributed to –OH groups of phenolic, carboxylic, and alcoholic groups in the samples. The peak in 1454 cm^{-1} also corresponds to phenolic –OH groups. The peaks at 2918, 2852 and 1372 cm^{-1} are the aliphatic C–H bonds. The peak at 1734 cm^{-1} corresponds to the C=O stretching of the carbonyl groups. The peak at 1051 cm^{-1} is a sign of the C–C bond, and the peaks between 1051–1237 cm^{-1} point out the presence of S=O groups in the structure. The peaks at 1646 and 1051 cm^{-1} are the stretching peaks of C=C and C–O bonds, and the peak at 892 cm^{-1} makes a sign to C–O–H groups [22–24].

The amounts of lactonic, phenolic, and carboxylic groups on the surface of natural and modified plane sawdust were determined by the Boehm titration method [25].
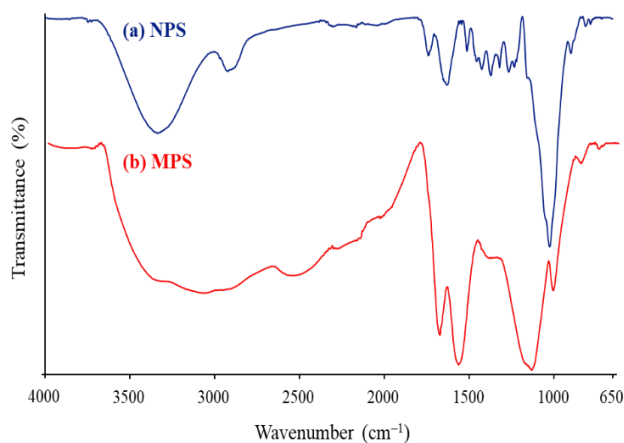

Figure 1. FTIR spectra of a) NPS and b) MPS

Table 1. Some characterization parameters of the adsorbents

Parameters	NPS	MPS
pH_{pzc}	4.6	–
Moisture content (%)	6.87	10.93
Surface acidic groups (mmol/g)		
Lactonic groups	1.23	2.14
Carboxylic groups	4.28	11.78
Phenolic groups	1.22	5.66
Total acidic groups (mmol/g)	6.73	19.58

Quantitative data of carboxylic, phenolic, and lactonic groups showed that surfaces of the adsorbents were rich in total acidic groups that increased by the modification process, especially the number of carboxylic groups increased the most (Table 1). As the temperature of the modification process, which increases the adsorption capacity and plays a significant role in the adsorptive removal of pollutants from aqueous solutions, is limited in the range of 200–400°C, high numbers of acidic oxides were obtained on the surface of the activated adsorbent [26].

3.2. Effect of pH on the adsorption process
The effect of the initial pH of the dye solutions in contact with each adsorbent was the first parameter studied for the best selection of the appropriate adsorbate-adsorbent systems since the initial pH directly affects the adsorption efficiency. MB and IC concentrations were 50 mg/L in separate solutions. MB solutions with a natural pH of 6.5 and adjusted pH values in the range of 2.0–8.0 and IC solutions with a natural pH and adjusted pH values in the range of 1.0–8.0 were tested for the optimization of the initial pH. Diluted HNO₃ and NaOH were used to adjust the pH of dye solutions. The NPS or MPS (5.0 g/L) was shaken with the dye solutions at various initial pH values on the mechanical shaker for 240 min and centrifuged at 3500 rpm for 5 min to separate the solid and the liquid phases. The concentrations of the remaining dyes in the supernatants were analyzed by the UV-Vis spectrophotometer.

As seen in Fig. 2 (a), the adsorption efficiency of the adsorbents performed best in the pH range of 6.0–8.0 in the adsorption of cationic MB dye. However, the adsorption efficiency in the MB adsorption onto NPS and MPS reached a value higher than 90% at pH 6.5 which corresponds to the natural (unadjusted) pH of the MB solution. The adsorption efficiencies of the MPS reached a value higher than 95% in the pH range of 2.0–8.0, also pointing out that not the electrostatic attractions only but also an ion-exchange-based mechanism may be possible to explain the adsorption process. In the adsorption of MB dye, natural adsorbent performed low adsorption efficiency, which increased by the increase in solution pH. On the other hand, the adsorption

efficiency reached its maximum value at pH 2.0 in the adsorption of IC dye, as seen in Fig. 2 (b). In the pH range of 1.0–2.0, the efficiencies of IC adsorption onto NPS and MPS are higher than 90%, yet the adsorption efficiencies decreased immediately as the initial pH of dye solutions increased.

The adsorption efficiencies are low in MB adsorption and high in IC adsorption in acidic initial pH values since the environments of the NPS and MPS are surrounded by H_3O^+ ions, and the functional groups of the solid adsorbents electrically charged positively in the acidic aqueous media. The electrostatic repulsion between the H_3O^+ ions and the cationic MB dye prevents the approaching of the adsorbent and the adsorbate. As the initial pH of the solution increases, the adsorption efficiency increases due to decreasing competitive adsorption behavior of H_3O^+ ions and cationic MB dye onto active sites. However, anionic IC dye approaches the positively charged surface of the adsorbent due to electrostatic attractions in low initial pH values. As the initial pH of the solution increases, the adsorption efficiency decreases due to the increased competitive adsorption behavior of OH^- ions and anionic IC dye onto active sites [27,28].

The pH_{pzc} value was found to be 4.6 for NPS, revealing that the number of acidic functional groups is higher than the basic functional groups in its chemical structure. Informative numerical data about the pH_{pzc} value of an adsorbent is essential to optimize the initial pH to reach the highest adsorption efficiency since the net surface charge of the adsorbent is positive if pH < pH_{pzc} and negative if pH > pH_{pzc} [29]. The cationic dyes are adsorbed better at pH values higher than pH_{pzc}, and the anionic dyes are adsorbed better at lower pH values than pH_{pzc} [30]. As a result, further experiments were planned through the optimized initial pH values of 6.5 for MB and 2.0 for IC adsorption.

3.3. Effect of contact time on the retention of MB and IC

Optimization of the contact time was evaluated by testing various periods of contact. Ten milliliters of MB solution with a natural pH of 6.5 or IC solution with an adjusted pH of 2.0 was added onto 5.0 g/L of NPS or MPS, which were weighed in polypropylene centrifuge tubes and processed for adsorption on the mechanical shaker for various periods ranging between 1–360 min. After shaking, the samples were centrifuged to separate the solution and the adsorbent from each other. The concentration of each dye remaining in the solution was determined by UV-Vis Spectrophotometer and used to calculate the amount of MB or IC dyes adsorbed onto 1 g of adsorbent (q_t) for different contact times.
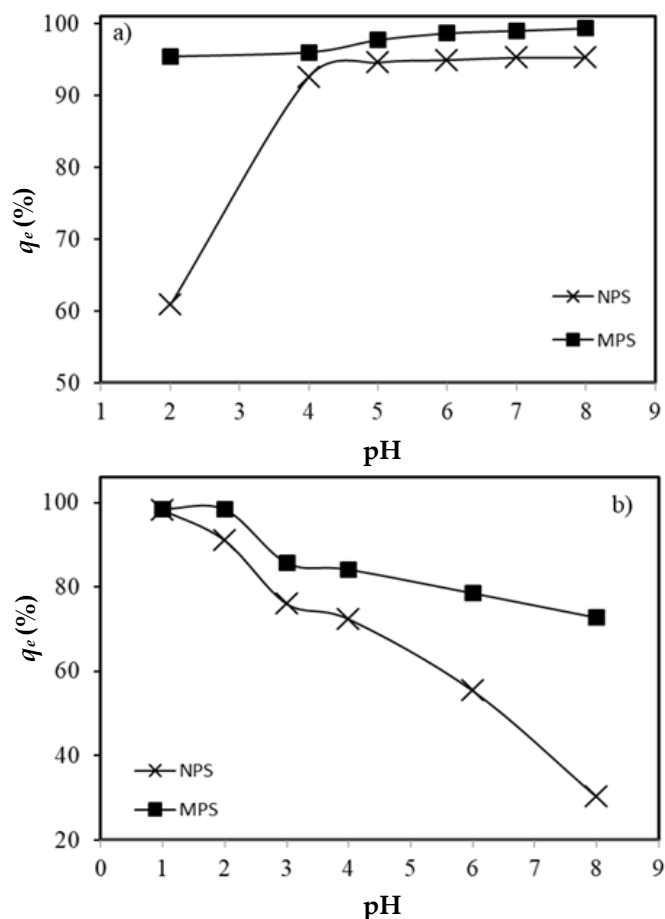

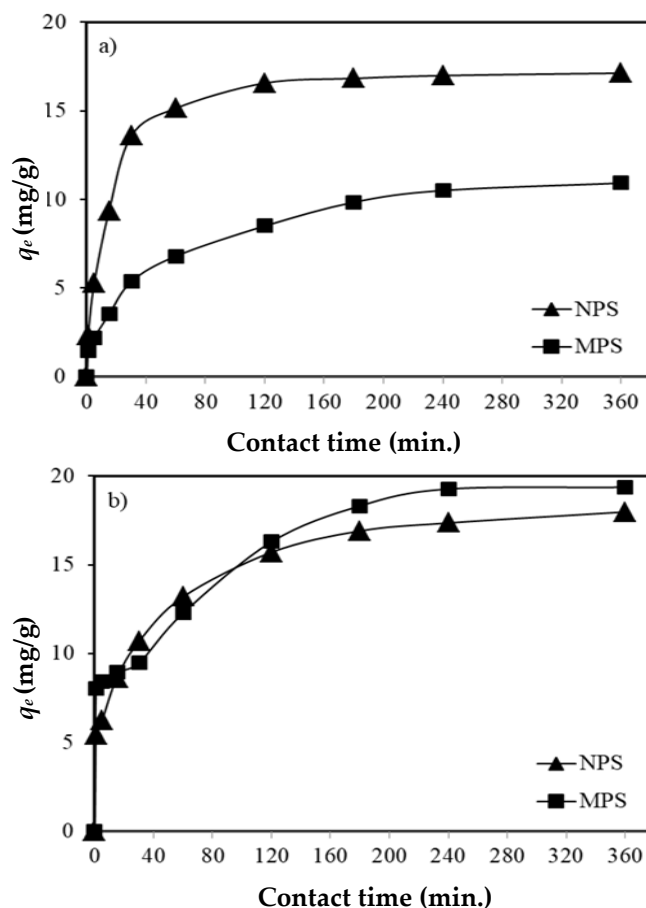Figure 2. Impact of initial pH on a) MB and b) IC uptake onto NPS and MPS

Figure 3. Influences of contact time on a) MB and b) IC uptake onto NPS and MPS

In the adsorption of MB onto NPS and MPS, optimum contact times to reach the equilibrium were determined to be 120 and 240 min, respectively (Fig. 3 (a)), while the process of IC adsorption onto NPS and MPS reached the equilibrium in 240 min (Fig. 3 (b)). The amount of adsorbed MB and IC onto all adsorbents became nearly stable after reaching the equilibrium. The dye sorption process occurs immediately in the first stages since the active sites of NPS and MPS surfaces were available for adsorption. The transportation of the dye molecules into the internal surfaces of the pores through diffusion slows down when the system becomes closer to equilibrium. After reaching the equilibrium, the amounts of adsorbed dye do not increase much according to the saturation of the adsorptive sites [31]. As a result, the equilibration time for both dyes was determined as 240 min in subsequent studies to ensure that the equilibrium was fully established.

3.4. Effect of initial dye concentration and isotherm studies

The solutions of MB and IC at various initial concentrations in the range of 50–1000 mg/L were added onto 5.0 g/L of NPS and MPS adsorbents separately to determine the effect of initial dye concentration on the adsorption process. Then the mixtures were shaken on the mechanical shaker at 350 rpm for 240 min to reach the equilibrium. After centrifuging the samples, the amount of unadsorbed MB or IC remaining in the supernatant was analyzed by UV-Vis spectrophotometer. The initial concentration of MB was plotted against the adsorbed amounts (q_e) and the removal percentage (%) of MB onto NPS and MPS (Fig. 4 (a,b), and the same parameters were plotted for the data obtained in IC's adsorption onto NPS and MPS as demonstrated in Fig. 4 (c,d). Increased initial concentrations of the dye resulted in increased amounts of MB or IC adsorbed per g of the adsorbent due to the occurring concentration gradient that improves the adsorption. On the other hand, the percentages of adsorption decreased at high initial dye concentrations because of the oversaturation of the active adsorption sites of the sorbents' surface [32].

The Langmuir, Freundlich, and Dubinin-Radushkevich isotherm models were fitted to the experimental data to get an idea of the surface structure of NPS and MPS and to interpret the MB and IC adsorption mechanism. According to the Langmuir isotherm model, the adsorbent has a homogenous surface consisting of a constant number of co-energized active sites, and there are no interactions between the adsorbate molecules [33]. Eq.3 and Eq.4 are the non-linear and linear forms of the Langmuir isotherm model.
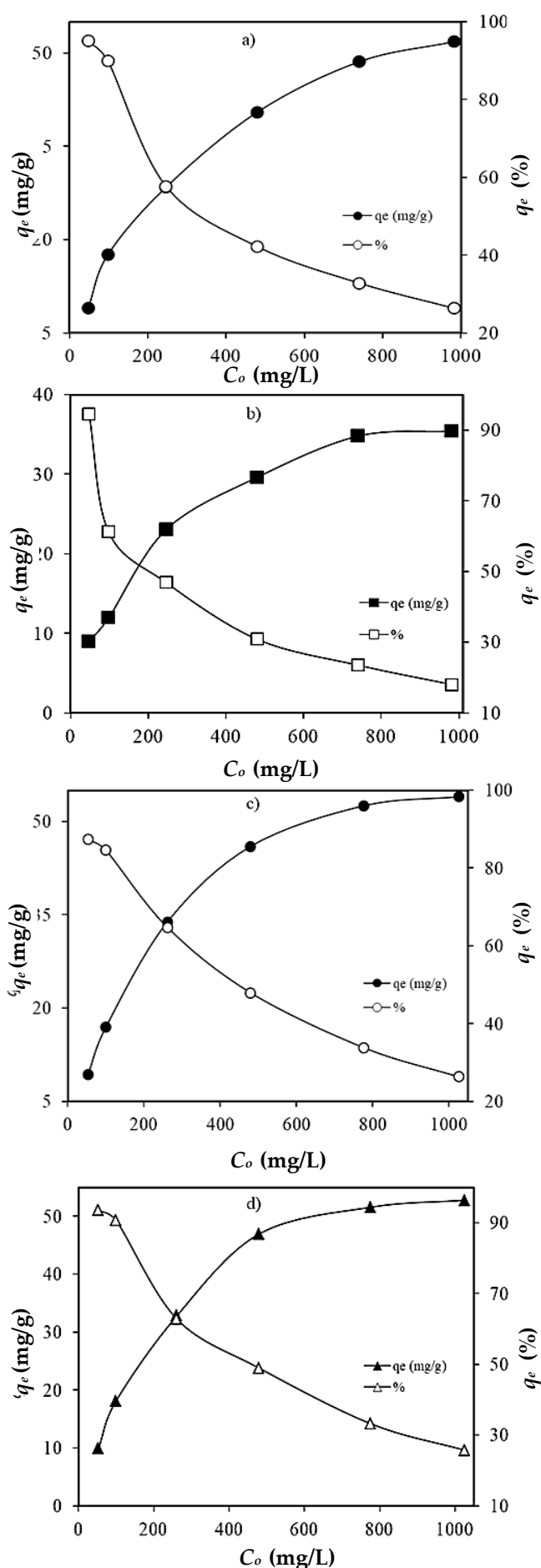
$$q_e = \frac{bC_e}{1 + bC_e} \qquad (3)$$

Figure 4. Effect of initial dye concentration on the adsorption of a) MB onto NPS b) MB onto MPS c) IC onto NPS d) IC onto MPS

$$\frac{C_e}{q_e} = \frac{C_e}{q_{max}} + \frac{1}{bq_{max}} \qquad (4)$$

q_e (mg/g) is the adsorbed amount of adsorbate onto 1 g of adsorbent, q_{max} (mg/g) is the adsorption capacity, C_e (mg/L) is the concentration of the remaining adsorbate in the solution at the equilibrium, and b (L/mg) is a constant related to the free energy. The slope and the intercept of the C_e/q_e vs. C_e plot are used to determine q_{max} and b.

Dimensionless R_L constant calculated by Eq.5 [34] gives an idea about the favorability of the adsorption process for an adsorbate-adsorbent pair.

$$R_L = \frac{1}{1 + bC_o} \qquad (5)$$

C_o (mg/L) is the initial concentration of the adsorbate in the solution, and b (L/mg) is the Langmuir constant. There are four possible values of R_L which are evaluated to four possible definitions as the adsorption process is,

i.   Favorable in the experimental conditions if $0 < R_L < 1$,
ii. Irreversible if $R_L = 0$,
iii. Linear if $R_L = 1$, and
iv. Unfavorable if $R_L > 1$.

The adsorptive sites on the surface of the adsorbent are accepted to be consisting of different types of sites and regions settled heterogeneously and energized variously in the Freundlich isotherm model as described in Eq. 6 [35] and linearizes to Eq. 7 by evaluating through the function of logarithms.

$$q_e = K_f \times C_e^{1/n} \qquad (6)$$

$$ln(q_e) = ln(K_f) + \frac{1}{n}ln(C_e) \qquad (7)$$

q_e (mg/g) is the amount of the adsorbed adsorbate onto 1 g of adsorbent, K_f (mg/g) is the adsorption capacity, C_e (mg/L) is the amount of unadsorbed adsorbate remaining in the solution at the equilibrium, and n is the density of adsorption. K_f and n are the constants obtained from the intercept and slope of the plot of $ln(q_e)$ vs. $ln(C_e)$, respectively. The heterogeneity factor (n) ranging between 1 and 10 is a sign of the favorability of the adsorption system [36].

Dubinin–Radushkevich (D–R) isotherm model (Eq. 8) explains the adsorption onto similarly porous surface structures [37], and this model reminds the Langmuir model in this respect.

$$ln(q_e) = ln(q_m) - K\varepsilon^2 \qquad (8)$$

q_e (mol/g) is the adsorbed amount of the adsorbate per g of adsorbent, q_m (mol/g) is the monolayer adsorption capacity, and K (mol²/kJ²) is the constant of adsorption energy. ε is Polanyi potential which is calculated by Eq. 9.

$$\varepsilon = RTln(1 + 1/C_e) \qquad (9)$$

R (J/mol/K) is the gas constant, C_e (mol/L) is the concentration of the unadsorbed adsorbate remaining in the solution at the equilibrium, and T (K) is the temperature. K and q_m values are obtained from the slope and intercept of the ε^2 vs. $ln\ q_e$ plot, respectively. K values obtained by the D–R isotherm are evaluated in Eq. 10 to calculate E (kJ/mol).

$$E = 1/(-2K)^{1/2} \qquad (10)$$

The average adsorption energy (E) gives information about the chemical and physical specifications of the adsorption. There are three possibilities about the value of E evaluated as the adsorption occurs,

i.   Physically if $E < 8$ kJ/mol,
ii. Through ion-exchange if $8 < E < 16$ kJ/mol, and
iii. Chemically if $E > 16$ kJ/mol [38].

Experimental data was applied to Langmuir, Freundlich, and D–R isotherm models to explain the mechanisms of MB and IC adsorption onto NPS and MPS. The non-linear equations of these three models were evaluated to obtain the isotherm plots (C_e vs. q_e) for MB adsorption onto NPS and MPS (Fig.5 (a,b)) and IC adsorption onto NPS and MPS (Fig.5 (c,d), respectively.

q_{max} and b are the Langmuir constants which were determined by the slope and the intercept of the C_e vs. C_e/q_e plot, respectively, while n and K_f are the constants of Freundlich isotherm, which were determined by the slope and the intercept of the $ln(C_e)$ vs. $ln(q_e)$ plot. The results of the calculations on the experimental data for MB and IC adsorption onto NPS and MPS were tabulated with the correlation coefficients (R^2) in Table 2.

The R^2 values obtained by the application of the Langmuir model were higher than those for the Freundlich model for both dyes, indicating that the active adsorption sites on the surfaces of NPS and MPS were distributed homogeneously [39]. Maximum MB adsorption capacities of NPS and MPS calculated as 55.56 and 38.46 mg/g by the Langmuir isotherm model, respectively, were compared to other adsorption studies in the literature.

Table 2. Isotherm model parameters

| Langmuir isotherm model	NPS-MB	MPS-MB	NPS-IC	MPS-IC
q_{max} (mg/g)	55.56	38.46	58.82	55.55
b (L/mg)	0.020	0.016	0.021	0.029
R^2	0.985	0.990	0.998	0.996
Freundlich isotherm model				
K_f (mg/g)	7.71	6.12	5.54	7.93
n	3.41	3.82	2.74	3.31
R^2	0.983	0.936	0.959	0.968
D–R isotherm model				
q_m (mg/g)	9.62	7.49	11.94	10.60
K (kJ^2/mol^2)	-0.002	-0.002	-0.003	-0.002
E (kJ/mol)	12.91	12.91	12.91	15.81
R^2	0.986	0.899	0.980	0.983

On the other hand, the maximum IC adsorption capacities were 58.82 and 55.55 mg/g for NPS and MPS adsorbents, yet there have not found enough studies about the adsorption of IC in the literature to compare with the results of this study. The adsorption capacities of NPS and MPS are higher than many adsorbents, which were expensive or not easily prepared, as seen in the table of comparison (Table 3) [29,40–49].

As the maximum adsorption capacities of natural and H$_2$SO$_4$-modified plane sawdust compared to each other, NPS performed better than MPS in MB adsorption, while there was no meaningful difference between the natural and modified adsorbents in IC adsorption. Closer adsorption capacities of natural and H$_2$SO$_4$-modified adsorbents in IC adsorption can be explained by the fact that although the surface areas of the modified adsorbents partially increased by the low-temperature modification process, the resulting sulfate salts may have clogged the pores.

As seen in Table 2, the constants of the D–R isotherm model were determined by the evaluation of the slope

Table 3. Comparison of the dye uptake capacities of the different sorbents from literature

Adsorbent	Adsorbate	q_{max} (mg/g)	Ref.
Celery residue modified with H$_2$SO$_4$ was	MB	476.19	[18]
Acorus calamus treated with H$_2$SO$_4$ and activated by KMnO$_4$	MB	1500	[19]
H$_2$SO$_4$-modified Aloe vera leaf shells	MB	192.3	[20]
Microwave assisted sawdust	MB	58.14	[29]
Canola residues	MB	13.22	[40]
Carbon nanotubes	MB	46.20	[41]
Titanium dioxide nanotube	MB	57.14	[42]
Magnetic ZnO/ZnFe$_2$O$_4$	MB	37.27	[43]
Peanut hull	MB	68.03	[44]
Activated carbons from sunflower oil cake modified by H$_2$SO$_4$	MB	16.43	[45]
Tartaric acid modified wheat bran	MB	25.18	[46]
Biochar derived from eucalyptus saw dust modified with acetic acid	MB	29.94	[47]
Orange peel	MB	13.90	[48]
Banana peel	MB	20.80	[48]
Original beech sawdust	MB	9.78	[49]
CaCl$_2$ treated beech sawdust	MB	13.02	[49]
Natural plane sawdust	MB and IC	55.56 and 58.82	This study
H$_2$SO$_4$-modified plane sawdust	MB and IC	38.46 and 55.55	This study
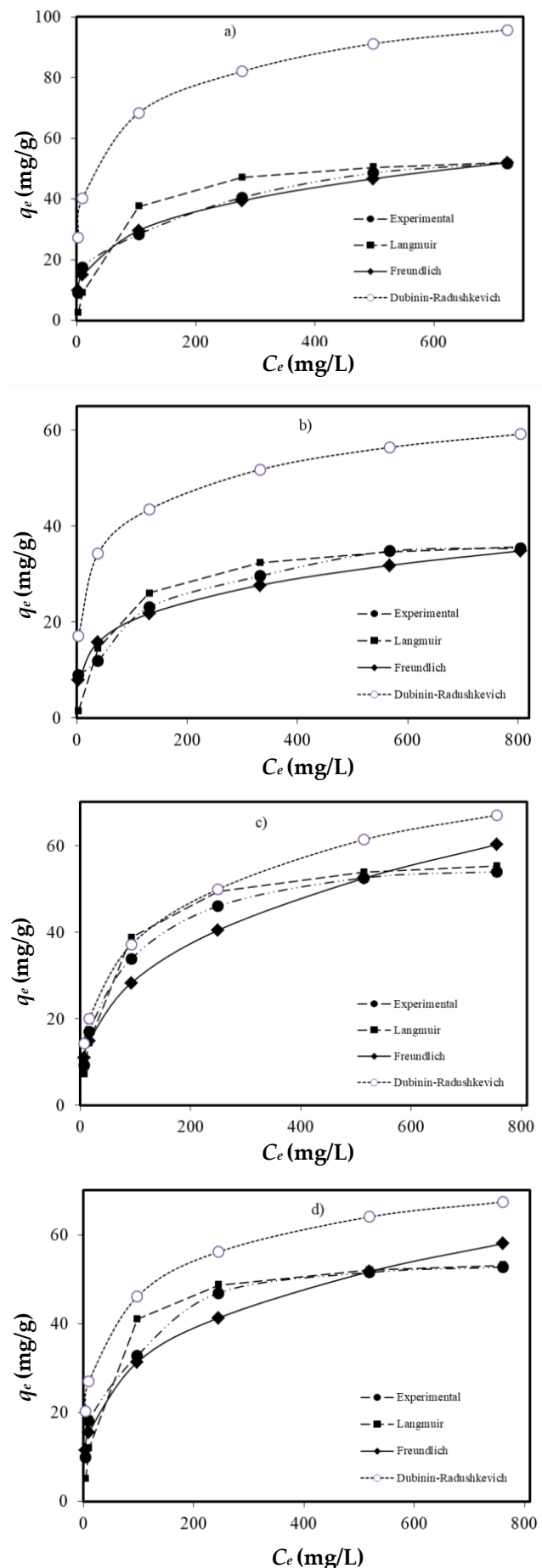
Figure 5. Adsorption isotherms of a) MB adsorption onto NPS a) MB adsorption onto NPS a) IC adsorption onto NPS a) IC adsorption onto NPS

and the intercept of the ε^2 versus $ln\ q_e$ plot as the values of K and q_m, respectively. E is the mean energy of the adsorption calculated from the value of K. E values were in the range of 8–16 kJ/mol in all calculations suggesting that ion-exchange mechanisms were also effective in the adsorption of MB and IC onto NPS and MPS [38].

R_L values were calculated to figure out the suitability of adsorption onto NPS and MPS and found to be in the range of 0–1, while the initial concentrations of MB and IC were between 50–1000 mg/L. As the initial dye concentration of the dye increased, the R_L values decreased in the range of $0 < R_L < 1$, suggesting that the processes in both dyes' adsorption onto the natural and H2SO4-modified plane adsorbents were favorable in the relevant experimental conditions. Additionally, n values obtained by the Freundlich isotherm model were in the 1–10 range, supporting the idea that MB and IC adsorption onto NPS and MPS were favorable.

3.5. Effect of adsorbent dosage on the adsorption efficiency

The suspensions consisting of 0.01–0.20 g (1.0–20.0 g/L) of NPS or MPS adsorbent and 200 mg/L MB or IC solutions were processed for 240 min on the mechanical shaker to investigate the effect of adsorbent dosage on the adsorption efficiency. After reaching the equilibrium, the concentrations of unadsorbed MB and IC remaining in the supernatants were determined by using a UV-Vis spectrophotometer. The adsorbed amounts (q_e) and removal percentages (%) of MB onto NPS and MPS were plotted against the amounts of NPS and MPS in Fig. 6 (a,b), and the adsorbed amounts (q_e) and removal percentages (%) of IC dyes against the amounts of NPS and MPS adsorbents were plotted as represented in Fig. 6 (c,d), respectively.

Increasing the amounts of NPS and MPS increased the unsaturated surfaces at the constant concentrations of MB and IC and decreased the amounts of adsorbed dye onto 1 gram of each adsorbent (q_e) due to the decreased surface area caused by a possible aggregation. However, increasing the dosage of NPS and MPS resulted in increased removal percentages caused by the number of active sites becoming higher in number [50].

3.6. Effect of foreign ions on the adsorption efficiency

Dye-contaminated wastewater sourced by textile industries may include high amounts of foreign ions, which cause ionic strength and decrease the adsorption efficiency. NaCl and BaCl2 solutions in various concentrations between 0.05–0.5 M were separately added to 100 mg/L MB and IC solutions and processed to investigate the effect of salts on the adsorption efficiency.
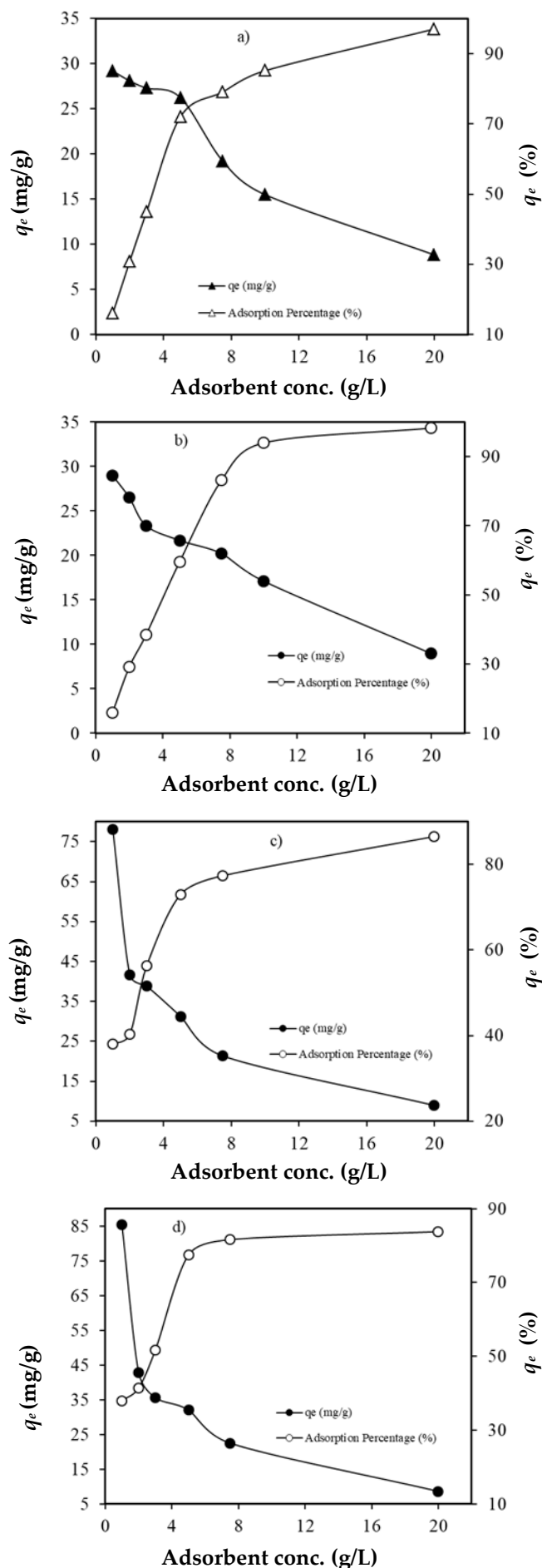

Figure 6. Effect of adsorbent amount on the adsorption of a) MB onto NPS b) MB onto MPS c) IC onto NPS d) IC onto MPS

The presence of salts may result in two effects opposite to each other. The first one is the prevention of the electrostatic interactions between the dye molecules and the active adsorption sites as the salt concentration increases, which decreases the adsorbed amounts of dye. This effect is observed in the adsorption of MB onto NPS and MPS (Fig. 7 (a,b)). The presence of both salts (NaCl and BaCl₂) in the solution prevents the attachment of MB molecules onto the active adsorptive sites of the adsorbent's surface, and the adsorption efficiency decreases when the salt concentration increases [51]. The other effect is an increase in the dissociation of dye molecules caused by ionic strength. The amount of adsorbed dye increases when the ionic strength increases since the dissociated dye molecules become free to bind onto the surface electrostatically, as observed in IC adsorption onto NPS and MPS (Fig. 7 (c,d)). Increased concentrations of NaCl and BaCl₂ caused increased adsorption according to the increased dissociation degree of IC [52].

4. Conclusion

In this study, the adsorption behaviors of natural and H₂SO₄-modified sawdust of plane (*Platanus orientalis* L.) were investigated for the adsorptive removal of pollutant methylene blue and indigo carmine dyes from aqueous media to suggest a new method for the treatment of dye contaminated industrial wastewater. Natural and H₂SO₄-modified adsorbents were characterized via FT–IR Spectroscopy, pH$_{pzc}$ and moisture content analysis, and the Boehm titration method. The optimum pH values at which the highest adsorption efficiencies were performed were determined as 6.0–8.0 range for cationic MB dye and 2.0 for anionic IC dye's adsorption onto NPS and MPS. The adsorption process reached the equilibrium in 240 min in IC adsorption onto NPS and MPS. On the other hand, the process reached equilibrium in 120 and 240 min in MB adsorption onto NPS and MPS, respectively. Both dyes were tested for all other parameters for 240 min of contact time. The amounts of adsorbed MB and IC per gram of any adsorbent decreased, and the percentage of adsorption increased with the increasing initial concentrations of both dyes. The adsorption of MB and IC fit well with the Langmuir isotherm model, suggesting that the surfaces of NPS and MPS consisted of homogeneous active sites in nature. The Langmuir maximum monolayer adsorption capacities of NPS and MPS adsorbents were higher than many expensive and hardly prepared adsorbents reported before. The information of decreasing R_L values in the 0–1 range while the concentrations of MB and IC dyes were increasing was supported by all the *n* values
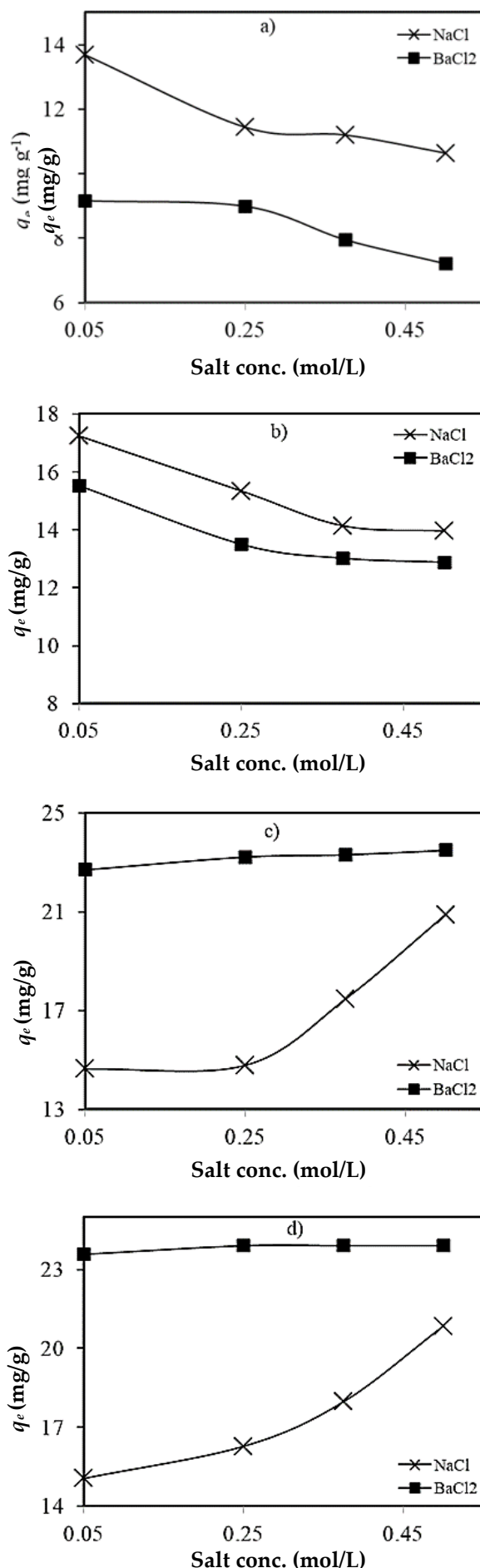

Figure 7. Effect of salt concentration on the adsorption of a) MB onto NPS b) MB onto MPS c) IC onto NPS d) IC onto MPS

corresponding to the range of 1–10 obtained from the Freundlich isotherm model, and these results indicated that the adsorption of both dyes onto NPS and MPS were favorable processes in this study. The adsorption efficiency decreased in MB adsorption and increased in IC adsorption due to the ionic strength in the presence of foreign ions, which were introduced to the aqueous media by NaCl and BaCl$_2$ salts. Natural and H$_2$SO$_4$– modified plane sawdust can be used as low-cost and effective adsorbents for the adsorptive removal of MB and IC.

Funding

References

[1] B.I. Musah, L. Peng, Y. Xu, Adsorption of Methylene Blue Using Chemically Enhanced *Platanus orientalis* Leaf Powder: Kinetics and Mechanisms, Nat Environ Pollut Technol, 19, 2020, 29–40.

[2] M. Peydayesh, A. Rahbar-Kelishami, Adsorption of methylene blue onto Platanus orientalis leaf powder: Kinetic, equilibrium and thermodynamic studies, J Ind Eng Chem, 21, 2015, 1014–1019.

[3] D. Morshedi, Z. Mohammadi, M.M.A. Boojar, F. Aliakbari, Using protein nanofibrils to remove azo dyes from aqueous solution by the coagulation process, Colloids Surf B Biointerfaces, 112, 2013, 245-254.

[4] X. Xiao, Y. Sun, W. Sun, H. Wu, C. Liu, Advanced treatment of actual textile dye wastewater by Fenton-flocculation process, Can J Chem Eng, 95(7), 2017, 1245–1252.

[5] M.F. Abid, M.A. Zablouk, A.M. Abid-Alameer, Experimental study of dye removal from industrial wastewater by membrane technologies of reverse osmosis and nanofiltration, Iranian J Environ Health Sci Eng, 9,2012, 17.

[6] M. Koç Keşir, G. Dilber, M. Sökmen, M. Durmuş, Use of new quaternized water soluble zinc phthalocyanin derivatives for effective dye sensitization of TiO$_2$, J Solgel Sci Technol, 93, 2020, 687–694.

[7] N.A. El Essawy, S.M. Ali, H.A. Farag, M. Elnouby, H.A. Hamad, Green synthesis of graphene from recycled PET bottle wastes for use in the adsorption of dyes in aqueous solution, Ecotoxicol Environ Saf, 145, 2017, 57–68.

[8] A.A. Mohammadi, S. Moghanlo, M.S. Kazemi, S. Nazari, S.K. Ghadiri, H.N. Saleh, M. Sillanpää, Comparative removal of hazardous cationic dyes by MOF-5 and modified graphene oxide, Sci Rep, 12, 2022,15314.

[9] F. Deniz, R.A. Kepekci, Biosorption of Food Green 3 by a novel green generation composite biosorbent from aqueous environment, Int J Phytoremediation, 19(6), 2017, 579–586

[10] A.A. Azzaz, S. Jellali, H. Akrout, A.A. Assadi, L. Bousselmi, Optimization of a cationic dye removal by a chemically modified agriculture by-product using response surface methodology: biomasses characterization and adsorption properties, Environ Sci Pollut R, 24(11), 2017, 9831–9846.

[11] T. Aftab, F. Bashir, B. Khan, J. Iqbal, R.A. Khan, Equilibrium and kinetics of color adsorption on agriculture by-products/wastes (Sugarcane bagasse, corncob, sawdust), Desalin Water Treat, 65, 2017, 109–116.

[12] V. Gupta, A. Agarwal, M.K. Singh, N.B. Singh, Removal of torque blue dye from aqueous solution by Kail Sawdust, Asian J Water Environ Pollut, 13(4), 2016, 59–67.

[13] H. Wang, X. Yuan, Z. Wu, L. Leng, G. Zeng, Removal of Basic Dye from Aqueous Solution using *Cinnamomum camphora* Sawdust: Kinetics, Isotherms, Thermodynamics, and Mass-Transfer Processes, Sep Sci Technol, 49, 2014, 2689–2699.

[14] M. Can, Equilibrium, kinetics and process design of acid yellow 132 adsorption onto red pine sawdust, Water Sci Technol, 71(12), 2015, 1901–1911.

[15] M. Jain, A. Mudhoo, V.K. Garg, Swiss blue dye sequestration by adsorption using *Acacia nilotica* sawdust, Int J Env Technol Manag, 14(1–4), 2011, 220–237.

[16] F.A. Khan, A. Ahad, S.S. Shah, M. Farooqui, Adsorption of crystal violet dye using *Platanus orientalis* (Chinar tree) leaf powder and its biochar: equilibrium, kinetics and thermodynamics study, Int J Environ Analyt Chem, 2021, 1–21.

[17] M. Mahmood-ul-Hassan, V. Suthor, E. Rafique, M. Yasin, Removal of Cd, Cr, and Pb from aqueous solution by unmodified and modified agricultural wastes, Environ Monit Assess, 187, 2015, 19.

[18] S. Mohebali, D. Bastani, H. Shayesteh, Methylene blue removal using modified celery (*Apium graveolens*) as a low-cost biosorbent in batch mode: Kinetic, equilibrium, and thermodynamic studies, J Mol Struct, 1173, 2018, 541–551.

[19] C. Djama, D. Chebli, A. Bouguettoucha, I. Doudou, A. Amrane, Statistical physics modelling of azo dyes biosorption onto modified powder of *Acorus calamus* in batch reactor, Biomass Convers Biorefinery, 13, 2023, 1013–1028.

[20] G. Zeydouni, S. R. Couto, H. Nourmoradi, H. Basiri, P. Amoatey, S. Esmaeili, S. Saeidi, F. Keishams, M. J. Mohammadi, Y. O. Khaniabadi, H$_2$SO$_4$-modified *Aloe vera* leaf shells for the removal of *P*-chlorophenol and methylene blue from aqueous environment, Toxin Reviews, 39 (1), 2020, 57–67.

[21] C. Duran, D. Ozdes, A. Gundogdu, M. Imamoglu, H.B. Senturk, Tea-industry waste activated carbon, as a novel adsorbent, for separation, preconcentration and speciation of chromium, Anal Chim Acta, 688, 2011, 75–83.

[22] A.W. Adamson, Physical Chemistry of Surfaces (2nd Edition), 1967, New York: Interscience.

[23] J. Guo, A.C. Lua, Textural and Chemical Characterizations of Adsorbent Prepared from Palm Shell by Potassium Hydroxide Impregnation at Different Stages, J Colloid Interf Sci, 254, 2002, 227–233.

[24] I.A.W. Tan, A.L. Ahmad, B.H. Hameed, Preparation of Activated Carbon from Coconut Husk: Optimization Study on Removal of 2,4,6-Trichlorophenol Using Response Surface Methodology, J Hazard Mater, 153, 2008, 709–717.

[25] H.P. Boehm, Chemical Identification of Surface Groups, Adv Catal, 16, 1966, 179–274.

[26] J.S. Mattson, H.B. Mark, Jr, Activated Carbon, 1971, New York: Marcel Dekker.

[27] V.K. Garg, A. Moirangthem, R. Kumar, R. Gupta, Basic dye (methylene blue) removal from simulated waste water by adsorption using Indian Rosewood Sawdust: timber industry waste, Dyes Pigments, 63, 2004, 243–250.

[28] V.K. Gupta, R. Jain, S. Malathi, A. Nayak, Adsorption-desorption studies of indigocarmine from industrial effluents by using deoiled mustard and its comparison with charcoal, J Colloid Interf Sci, 348(2), 2010, 628-633.

[29] S. Suganya, P. Senthil Kumar, A. Saravanan, P. Sundar Rajan, C. Ravikumar, Computation of adsorption parameters for the removal of dye from wastewater by microwave assisted sawdust: Theoretical and experimental analysis, Environ Toxicol Pharmacol, 50, 2017, 45–57.

[30] A.S. Mestre, J. Pires, J.M.F. Nogueira, A.P. Carvalho, Activated Carbons for the Adsorption of Ibuprofen, Carbon, 45, 2007, 1979–1988.

[31] M. Heidarizad, S.S. Sengor, Synthesis of graphene oxide/magnesium oxide nanocomposites with high-rate adsorption of methylene blue, J Mol Liq, 224, 2016, 607–617.

[32] Y. Feng, D.D. Dionysiou, Y. Wu, H. Zhou, L. Xue, S. He, L. Yang, Adsorption of dyestuff from aqueous solutions through oxalic acid-modified swede rape straw: adsorption process and disposal methodology of depleted bioadsorbents, Bioresource Technol, 138, 2013, 191–197.

[33] I. Langmuir, The adsorption of gases on plane surfaces of glass, mica and platinum, J Am Chem Soc, 40, 1918, 1361–1403.

[34] G. McKay, H.S. Blair, J.R. Gardner, Adsorption of dyes on chitin. I. Equilibrium studies, J Appl Polym Sci, 27, 1982, 3043–3057.

[35] H.M.F. Freundlich, Über die adsorption in lösungen, Z Phys Chemie, 57, 1906, 385–470.

[36] L.F.M. Ismail, H.B. Sallam, S.A. Abo Farha, A.M. Gamal, G.E.A. Mahmoud, Adsorption behaviour of direct yellow 50 onto cotton fiber: Equilibrium, kinetic and thermodynamic profile, Spectrochim Acta A, 131, 2014, 657–666.

[37] M.M. Dubinin, L.V. Radushkevich, Equation of the characteristics curve of activated charcoal, Chem Zent, 1, 1947, 875.

[38] F. Helfferich, Ion Exchange, 1962, New York: McGraw-Hill.

[39] H.B. Senturk, D. Ozdes, C. Duran, Biosorption of Rhodamine 6G from aqueous solutions onto almond shell (Prunus dulcis) as a low cost biosorbent, Desalination, 252, 2010, 81–87.

[40] D. Balarak, J. Jaafari, G. Hassani, Y. Mahdavi, I. Tyagi, S. Agarwal, V.K. Gupta, The use of low-cost adsorbent (Canola residues) for the adsorption of methylene blue from aqueous solution: isotherm, kinetic and thermodynamic studies, Colloid Interface Sci Commun, 7, 2015, 16–19.

[41] Y. Yao, F. Xu, M. Chen, Z. Xu, Z. Zhu, Adsorption behavior of methylene blue dye on carbon nanotubes, Bioresour Technol, 101(9), 2010, 3040–3046.

[42] T.S. Natarajan, H.C. Bajaj, R.J. Tayade, Preferential adsorption behavior of methylene blue dye onto surface hydroxyl group enriched TiO2 nanotube and its photocatalytic regeneration, J Colloid Interface Sci, 433, 2014, 104–114.

[43] J. Feng, Y. Wang, L. Zou, B. Li, X. He, Y. Ren, Y. Lv, Z. Fan, Synthesis of magnetic ZnO/ZnFe2O4 by a microwave combustion method, and its high rate of adsorption of methylene blue, J Colloid Interface Sci, 438, 2015, 318–322.

[44] R. Gong, M. Li, C. Yang, Y. Sun, J. Chen, Removal of cationic dyes from aqueous solution by adsorption on peanut hull, J Hazard Mater, 121(1–3), 2005, 247–250.

[45] S. Karagoz, T. Tay, S. Ucar, M. Erdem, Activated carbons from waste biomass by sulfuric acid activation and their use on methylene blue adsorption, Bioresour Technol, 99(14), 2008, 6214–6222.

[46] S. Yao, H. Lai, Z. Shi, Biosorption of methyl blue onto tartaric acid modified wheat bran from aqueous solution, Iranian J Environ Health Sci Eng, 9(1), 2012, 16.

[47] L. Sun, D. Chen, S. Wan, Z. Yu, Performance, kinetics, and equilibrium of methylene blue adsorption on biochar derived from eucalyptus saw dust modified with citric, tartaric, and acetic acids, Bioresour Technol, 198, 2015, 300–308.

[48] G. Annadurai, R.-S. Juang, D.-J. Lee, Use of cellulose-based wastes for adsorption of dyes from aqueous solutions, J Hazard Mater, 92(3), 2002, 263–274.

[49] F.A. Batzias, D.K. Sidiras, Dye adsorption by calcium chloride treated beech sawdust in batch and fixed-bed systems, J Hazard Mater, 114(1–3), 2004, 167–174.

[50] G. Crini, H.N. Peindy, F. Gimbert, C. Robert, Removal of C.I. basic green 4 (malachite green) from aqueous solutions by adsorption using cyclodextrin-based adsorbent: Kinetic and equilibrium studies, Sep Sci Technol, 53, 2007, 97–110.

[51] Y. Ozdemir, M. Dogan, M. Alkan, Adsorption of cationic dyes from aqueous solutions by sepiolite, Micropor Mesopor Mat, 96, 2006, 419–427.

[52] N. Tekin, O. Demirbas, M. Alkan, Adsorption of cationic polyacrylamide onto kaolinite, Micropor Mesopor Mat, 85 (3), 2005, 340–350.

Turkish Journal of

Analytical Chemistry

www.turkjac.org
2019

TurkJAC

Biosynthesis and characterization of α-FeOOH nanoparticles using Isabella grape (*Vitis labrusca* L.) extract

Huseyin Ozcan[1] (iD), Aslihan Dalmaz[2] (iD), Mesut Ozdincer[3] (iD), Kubra Zenkin[1] (iD), Sefa Durmus[4*] (iD)

[1] Düzce University, Graduate Education Institute, Department of Chemistry, 81620, Düzce, Türkiye
[2] Düzce University, Graduate Education Institute, Department of Natural and Herbal Products/Cosmetic Products, 81620, Düzce, Türkiye
[3] Düzce University, Graduate Education Institute, Department of Composite-Materials, 81620, Düzce, Türkiye
[4] Düzce University, Faculty of Art and Science, Department of Chemistry, 81620, Düzce, Türkiye

Abstract

The advancement of environmentally sustainable and eco-friendly approaches to nanoparticle synthesis has gained significant importance in analytical chemistry. This research examined the green synthesis of iron oxyhydroxide nanoparticles, utilizing *Vitis labrusca* L. (Isabella grape) extract as both a reducing and stabilizing agent. The application of this natural extract offers an environmentally friendly alternative to conventional chemical synthesis techniques and is expected to meet the growing demand for sustainable applications. The synthesized iron oxyhydroxide nanoparticles were characterized using advanced techniques, including X-ray diffraction, scanning electron microscopy, energy-dispersive X-ray analysis and fourier transform infrared spectroscopy, to verify their composition and structure. The findings reveal the successful synthesis of iron oxyhydroxide nanoparticles with a uniform size distribution and excellent stability.

Keywords: *Vitis labrusca* L., α-FeOOH, nanoparticle, biosynthesis

1. Introduction

Nanotechnology has made great advances in recent years, with applications in medicine, chemistry, biotechnology, and has become a field that is attracting attention [1,2]. Nanoparticles are one of the basic units of nanotechnology, and have great potential in various applications [3]. Nano-sized particles are particularly attractive thanks to their high surface-to-volume ratios. Nanoparticles can be more reactive than other materials due to the fact that the atoms on the surface are more active than those in the center. With these unique and unusual physical and chemical properties, metal oxide nanoparticles offer new opportunities in nanoscale science [4–10]. Among metal oxide nanoparticles, iron-based nanoparticles are of great interest given the wide range of applications [11,12]. With applications as diverse as magnetic recording devices [13], ferrofluids [14], drug delivery systems, magnetic resonance imaging [15,16], and paint pigments, iron oxides are remarkable. In addition, it is desirable for nanoparticles that are used in biological applications to have superparamagnetic properties. Magnetic properties of particles change

depending on particle size. In this sense, the synthesis of particles of the desired size gains importance in terms of application areas.

Among iron compounds, α-FeOOH nanoparticles (goethite, iron oxyhydroxide) are used in various technical applications such as pigment industries, environmental remediation and medical supplements. The α-FeOOH nanoparticles can be particularly effective in the removal of metallic cation pollutants such as arsenic and chromium [17,18]. Additionally, α-FeOOH nanoparticles have the ability to remove fluoride from contaminated aqueous media. In addition to their high adsorption capacity, these particles can be used as an effective nanocatalyst in chemical reduction reactions. The increasing use of α-FeOOH nanoparticles in a wide range of applications has led to a growing demand for the sustainable production of these nanostructures. α-FeOOH nanoparticles are usually synthesized at high temperature, and this process can become energy consuming, and non-economical. These nanoparticles can be synthesized by physical [19], chemical [20] or

biological methods [21]. Various physical and chemical methods such as hydrothermal [22], sol-gel [23] synthesis may require special equipment, and qualified work force. In addition, they have toxic effects harmful to health. However, it has been observed that nanoparticles obtained by the green synthesis method are cost-effective, non-toxic, and biodegradable in nature [24–27]. For this reason, the production of metal oxide nanoparticles using the principles of green chemistry has become an important area of research.

Many efforts have been made to use various plant extracts for the preparation of nanoscale metal oxides [28,29]. Secondary metabolites such as phenolics, polysaccharides, and flavonoids, which possess redox capacities [29,30], play a crucial role in the synthesis of metal oxide nanoparticles. In the field of nanotechnology, the use of natural capping agents, such as *Vitis labrusca* L., has gained interest due to their perceived eco-friendliness, and biocompatibility compared to traditional synthetic surfactants, and reducing agents. *Vitis labrusca* L. extracts contain a variety of organic compounds, including flavonoids, and tannins [31,32], which have been shown to be effective in stabilizing, and reducing metal ions during the synthesis of metal oxide nanoparticles. However, it is important to acknowledge that the efficacy of *Vitis labrusca* L. as a sequestrant and reducing agent in the synthesis of metal oxide nanoparticles depends on several factors, including the extraction method, the extract concentration, and the specific type of metal oxide nanoparticle under consideration. Further research is needed to fully understand the potential of *Vitis labrusca* L. as a capping, and reducing agent in metal oxide nanoparticles synthesis. Notably, some studies have reported the successful synthesis of metal oxide nanoparticles using *Vitis labrusca* L. extract as a green reducing agent [33]. For example, Raota et al. demonstrated the synthesis of silver nanoparticles using grape pomace extract, which was evaluated for its phenolic compound content, and subsequently used as a stabilizing reducing agent [34]. The researchers also investigated the application of silver nanoparticles in the disinfection of raw wastewater.*Vitis labrusca* L., a fragrant grape found only in the Black Sea region, was chosen for its affordability, accessibility, and sustainable nature. In this work, we present a new method for the synthesis of α-FeOOH nanoparticles using *Vitis labrusca* L. as a coating, and reducing agent. The resulting nanoparticles were then characterized using a variety of techniques, including scanning electron microscopy (SEM), energy-dispersive X-ray spectroscopy (EDX), X-ray diffraction (XRD), and fourier transform infrared spectroscopy (FT-IR) analysis.

2. Materials and Methods

2.1. Chemicals and Instrumentations

All of the chemical materials used in the study were of analytical grade purity and were used without any purification. $Fe(NO_3)_3.9H_2O$ and NaOH were obtained from Merck company. In this study, the *Vitis labrusca* L., which was used as a reducing agent, was obtained from Duzce at the time of harvest. The image of *Vitis labrusca* L. is shown in Fig. 1.

Figure 1. Image of *Vitis labrusca* L.

FT-IR spectroscopy results were recorded using a Perkin Elmer Spectra Two UATR FT-IR spectrophotometer. Scanning electron microscopy (FEI Quanta FEG 250) was employed to determine the size, and morphology of nanoparticles, while energy dispersive X-ray analysis was utilized to determine their elemental composition. The X-ray diffraction pattern of nanoparticles was obtained using a Bruker D8 Discover instrument with Cu-Kα radiation (1.5406 Å). The maximum peaks in the XRD patterns of the nanoparticles were matched with JCPDS cards.

The pH control of the reaction mixture was measured using an Isolab brand pH meter. A VWR brand centrifuge device was employed to separate the obtained product from the supernatant. The drying process of the obtained product was conducted using an Elektromag M5040P brand oven. A Heidolph brand MR Hei-Standard model magnetic stirrer was utilized to complete the dissolution process, and ensure the mixing of the solutions until the reaction was complete.
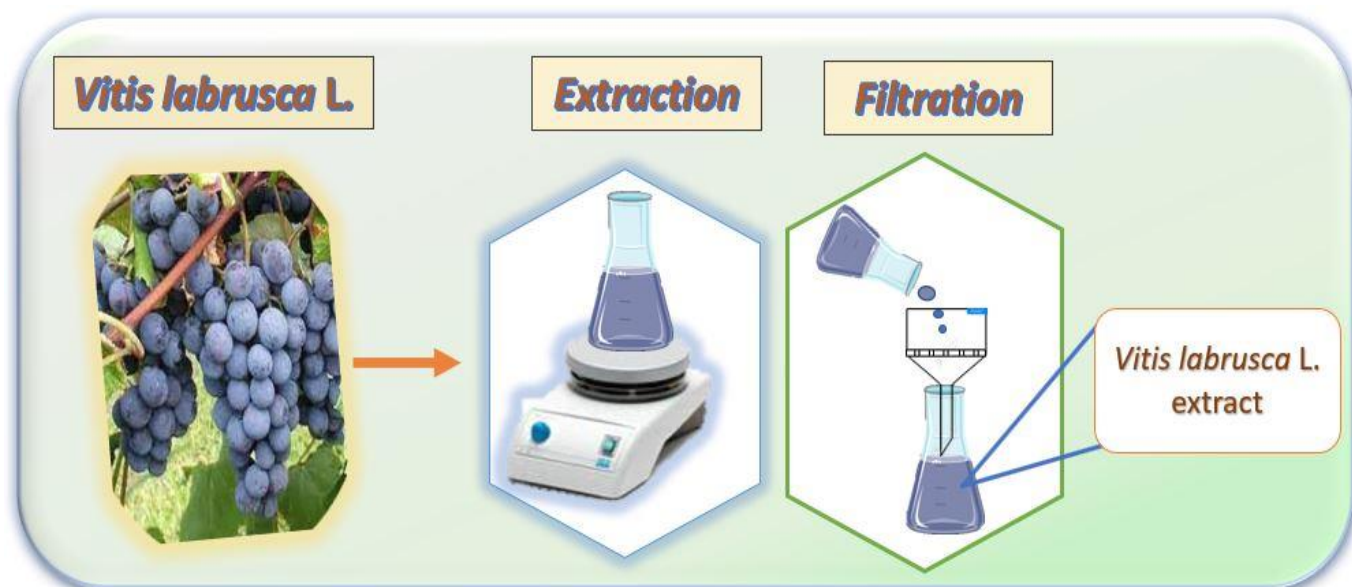
Figure 2. Representative illustration of *Vitis labrusca* L. extract preparation

The filtration processes of *Vitis labrusca* L. extract, and the product obtained were carried out using an Isolab brand vacuum pump. All weighing processes during the study were conducted using Radwag brand electronic scales.

2.2. Preparations of *Vitis labrusca* L. Extract

Vitis labrusca L. was rigorously cleaned by washing several times with deionized water to remove dust and other impurities. Then *Vitis labrusca* L. extract was prepared by boiling 20 g grapes in 250 mL deionized water in a magnetic stirrer for 90 minutes. The prepared extract was cooled, filtered through Whatman filter paper and stored in a refrigerator at 4 °C to be used in the synthesis of α-FeOOH nanoparticles (Fig. 2).

2.3. Green Synthesis of α-FeOOH Nanoparticles

A solution of 2,8 g $Fe(NO_3)_3.9H_2O$ salt in deionized water was added to 25 mL of *Vitis labrusca* L. extract, the temperature of which was kept constant at 60 °C. Then the pH of the solution was adjusted to 8 with 0.1 M NaOH. It was mixed with a magnetic stirrer for one hour at 60 °C and a completely homogeneous mixture was obtained. The obtained homogeneous mixture was centrifuged at 5000 rpm for 5 minutes, and then washed several times with deionized water. The obtained product was left to dry in an oven at 70 °C for 24 hours and then calcined at 550 °C for 3 hours. The resulting dark brown α-FeOOH nanoparticles were stored in a desiccator.
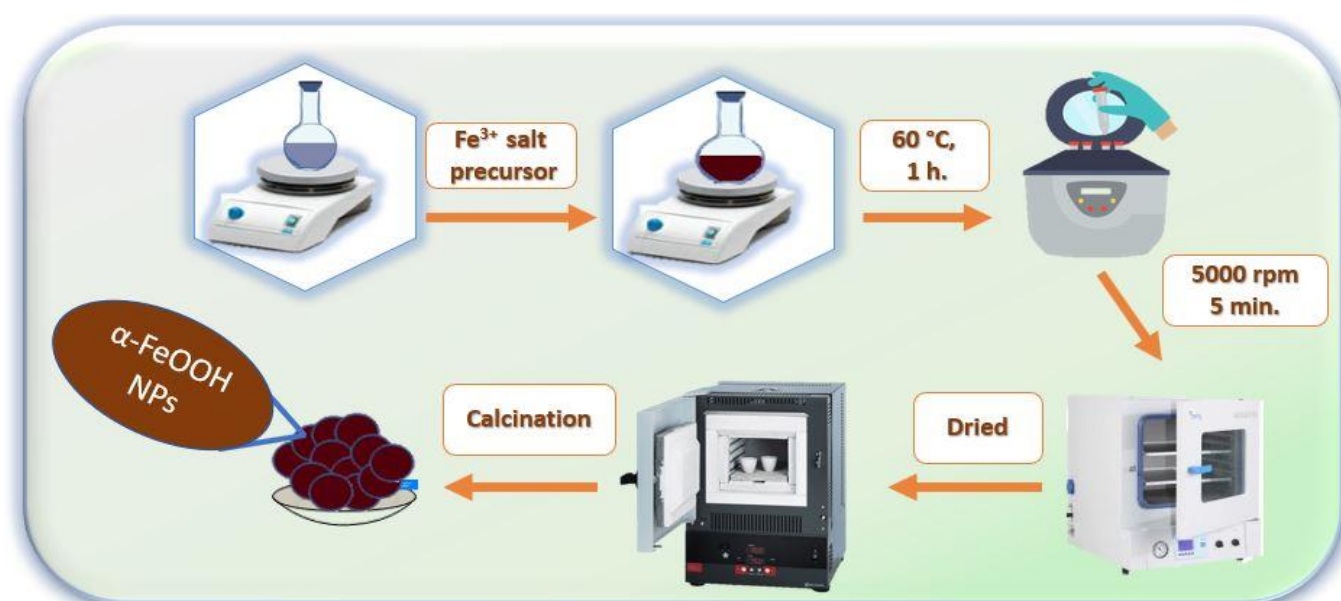

Figure 3. Schematic representation for green synthesis of α-FeOOH nanoparticles

3. Results and Discussion

3.1. FT-IR spectra

3.1.1. *Vitis labrusca L. Extract*

FT-IR spectroscopy analysis was performed to investigate the presence of functional biomolecule groups in *Vitis labrusca* L. extract and synthesized metal oxide nanoparticles. When the FT-IR spectrum of *Vitis labrusca* L. shown in Fig. 4 is examined, the band seen at 3283 cm^{-1} is due to O-H stretching vibrations in the structure of polyphenols. The asymmetric C-H stretching vibration of -CH_3 groups in the structure of biomolecules was observed at 2932 cm^{-1} and the peak of the carbonyl (C=O) functional group was observed at 1720 cm^{-1}. The peak observed at 1604 cm^{-1} in the FT-IR spectrum indicates the presence of the O-H group in the structure of water. Furthermore, the peaks corresponding to aliphatic C-H stretching and CH_3 symmetrical bending vibrations are observed at 1408 cm^{-1} and 1343 cm^{-1}, respectively. The C-O stretch vibration of hydroxy flavonoids in the biostructure of *Vitis labrusca* L. is observed at 1251 cm^{-1}, while the band at 1026 cm^{-1} corresponds to the C-O stretch of primary alcohols. Besides, the vibration of the C=O bending band in the structure of fatty acids was observed at 917 cm^{-1}[35]. In addition, the absorption bands shown at 865, 815 and 776 cm^{-1} can be assigned to the =C-H flexure, which is consistent with the polyphenolic or flavonoid compounds present in the extract [36].

3.1.2. *α-FeOOH Nanoparticles*

The FT-IR spectrum of α-FeOOH nanoparticles is given in Fig. 4. In the FT-IR spectrum of α-FeOOH nanoparticles, vibrations at 3168, 1590, 1375, 800, 700, 548 and 397 cm^{-1} were noted. The 3168 cm^{-1} vibration is attributed to the O-H group stretching vibrations of polyphenols found in the *Vitis labrusca* L. plant extract, while the 1575 cm^{-1} vibration corresponds to carbonyl group vibrations of the same polyphenols. Additionally, the in-plane bending vibration at 891 cm^{-1} and the out-of-plane bending vibration at 794 cm^{-1} are specific to the Fe-OH bending vibration of the goethite particles. It is worth noting that the thermal transformation from goethite to hematite results in hematite characteristic vibrations at 533 and 454 cm^{-1}, which have been previously reported for similar findings in goethite [37].

3.2. XRD Analysis

In the XRD pattern of α-FeOOH nanoparticles as shown in Fig. 5, distinct peaks were observed at 2θ=22.42°, 34.08°, 36.78°, 39.72°, 44.82° and 59.39°. These peaks were interrelated to (110), (130), (111), (200), (131) and (151) hkl planes. All these diffraction peaks are consisted to orthorhombic goethite compatible with JCPDS Card No. 29-0713 and space group $P2_1nm$. The cell parameters of the α-FeOOH nanoparticles a= 4.61 Å, b = 9.95 Å and c = 3.02 Å as shown in Table 1. Since there are no different peaks in the substance, the product does not contain impurities [38].
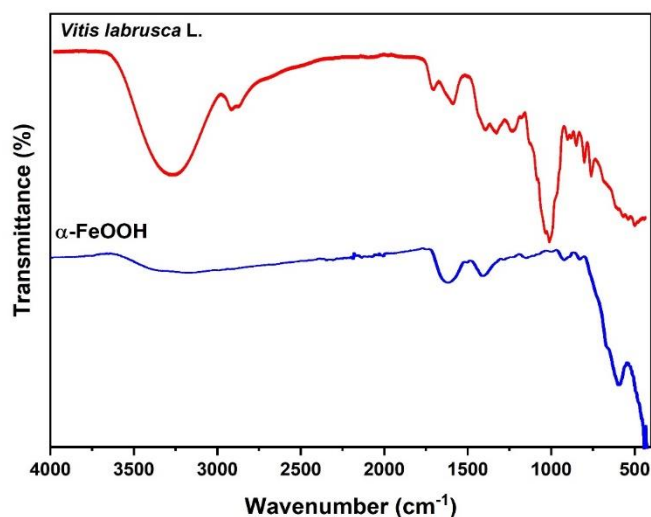

Figure 4. FT-IR spectra of dry *Vitis labrusca* L. extract and α-FeOOH nanoparticles

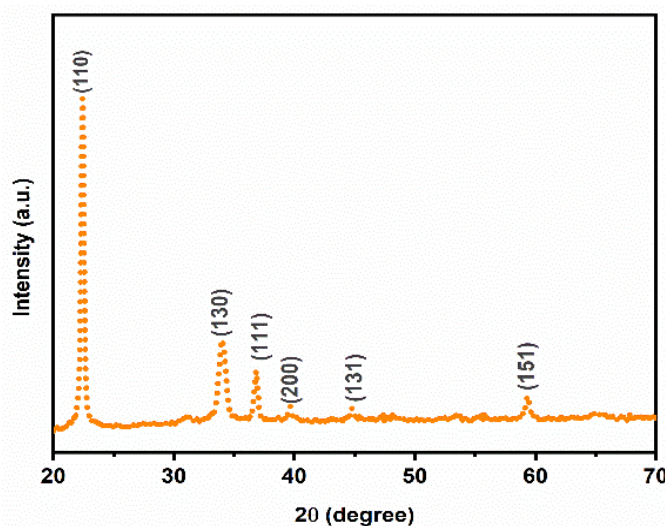**Figure 5.** Powder XRD pattern and illustration of the crystal structure of α-FeOOH nanoparticles

Table 1. The structural parameters of the prepared α-FeOOH nanoparticles obtained from XRD analysis

Sample	JCPDS Card no:	Crystal Structure	Space Group	Lattice Parameters (Å)	Cell Volume (Å³)	Distance (Å)
α-FeOOH	29-0713	Orthorhombic	$P2_1nm$	a= 4.61 b= 9.95 c= 3.02	138.52	Fe1-Fe2= 2.32 Fe1-O1= 2.04 Fe2-O1= 2.06 Fe2-H1= 1.69 O1-H1= 1.22

3.3. SEM-EDX Analysis

The basic composition of the synthesized materials is determined by EDX, a microanalytical technique used in conjunction with SEM. EDX detects X-rays emitted by the sample as a result of electrons bombarding the material surface. The measurement of density and energy provides information on chemical composition. The EDX spectrum for each energy level shows the frequency of X-rays as counts. By determining the intensity of the peak, information about the amount of the element in the sample is obtained.

A morphological analysis of goethite by SEM in Fig. 6 showed that it was composed of agglomerated pseudo-spheres with a spongy appearance, consistent with its low crystallinity [39]. The size of the nanoparticles is in the range of 20–38 nm. When the EDX analysis result of α-FeOOH nanoparticles was examined, the main iron peaks were located at approximately 0.75 keV, 6.5 keV and 7.2 keV. The peak corresponding to oxygen was observed at 0.5 keV (Fig. 7). The peak corresponding to oxygen was observed at 0.5 keV. The atomic percentages of oxygen and iron elements without any impurities were found to be 40.05/59.95 [40].
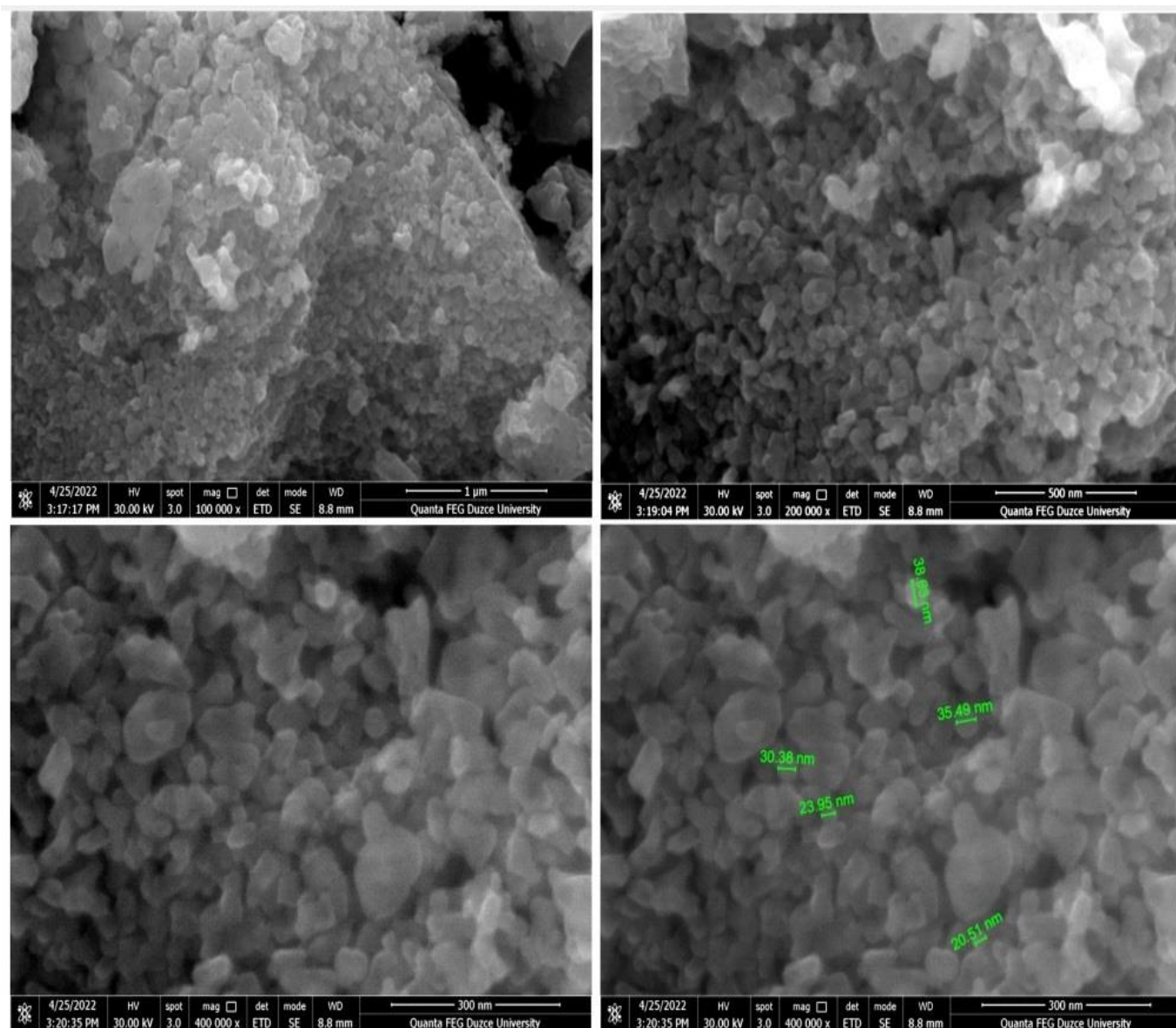
Figure 6. SEM images of the synthesized α-FeOOH nanoparticles, observed at various magnification levels
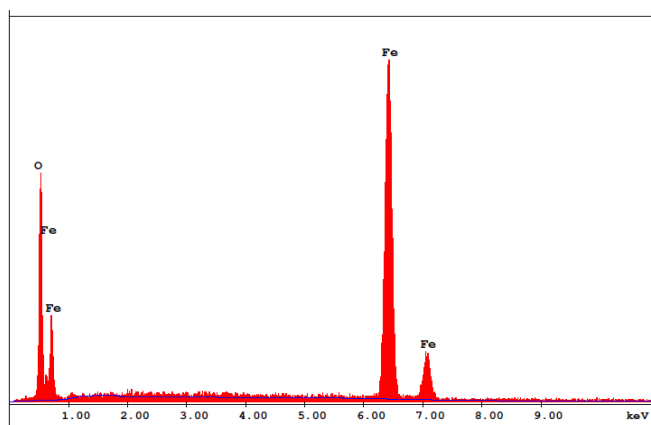
Figure 7. EDX spectrum of α-FeOOH nanoparticles

4. Conclusions

In summary, the aqueous extract of *Vitis labrusca* L. serves as an excellent reducing and stabilising agent for the synthesis of α-FeOOH nanoparticles. The growing interest in green chemistry approaches stems from their resource efficiency and eco-friendliness. Moreover, green-synthesized nanoparticles are devoid of harmful byproducts, making them suitable for biomedical and biotechnological applications. In this study, we successfully synthesized α-FeOOH nanoparticles using a green method mediated by the aqueous extract of *Vitis labrusca* L. We employed FT-IR, XRD, and SEM-EDX analyses to characterize the synthesized α-FeOOH nanoparticles. The FT-IR and XRD results confirmed the purity of the synthesized α-FeOOH nanoparticles, without the presence of other iron compounds. SEM-EDX analysis revealed that the α-FeOOH nanoparticles have a pseudo-spherical structure and fall within the size range of 20–38 nm. This study serves as a valuable reference for the preparation of environmentally friendly, cost-effective, and high-yield α-FeOOH nanoparticles with strong adsorption capacity for analytical applications.

Acknowledgement

References

[1] S. Nimesh, Nanotechnology: an introduction, Gene Therapy, 2013, USA, Elsevier.

[2] A. Afkhami, T. Madrakian, M. Ahmadi, Chapter 3 - Nanotechnology and analytical chemistry, Analytical Nanochemistry, 2023, İndia, Elsevier.

[3] A. Thakur, P. Thakur, S.M.P. Khurana, Synthesis and applications of nanoparticles, 2022, Singapore, Springer Nature Singapore.

[4] P.G. Jamkhande, N.W. Ghule, A.H. Bamer, M.G. Kalaskar, Metal nanoparticles synthesis: An overview on methods of preparation, advantages and disadvantages, and applications, J Drug Deliv Sci Technol, 53, 2019, 101174.

[5] D. Gnanasangeetha, M. Suresh, A review on green synthesis of metal and metal oxide nanoparticles, Nat Environ Pollut Technol, 19, 2020, 1789-1800.

[6] M.S. Chavali, M.P. Nikolova, Metal oxide nanoparticles and their applications in nanotechnology, SN Appl Sci, 1(6), 2019.

[7] S. Durmus, A. Dalmaz, M. Ozdincer, S. Sivrikaya, Preparation of cerium oxide nanoparticles: an efficient catalyst to the synthesis of dimeric disulphide Schiff bases, CBU J of Sci, 13 (1), 2017, 25-30.

[8] A. Dalmaz, S. Durmuş, G. Dülger, M. Alpay, Thio-Schiff bases derived from 2,2'-disulfanedianiline via nanocerium oxide: antimicrobial effect and antiproliferative effects in melanoma cells, Turk J Chem, 46, 2022, 1055–1068.

[9] A. Dalmaz, S. Durmuş, G. Dulger, B. Dülger, Synthesis and characterization of dimeric thio-Schiff bases by nano cerium oxide and examination of their antimicrobial activities, SAUJS, 25, 2021, 364–378.

[10] S. Durmus, A. Dalmaz, E. Calıskan, G. Dulger, Synthesis and characterization of disulfide-Schiff base derivatives and in vitro investigation of their antibacterial activity against multidrug-resistant acinetobacter baumannii isolates: a new study, Russ J Gen Chem, 88, 2018, 305–311.

[11] L. Dong, G. Chen, G. Liu, X. Huang, X.M. Xu, L. Li, Y. Zhang, J. Wang, M. Jin, D. Xu, A.M. Abd El-Aty, A review on recent advances in the applications of composite Fe_3O_4 magnetic nanoparticles in the food industry, Crit Rev Food Sci Nutr, 2022, 1-29.

[12] M. Özdinçer, S. Durmuş, A. Dalmaz, Magnetic spinel-type $CoFe_2O_4$ nanoparticles: synthesis and investigation of structural, morphological properties, SDU Fen Bilimleri Enstitüsü Dergisi, 21, 2017, 311.

[13] I. Dumitru, O.F. Caltun, Ferrites use in magnetic recording, in: Ferrite Nanostructured Magnetic Materials, Elsevier, 2023, 733–745.

[14] M. Imran, A.A. Chaudhary, S. Ahmed, Md.M. Alam, A. Khan, N. Zouli, J. Hakami, H.A. Rudayni, S.-U.-D. Khan, Iron oxide nanoparticle-based ferro-nanofluids for advanced technological applications, Molecules, 27, 2022, 7931.

[15] Y. Li, L. Wang, A. Orza, H. Mao, Iron oxide nanoparticles for magnetic resonance imaging, Encyclopedia of Nanomaterials, 3, 2023, 356–373.

[16] L. Chen, J. Xie, H. Wu, F. Zang, M. Ma, Z. Hua, N. Gu, Y. Zhang, Improving sensitivity of magnetic resonance imaging by using a dual-targeted magnetic iron oxide nanoprobe, Colloids Surf B Biointerfaces, 161, 2018, 339–346.

[17] S.R. Safi, K. Senmoto, T. Gotoh, T. Iizawa, S. Nakai, The effect of γ-FeOOH on enhancing arsenic adsorption from groundwater with DMAPAAQ + FeOOH gel composite, Sci Rep, 9, 2019, 11909.

[18] N. Guo, X. Lv, Q. Li, T. Ren, H. Song, Q. Yang, Removal of hexavalent chromium from aqueous solution by mesoporous α-FeOOH nanoparticles: Performance and mechanism, Microporous Mesoporous Mater, 299, 2020, 110101.

[19] L. Krishnia, P. Thakur, A. Thakur, Synthesis of nanoparticles by physical route, in: synthesis and applications of nanoparticles, 2022, Singapore, Springer Nature Singapore.

[20] S. Taneja, P. Punia, P. Thakur, A. Thakur, Synthesis of nanomaterials by chemical route, in: synthesis and applications of nanoparticles, 2022, Singapore, Springer Nature Singapore.

[21] A. Thakur, D. Chahar, P. Thakur, Synthesis of nanomaterials by biological route, in: synthesis and applications of nanoparticles, 2022, Singapore, Springer Nature Singapore.

[22] X. Liu, G. Qiu, A. Yan, Z. Wang, X. Li, Hydrothermal synthesis and characterization of α-FeOOH and α-Fe_2O_3 uniform nanocrystallines, J Alloys Compd, 433, 2007, 216–220.

[23] M.A. Dar, S.K. Kulkarni, Z.A. Ansari, S.G. Ansari, H.-S. Shin, Preparation and characterization of α-FeOOH and α-Fe_2O_3 by sol–gel method, J Mater Sci, 40, 2005, 3031–3034.

[24] A. Gour, N.K. Jain, Advances in green synthesis of nanoparticles, Artif Cells Nanomed Biotechnol, 47, 2019, 844–851.

[25] N.A.I. M. Ishak, S.K. Kamarudin, S.N. Timmiati, Green synthesis of metal and metal oxide nanoparticles via plant extracts: an overview, Mater Res Express, 6, 2019, 112004.

[26] M. Kaur, A. Gautam, P. Guleria, K. Singh, V. Kumar, Green synthesis of metal nanoparticles and their environmental applications, Curr Opin Environ Sci Health, 29, 2022, 100390.

[27] R. Bekem, S. Durmuş, A. Dalmaz, G. Dulger, *Agaricus bisporus* ekstraktı kullanılarak Zno nanopartiküllerinin yeşil sentezi: yapısal karakterizasyonu ve biyolojik aktivitelerinin incelenmesi, Düzce Üniversitesi Bilim ve Teknoloji Dergisi, 11, 2023, 551–562.

[28] S. Marouzi, Z. Sabouri, M. Darroudi, Greener synthesis and medical applications of metal oxide nanoparticles, Ceram Int, 47, 2021, 19632–19650.

[29] L. Soltys, O. Olkhovyy, T. Tatarchuk, M. Naushad, Green synthesis of metal and metal oxide nanoparticles: Principles of green chemistry and raw materials, Magnetochemistry. 7, 2021, 145.

[30] M. Jamzad, B. Mokhtari, P.S. Mirkhani, Green synthesis of metal nanoparticles mediated by a versatile medicinal plant extract, Chemical Papers, 2022.

[31] H. Tahmaz, D.Y. Kusku, G. Soylemezoglu, H. Celik, Phenolic compound and antioxidant capacity contents of *Vitis labrusca* L. genotypes, J Tekirdag Agricultural Faculty, 19, 2022, 318–331.

[32] S. Aydın, C. Demir Gökışık, Total phenolic and flavonoid contents and antioxidant capacity of home-made Isabella grape (Vitis labrusca L.) vinegar, Int J Chem Technol, 3, 2019, 11–16.

[33] A. Shamaa Anjum, A. Rajasekar, S. Rajeshkumar, Synthesis and characterization of grape seed mediated titanium dioxide nanoparticles: An in vitro study, Plant Cell Biotechnol Mol Biol, 21, 2020, 17–23.

[34] C.S. Raota, A.F. Cerbaro, M. Salvador, A.P.L. Delamare, S. Echeverrigaray, J. Da Silva Crespo, T.B. Da Silva, M. Giovanela, Green synthesis of silver nanoparticles using an extract of Ives cultivar (Vitis labrusca) pomace: Characterization and application in wastewater disinfection, J Environ Chem Eng, 7, 2019.

[35] N.H. Arbain, J. Salimon, Synthesis and characterization of ester trimethylolpropane based jatropha curcas oil as biolubricant base stocks, J Sci Technol, 2(2), 2010.

[36] M.R. Kamli, E.A. Alzahrani, S.M. Albukhari, A. Ahmad, J.S.M. Sabir, M.A. Malik, Combination effect of novel bimetallic Ag-Ni nanoparticles with fluconazole against candida albicans, J Fungi, 8, 2022, 733.

[37] H.D. Ruan, R.L. Frost, J.T. Kloprogge, L. Duong, Infrared spectroscopy of goethite dehydroxylation: III. FT-IR microscopy of in situ study of the thermal transformation of goethite to hematite, Spectrochim Acta A Mol Biomol Spectrosc, 58, 2002, 967–981.

[38] J.Z. Marinho, R.H.O. Montes, A.P. de Moura, E. Longo, J.A. Varela, R.A.A. Munoz, R.C. Lima, Rapid preparation of α-FeOOH and α-Fe$_2$O$_3$ nanostructures by microwave heating and their application in electrochemical sensors, Mater Res Bull, 49, 2014, 572–576.

[39] D. Alonso-Domínguez, M. Pico, I. Álvarez-Serrano, M. López, New Fe$_2$O$_3$-Clay@C nanocomposite anodes for li-ion batteries obtained by facile hydrothermal processes, Nanomaterials, 8, 2018, 808.

[40] H. Gupta, R. Kumar, H.-S. Park, B.-H. Jeon, Photocatalytic efficiency of iron oxide nanoparticles for the degradation of priority pollutant anthracene, Geosystem Engineering, 20, 2017, 21–27.

A "Turn-off" fluorescence sensor for Fe²⁺, Fe³⁺, and Cu²⁺ ions based on novel pyrene-functionalized chitosan

İpek Ömeroğlu* (iD), Vildan Şanko (iD)

Gebze Technical University, Faculty of Science, Department of Chemistry, 41400, Kocaeli, Türkiye

Abstract

The detection of iron and copper ions is very important for environmental and biological processes. In this work, a novel pyrene-functionalized Schiff base chitosan (**Chit-Pyr**) was synthesized, and this hybrid material was used as a "turn-off" fluorescence sensor for the detection of Fe²⁺, Fe³⁺, and Cu²⁺ ions. FTIR, UV-Vis, TGA, and SEM were used to examine for structural, thermal, and morphological properties of **Chit-Pyr**. This sensor exhibited a selectivity towards Fe²⁺, Fe³⁺, and Cu²⁺ ions among several common metal cations in the DMF dispersion. The results showed that the proposed "turn-off" fluorescence sensing mechanism of **Chit-Pyr** was simple and sensitive for the determination of Fe²⁺, Fe³⁺, and Cu²⁺ ions.

Keywords: Fluorescence sensor, iron and copper, chitosan, pyrene

1. Introduction

Improving sensors for the detection and determination of transition metal ions is very important for environmental and biological processes [1]. Iron and copper ions, which are biological metals, play significant roles in these processes [2–4]. Iron exists in the form of ferrous (Fe²⁺) and ferric (Fe³⁺) ions and is indispensable in physiological processes such as oxygen binding, respiration, and enzymatic reactions [5–8]. Although it is of great importance in physiological processes, iron deficiency causes diabetes, anemia, liver, heart, and kidney damage, and iron accumulation causes serious diseases such as cancer, Parkinson's, and Alzheimer's [9–11]. Copper is the third most abundant transition metal in the human body, and excess copper in the human body causes diseases such as vomiting, increased blood pressure and respiratory rate, acute hemolytic anemia, and liver damage [12]. Therefore, it is very important to improve simple, sensitive, fast, cost-effective, and portable alternating for metal ion definition [13]. Many analytical techniques such as high-performance liquid chromatography (HPLC), anodic stripping voltammetry, inductively coupled plasma-mass spectrometry (ICP-MS), and atomic absorption spectrometry (AAS) have been improved for the definition of iron and copper [14–21]. In addition to

traditional analytical methods, fluorescence probes have been widely used in recent years for the detection of any analyte [22]. Fluorescence probes are of great interest for applications such as optical imaging and analytical sensing due to their high sensitivity, simplicity, and fast response times [23]. Fluorescence detection, which has turned into an effective tool for real-time detection and monitoring of biological species and physiological processes, is non-invasive, well-operative, and extremely susceptible [24].

Biopolymers, which can be divided into natural and synthetic based on their origin, are long chain-like molecules containing repeating monomer units that are environmentally degradable [25,26]. Cellulose, chitosan, and chitin are polysaccharide derivative biopolymers in the natural biopolymer class [27]. Chitosan, the second most abundant biopolymer on Earth after cellulose, is a polycationic polysaccharide derived from chitin, consisting of *N*-acetyl-d-glucosamine units linked by β-(1,4)-glycosidic bonds [28,29]. It is soluble in aqueous solutions such as acetic acid and lactic acid, and its solubility depends on the degree of deacetylation (DD) and molecular weight [30]. It is used in many applications due to its non-toxic, low-cost, versatility,

biodegradability, biocompatibility, digestibility, antibacterial, anti-tumor, hemostatic, and antioxidant properties [31–34]. Chitosan has shortcomings such as low mechanical properties, thermal stability, and high sensitivity to moisture. To overcome these shortages, chitosan is functionalized using physical, chemical, and biological modification methods [30]. Also, in fluorescence sensor applications, the fact that it does not have fluorescence properties requires modification with new groups.

Pyrene, one of the polyaromatic hydrocarbon family, is widely used as a fluorescence probe in many applications. It is well-known that pyrene and its derivatives show both monomeric and excimer fluorescence emission [35]. The pyrene displays the monomer emission wavelength in the range of ~380–410 nm and the excimer emission wavelength in the range of ~450–500 nm [36]. The formation of the excimer causes the emission wavelength of the pyrene compound to exhibit a bathochromic shift to a longer wavelength [37]. Excimer emission of pyrene due to interactions between pyrene units, one of which is excited, both in the solution and in the solid state under different conditions, may result from an intermolecular or intramolecular process [38]. Although pyrene-modified chitosan biopolymers have been reported in the literature, they differ from our study in terms of synthesis and application. Jatunov *et al.* synthesized a biopolymer expressing molecules with different physicochemical properties by adding equimolar amounts of aldehydes (4-*N,N*-diphenylaminobenzaldehyde, 4-*N,N*-dimethylamino-1-naphthaldehyde, and 1-pyrenecarboxaldehyde) to a methanolic suspension of chitosan [39]. Franconetti *et al.* developed aromatic and heteroaromatic aldehydes with malononitrile, a symmetric active methylene compound. Then, the catalytic activities of organocatalysts, chitosan hydrogel beads, and hydrogel disks formed by ureidyl-chitosan derivatives were evaluated as a function of pH, temperature, and catalyst concentration [40]. Sirajunnisa *et al.* synthesized the β-amino derivative of lawsone using chitosan and 1-pyrenecarboxaldehyde *via* the Mannich reaction. Also, they prepared quaternization of a Mannich base and following intercalation into bentonite clay produced the organic-inorganic hybrid systems [41]. However, as far as we know 1-pyrenecarboxaldehyde-modified chitosan prepared as a fluorescence sensor for the detection of metal ions is not yet available in the literature. In addition, chitosan and its derivatives are used in the fluorometric determination of various analytes. Although chitosan compound containing 1-pyrenecarboxaldehyde is not available in the literature, these biopolymers containing different fluorescent groups are used as a fluorescence sensor for the detection of metal ions [42–44].

In this work, novel pyrene-functionalized Schiff base chitosan was synthesized as a "turn-off" fluorescence determination of Fe^{2+}, Fe^{3+}, and Cu^{2+} ions. The characterization, morphological, and thermal properties of **Chit-Pyr** were investigated by FTIR, SEM, and TGA. The photophysical and fluorescence sensor properties were measured by UV-Vis and fluorescence spectroscopies. Also, the change of color was observed by adding Fe^{2+} and Fe^{3+} ions to the dispersion of **Chit-Pyr** in DMF. As a result, new photophysical, thermal, and morphological properties were gained to the biopolymer by functionalizing the chitosan with the pyrene compound.

2. Experimental

2.1. Materials and equipments

Chitosan, 1-pyrenecarboxaldehyde, glacial acetic acid, absolute ethanol (EtOH), dichloromethane (DCM), tetrahydrofuran (THF), acetonitrile (ACN), dimethyl sulfoxide (DMSO), dimethylformamide (DMF), $AgNO_3$, $BaCl_2$, $CaCl_2$, $CdCl_2$, $CsCl$, $CuCl_2$, $FeCl_2$, $FeCl_3$, $HgCl_2$, KCl, $LiCl$, $MgCl_2$, $MnCl_2$, $NaCl$, $PbCl_2$, and $ZnCl_2$ metal salts were obtained from commercial suppliers. Ultrapure water (18.2 MΩ) was used for chemical reaction and sensor measurements.

Fourier-transform infrared spectroscopy (FTIR) spectra were recorded on a Perkin Elmer Spectrum 100 spectrophotometer. Scanning Electron Microscopy (FEI, Nova Nano SEM 450) was used for the analysis of surface morphological properties. Thermogravimetric analysis (TGA) was performed by Thermal Analysis System (Mettler Toledo STARe) and the heating rate was adjusted to 10 °C/min when the N_2 flow rate was kept at 50 mL/min. Absorption spectra were recorded with a Shimadzu 2101 UV-Vis spectrophotometer. Fluorescence emission spectra were obtained by a Varian Eclipse spectrofluorometer.

2.2. Synthesis of pyrene-modified chitosan (Chit-Pyr)

0.50 g of low molecular weight chitosan was dissolved in 20 mL of ultrapure water and five drops of glacial acetic acid (AcOH). It was stirred at 50 °C for two hours to completely dissolve the chitosan. Then, an excess amount of 1-pyrenecarboxaldehyde dissolved in 10 mL of ethanol was added to the reaction mixture under an inert atmosphere and refluxed for 24 hours. After that time, the reaction solvent was removed and the solid product was washed several times with THF, DCM, and ethanol to remove unreacted 1-pyrenecarboxaldehyde. The light-yellow product was dried in a vacuum oven at 55 °C.
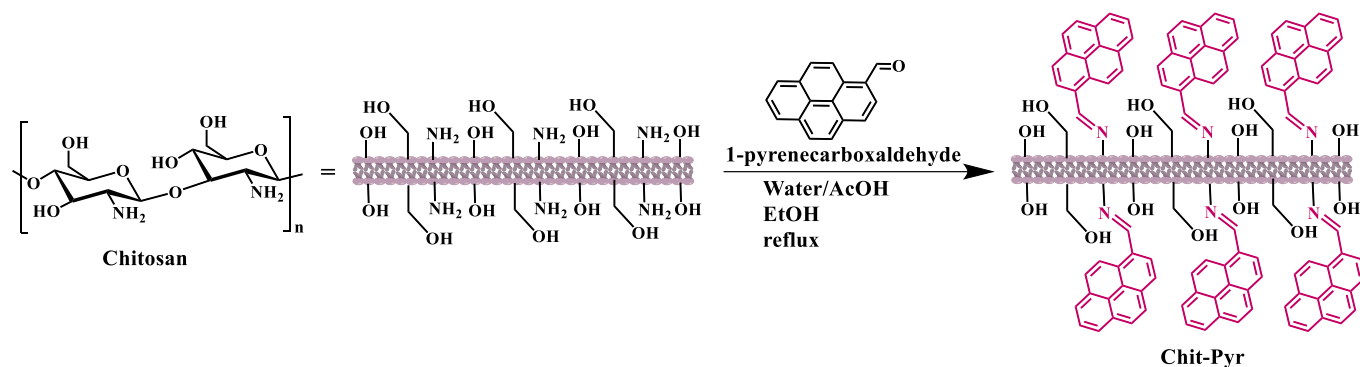
Scheme 1. The synthetic procedure of pyrene-modified chitosan (**Chit-Pyr**)

2.3. "Turn-off" fluorescence sensor measurements

Absorption and emission changes upon the addition of metal ions (Ag^+, Ba^{2+}, Ca^{2+}, Cd^{2+}, Cs^+, Cu^{2+}, Fe^{2+}, Fe^{3+}, Hg^{2+}, K^+, Li^+, Mg^{2+}, Mn^{2+}, Na^+, Pb^{2+}, Zn^{2+}) to the **Chit-Pyr** dispersion were determined using a UV-Vis and fluorescence spectrophotometer. Absorption and fluorescence emission spectra in "turn-off" fluorescence sensor measurements were performed **Chit-Pyr** in the DMF dispersion (0.4 mg/mL) at room temperature. The aqueous solutions of the metal chlorides (nitrate derivative for Ag^+ ion, 0.1 M) were used as the source of metal ions in these measurements. Spectra were routinely acquired at 25 °C in a 1 cm path-length quartz cuvette by adding 0.1 M different metal ions (Ag^+, Ba^{2+}, Ca^{2+}, Cd^{2+}, Cs^+, Cu^{2+}, Fe^{2+}, Fe^{3+}, Hg^{2+}, K^+, Li^+, Mg^{2+}, Mn^{2+}, Na^+, Pb^{2+}, Zn^{2+}) to 2 mL solution. The metal solutions used in the measurements were prepared as 0.1 M stock solutions in ultrapure water using metal salts ($AgNO_3$, $BaCl_2$, $CaCl_2$, $CdCl_2$, $CsCl$, $CuCl_2$, $FeCl_2$, $FeCl_3$, $HgCl_2$, KCl, $LiCl$, $MgCl_2$, $MnCl_2$, $NaCl$, $PbCl_2$, and $ZnCl_2$).

3. Results and discussion

3.1. Synthesis and characterization

Chitosan containing primary amine was substituted with pyrene, a fluorophore group with good photophysical properties, using a chemical modification method and utilized in the fluorescence detection platform. The pyrene-modified chitosan (**Chit-Pyr**) was synthesized *via* Schiff base reaction as a fluorescent sensor for "turn-off" fluorescence determination of Fe^{2+}, Fe^{3+}, and Cu^{2+} (Scheme 1).

The chemical, thermal, and morphological characterizations of the final product **Chit-Pyr** are given in Fig. 1.
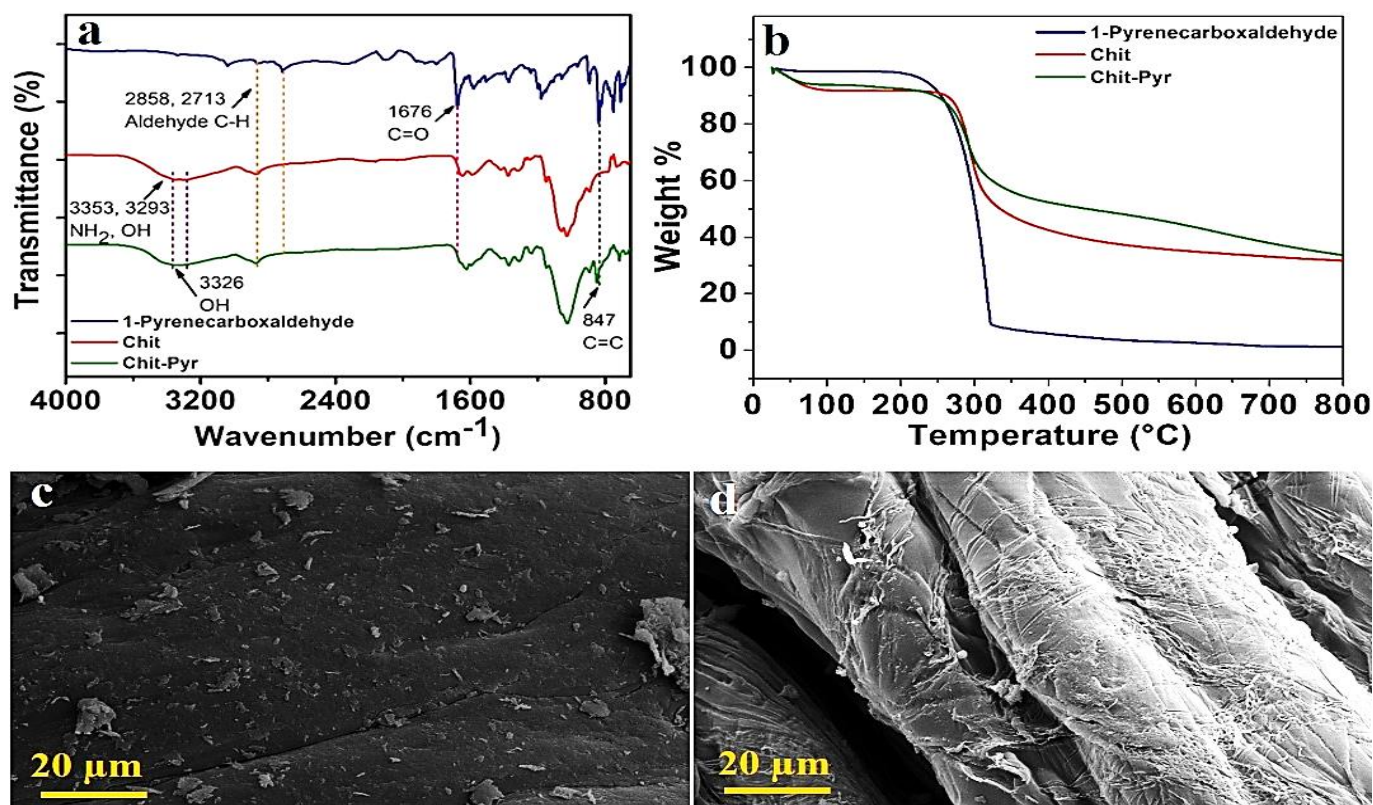

Figure 1. (a) FTIR spectra, (b) TGA diagrams of 1-pyrenecarboxaldehyde, Chit, **Chit-Pyr** and SEM images of (c) Chit and (d) **Chit-Pyr** surfaces with X1000 magnification

Also, the chemical and thermal characterizations of the starting compounds Chit and 1-pyrenecarboxaldehyde are shown in Fig. 1a–b. In the FTIR spectra (Fig. 1a), the peaks representing the 1-pyrenecarboxaldehyde structure, which is one of the starting materials, were detected by the literature. The presence of aldehyde C-H peaks at 2858–2713 cm^{-1} and C=O peak at 1676 cm^{-1} support the structure [45]. The characteristic peaks of the Chit structure, N-H and O-H peaks at 3353–3293 cm^{-1}, symmetrical and asymmetrical C-H stretching vibrations at 2880 cm^{-1}, C=O at 1657 cm^{-1} and C-O stretching vibrations at 1059 cm^{-1} confirm the structure [46]. In the FTIR spectrum of **Chit-Pyr**, which is the product obtained after modification, the peaks of chitosan are prominently present, while at the same time, the peak modification at 1623 cm^{-1} for the C-N bond vibration, which indicates the formation of Schiff base, confirms the modification [45].

Changes in the thermal properties of materials are also one of the important characterizations supporting whether the modification has taken place. Therefore, for this study, the thermal properties of the study groups were examined, and the thermal diagrams obtained are given in Fig. 1b. It has been determined that chitosan undergoes thermal decomposition at approximately 350 °C with a significant mass loss of 48%. 1-pyrenecarboxaldehyde lost about 90% of its mass at 323 °C. The temperature at which mass loss of **Chit-Pyr** was observed also showed similar characteristics with Chit. The fact that the thermal decomposition temperatures of the bonded organic group and Chit structures were very close caused the obtained product to undergo thermal decomposition at a similar temperature point. However, some variation in the percent mass loss was detected. A mass loss of 40% indicates that the thermal properties of the Chit structure increase after modification. In addition, the difference in the thermal course after the temperature range (350-800 °C) where rapid mass loss is observed supports the modification [47,48].

For morphological characterization, the images of chitosan particles before (Fig. 1c) and after (Fig. 1d) were modified with 1-pyrenecarboxaldehyde were examined. The surface of the chitosan particles appears to be smoother and relatively more homogeneous. In addition, it was determined that the surface of **Chit-Pyr** particles changed considerably to support the modification and had a rougher and non-homogeneous surface.

Normalized absorption spectra of 1-pyrenecarboxaldehyde, Chit, and **Chit-Pyr** in DMF were given in Fig. 2. As seen in Fig. 2, no apparent absorption peaks were monitored in the region of 270–570 nm in the UV-Vis absorption spectrum of Chit. After the chitosan was modified with pyrene (**Chit-Pyr**), the novel hybrid material showed a new absorption peak at 275–293 nm and 340–396 nm which were attributed to π-π* transitions of the pyrene moieties [49]. Thus, the absorption spectrum of the hybrid material (**Chit-Pyr**) confirmed that the pyrene has been modified to the chitosan surface.
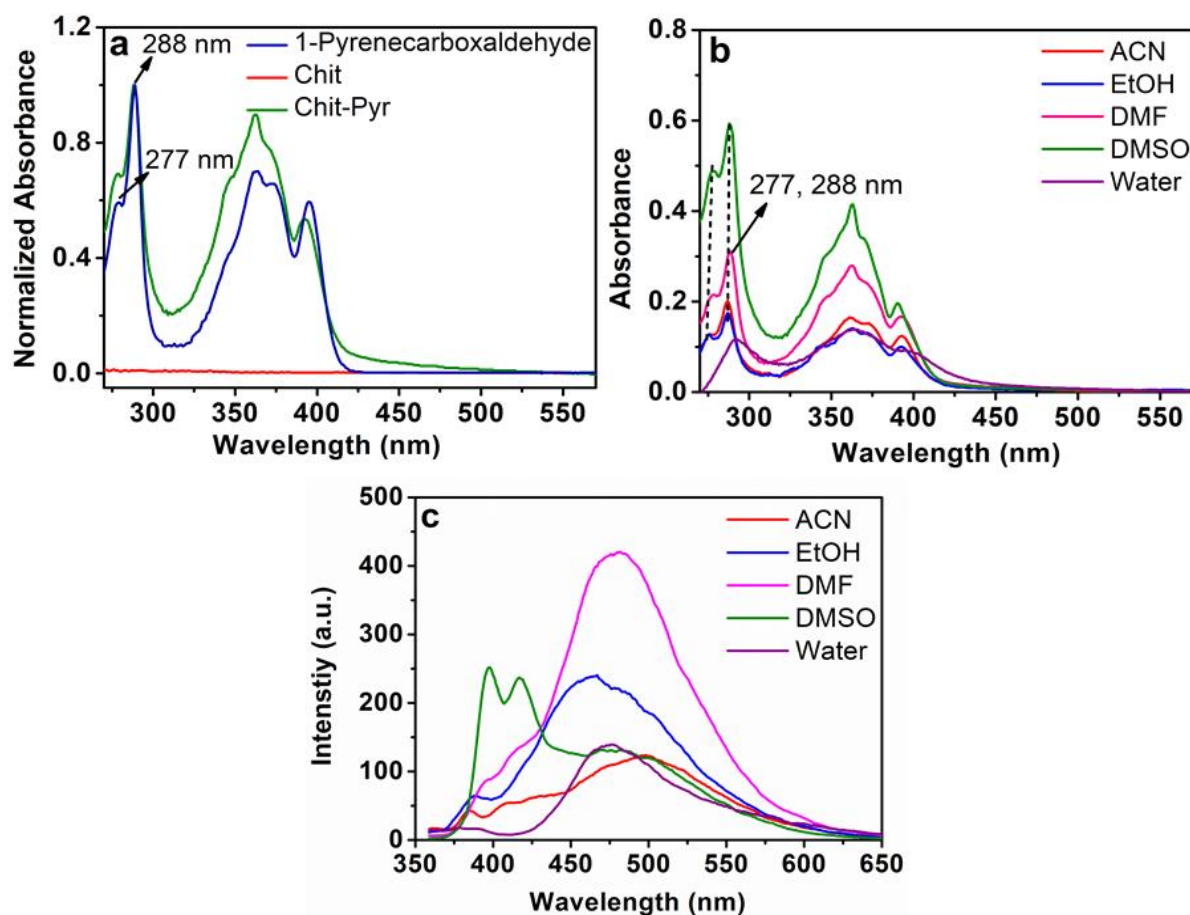

Figure 2. (a) Normalized UV-Vis absorption spectra of 1-pyrenecarboxaldehyde, Chit, and **Chit-Pyr** in DMF, (b) UV-Vis absorption spectra of 0.4 mg/mL **Chit-Pyr** in different solvents, and (c) fluorescence emission spectra of 0.4 mg/mL **Chit-Pyr** in different solvents (λ_{ex}=345 nm)

3.2. Photophysical studies

The absorption and fluorescence properties of pyrene-modified chitosan hybrid (**Chit-Pyr**) were investigated in different water-miscible solvents such as THF, ACN, EtOH, DMF, DMSO, and water at the same concentration (0.4 mg/mL, Fig. 2b–c). In addition, absorption and emission spectra of **Chit-Pyr** at different concentrations from 0.4 mg/mL to 0.1 mg/mL and in different solvents were measured to examine the effect of on the UV-Vis and emission absorption properties of **Chit-Pyr**. The absorbance values were decreased comparatively when the concentration of **Chit-Pyr** was decreased without a significant change in the absorption wavelength (Fig. 3).
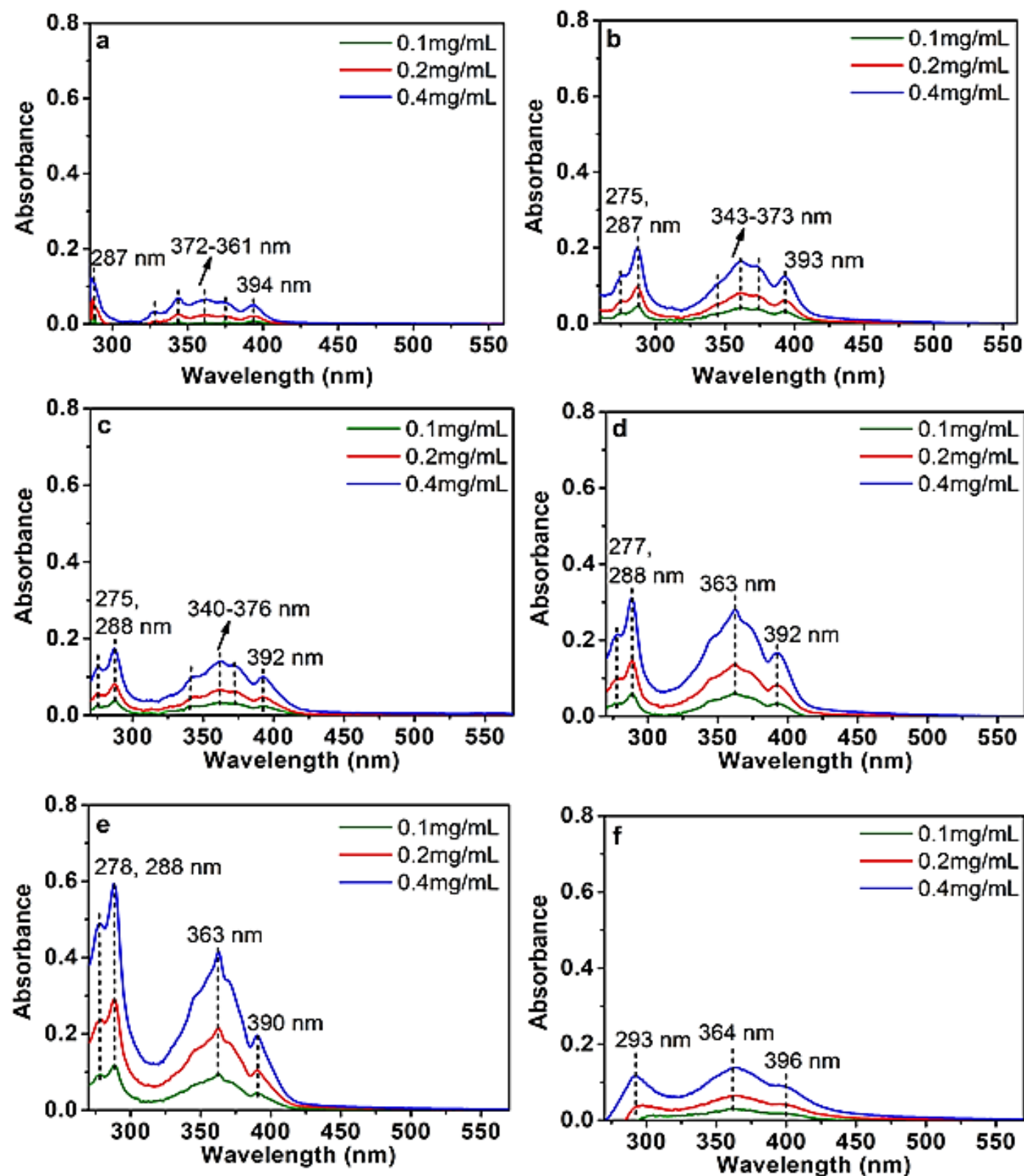

Figure 3. UV-Vis absorption spectra of Chit-Pyr in (a) THF, (b) ACN, (c) EtOH, (d) DMF, (e) DMSO, and (f) water at different concentrations

The emission characteristic of **Chit-Pyr** was investigated at different concentrations from 0.4 mg/mL to 0.1 mg/mL and in different solvents when excited at 345 nm (Fig. 4). It was determined that the excimer emission of **Chit-Pyr** obtained in ethanol and water, which are polar protic solvents, was blue-shifted compared to polar aprotic solvents [50]. In addition, emission bands of both monomer and excimer of the **Chit-Pyr** were obtained in solvents such as THF, ACN, EtOH, and DMSO. The emission intensity of the monomer emission (398 and 418 nm) was determined as DMSO higher than the excimer emission (481 nm) compared to other solvents. Also, the excimer *vs.* monomer emission intensity ratio (I_e/I_m) of **Chit-Pyr** in DMSO was calculated as ~0.6, and this ratio remained the same with increasing or decreasing concentration. Among all solvents studied, DMF was chosen as the solvent in "turn-off" fluorescence sensor studies, because **Chit-Pyr** showed a high emission peak in DMF which is miscible in water.
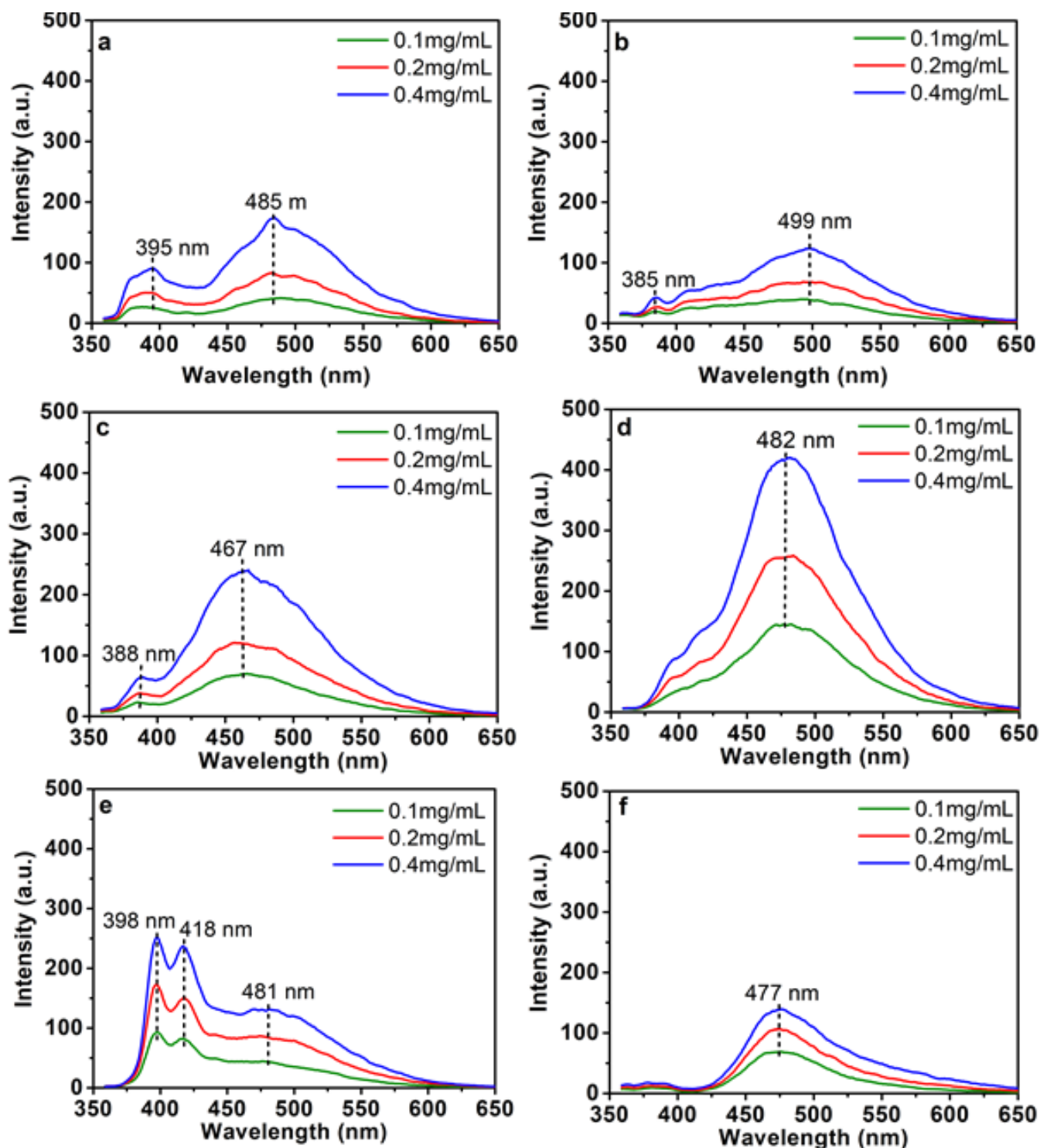

Figure 4. Fluorescence emission spectra of **Chit-Pyr** in (a) THF, (b) ACN, (c) EtOH, (d) DMF, (e) DMSO, and (f) water at different concentrations (λ_{ex}=345 nm)
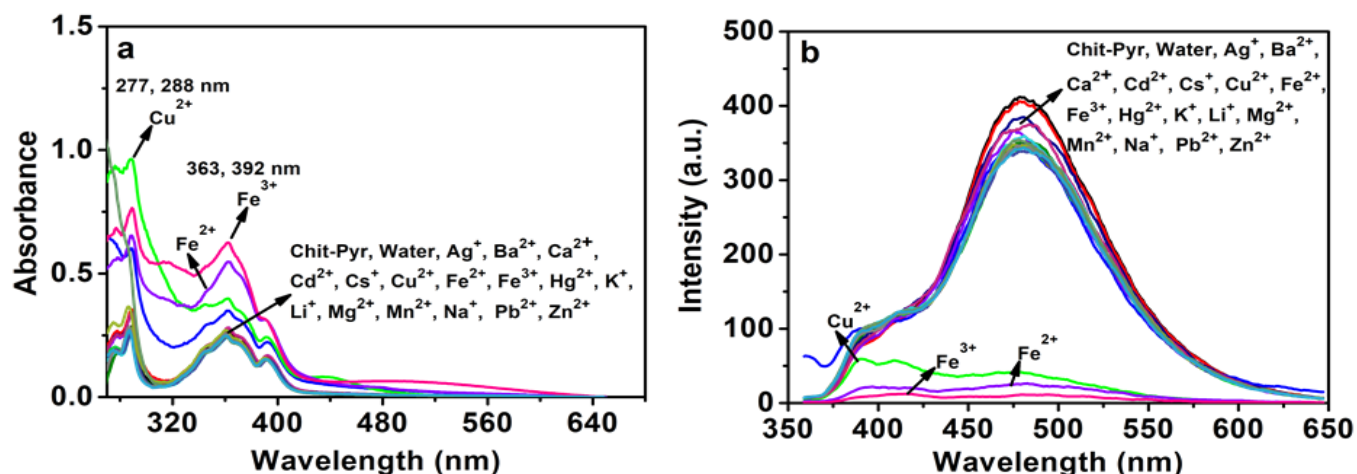
Figure 5. (a) UV-Vis absorption spectra and (b) fluorescence emission spectra of Chit-Pyr (0.4 mg/mL in DMF λ_{ex} = 345 nm) upon addition of 0.1 M of various metal ions (Ag$^+$, Ba^{2+}, Ca^{2+}, Cd^{2+}, Cs$^+$, Cu^{2+}, Fe^{2+}, Fe^{3+}, Hg^{2+}, K$^+$, Li$^+$, Mg^{2+}, Mn^{2+}, Na$^+$, Pb^{2+}, Zn^{2+})

3.3. "Turn-off" fluorescence sensor studies

The pyrene-modified chitosan (**Chit-Pyr**) was dispersed in DMF and "turn-off" fluorescence sensor studies were performed at a concentration of 0.4 mg/mL. **Chit-Pyr** was dispersed in DMF with an ultrasonic bath and 5 µL of 0.1 M of various metal ions (Ag$^+$, Ba^{2+}, Ca^{2+}, Cd^{2+}, Cs$^+$, Cu^{2+}, Fe^{2+}, Fe^{3+}, Hg^{2+}, K$^+$, Li$^+$, Mg^{2+}, Mn^{2+}, Na$^+$, Pb^{2+}, Zn^{2+}) were added to the dispersion of **Chit-Pyr**. Then, the absorption and emission responses of **Chit-Pyr** were evaluated after adding metal ions (Fig. 5). As seen in Fig. 5a, absorption properties of **Chit-Pyr** considerably changed after the addition of Fe^{2+}, Fe^{3+}, and Cu^{2+} ions to a dispersion of **Chit-Pyr**. The absorption peaks of **Chit-Pyr**, observed at 277 and 288 nm, were increased 2.9- and 2.3-fold for Fe^{2+}, 3.6- and 2.7-fold for Fe^{3+}, and 4.9- and 3.4-fold for Cu^{2+}, respectively. Also, the absorption peaks of **Chit-Pyr**, monitored at 363 and 392 nm, were increased 2.1- and 2.0-fold for Fe^{2+}, 2.4- and 2.0-fold for Fe^{3+}, and 1.5- and 1.5-fold for Cu^{2+}, respectively. No blue

or red shifts were detected in the absorption bands with the addition of metal ions (Ag$^+$, Ba^{2+}, Ca^{2+}, Cd^{2+}, Cs$^+$, Cu^{2+}, Fe^{2+}, Fe^{3+}, Hg^{2+}, K$^+$, Li$^+$, Mg^{2+}, Mn^{2+}, Na$^+$, Pb^{2+}, Zn^{2+}).

The emission spectra of **Chit-Pyr** were obtained towards Fe^{2+}, Fe^{3+}, and Cu^{2+} ions at the same analytical conditions with absorption measurements. As shown in Fig. 5b, the emission bands of **Chit-Pyr** with moderate emission intensity at 482 nm were decreased 15.8-fold for Fe^{2+}, 37.4-fold for Fe^{3+}, and 10.3-fold for Cu^{2+}. No significant changes were determined in the emission band with the addition of other metals (Ag$^+$, Ba^{2+}, Ca^{2+}, Cd^{2+}, Cs$^+$, Hg^{2+}, K$^+$, Li$^+$, Mg^{2+}, Mn^{2+}, Na$^+$, Pb^{2+}, Zn^{2+}). The addition of other metals did not cause any significant changes in the emission band of **Chit-Pyr**.

As seen in Fig. 6a, the relative fluorescence response of **Chit-Pyr** confirmed the high selectivity of **Chit-Pyr** against Fe^{2+}, Fe^{3+}, and Cu^{2+} ions and showed that it was unaffected by competitive species. The addition of Fe^{2+}
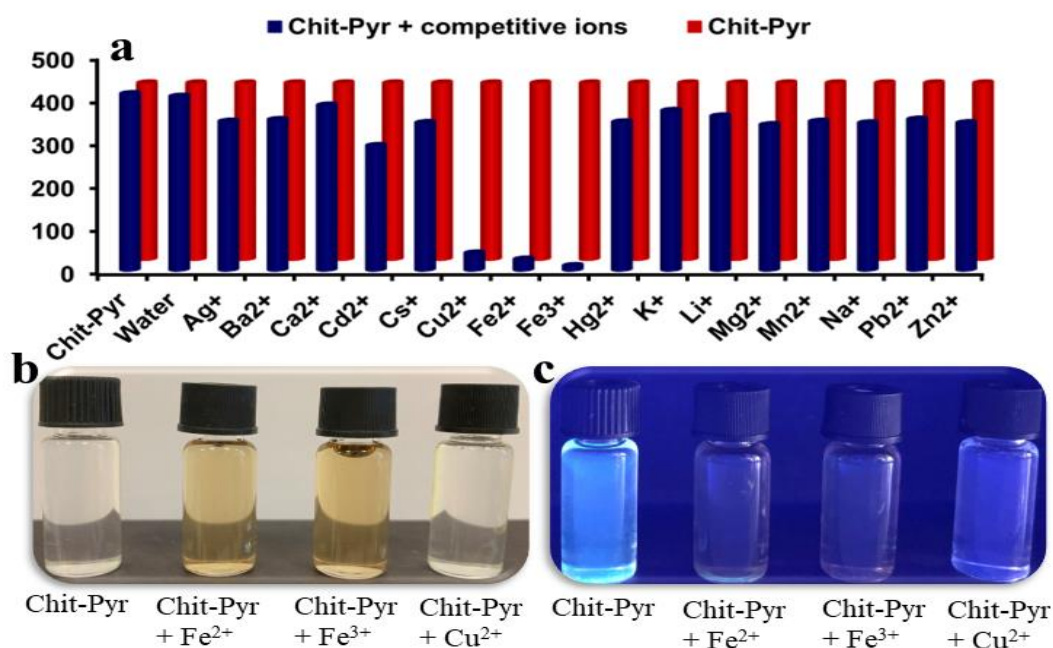

Figure 6. (a) Fluorescence signal change of Chit-Pyr in DMF addition of various competitive ions, the color change of Chit-Pyr in DMF (0.4 mg/mL) (b) daylight, and (c) UV light

and Fe^{3+} ions to **Chit-Pyr** solution dispersed in DMF caused significant color changes to the naked eye (colorless to light brown, Fig. 6b) and under UV light (blue/green to colorless, Fig. 6c). While there was no visible color change after addition of Cu^{2+} was added, a color change from blue/green to colorless was observed under UV light (Fig. 6c). Thus, it was determined that the newly synthesized pyrene modified chitosan hybrid (**Chit-Pyr**) indicated "turn-off" fluorescence sensor properties against these metals. Also, the color change after the addition of Fe^{2+} and Fe^{3+} ions indicated that this hybrid material can be used as both a colorimetric and fluorometric sensor platform.

Fluorescence titration of **Chit-Pyr** with an increased amount of Fe^{2+}, Fe^{3+}, and Cu^{2+} ions was measured in DMF

to define the linear "turn-off" response of the **Chit-Pyr** towards the selective metal ions (Fig. 7). The fluorescence signals of **Chit-Pyr** were gradually "turn-off" upon the addition of Fe^{2+}, Fe^{3+}, and Cu^{2+} ions, respectively.

The linear regression equation for selective metal ions was calculated as $y = -8.1857 [Fe^{2+}] + 401.14$ ($R^2 = 0.9971$), $y = -9.4774 [Fe^{3+}] + 424.94$ ($R^2 = 0.985$), and $y = -8.9291 [Cu^{2+}] + 393.32$ ($R^2 = 0.9948$) (Fig. 8). The limit of detection (LOD) is calculated with $3\sigma/K$ where σ and K represent the standard deviation of the blank sample and slope of calibration curves, respectively. LODs were determined as 2.52 μM for Fe^{2+}, 1.74 μM for Fe^{3+}, and 1.96 μM for Cu^{2+}. Also, the limit of quantification (LOQ) for Fe^{2+}, Fe^{3+}, and Cu^{2+} were calculated as 7.56 μM, 5.21 μM and 5.89 μM with $9\sigma/K$, respectively.
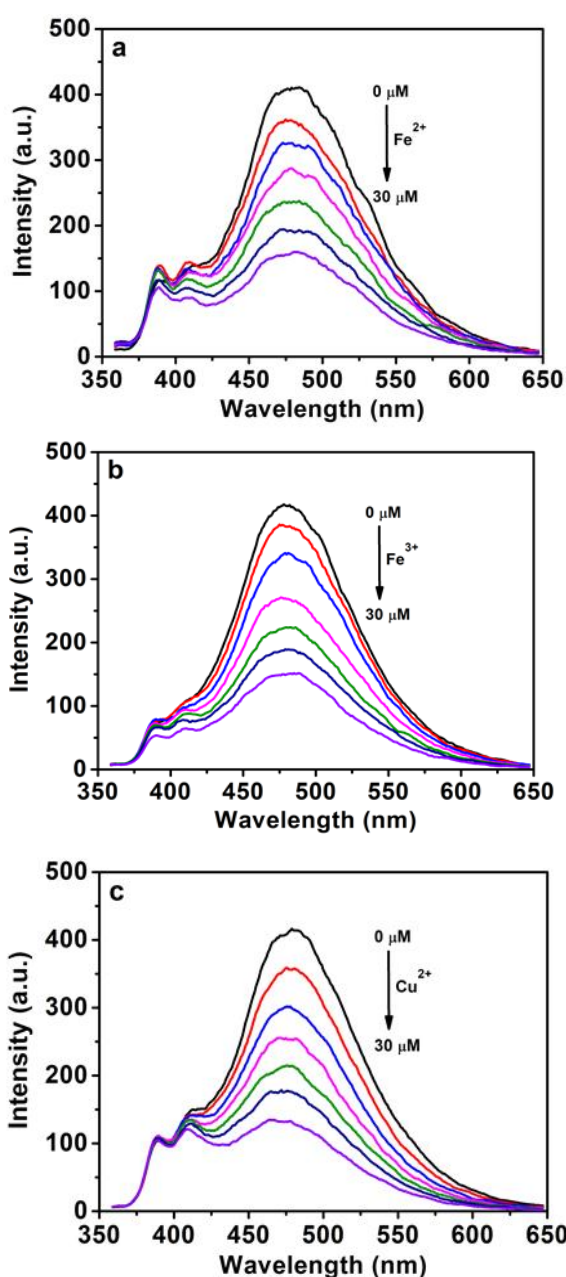

Figure 7. Fluorescence titration of **Chit-Pyr** (0.4 mg/mL) (a) Fe^{2+}, (b) Fe^{3+}, and (c) Cu^{2+} with a gradually increased concentration in DMF ($\lambda_{ex} = 345$ nm)
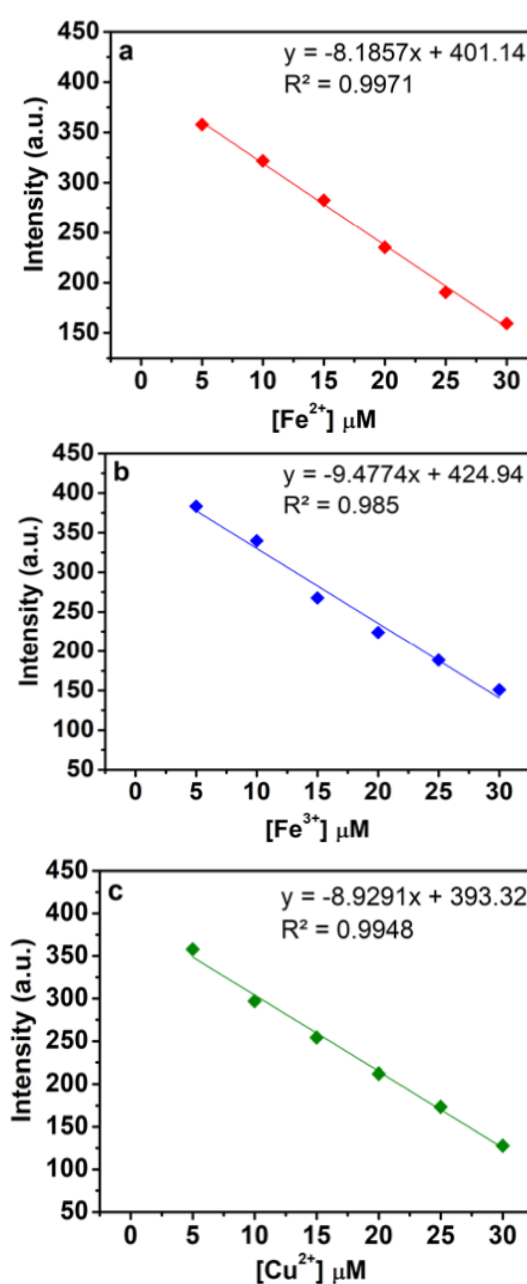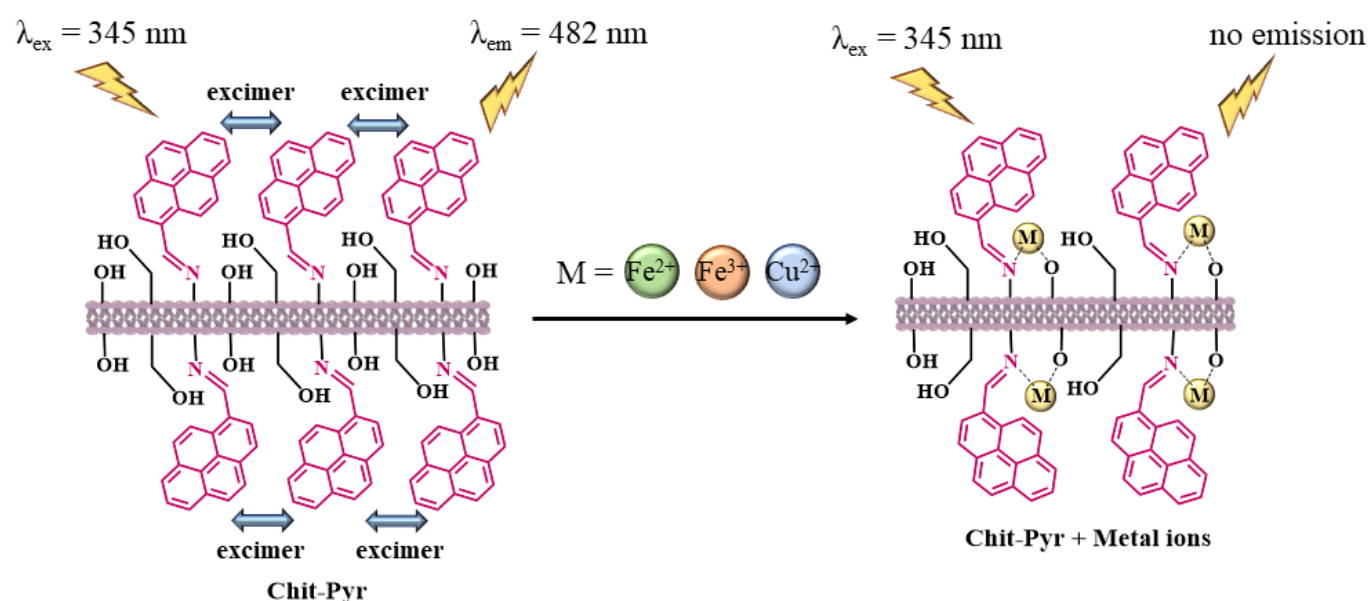
Figure 8. The linear relationship between fluorescence responses of **Chit-Pyr** and metal ions (a) Fe^{2+}, b) Fe^{3+}, and (c) Cu^{2+}.

Scheme 2. Proposed "turn-off" fluorescence sensing mechanism of Fe^{2+}, Fe^{3+}, and Cu^{2+} with **Chit-Pyr**.

Heavy metals such as iron and copper, which chelate with the -OH and $-NH_2$ groups in chitosan, cause a change in the emission signal due to the photoinduced electron transfer (PET) mechanism. Electron transfer occurs from the excited compound to the electron-deficient metal ions with Lewis acid character and quenches the emission signal of the fluorescence compound [51]. The -OH groups that provide charge transfer from the ligand to the metal ion were deprotonated after the interaction of **Chit-Pyr** with Fe^{2+}, Fe^{3+}, and Cu^{2+}. The coordination between Fe^{2+}, Fe^{3+}, Cu^{2+}, and **Chit-Pyr** was accomplished through the hydroxyl oxygen atom and the imine nitrogen atom [2,52]. Scheme 2 indicates the proposed "turn-off" fluorescence sensing mechanism of Fe^{2+}, Fe^{3+}, and Cu^{2+}.

4. Conclusion

Interest in biopolymer-based fluorescent sensors is increasing, as they exhibit cost-effective, biodegradable, and environmentally friendly properties. Also, biopolymers with new properties are obtained by functionalization with alternative groups. In this study, novel, sensitive, and simple "turn-off" fluorescence studies were performed using pyrene-modified chitosan hybrid (**Chit-Pyr**) against Fe^{2+}, Fe^{3+}, and Cu^{2+} ions. FTIR, UV-Vis, TGA, and SEM were used to examine for structural, thermal, and morphological properties of **Chit-Pyr**. Photophysical properties of **Chit-Pyr** were determined by UV-Vis absorption and fluorescence studies. The selective "turn-off" fluorescence response for **Chit-Pyr** was obtained towards Fe^{2+}, Fe^{3+}, and Cu^{2+} ions in different competitive species. It is thought that this study will contribute to the preparation of stable, economical, and sustainable new hybrid biopolymers for use in fluorescence sensor studies.

References

[1]   P. Kumar, V. Kumar, R. Gupta, Arene-based fluorescent probes for the selective detection of iron, RSC Adv, 5, 2015, 97874–97882.

[2]   X. Zhu, Y. Duan, P. Li, H. Fan, T. Han, X. Huang, A highly selective and instantaneously responsive Schiff base fluorescent sensor for the "turn-off" detection of iron(iii), iron(ii), and copper(ii) ions, Anal Methods, 11, 2019, 642–647.

[3]   G.J. Park, G. R. You, Y. W. Choi, C. Kim, A naked-eye chemosensor for simultaneous detection of iron and copper ions and its copper complex for colorimetric/fluorescent sensing of cyanide, Sensor Actuat B-Chem, 229, 2016, 257–271.

[4]   G. T. Selvan, C. Varadaraju, R. T. Selvan, I. V. M. V. Enoch, P. M. Selvakumar, On/Off Fluorescent Chemosensor for Selective Detection of Divalent Iron and Copper Ions: Molecular Logic Operation and Protein Binding, ACS Omega, 3, 2018, 7985–7992.

[5]   A. Parsaei-Khomami, A. Badiei, Z. S. Ghavami, J. B. Ghasemi, A new fluorescence probe for simultaneous determination of Fe^{2+} and Fe^{3+} by orthogonal signal correction-principal component regression, J Mol Struct, 1252, 2022, 131978.

[6]   A. Paterek, U. Mackiewicz, M. Mączewski, Iron and the heart: A paradigm shift from systemic to cardiomyocyte abnormalities, J Cell Physiol 234, 2019, 21613–21629.

[7]   J. Kaplan, D. M. Ward, R. J. Crisp, C. C. Philpott, Iron-dependent metabolic remodeling in S. cerevisiae, Biochim Biophys Acta-Mol. Cell Res, 1763, 2006, 646–651.

[8]   K. Pantopoulos, S. K. Porwal, A. Tartakoff, L. Devireddy, Mechanisms of Mammalian Iron Homeostasis, Biochem, 51, 2012, 5705–5724.

[9]   A. M. Şenol, Y. Onganer, K. Meral, An unusual "off-on" fluorescence sensor for iron(III) detection based on fluorescein–reduced graphene oxide functionalized with polyethyleneimine, Sens Actuat B-Chem, 239, 2017, 343–351.

[10] S. O. Tümay, S.Y. Sarıkaya, S. Yeşilot, Novel iron(III) selective fluorescent probe based on synergistic effect of pyrene-triazole units on a cyclotriphosphazene scaffold and its utility in real samples, J Lumin, 196, 2018, 126–135.

[11]   S. O. Tümay, M. H. Irani-nezhad, A. Khataee, Design of novel anthracene-based fluorescence sensor for sensitive and selective determination of iron in real samples, J Photoc Photobio A, 402, 2020, 112819.

[12]   S. O. Tümay, E. Okutan, I. F. Sengul, E. Özcan, H. Kandemir, T. Doruk, M. Çetin, B. Çoşut, Naked-eye fluorescent sensor for Cu(II) based on indole conjugate BODIPY dye, Polyhedron, 117, 2016, 161–171.

[13]   Z. Khoshbin, M. R. Housaindokht, A. Verdian, M. R. Bozorgmehr, Simultaneous detection and determination of mercury (II) and lead (II) ions through the achievement of novel functional nucleic acid-based biosensors, Biosens Bioelectron, 116, 2018, 130–147.

[14]   S. García-Marco, A. Torreblanca, J.J. Lucena, Chromatographic Determination of Fe Chelated by Ethylenediamine-N-(o-hydroxyphenylacetic)-N'-(p-hydroxyphenylacetic) Acid in Commercial EDDHA/Fe^{3+} Fertilizers, J Agr Food Chem, 5, 2006, 1380–1386.

[15]   N. Scheers, T. Andlid, M. Alminger, A. S. Sandberg, Determination of Fe^{2+} and Fe^{3+} in Aqueous Solutions Containing Food Chelators by Differential Pulse Anodic Stripping Voltammetry, Electroanal, 22, 2010, 1090–1096.

[16]   R. Ferreira, J. Chaar, M. Baldan, N. Braga, Simultaneous voltammetric detection of Fe^{3+}, Cu^{2+}, Zn^{2+}, Pb^{2+} e Cd^{2+} in fuel ethanol using anodic stripping voltammetry and boron-doped diamond electrodes, Fuel, 291, 2021, 120104.

[17]   Y. Guo, N. Huang, B. Yang, C. Wang, H. Zhuang, Q. Tian, Z. Zhai, L. Liu, X. Jiang, Hybrid diamond/graphite films as electrodes for anodic stripping voltammetry of trace Ag$^+$ and Cu^{2+}, Sens Actuat B-Chem, 231, 2016, 194–202.

[18]   E. Bakkaus, R. N. Collins, J.-L. Morel, B. Gouget, Anion exchange liquid chromatography–inductively coupled plasma-mass spectrometry detection of the Co^{2+}, Cu^{2+}, Fe^{3+} and Ni^{2+} complexes of mugineic and deoxymugineic acid, J Chromatogr A, 1129, 2006, 208–215.

[19]   A. Spolaor, P. Vallelonga, J. Gabrieli, G. Cozzi, C. Boutron, C. Barbante, Determination of Fe^{2+} and Fe^{3+} species by FIA-CRC-ICP-MS in Antarctic ice samples, J Anal Atom Spectrom, 27, 2012, 310–317.

[20]   M. Yaman, G. Kaya, Speciation of iron (II) and (III) by using solvent extraction and flame atomic absorption spectrometry, Anal Chim Acta, 540, 2005, 77–81.

[21]   M. Ghaedi, K. Niknam, K. Taheri, H. Hossainian, M. Soylak, Flame atomic absorption spectrometric determination of copper, zinc and manganese after solid-phase extraction using 2,6-dichlorophenyl-3,3-bis(indolyl)methane loaded on Amberlite XAD-16, Food Chem Toxicol, 48, 2010, 891–897.

[22]   T. Verma, P. Verma, U. P. Singh, A multi responsive phosphonic acid based fluorescent sensor for sensing Fe^{3+}, benzaldehyde and antibiotics, Microchem J, 191, 2023, 108771.

[23]   S. H. Park, N. Kwon, J. H. Lee, J. Yoon, I. Shin, Synthetic ratiometric fluorescent probes for detection of ions, Chem Soc Rev, 49, 2020, 143–179.

[24]   W. Wang, L. Chai, X. Chen, Z. Li, L. Feng, W. Hu, H. Li, G. Yang, Imaging changes in the polarity of lipid droplets during NAFLD-Induced ferroptosis via a red-emitting fluorescent probe with a large Stokes shift, Biosens Bioelectron, 231, 2023, 115289.

[25]   P. R. Yaashikaa, P. S. Kumar, S. Karishma, Review on biopolymers and composites – Evolving material as adsorbents in removal of environmental pollutants, Environ Res, 212, 2022, 113114.

[26]   A. Das, T. Ringu, S. Ghosh, N. Pramanik, A comprehensive review on recent advances in preparation, physicochemical characterization, and bioengineering applications of biopolymers, Polym Bull, 2022, 1–66.

[27]   M. Nasrollahzadeh, M. Sajjadi, S. Iravani, R. S. Varma, Starch, cellulose, pectin, gum, alginate, chitin and chitosan derived (nano)materials for sustainable water treatment: A review, Carbohyd Polym, 251, 2021, 116986.

[28]   W. Wang, C. Xue, X. Mao, Chitosan: Structural modification, biological activity and application, Int J Biol Macromol, 164, 2020, 4532–4546.

[29]   R. Priyadarshi, J.W. Rhim, Chitosan-based biodegradable functional films for food packaging applications, Innov Food Sci Emerg, 62, 2020, 102346.

[30]   Y. Chen, Y. Liu, Q. Dong, C. Xu, S. Deng, Y. Kang, M. Fan, L. Li, Application of functionalized chitosan in food: A review, Int J Biol Macromol, 235, 2023, 123716.

[31]   P. S. B, D. Selvakumar, K. Kadirvelu, N. S. Kumar, Chitosan as an environment friendly biomaterial – a review on recent modifications and applications, Int J Biol Macromol, 150, 2020, 1072–1083.

[32]   M. Zhang, F. Zhang, C. Li , H. An, T. Wan, P. Zhang, Application of Chitosan and Its Derivative Polymers in Clinical Medicine and Agriculture, Polymers-Basel, 14, 2022, 958.

[33]   R. Jayakumar, M. Prabaharan, S.V. Nair, S. Tokura, H. Tamura, N. Selvamurugan, Novel carboxymethyl derivatives of chitin and chitosan materials and their biomedical applications, Prog Mater Sci, 55, 2010, 675–709.

[34]   B. I. Andreica, X. Cheng, L. Marin, Quaternary ammonium salts of chitosan. A critical overview on the synthesis and properties generated by quaternization, Eur Polym J, 139, 2020, 110016.

[35]   H. A.Alidağı, S. O. Tümay, A. Şenocak, S. Yeşilot, Pyrene functionalized cyclotriphosphazene-based dyes: Synthesis, intramolecular excimer formation, and fluorescence receptor for the detection of nitro-aromatic compounds, Dyes Pigments, 153, 2018, 172–181.

[36]   V. Kumar, B. Sk, S. Kundu, A.Patra, Dynamic and static excimer: a versatile platform for single component white-light emission and chelation-enhanced fluorescence, J Mater Chem C, 6, 2018, 12086–12094.

[37]   L. Gai, H. Chen, B. Zou, H. Lu, G. Lai, Z. Li, Z. Shen, Ratiometric fluorescence chemodosimeters for fluoride anion based on pyrene excimer/monomer transformation, Chem Commun, 48, 2012, 10721–10723.

[38]   M. Belovari, D. Nestić, I. Marić, D. Majhen, M. Cametti, Z. Džolić, Photophysical characterization and the self-assembly properties of mono- and bis-pyrene derivatives for cell imaging applications, New J Chem, 46, 2022, 22518–22524.

[39]   S. Jatunov, A. Franconetti, R. Prado-Gotor, A. Heras, M. Mengíbar, F. Cabrera-Escribano, Fluorescent imino and secondary amino chitosans as potential sensing biomaterials, Carbohyd Polym, 123, 2015, 288–296.

[40]   A. Franconetti, P. Domínguez-Rodríguez, D. Lara-García, R. Prado-Gotor, F. Cabrera-Escribano, Native and modified chitosan-based hydrogels as green heterogeneous organocatalysts for imine-mediated Knoevenagel condensation, Appl Catal A-Gen, 517, 2016, 176–186.

[41]   P. Sirajunnisa, C. Sabna, A. Aswin, S. Prathapan, G. S. Sailaja, Lawsone-bentonite hybrid systems for pH-dependent sustained release of ciprofloxacin, New J Chem, 46, 2022, 9560–9571.

[42]   H. M. Lee, M. H. Kim, Y. I. Yoon, W. H. Park, Fluorescent Property of Chitosan Oligomer and Its Application as a Metal Ion Sensor, Mar Drugs, 15, 2017, 105.

[43]   D. Wang, L. Marin, X. Cheng, Fluorescent chitosan-BODIPY macromolecular chemosensors for detection and removal of Hg^{2+} and Fe^{3+} ions, Int J Biol Macromol, 198, 2022, 194–203.

[44]   Z. Meng, Z. Wang, Y. Liang, G. Zhou, X. Li, X. Xu, Y. Yang, S. Wang, A naphthalimide functionalized chitosan-based fluorescent probe for specific detection and efficient adsorption, Int J Biol Macromol, 239, 2023, 124261.

[45]   S. O. Tümay, V. Şanko, E. Demirbaş, A. Şenocak, Fluorescence determination of trace level of cadmium with pyrene modified nanocrystalline cellulose in food and soil samples, Food Chem Toxicol, 146, 2020, 11184.

[46]   M. A. Ahghari, M. R. Ahghari, M. Kamalzare, A. Maleki, Design, synthesis, and characterization of novel eco-friendly chitosan-

AgIO$_3$ bionanocomposite and study its antibacterial activity, Sci Rep-UK, 12, 2022, 10491.

[47] T. Jiang, C. Wang, W. Liu, Y. Li, Y. Luan, P. Liu, Optimization and characterization of lemon essential oil entrapped from chitosan/cellulose nanocrystals microcapsules, J Appl Polym Sci, 138, 2021, 51265.

[48] S. O. Tümay, V. Şanko, A. Şenocak, E. Demirbaş, A hybrid nanosensor based on novel fluorescent iron oxide nanoparticles for highly selective determination of Hg^{2+} ions in environmental samples, New J Chem, 45, 2021, 14495–14507.

[49] H. Ardic Alidagi, S. O. Tümay, A. Şenocak, Ö. F. Çiftbudak, B. Çoşut, S. Yeşilot, Constitutional isomers of dendrimer-like pyrene substituted cyclotriphosphazenes: synthesis, theoretical calculations, and use as fluorescence receptors for the detection of explosive nitroaromatics, New J Chem, 43, 2019, 16738–16747.

[50] P. K. Lekha, E. Prasad, Tunable Emission of Static Excimer in a Pyrene-Modified Polyamidoamine Dendrimer Aggregate through Positive Solvatochromism, Eur J Chem, 17, 2011, 8609–8617.

[51] H. Gupta, K. Kaur, R. Singh, V. Kaur, Chitosan Schiff base for the spectrofluorimetric analysis of E-waste toxins: Pentabromophenol, Fe^{3+}, and Cu^{2+} ions, Cellulose, 30, 2023, 1381–1397.

[52] T. Sun, Q. Niu, T. Li, Z. Guo, H. Liu, A simple, reversible, colorimetric and water-soluble fluorescent chemosensor for the naked-eye detection of Cu^{2+} in ~100% aqueous media and application to real samples, Spectrochim Acta A, 188, 2018, 411–417.

The investigation of the effect of sodium chlorite and phosphonic acid catalysts on cotton bleaching process conditions

Salih Zeki Yıldız[1] iD , Sami Dursun[2]* iD

[1] Sakarya University, Department of chemistry, 54050, Sakarya, Türkiye
[2] Konya Technical University, Department of Metallurgical and Materials Engineering, 42130, Konya, Türkiye

Abstract

Traditional textile bleaching techniques need to be given another look in light of the environment and lifestyle of today. To achieve higher whiteness values while using less water and chemicals during the bleaching process, it is crucial for both the environment and the economy. The most effective disinfectant, chlorine dioxide (ClO_2), is produced by sodium chlorite ($NaClO_2$), which is a suitable oxidant for the job. During the COVID-19 pandemic, $NaClO_2$ gained popularity and became more widely available. The use of $NaClO_2$ as a bleaching agent offers many benefits, including a decrease in the number of washing steps and an increase in cotton strength. This reagent's ability to produce less weight loss in the fabric than other reagents is another benefit. Therefore, the present work was intended to improve the process conditions (different temperatures, concentrations, and times) of bleaching of cotton fabric by using $NaClO_2$. A high whiteness index (W.I. = 88) was obtained by utilizing phosphonic acid (HEDP), and the ideal temperature and duration were found to be 30 min at 65 °C and 30 min at 85 °C. Moreover, the tensile strength, weight loss and morphologies of the samples were examined. Because sodium chlorite does not leave behind any alkaline residues, it has been found to do less harm to cotton fibers and use less water for rinsing.

1. Introduction

The economy and environment of the textile industry are greatly impacted by the bleaching of cotton fabric [1,2]. Cotton fibers are naturally yellow or brown because of their structural makeup. Pigments that are naturally present may be the cause of this yellowish and brown discoloration [3]. Additionally, this color pollution may be brought on by environmental factors such as soil, climate, drought, frost, dust, and insects [4–6]. Before dyeing and finishing, which is one of the crucial steps, cotton fibers must typically undergo pretreatment to remove the natural pigments [7]. Bleaching is used to turn colored materials into the white fabric while causing the least amount of fiber deterioration possible. To achieve the desired whiteness, the bleaching chemicals either oxidize or decrease the coloring matter [8]. Washing off the treated colours and material yields satisfactory whiteness [1,9].

For a long time, textile and paper pulp have been bleached to a high white without losing strength using sodium chlorite ($NaClO_2$), which is a known commercial chemical [10,11]. $NaClO_2$ is also easy to obtain and stores reasonably well. Additionally, it is a persistent free radical that acts as a one-electron oxidant in reactions with reducing substrates such as amines, sulfides, and phenols [12,13]. The activation of stable aqueous $NaClO_2$ solutions under alkaline conditions requires acidification. The rate at which sodium chlorite decomposes into chlorine dioxide (ClO_2), a potent oxidizing gas, increases with decreasing pH values and increasing bleach bath temperature (over 70 °C) [14,15]. The amount of $NaClO_2$ in the solution has a direct relationship to the rate of ClO_2 production. Maximum ClO_2 synthesis occurs between pH 2.5 and 3.0 [1]. Since the rate of ClO_2 generation almost doubles for each 0.4 pH drop at 85 °C, an acid like formic, acetic, or phosphoric acid is advised to alter pH values between 5.0 and 3.0 [16,17].

The ineffective storage of ClO_2, the possibility of a gaseous explosion, and the fact that it is typically coupled with hypochlorite hinder the effective usage of

ClO_2 even though it is a potent and affordable oxidant and disinfectant [18]. However, since the current pandemic, chlorine dioxide use has grown significantly and is still growing [19,20]. It was decided at this point that it would be advantageous to revisit the $NaClO_2$ bleaching procedures to dispel some myths, particularly in the textile industry, and to improve their usability and safety.

The present work aims to find the most appropriate and environmentally safe process conditions to bleach cotton using $NaClO_2$, caring about the quality of the bleached fabric. In this study, in addition to other bleaching studies, some phosphonic acids were used and it was determined that the whiteness value of the bleached fabric increased significantly. In addition, it has been determined that the bleaching process can be performed without the use of wetting agent thanks to the phosphonic acid used, and thus the cost is reduced. As a result of the characterizations performed on the bleached fabric, it was determined that the morphology of the fabric was less damaged than the fabrics bleached by another bleaching method. In addition, this study is remarkable in terms of being environmentally friendly and obtaining cotton fabrics with good stretching properties by the bleaching process.

2. Experimental

2.1. Equipments, materials and chemicals

With pots of 200 mL capacity constructed of AISI 316L stainless steel (thickness of 2 mm), the TM-Termal™ was utilized as a laboratory-size dyeing apparatus. The device has a 20-step, 36 programs, PT-100 temperature sensor, and 1–3 °C/min temperature control mechanism. 5 °C to 140 °C operational temperature range and heating rate. The Konica Minolta Spectrophotometer, CM-3600d, assessed the reflectance of the bleached samples' whiteness. meterLab Ag/AgCl electrode and analytical KCl were utilized with the pH meter 210 Standard. The Turkish company NUR Textile Co. provided the plain weave, 100 percent cotton. These were the fabric's specifications: 150 g/m^2 fabric weight, 30 weft yarns per centimeter, and 36 warp yarns per cm. Turoksi Chemical Co. supplied sodium chlorite as a 31% solution in water. Technical grade sodium tripolyphosphate STPP), ethylenediaminetetraacetic acid (EDTA), amino trimethylene phosphoric acid (AMTP), polyacrylic acid (PAA), and 1-hydroxy ethylidene-1,1-diphosphonic acid (HEDP)were all provided by the Turkish domestic market. The following chemicals were acquired from Merck Chemical Company: acetic acid (CH_3COOH, 99%), sodium thiosulfate anhydrous ($Na_2S_2O_3$, 98.0%), citric acid ($C_6H_8O_7$, 99%), phosphoric acid (H_3PO_4, 85%), formic acid (CH_2O_2, 96%), sulfuric acid (H_2SO_4, 95.0–98.0%), and potassium iodide (KI, 99.0%).

2.2. Process conditions

For bleaching trials, fabrics were weighed out to around 10 g for each one immersed in a liquor solution. The main components of the liquors include acids that are used to modify the pH from 2.5 to 4.0, wetting agents, various stabilizers, and sodium chlorite. The mentioned amounts of chemicals given in the recipes were added to provide a material to liquor ratio of 1/10. Wetting agent (1 g/L), stabilizer (1 g/L), and $NaClO_2$ (0.850 g–5.225 g/L) were all used. The stabilizer agent STPP was employed. Acids including formic acid (FA), acetic acid (AA), phosphoric acid (PA), citric acid (CA), 1-hydroxy ethylidene-1,1-diphosphonic acid (HEDP), polyacrylic acid (PAA), and amino trimethylene phosphoric acid (AMTP) were used to change the pH of the solution. Both a pH regulator and a stabilizer are employed with HEDP. The completed mixture was put into 200 mL stainless steel HT tubes with fabric, and the tube lids were tightly sealed. The alphabetical order of a, b, c, d given in Fig. 1 is the order in which the reagents are added to the process. The heating program was run following the replacement of the tubes on the dying machine heel (Fig. 1). After the period, the tubes were taken out of the device and opened. First, warm water was used to rinse the bleached materials, and then tap water was used.

If the investigations are treated chronologically, the trials were conducted at various times (0.5, 1.0, 1.5, and 3.0 h), but the best time to access the other conditions were maintained constant. Trials were then undertaken at various temperatures (30, 50, 70, and 95 °C) while maintaining other parameters constant to identify the ideal temperature, which is identical to the ideal length setting. Following the establishment of the ideal times and temperatures, the ideal bleach concentration was established using a range of $NaClO_2$ concentrations (0.85, 1.70, 3.40, 4.25, and 5.25 g). Finally, experiments were carried out at various pH values (2.5, 3.0, 3.5, and 4.0) to find the ideal pH value, which has a significant impact on bleaching.

2.3. Preparation of reference fabrics

The reference fabric served as a witness throughout the investigation as it was used to compare research fabrics bleached with $NaClO_2$ to reference fabrics bleached with H_2O_2. The witness fabric was bleached with 5g/L H_2O_2. A solution of sodium hydroxide was used to modify the pH before bleaching, which was done at a pH of 10.5.
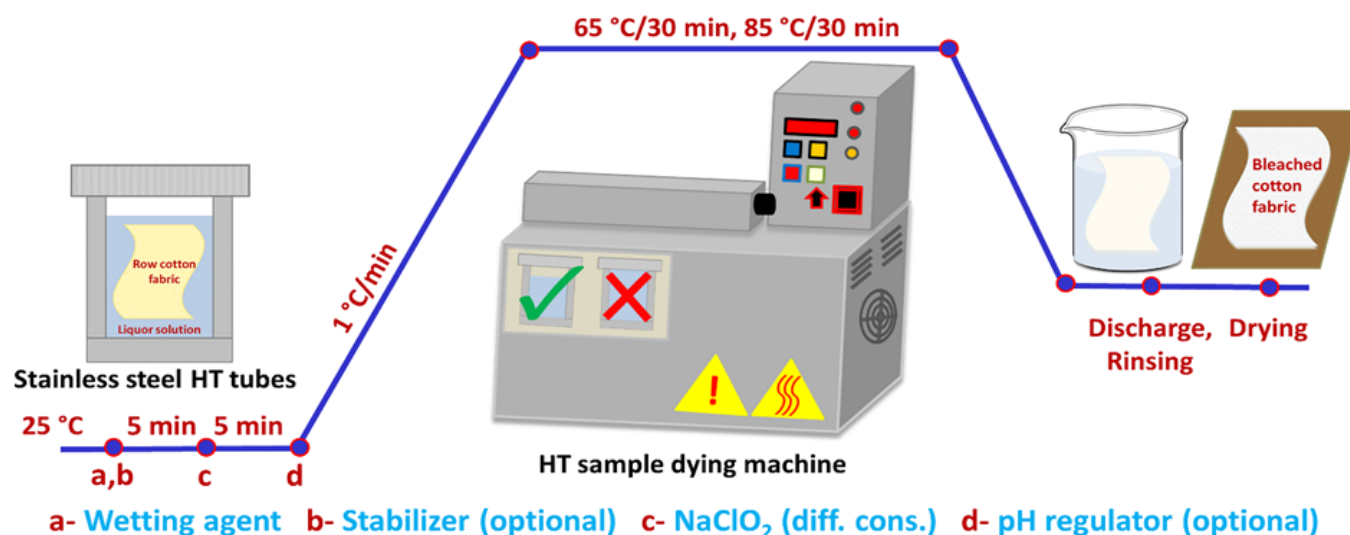
Figure 1. Schematic presentation of the cotton fabric bleaching process

The optimal bleaching time and temperature were found to be 2 h and 95 °C, respectively, and a nonionic STPP agent was utilized as the wetting agent.

2.4. Degree of whiteness

Necessary comparisons were made by carrying out the whiteness measurements of the experimental fabrics bleached with $NaClO_2$ and the reference fabrics bleached with H_2O_2. At 400 nm, the whiteness was measured. The degree of whiteness of bleached cotton samples, expressed as the whiteness index (W.I.), was measured using a Konica Minolta spectrophotometer (CM-3600d). The equation (ASTM Method E31373) was used to compute the W.I. in terms of the CIE Y (blue) and (green) reflectance components [21].

$$W.I. = \frac{4Z}{1.18} - 3Y \quad (1)$$

where Y and Z are the readings of the device.

2.5. Weight Loss

The following calculation was used to determine fabric weight decrease based on dry weight:

$$Weight\ Loss\ (\%) = \frac{W_1 - W_2}{W_1} \times 100 \quad (2)$$

where W_1 and W_2 represent the cotton fabric's dry weights before and after the bleaching process, respectively.

2.6. UV-visible absorption spectra of species

The spectrum of absorbance of $NaClO_2$ solutions with the addition of various quantities of acid was examined using a UV-Vis spectrophotometer (3100-PC) in the 240–500 nm wavelength range.

2.7. Tensile strength (RT)

Cotton samples' tensile strength was assessed using the strip method by ASTM procedure D 2256-66T [22].

2.8. Field Emission Scanning Electron Microscopy (FE-SEM) analysis of cotton samples

Cotton samples were analyzed using a Hitachi S-4700 scanning electron microscope (SEM) to learn more about the microstructure of the cotton samples and determine whether the residues had been successfully removed after bleaching. A sputter machine (Cressington 108 auto sputter coater) was used to coat cotton cloth. Using ImageJ software, the measurement of the diameter and size of at least 50 randomly selected cotton fibers were measured to ascertain the size, diameter, and size distribution of the cotton fibers.

2.9. Fourier transforms infrared (FT-IR) analysis

In order to determine if chemical bonding exists in raw and bleached cotton in the range of 4000–400 cm^{-1} at a resolution of 4 cm^{-1}, Bruker Fourier transform infrared (FT-IR, Vertex-70) spectroscopy was utilized.

3. Results and discussions

According to earlier research, sodium chlorite breaks down into a strong oxidizing gas called ClO_2 and decomposes more quickly at low pH levels and higher temperatures [23,24]. Taking into account this information, the study's optimal timing and temperature were first established. The optimum temperature and time required for cotton fabrics to have a sufficient degree of whiteness were determined as a result of a series of bleaching experiments given in Table 1. As a result of the experiments performed at different temperatures and times using the same wetting agent

and acid conditioner, the ideal time and temperature were found to be 65 °C 30 min and 85 °C 30 min.

Examining the impact of the chemicals used to modify pH on cotton bleaching is one of the most crucial aspects of this study. The following substances are used to change the pH: AA, CA, PA, FA, AMTP, PAA, and HEDP. Utilizing sodium chlorite solutions of various concentrations and acids, information regarding the ideal concentration and acid was discovered to explore the bleaching impacts of $NaClO_2$ concentration and acidity controllers on cotton fabric bleaching. The experiment process was determined as a total of 60 min at pH = 3.0, 65 °C/30 min and 85 °C/30 min time/temperature.

The influence of acidity regulators and $NaClO_2$ concentration on the whiteness of cotton fabric is depicted in Fig. 2. In all acid tests, as shown in the figure (Fig. 2a), the amount of whiteness of the cotton fabric rises as the bleach concentration rises. It was discovered that the determined whiteness levels were on the equation with or higher than the reference sample following bleaching studies where the bleaching intensity ranged from 4.50 to 5.25. The most noteworthy acids among the used acid regulators were found to be FA and HEDP.

The whiteness rating of the bleaching experiments utilizing FA and HEDP at various $NaClO_2$ concentrations is contrasted with the whiteness rating of the reference fabric in Fig. 2b. The fabric's whiteness index was found to be low in the lower concentration tests (0.85, 1.70), to be reasonable in the slightly higher concentration test (3.40), and to be equal to or better in the experiments with concentrations of 4.25 and 5.25 for the reference fabric. The bleaching procedure utilizing an HEDP acid inhibitor at a concentration of 5.25 g/L $NaClO_2$ produces the best whiteness index (W.I. = 83).

One of the most crucial parameters, pH, was tuned at this point after the ideal temperature and time changes had been established in the initial phase of the study. The rate of sodium chlorite breakdown accelerates at low pH levels and high temperatures, according to earlier research [23]. To analyze the changes in the whiteness index of the fabrics, a variety of acid regulators (AA, CA, PA, FA, AMTP, PAA, and HEDP) were used during the bleaching trials at various pH levels (2.5, 3.0, 3.5, and 4.0) in Fig. 3a. As the pH level decreases, it can be observed in Fig. 3a that the whiteness value of the fabrics increases significantly. In all of the acid regulators utilized in the study, pH 2.5 and 3.0 produced the best whiteness results. This outcome is in line with research in the literature that looked at $NaClO_2$ and pH.
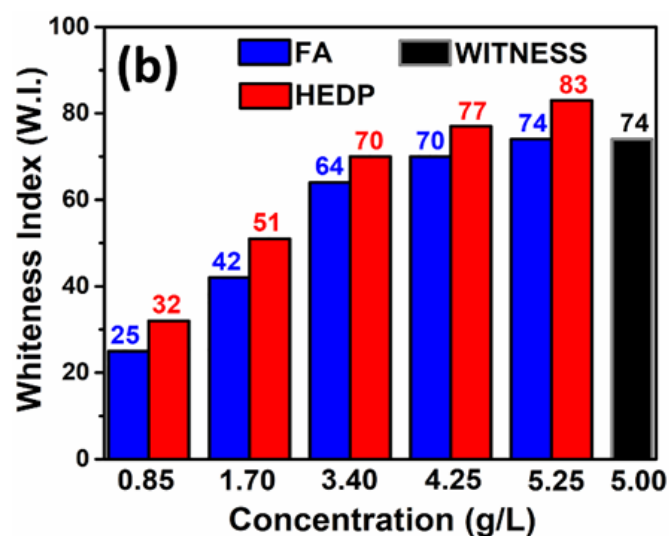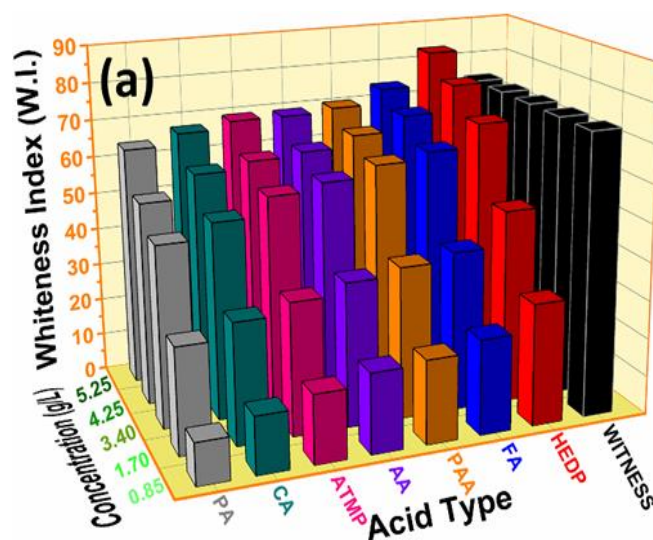

Figure 2. (a) The effect of sodium chloride amount and acid types on cotton bleaching and (b) the whiteness values obtained in the bleaching experiments with FA and HEDP compared with the whiteness value of the reference fabric

Table 1. Determination of optimum duration and temperature in cotton bleaching

Code	Temp. (°C)	Duration (min)	Whiteness Index(%)
1	30	30	44
2	30	60	50
3	30	90	55
4	30	180	58
5	50	30	61
6	50	60	64
7	50	90	71
8	50	180	74
9	65	30	63
10	70	30	65
11	70	60	72
12	70	90	75
13	70	180	80
14	85	30	67
15	95	30	69
16	95	60	78
17	95	90	80
18	95	180	82

$NaClO_2$: 5.25 (g/L) pH regulator: Formic acid, pH: 3.0, Stabilizer: STPP, Liquor Ratio: 1/10

Figure 4. FT-IR spectra of raw cotton fabric and NaClO₂ bleached cotton fabric
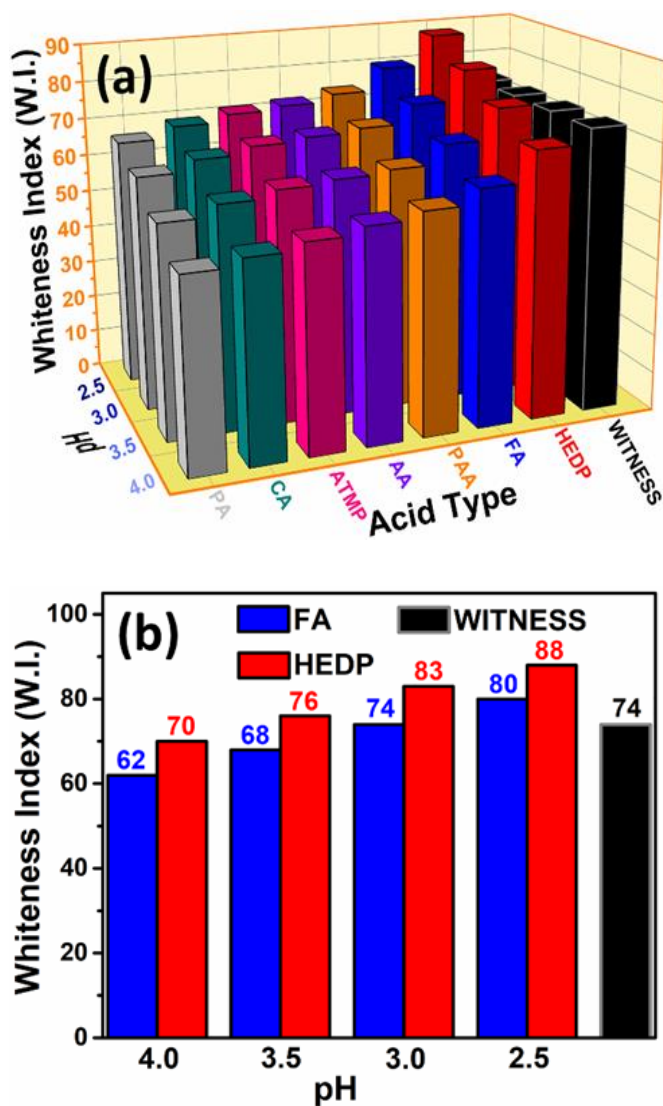

Figure 3. (a) The effect of pH on bleaching and (b) Comparison of the bleaching processes performed at different pH values by means of FA and HEDP with the reference fabric

The greatest whiteness index amongst acid controllers is provided by the HEDP acid, which can be better compared using Fig. 3b. It performs higher than the whiteness rating of the witness textile sample even when the pH level is 3.5.

The FTIR spectra of the unbleached fabric and the fabric bleached with sodium chlorite are shown in Fig. 4. The weak band at 1240 cm^{-1} is assigned to pectin's C-O side chain vibration [25]. However, this peak is not seen in the FT-IR spectrum of the bleached cotton, indicating that pectin was removed as a result of the bleaching process. At 1155 cm^{-1}, a comparable condition is also observed. This finding suggests that the bleaching process deforms the anti-symmetric C-O-C bond [26,27].

The raw and bleached cotton peak measurements of 1027 and 885 cm^{-1} and 1024 and 882 cm^{-1}, respectively, show that pectin and hemicelluloses are present in the cotton fiber [28]. The O-H frequency is also responsible for the broad peaks at 3328 and 3325 cm^{-1} in both spectra,
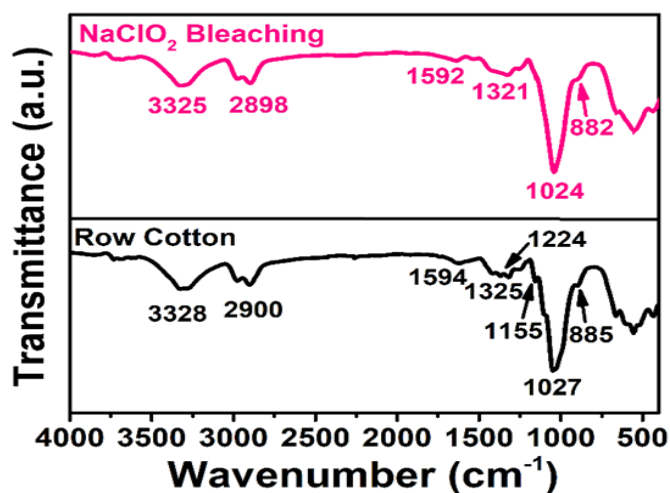
whereas the C-H stretch bands are responsible for the peaks at 2900 and 2898 cm^{-1} [29].

Fig. 5a and Fig. 5b show, respectively, the structure of the reference bleaching with H₂O₂ and the test sample bleached with NaClO₂. The reference cloth bleached with H₂O₂ and the untreated fabric utilized in the experimental research come from the same raw fabric roll. According to Fig. 5a, the structure of H₂O₂ bleached cloth is made up of fibers of comparable sizes. Inset in Fig. 5a depicts the periodicity of the fibers' measured diameters. 142 nm was the average diameter determined. The red dashed circle in Fig. 5a highlights the area where the fiber ripped following bleaching with H₂O₂. The surface of the fiber has deformations, as shown in the image. Furthermore, as shown by the red arrow, it is apparent that there are contaminants or chemical residues from bleaching agents on or between the fibers.

The cotton fabric in Fig. 5b has been bleached with NaClO₂ at pH = 3.0 with the help of the HEDP, pH regulator. The smooth fibers in the figure are greater in diameter than the fibers in Fig. 5a, and they are also not distorted. An inset of Fig. 5b displays the frequencies of the fiber sizes that were measured. Its 213 nm average diameter was determined. When comparing the two bleaching methods, it can be seen that the bleached with NaClO₂ results in less fiber deformation and leaves no bleaching residue on the cloth. These findings agree with previous research [10].

Finding out how much weight is lost in the fabric after bleaching is one of the key aspects of fabric bleaching. The weight of the fiber cotton is affected by various NaClO₂ concentrations and acidity regulators, as shown in Fig. 6a. As can be observed in the image, fabrics bleached with FA and HEDP have the highest decreased weight among acid regulators. As can be seen in Fig. 6a,
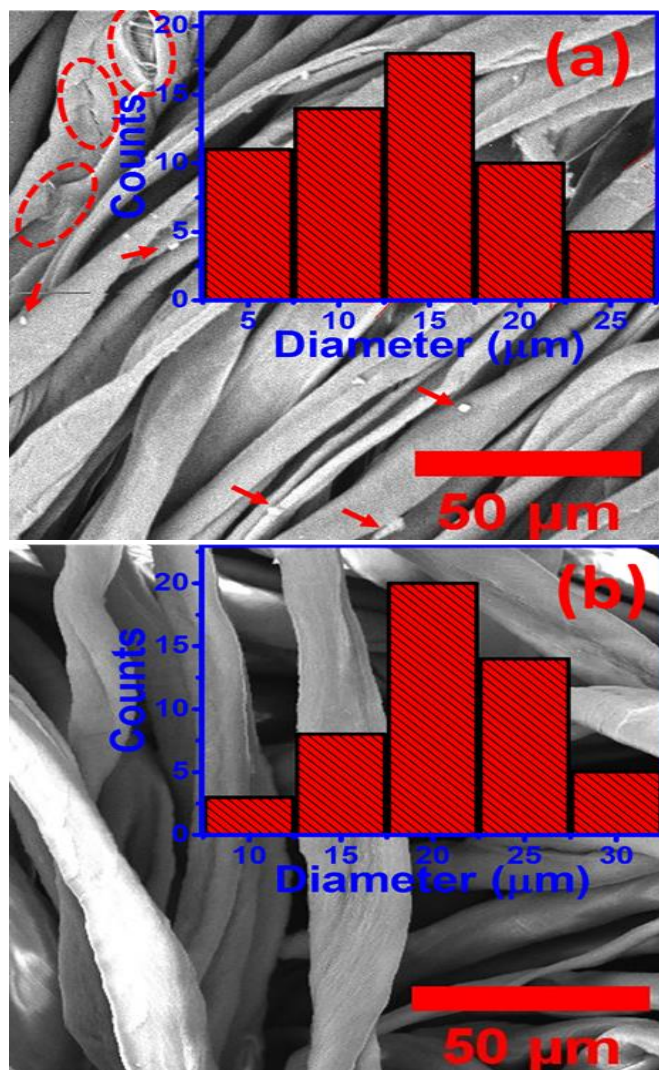
Figure 5. SEM images of (a) a reference fabric sample bleached with H_2O_2 and (b) an experimental cotton fabric sample bleached with $NaClO_2$ (top appendices in each figure show the frequency of the calculated diameters of the fibers)
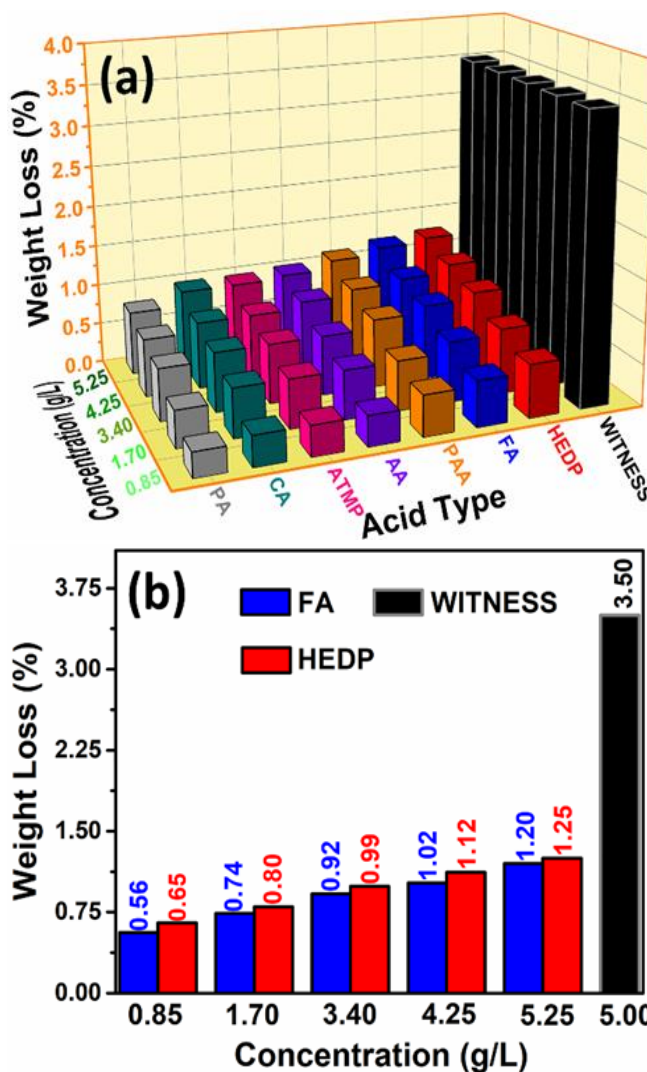

Figure 6. (a) The effect of $NaClO_2$ concentration on fabric weight and (b) Comparison of the percent loss in fabric weight as a result of bleaching processes performed at different $NaClO_2$ concentrations with the reference fabric

acid controllers in terms of the bleaching trials' whiteness indices.

Fig. 6b is included so that you may more clearly understand how these two acid controllers and various $NaClO_2$ concentrations affect weight loss. The bleached fabric loses weight as the sodium chlorite concentration rises, as shown in the figure. In conclusion, the bleaching and elimination of contaminants in the bleached cotton fabric is the cause of the fabric's increased weight loss with a rise in the whiteness index. The most startling finding is that even though the sodium chlorite

bleaching used in our investigation produced whiter results than the reference sample's whiteness, there was still a weight loss of about a third. This could imply that bleaching with $NaClO_2$ is cost-effective for techniques that do not result in a significant loss in fabric weight. The mechanical characteristics of bleached cotton fabrics, including tenacity and elongation% at the break, are shown in Table 2 and Table 3. Effect of pH and $NaClO_2$ concentration on the physical properties and whiteness index of the bleached cotton fabric. The table shows that as the concentration of $NaClO_2$ rises, the tenacity of the bleached fabric gradually declines.

Table 2. Effect of $NaClO_2$ concentration on the physical properties and whiteness index of the bleached cotton fabric

Code	$NaClO_2$ (g/L)	Whiteness Index (%)	Tenacity (kg f)	Elongation (%)
1	0.85	32	59.2	30.3
2	1.70	51	58.5	31.7
3	3.40	70	57.6	32.1
4	4.25	77	56.4	32.5
5	5.25	83	54.5	33.1
Witness	5.00 H_2O_2	74	51.2	34.3
Raw Cotton	—	—	68	21.3

Table 3. Effect of pH on the physical properties and whiteness index of the bleached cotton fabric

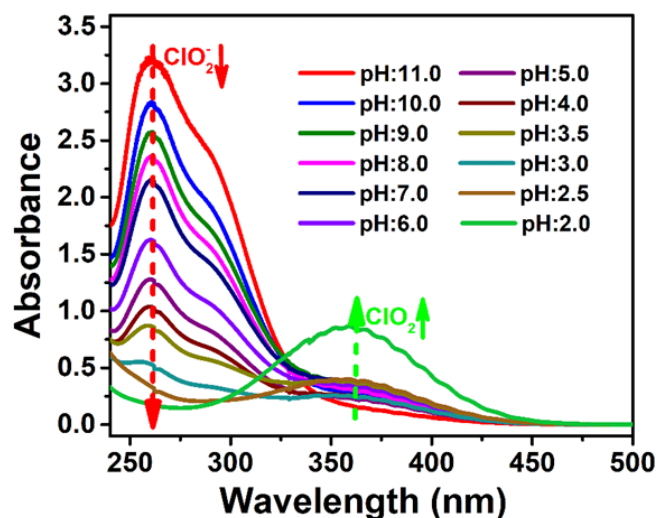| Code	pH	Whiteness Index (%)	Tenacity (kg f)	Elongation (%)
1	2.5	88	53	34
2	3.0	83	54.5	33.1
3	3.5	76	56.6	32.1
4	4.0	70	57.4	32.8
Witness	10.5	74	51.2	34.3
Raw Cotton	—	—	68	21.3

Figure 7. UV–visible absorption spectra of ClO_2^- and ClO_2 species in NaClO_2 solution under differrent pH irradiation (NaClO_2 concentration 0.8 g/L)

The situation is different when expressed as a percentage of elongation. Similarly, bleaching at low pH causes a decrease in the fabric's strength while increasing the whiteness index, percent elongation, and percent loss of weight of treated materials. The previous image discussed how bleach concentration increased as the weight of bleached materials increased.

As a result of the elimination of non-cellulosic components from cotton, it may be inferred that the weight loss, strength, and elongation have all increased, decreased, and are all increasing. A conclusion that can be drawn from the data is that the bleaching concentration and pH that should be utilized in the bleaching process are 5.25 g at pH = 3.0, which results in a desirable whiteness index and greatly protects the mechanical characteristics of the cotton fabric.

Considering the economic climate, even a 4.25 g concentration of bleach may be sufficient, according to the data gathered. However, the bleach concentration producing the best whiteness value is 5.25 g. Additionally, it has been found that bleach at this concentration provides a sufficient whiteness index and considerably safeguards the mechanical qualities of cotton fabric. The successful removal of these components may result in an increase in the whiteness index and a decrease in fabric weight since non-cellulosic substances in cotton fabric's natural structure darken the fabric's color.

Fig. 7 displays the absorbance spectrum of NaClO_2 solutions in various HEDP acid concentrations. This illustration depicts the absorption peaks of and at wavelengths of 260 nm and 360 nm, respectively [30]. As was already established, a rise in the amount of H⁺ has a beneficial impact on the ability to oxidize. The fact that sodium chlorite can decompose into poisonous and highly corrosive ClO$_2$ gas is also known [31]. Because of this, experiments were conducted to identify the ideal

pH level by taking measurements at various pH levels. Once the UV-vis spectra were studied, it was found that at high pH values, there was no discernible change in the concentration of NaClO_2 and that NaClO_2 got used as the environment turned acidic, or as the pH value declined. It becomes an unfavorable gas as the pH value decreases (2 and below) [32]. It was decided to conduct cotton bleaching experiments between pH: 4.0 and 2.5 as a consequence of the data gathered.

When water-soluble sodium chlorite is dissolved;

$$NaClO_2 + H_2O \rightarrow NaOH + HClO_2 \qquad (3)$$

A straightforward solution is found using Eq. 3. Agster claims that bleaching is provided by acid chlorite, not sodium chlorite or its ions. According to the equations below (Eq. 4), chlorite acid bleaches by releasing active oxygen.

$$HClO_2 \rightarrow HCl + 2O \qquad (4)$$
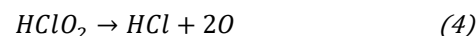
When bleaching, chlorine acid (HClO$_2$) rapidly breaks down into chlorine dioxide (ClO$_2$), the species that is active (Eq. 5), whose generation rate is related to the solution's sodium chlorite content.

$$NaClO_2 + HCl \rightarrow NaCl + HClO_2 \qquad (5)$$
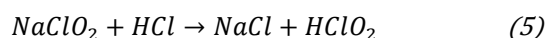
They can produce the reactions described in Eq. 6 and Eq. 7, as well as the chlorous acid emitted in the acidic environment, generating a reaction as given in Eq. 5.

$$5HClO_2 \rightarrow 4HClO_2 + HCl + 2H_2O \qquad (6)$$

$$3HClO_2 \rightarrow 2HClO_2 + HCl \qquad (7)$$
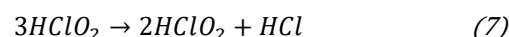
4. Conclusion

In this study, first, the optimum temperature and time parameters were determined. The optimum temperature and time were determined as 65 °C for 30 min and 85 °C for 30 min. In addition, the effect of NaClO_2 concentration on whiteness was investigated, and it was determined that the whiteness values obtained as a result of the bleaching study performed using 4.25 and 5.25 g/L NaClO$_2$ were better than the whiteness value of the reference fabric. Moreover, the effect of pH on bleaching was investigated, and it was observed that as the acidity of the medium increased, the whiteness increased in direct proportion. However, when working at very low pH values, undesirable ClO$_2$ gas output has

been observed. In addition to these, the effect of different acid types on bleaching was investigated, and the highest whiteness value was reached when HEDP was used (W.I. = 88). HEDP has reduced the use of chemicals, both because it acts as a wetting agent such as STPP, and because it enables fabrics to exhibit high whiteness even at low NaClO2 concentrations. As a result of the calculations, it was seen that the weight loss in fabrics bleached with NaClO2 was very small compared to the weight loss in the reference fabric. These results show that the bleaching process within the scope of this study is very economical. Moreover, it was observed that the bleaching process used in this study did little damage to cotton fibers and there was no alkali residue in bleached fabrics, so less water was needed to rinse the product and remove sodium. In addition, in this study, NaClO2, which is the source of ClO2, which has recently attracted a lot of attention as a disinfectant, was used. These results show that the bleaching process within the scope of this study is a very environmentally friendly process.

Acknowledgments

References

[1] E.S. Abdel-Halim, Simple and economic bleaching process for cotton fabric, Carbohydr Polym, 88, 2012 1233–8.

[2] H. Liu, C. Wang, and G. Wang, Photocatalytic advanced oxidation processes for water treatment: recent advances and perspective, Chem-Asian J, 15, 2020, 3239–3253.

[3] G.K. Günaydin, O. Avinc, S. Palamutcu, A. Yavas, A.S. Soydan, Naturally colored organic cotton and naturally colored cotton fiber production, Organic cotton, Springer, 2019, 81–99.

[4] A.K. Samanta, A. Konar, Dyeing of textiles with natural dyes, Nat dyes, 2011, 30–56.

[5] A. Davulcu, H. Benli, Y. Şen, M.I. Bahtiyari, Dyeing of cotton with thyme and pomegranate peel, Cellulose, 21, 2014, 4671–4680.

[6] A. Nadi, A. Boukhriss, A. Bentis, E. Jabrane, S. Gmouh, Evolution in the surface modification of textiles: a review, Text Prog, 50, 2018, 67–108.

[7] A. Haji, M. Naebe, Cleaner dyeing of textiles using plasma treatment and natural dyes: A review, J Clean Prod, 265, 2020, 121866.

[8] T. Adane, A. T. Adugna, E. Alemayehu, Textile industry effluent treatment techniques, J Chem, 2021,1–14.

[9] N. J. Lant, A. S. Hayward, M. M. Peththawadu, K. J. Sheridan, J. R. Dean, Microfiber release from real soiled consumer laundry and the impact of fabric care products and washing conditions, PloS one, 15, 2020, 1–18.

[10] C.A.H. Aguilar, J. Narayanan, N. Singh, P. Thangarasu, Kinetics and mechanism for the oxidation of anilines by ClO2: a combined experimental and computational study, J Phys Org Chem, 27, 2014, 440–449.

[11] A. Ivanovska, L. Pavun, B. Dojčinović, M. Kostić, Kinetic and isotherm studies for the biosorption of nickel ions by jute fabrics, J Serb Chem Soc, 86, 2021, 885–897.

[12] S. Xu, D. Huo, K. Wang, Q. Yang, Q. Hou, F. Zhang, Facile preparation of cellulose nanofibrils (CNFs) with a high yield and excellent dispersibility via succinic acid hydrolysis and NaClO2 oxidation, Carbohydr Polym, 266, 2021, 118118.

[13] M. Beroual, L. Boumaza, O. Mehelli, D. Trache, A. F. Tarchoun, K. Khimeche, Physicochemical properties and thermal stability of microcrystalline cellulose isolated from esparto grass using different delignification approaches, J Polym Environ, 29, 2021, 130–42.

[14] C.A. Hubbell, A. J. Ragauskas, Effect of acid-chlorite delignification on cellulose degree of polymerization, Bioresour Technol, 101, 2010, 7410–7415.

[15] G.D. Callachan, Novel methods for the removal of chlorine dioxide gas from aqueous solution and sodium chlorite production, Master's Thesis, Heriot Watt University, School of Engineering and Physical Sciences, 2019.

[16] M. Hirota, N. Tamura, T. Saito, A. Isogai, Oxidation of regenerated cellulose with NaClO2 catalyzed by TEMPO and NaClO under acid-neutral conditions, Carbohydr Polym, 78, 2009, 330–335.

[17] W. Ye, Y. Hu, H. Ma, L. Liu, J. Yu, Y. Fan, Comparison of cast films and hydrogels based on chitin nanofibers prepared using TEMPO/NaBr/NaClO and TEMPO/NaClO/NaClO2 systems, Carbohydr Polym, 237, 2020, 116125.

[18] T.L. Chen, Y.H. Chen, Y.L. Zhao, P.C. Chiang, Application of gaseous ClO2 on disinfection and air pollution control: A mini review, Aerol Air Qual Res, 20, 2020, 2289–2298.

[19] I.C. Eduardo, B.G. Blanca, A. Yohanny, C. Patricia, S.A. Maria, A.B.A. San Martín, C.O. Gonzales, Determination of the Effectiveness of Chlorine Dioxide in the Treatment of COVID 19, Mol Genet Genomic Med, 2021, 1–11.

[20] B. A. Annous, D. A. Buckley, D. H. Kingsley, Efficacy of chlorine dioxide gas against hepatitis A virus on blueberries, blackberries, raspberries, and strawberries, Food Environ Virol, 13, 2021, 241–247.

[21] D. ASTM, E313-73: Standard Test Method for Indices of Whiteness and Yellowness of Near-White, Opaque Mater, 1993.

[22] H. Fahmy, Enhancing some performance properties of ester crosslinked cotton fabric by pre-quaternization, Egypt J Chem, 47, 2004, 627–640.

[23] S. R. Karmakar, Chemical technology in the pre-treatment processes of textiles: Elsevier, 1999.

[24] C. A. Hubbell, A. J. Ragauskas, Effect of acid-chlorite delignification on cellulose degree of polymerization, Bioresource technol, 101,2010, 7410–7415.

[25] A. Kozioł, K. Środa-Pomianek, A. Górniak, A. Wikiera, K. Cyprych, M. Malik, Structural determination of pectins by spectroscopy methods, Coatings, 12, 2022, 546.

[26] J. Sun, F. Xu, X. Sun, B. Xiao, R. Sun, Physico-chemical and thermal characterization of cellulose from barley straw, Polym Degrad Stab, 88, 2005, 521–531.

[27] Z. Yang, S. Xu, X. Ma, S. Wang, Characterization and acetylation behavior of bamboo pulp, Wood Sci Technol, 42, 2008, 621–632.

[28] V. Sangeetha, T. Varghese, S. K. Nayak, Isolation and characterisation of nanofibrillated cellulose from waste cotton: effects on thermo-mechanical properties of polylactic acid/MA-g-SEBS blends, Iran Polym J, 28, 2019, 673–683.

[29] M. Joonobi, J. Harun, P. M. Tahir, L. H. Zaini, S. SaifulAzry, M. D. Makinejad, Characteristic of nanofibers extracted from kenaf core, BioResour, 5, 2010, 2556–2566.

[30] S. Yang, X. Pan, Z. Han, D. Zheng, J. Yu, P. Xia, B. Liu, Z. Yan, Nitrogen oxide removal from simulated flue gas by UV-irradiated sodium chlorite solution in a bench-scale scrubbing reactor, Ind Eng Chem Res, 56, 2017, 3671–3678.

[31] R. Hao, X. Wang, Y. Liang, Y. Lu, Y. Cai, X. Mao, B. Yuan, Y. Zhao, Reactivity of NaClO2 and HA-Na in air pollutants removal: active species identification and cooperative effect revelation, J Chem Eng, 330, 2017, 1279–1288.

[32] P. Gong, X. Li, Promoting effect of H+ and other factors on NO removal by using acidic $NaClO_2$ solution, Energies, 12, 2019, 2966.
[33] T. L. Vigo, Textile processing and properties: Preparation, dyeing, finishing and performance: Elsevier, 2013.

Dispersive liquid-liquid microextraction for the spectrophotometric determination of Fe³⁺ with a water soluble Cu(II) phthalocyanine compound

Yasemin Çağlar [iD]

Giresun University, Faculty of Engineering, Department of Genetic and Bioengineering, 28200, Giresun, Türkiye

Abstract

DLLME, which is a method that minimizes organic solvent consumption and waste generation, is frequently used for trace analyte determination. In the present work, a simple, selective and sensitive spectrophotometric method based on the dispersive liquid-liquid microextraction was reported. The procedure is based on the formation of a 1:1 complex between Fe^{3+} and a water-soluble Cu(II) phthalocyanine and then extraction of this complex into dichloromethane by dispersive effect of acetone. The experimental parameters that effecting the DLLME such as amount of extractive and disperser solvents, pH, salt concentration, Cu(II) phthalocyanine concentration and centrifuging time and rate were optimized. The linear range of the method is 0.4–70.0 ng/mL with a good correlation coefficient (R^2) of 0.9912. The limits of detection (LOD) and quantification (LOQ) are 0.47 and 1.86 ng/mL, respectively. The relative standart deviation (RSD, %) of the method for 40 ng/mL Fe^{3+} in sample solution (n=11) was 1.4% and the enrichment factor was calculated 240.

Keywords: DLLME, spectrophotometry, iron, Cu(II) phthalocyanine

1. Introduction

Iron is an essential element for biological processes. [1,2]. An healty adult human body contains about 4 grams of iron, mostly in hemoglobin and myoglobin and is lost every day for a variety of reasons. The daily loss must be compensated to maintain the body's iron balance [3,4]. One of the important tasks of iron, which is an element prone to oxidation due to its structure, in the human body is to carry oxygen. Heme iron binds to hemoglobin in the blood and to myoglobin in the muscles, performing the task of transporting oxygen. The human body also needs iron to make some hormones responsible for growth and development. Iron is found in the active site of many important redox enzymes in plants and animals. It increases the efficiency of copper and calcium by helping enzymes in protein metabolism [5–8].

Chemically, the most common oxidation states of iron are Fe^{2+} and Fe^{3+}. Dietary iron exists in two forms, heme iron (Fe^{2+}) and non-heme iron (Fe^{3+}). Heme iron is found in animal sources such as red meat, eggs, fish and chicken. Non-heme iron is obtained from plant sources. Heme iron is better absorbed by the body than non-heme iron. Low pH and the presence of ascorbic acid increase non-heme iron absorption. However, polyphenols such as tannins and chlorogenic acids found in tea, coffee, and some other foods inhibit iron absorption. Although conventional views agree that polyphenols only affect non-heme iron absorption, recent experiments have provided evidence that polyphenolic compounds can inhibit the absorption of heme and non-heme iron. It also showed that polyphenols have a dose-dependent inhibitory effect [9–14].

When the hemoglobin protein in the blood falls below the normal level, it is called anemia. The most common cause of anemia is iron deficiency. Iron deficiency reduces oxygen delivery to cells, leading to fatigue and weakening of the immune system. Iron deficiency, which is commonly observed in children and infants, delays mental development. Iron deficiency is a serious health problem in both developing and developed countries. Chronic blood loss and insufficient absorption in the small intestines are important factors in iron deficiency. However, it is mostly caused by insufficient iron intake in the daily diet [15–18].

Iron is a micronutrient. But high doses of iron are toxic to humans and can cause serious health problems

such as depression, difficulty breathing, convulsions and heart attacks. Excessive intake of Fe^{2+} creates free radicals in the body. Long-term exposure to high doses of iron can cause diabetes, liver poisoning, and graying of the skin [19–22].

Quantitative determination of iron is especially important for the biological and environmental fields. That is why, various methods have been suggested to determine iron concentration including inductively coupled plasma mass spectrometry (ICP-MS) [23], flame atomic absorption spectrometry (FAAS) [24], polarography [25], high performance liquid chromatography (HPLC) [26], ion chromatography [27] and spectrophotometry [28,29].

Despite the development of high precision analytical instruments for the analysis of trace analytes, problems are often encountered in direct analysis from the sample matrix. Therefore, pretreatment is usually required for the separation and concentration of the analytes from the matrix medium. Microextraction methods, which minimize the use of organic solvents and provide a high enrichment factor, are intensely preferred for sample pretreatment todays [30–32].

Dispersive liquid-liquid microextraction (DLLME) is a relatively novel miniaturized sample pretreatment protocol. It was suggested by Rezae at al. in 2006 [33]. It based on a ternary component solvent system inclusive extractive solvent, dispersive solvent and aqueous sample phase. The mixture of appropriate amounts of extractive and dispersive solvents are quickly applied to the aqueous sample phase by a syringe. Extraction is completed in a short time after formation of cloudy solution because of huge surface area between the extractive and aqueous phases. Following centrifugation, the small droplets of extraction solvent containing analyte is gathered at the base of test tube. Finally, appropriate instrumental technique is applied to the residue for quantitative calculations about analyte [34–39].

In this study, a novel spectrophotometric iron determination method based on DLLME has been reported. The short content of this method is the extraction of Fe^{3+} from the sample medium by the DLLME method, following the formation of a complex with a water soluble Cu(II) phthalocyanine (Cu(II)-Pc) ligand that was prepared as stated in relevant literature [40].

Phthalocyanines are synthetic macrocyclic compounds with a highly conjugated planar 18-π electron system. Phthalocyanines, which are formed by the condensation of four iminoisoindoline units, have a very tense structure. During the production of metal phthalocyanines, the template effect of the metal ion in the environment increases the product yield. The chemical properties of a phthalocyanine compound depend on the central atom and the substituents. They have high thermal stability and blue-green color. Phthalocyanines can be coordinated with almost all metals. The most important limitation in the application of phthalocyanines is their low solubility in water and most organic solvents. [41–43].

2. Experimental

2.1. Materials
All the reagents and solvents were analytical grade from Merck (Darmstadt, Germany) and Sigma Aldrich (Taufkirchen, Germany). Ultrapure water was used for the entire study from Sartorius (Arium-Pro). Fe^{3+} working standard solutions were prepared by daily stepwise dilution of standard stock solution ($Fe(NO_3)_3 \cdot 6H_2O$, 1×10^{-3} mol/L). The sensor (1×10^{-5} mol/L) solution was prepared weekly by dissolving an appropriate amount of Cu(II)-Pc in 25 mL of water and kept at 4 °C.

2.2. Equipment
A Thermo Scientific Evaluation Array Spectrophotometer and a 250 μL volume quartz cuvette were used for the absorbance measurements. The pH values were measured by a Hanna HI 2211 model pH meter. Benchtop Centrifuge, K2015R model centrifuge was used to achieve phase separation.

2.3. Preconcentration procedure
For DLLME, initially 10 mL of water solution containing the Fe^{3+} analyte was poured into a 15 ml conical glass tube. Then 400 μL of Cu(II)-Pc (1×10^{-5} mol/L) was added as sensor. The pH of the tube was adjusted to 4.0 with 0.1 mol/L di-sodium hydrogen phosphate/potassium dihydrogen phosphate buffer solution after 150 μL of NaCl (1.0 M) was joined. Complexation was waited for 1 min. Followed by the mixed solution of 120 μL dichloromethane and 1.0 mL acetone was rapidly sheded onto the mixture by a 2.0 mL syringe. It was observed that the solution became cloudy because of dispersing of very fine dichloromethane droplets. So, the formed complex between Fe^{3+} ion and Cu(II)-Pc was extracted into these fine droplets. After that, the solution was centrifuged at 4000 rpm for 3 min. The dispersed slim droplets of dichloromethane were collapsed at the ground of the glass tube. The supernatant aqueous phase was ejected with a glass Pasteur pipette. After all, the organic phase was diluted to 400 μL with ethanol and absorbance was measured by using a quartz micro-cell at 355 nm.

3. Results and Discussion

3.1. Absorption spectra

Phthalocyanine compounds have strong $\pi \rightarrow \pi^*$ transitions, known as the Q band, in the 600–700 nm range. Metallic phthalocyanines form a single band in this region. The n-π^* transitions observed in the range of 320–400 nm resulting from the characteristic colors of the phthalocyanine compounds are called the B (Soret) band. In accordance with the literature, the absorption spectra of the water soluble Cu(II)-Pc ligand has a sharp Q band at 680 nm and a B band at 335 nm.

The spectral changes were recorded in the 320–500 nm range after the DLLME procedure. It was observed that increasing Fe^{3+} concentration in the range of 0.4–70.0 ng/mL at 355 nm regularly increased the absorbance of the ligand (Fig. 2).

3.2. Optimization of DLLME

3.2.1. Effect of extractive solvent kind and volume

The choice of organic solvent which is one of the basic parameters of DLLME significantly affects the enrichment factor. To allow phase separation, it must be immiscible with water while miscible with disperser solvent. Besides, the extractive solvent must be denser than water [44–46]. For the proposed DLLME procedure, various organic solvents such as chloroform, carbon tetrachloride and dichloromethane were tested.
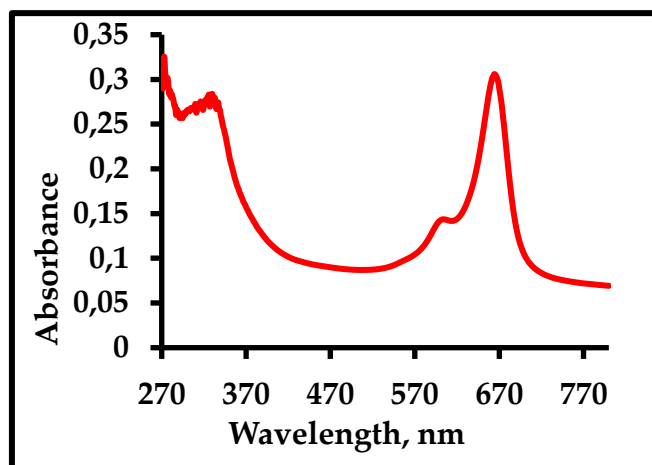

Figure 1. The Uv-Vis spectra of Cu(II)-Pc in water (1x10^{-5} mol/L)

When the experimental data were examined (Fig. 1), it was seen that the extraction efficiency of dichloromethane was higher than all of them due to the highest absorbance value. Therefore, dichloromethane was chosen as the extractive solvent.

To state the effect of selected extractive solvent volume on the proposed DLLME procedure, varied volumes (40, 80, 120, 160, 200, 240 and 280 μL) of dichloromethane were applied to experimental procedure. Since after 120 μL of dichloromethane the extraction efficiency decreases as the solvent volume increases, as seen in Fig. 2, 120 μL of dichloromethane was chosen as the optimum extractive solvent volume.
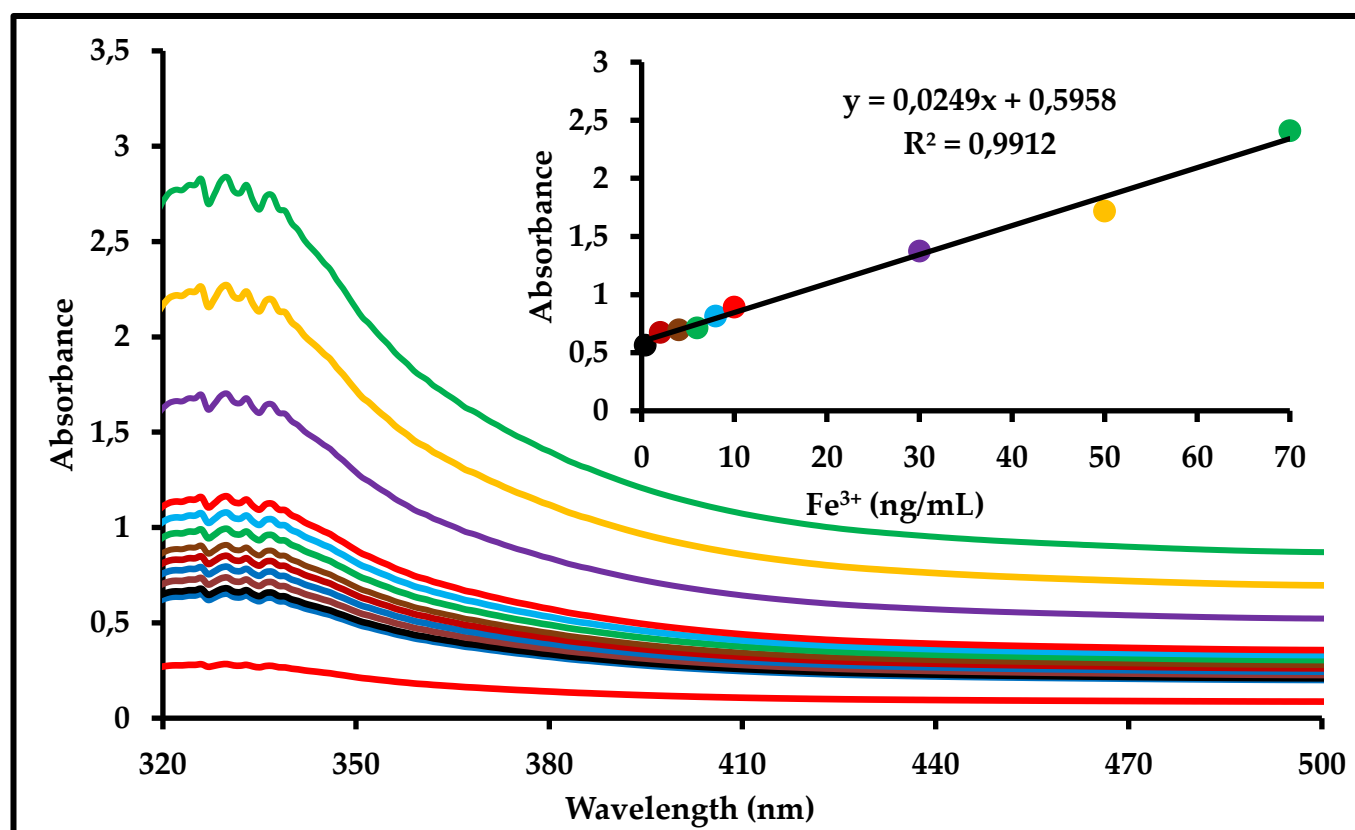

Figure 2. Changes in absorption spectra of Fe^{3+}:Cu(II)-Pc after DLLME procedure Extraction conditions: 10.0 mL sample volume; 120 μL dichloromethane; 1.0 mL acetone; 1x10^{-5} mol/L Cu(II)-Pc; 1.0 M NaCl; pH 4.0 Inset: Changes in absorbance in 355 nm. Iron(III) concentration is between 0.4–70.0 ng/mL

3.2.2. Effect of nature and volume of disperser solvent

The choice of a dispersing solvent depends on its miscibility in both the extraction solvent and the aqueous sample solution [47–49]. Ethanol, methanol, acetone and acetonitrile that are the most commonly used dispersion solvents in DLLME procedures were tried for this proposed method. It was observed that the precipitated phase was the highest when acetone was used as the dispersing solvent. Looking at Fig. 3, it is clear that the absorbance value agree with the observation. Therefore, acetone was chosen as the disperser solvent.

For the best disperser solvent volume the enrichment factors of the samples containing different volumes of acetone 0.25, 0.50, 0.75, 1.0, 1.5 and 2.0 mL containing 120 µL of dichloromethane were compared. In the presence of 0.25 mL of acetone, the enrichment factor is somewhat lower because dichloromethane is not sufficiently dispersed as seen in Fig. 4. The enrichment factor decreased after the acetone volume exceeded 1.0 ml because excess acetone volume increased the solubility of the complex. As a result of detailed examination of Fig. 4, 1.0 mL was chosen as the optimum dispersive solvent volume.

3.2.3. Effect of sample pH

Sample pH has a major role in the metal-ligand interaction and the following microextraction procedure especially in ternary complex formation [50]. The effect of pH on the extraction of Fe^{3+} was studied in the pH range of 2.0 to 12.0. Experimental results (Fig. 5) showed that absorption had reached its maximum at pH 4.0. Considering the results, a pH value of 4.0 was selected as optimum for microextraction procedure.

3.2.4. Effect of salt

The varied NaCl concentrations (0.0–2.0 M) were studied to investigate the ionic strength effect on DLLME procedure. The result showed that (Fig. 6), the addition of salt increased the extraction efficiency in 1.0 M NaCl. The addition of more salt caused a decrease in absorbance as it prevented the transition of Fe^{3+}:Cu(II)-Pc complex to the extractive solvent [51].

3.2.5. Study of centrifuging time and rate

To understand of effect of centrifuging parameters such as the centrifuging time and rate on the proposed DLLME procedure, they were studied in the range of 1.0 to 8.0 min and 1000–6000 rpm, respectively. According to the results of the experiment, 3 min and 4000 rpm were chosen as the optimum centrifugation parameters.
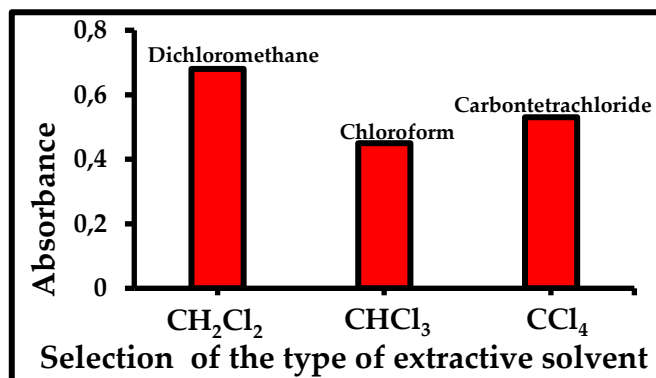

Figure 3. The selection of the extractive solvent kind. Extraction conditions: 10.0 mL sample volume; 1.0 mL acetone; 1×10^{-5} mol/L Cu(II)-Pc; 1.0 M NaCl; pH 4.0

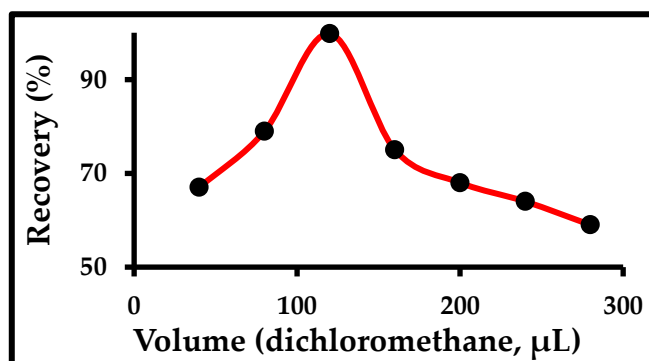**Figure 4.** The effect of the dichloromethane volume on extraction recovery. Extraction conditions: 10.0 mL sample volume; 1.0 mL acetone; 1×10^{-5} mol/L Cu(II)-Pc; 1.0 M NaCl; pH 4.0
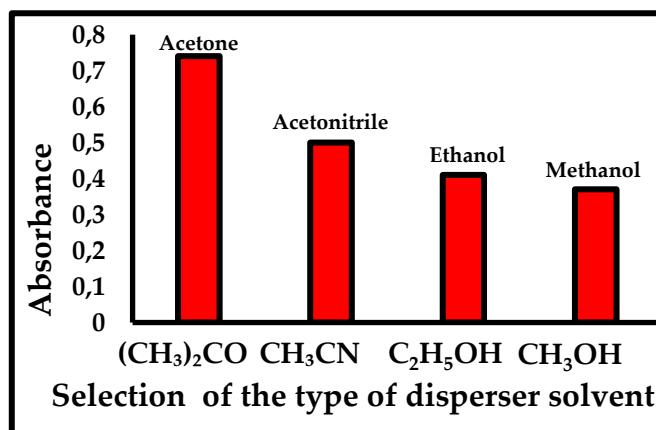

Figure 5. The selection of the disperser solvent kind. Extraction conditions: 10.0 mL sample volume; 120 µL dichloromethane; 1×10^{-5} mol/L Cu(II)-Pc; 1.0 M NaCl; pH 4.0
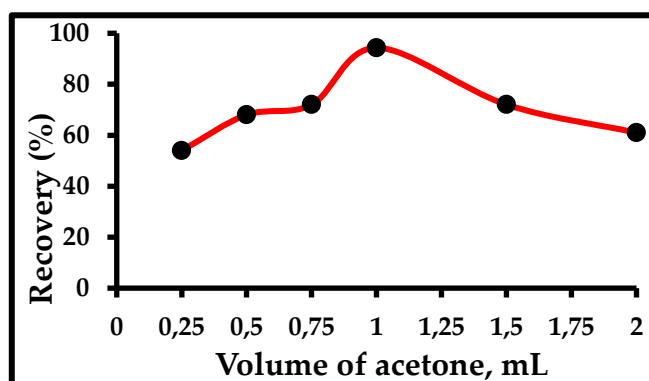

Figure 6. The effect of the acetone volume on extraction recovery. Extraction conditions: 10.0 mL sample volume; 120 µL of dichloromethane; 1×10^{-5} mol/L Cu(II)-Pc; 1.0 M NaCl; pH 4.0

3.2.6. Effect of concentration of Cu(II)-Pc

The effect of different concentration of the Cu(II)-Pc in the range of 1×10^{-4} to 1×10^{-6} mol/L were studied while the other parameters were kept constant. The highest absorbance was seen for 1×10^{-5} mol/L Cu(II)-Pc. Last of all, 1×10^{-5} mol/L Cu(II)-Pc was optimum for Fe^{3+} detection.

3.2.7. Assessment of probable interferences

In order to show the selectivity of Fe^{3+} determination with the proposed DLLME method, the effects of several probable interfering metal cations were carefully studied. Different concentrations of these ions were added to samples containing 40 ng/mL Fe^{3+}. The highest concentrations of probable interfering ions no causing more than 5% change in sample absorption were calculated as the tolerance limit. As can be seen in Table 1, since the tolerance limits of the studied ions are quite high, the matrix effect can be neglected in Fe^{3+} analysis in real samples with the proposed DLLME method.

3.3. Complex stoichiometry

The Job method was applied to determine the stoichiometries of Fe^{3+}:Cu(II)-Pc complex formed. The resulting Job graph showed us that the M:L ratio was 1:1.

3.4. Method validation

Validation of the proposed method under optimum conditions was evaluated based on limits of detection (LOD), limits of quantification (LOQ), linear range, enrichment factor and relative standard deviation (RSD, %). The LOD was 0.47 ng/mL defined as 3 times the ratio of the standard deviation of the blank to the calibration graph. The LOQ was 1.86 ng/mL defined as 10 times the ratio of the standard deviation of the blank to the calibration graph. The calibration curve is linear in the range of 0.4–70.0 ng/mL with a good correlation coefficient (R^2) of 0.9912. The relative standard deviation (RSD, %) of the proposed method for 40 ng/mL Fe^{3+} in sample solution (n = 11) was 1.4%. The enrichment factor was calculated 240.

Table 1. Tolerance limits of coexisting ions for the spectrophotometric determination of Fe^{3+} at 355 nm

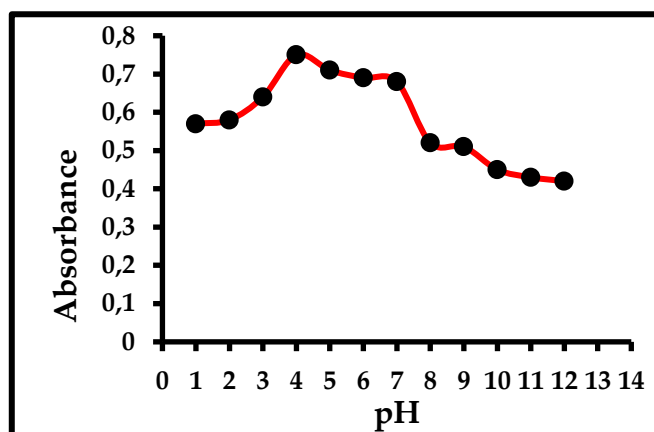| Foreign ion added	DLLME
Ag^+	165
Cu^{2+}	118
Co^{2+}	93
Cr^{3+}	152
Pb^{2+}	141
Ni^{2+}	68
Cd^{2+}	199
Zn^{2+}	227
Mn^{2+}	106
Na^+	356
NO_3^-	235
SO_4^{2-}	94
PO_4^{3-}	178

Figure 7. The effect of pH on extraction procedure. Extraction conditions: 10.0 mL sample volume; 120 µL of dichloromethane; 1.0 mL acetone; 1×10^{-5} mol/L Cu(II)-Pc; 1.0 M NaCl
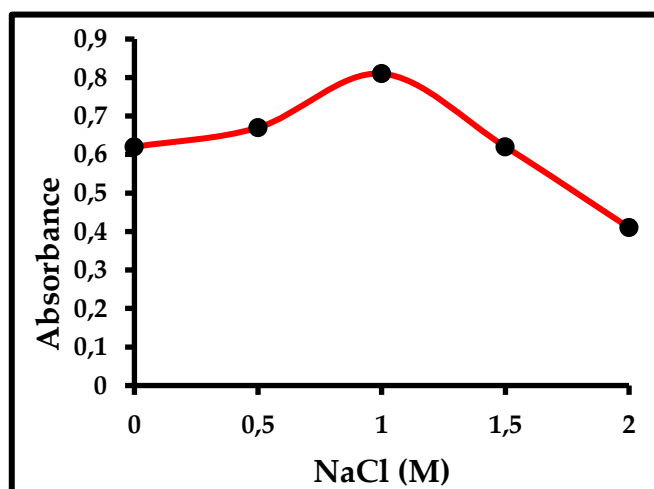

Figure 8. The effect of concentration of salt on extraction procedure. Extraction conditions: 10.0 mL sample volume; 120 µL of dichloromethane; 1.0 mL acetone; 1×10^{-5} mol/L Cu(II)-Pc; pH 4.0

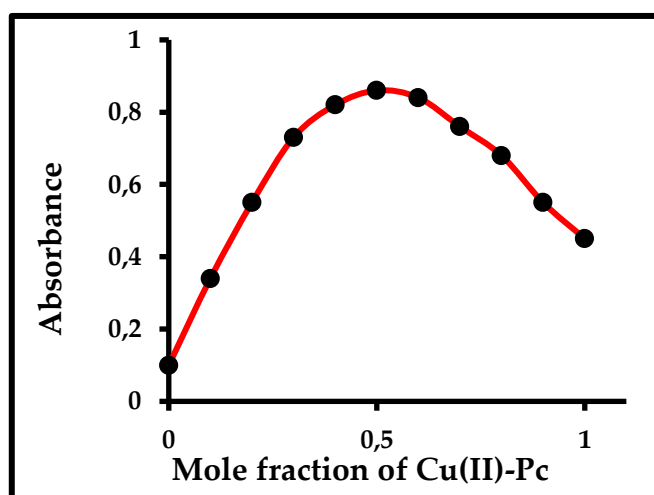**Figure 9.** The Job plot to determine the Fe3+:Cu(II)-Pc stoichiometry

Table 2. The analytical features of the optimized method

Parameter	
Correlation coefficient (R^2)	0.9912
Linear range (ng/mL)	0.4–70.0
LOD (ng/mL)	0.47
LOQ (ng/mL)	1.86
RSD,% (n=11)	1.4
Enrichment factor	240

4. Conclusion

In the DLLME procedure, the selection of the chelating reagent is a very important parameter that affects the extraction efficiency. Phthalocyanines are very suitable materials for developing chelating cation sensors. As the synthesis of water-soluble phthalocyanines increases, their utility in spectroscopic metal determination also increases. In this proposed DLLME method, a water-soluble Cu(II) phthalocyanine containing 3- (pyridin-4-yl) propane-1-oxy groups in non-peripheral positions is used as the chelating reagent. The method is simple, selective, and low cost.

Acknowledgments

References

[1] D. Stoyanovsky, Y. Tyurina, I. Shrivastava, I. Bahar, V. Tyurin, O. Protchenko, S. Jadhav, S. Bolevich, A. Kozlov, Y. Vladimirov, Iron catalysis of lipid peroxidation in ferroptosis: Regulated enzymatic or random free radical reaction, Free Radic Biol Med, 133, 2019, 153–161

[2] Y. Bi, A. Ajoolabady, L.J. Demillard, W. Yu, M.L. Hilaire, Y. Zhang, J. Ren, Dysregulation of iron metabolism in cardiovascular diseases: From iron deficiency to iron overload, Biochem Pharmacol, 190, 2021, 114661–114673.

[3] A.D. Sheftel, A.B. Mason, P. Ponka, The long history of iron in the universe and in health and disease, Bichim Biophysic Acta, 1820, 2012, 161–187.

[4] J. Mao, Q. He, W. Liu, A.D. Sheftel, A.B. Mason, P. Ponka, An rhodamine-based fluorescence probe for iron(III) ion determination in aqueous solution, Talanta, 20, 2010, 2093–2098.

[5] B. Uttara, A.V. Singh, P. Zamboni, R.T. Mahajan, Oxidative stress and neurodegenerative diseases: a review of upstream and downstream antioxidant therapeutic options, Curr Neuropharmacol, 7, 2009, 65–75.

[6] Y. Chen, P. Barak, Iron nutrition of plants in calcareous soils, Adv Agron, 35, 1982, 217–240.

[7] S. Lakhal-Littleton, Mechanisms of cardiac iron homeostasis and their importance to heart function, Free Radic Biol Med, 133, 2019, 234–237.

[8] C. Camaschella, Iron-deficiency anemia, N Engl J Med, 372(19), 2015, 1832–1843.

[9] J.R. Hunt, Bioavailability of iron, zinc, and other trace minerals from vegetarian diets. Am J Clin Nutr, 78(3), 2003, 633–639.

[10] P.J. Gregory, A. Wahbi, J. Adu-Gyamfi, M. Heiling, R. Gruber, E.J.M. Joy, M.R. Broadley, Approaches to reduce zinc and iron deficits in food systems, Glob Food Sec, 15, 2017. 1–10.

[11] S.O. Fakayade, A.G. King, M. Yakubu, A.K. Mohammed, D.A. Pollard, Determination of Fe content of some food items by flame atomic absorption spectroscopy (FAAS): a guided-inquiry learning experience in instrumental analysis laboratory, J Chem Educ, 89, 2012, 109–113.

[12] E.C. Theil, Iron regulatory elements (IREs): a family of mRNA non-coding sequences, Biochem J, 304, 1994, 1–11.

[13] M.W. Hentze, L.C. Kuhn, Molecular control of vertebrate iron metabolism: mRNA-based circuits operated by iron, nitric oxide, and oxidative stress, Proc Natl Acad Sci USA, 93, 1996, 8175–8182.

[14] T.A. Rouault, R.D. Klausner, Post-transcriptional regulation of genes of iron metabolism in mammalian cells, J Biol Inorg Chem, 1, 1996, 494–499.

[15] R.V.C. Cardoso, A. Fernandes, A.M. Gonzaléz- Paramás, L. Barros, I.C.F.R. Ferreira, Flour fortification for nutritional and health improvement: A review, Food Research Int, 125, 2019, 108576–108587.

[16] M. Auerbach, J.W. Adamson, How we diagnose and treat iron deficiency anemia, Am J Hematol, 91, 2015, 31–38.

[17] H. Tapiero, L. Gate, K. Tew, Iron: deficiencies and requirements, Biomed Pharmacother, 55, 2001, 324–332.

[18] F.E. Viteri, Iron supplementation for the control of iron deficiency in populations at risk, Nutr Rev, 55, 1997, 195–209.

[19] T.A. Rouault,. Iron metabolism in the CNS: implications for neurodegenerative diseases, Nat Rev Neurosci, 14, 2013, 551–564.

[20] M.A. Smith, P.L.R. Harris, L.M. Sayre, G. Perry, Iron accumulation in Alzheimer disease is a source of redox-generated free radicals. Proc Natl Acad Sci USA 94, 1997, 9866–9868,

[21] A. Shander, M.D. Cappellini, L.T. Goodnough, Iron overload and toxicity: the hidden risk of multiple blood transfusions, Vox Sang, 97, 2009, 185–197.

[22] Y. Kohgo, K. Ikuta, T. Ohtake, Y. Torimoto, J. Kato, Body iron metabolism and pathophysiology of iron overload, Int J Hematol, 88(1), 2008, 7–15.

[23] M.S. Wheal, E. DeCourcy-Ireland, J.R. Bogard, S.H. Thilsted , J.C.R. Stangoulis, Measurement of haem and total iron in fish, shrimp and prawn using ICP-MS: implications for dietary iron intake calculations, Food Chem, 201, 2016, 222–229.

[24] E. Canfranc, A. Abarca, I. Sierra, M.L. Marina, Determination of iron and molybdenum in a dietetic preparation by flame AAS after dry ashing, J Pharm Biomed Analysis, 25 (1), 2001, 103–108.

[25] L. Yang, L. Wang, L. Lın, Z. Peng, G. Lu, Polarographic determination of total iron content using a $Fe^{2+/3+}$-Methylthymol Blue-NO_2^- System, Analyt Scienc, 20, 2004, 1655-1659.

[26] V. Fernández, G. Winkelmann, The determination of ferric iron in plants by HPLC using the microbial iron chelator desferrioxamine E, Biometals, 18, 2005, 53–62.

[27] F. Deutsch, P. Hoffman, H.M. Ortner, Field experimental investigations on the Fe (II)-and Fe (III)-content in cloudwater samples, J Atmos Chem, 40(1), 2001, 87–105.

[28] M.J. Ahmed, U.K. Roy, A simple spectrophotometric method for the determination of iron(II) aqueous solutions, Turk. J. Chem, 33, 2009, 709–726.

[29] M.A. Kassem, A.S. Amin, Spectrophotometric determination of iron in environmental and food samples using solid phase extraction, Food Chem, 141, 2013, 1941–1946.

[30] L.K. Tintrop, A. Salemi, M.A. Jochmann, W.R. Engewald, T.C. Schmidt, Improving greenness and sustainability of standard analytical methods by microextraction techniques: A critical review, Anal Chim Acta, 1271, 2023, 341468–341472.

[31] A. Sarafraz-Yazdi, A. Amiri, Liquid phase microextraction, Trends Anal Chem, 29, 2010, 1–14.

[32] S. Armenta, S. Garriguez, M. de la Guardia, The role of green extraction techniquesin green analytical chemistry, Trends Anal Chem, 71, 2015, 2–8.

[33] M. Rezaee, Y. Assadi, M.R. Milani Hosseini, E. Aghaee, F. Ahmadi, S. Berijani, Determination of organic compounds in water using dispersive liquid-liquid microextraction, J Chromatogr A, 1116, 2006, 1–9.

[34] A. Bidari, E. Zeini Jahromi, Y. Assadi, M.R. Milani Hosseini, Monitoring of selenium in water samples using dispersive liquid-liquid microextraction followed by iridium-modified tube graphite furnace atomic absorption spectrometry, Microchem J, 87, 2007, 6–12.

[35] M. Gharehbaghi, F. Shemirani, M. Baghdadi, Dispersive liquid-liquid microextraction and spectrophotometric determination of cobalt in water samples, Int J Environ Anal Chem, 88, 2008, 513–523.

[36] P. Liang, H. Sang, Determination of trace lead in biological and water samples with dispersive liquid-liquid microextraction preconcentration, Anal Biochem, 380, 2008, 21–25.

[37] P. Liang, L. Peng, P. Yan, Speciation of As(III) and As(V) in water samples by dispersive liquid-liquid microextraction separation and determination by graphite furnace atomic absorption spectrometry, Microchim Acta, 166, 2009, 47–52.

[38] A.B. Tabrizi, Development of a dispersive liquid-liquid microextraction method for ıron speciation and determination in different water samples, J Hazard Mater, 183, 2010, 688–693.

[39] H. Yan, H. Wang, Recent development and applications of dispersive liquid-liquid microextraction, J Chromatogr A, 1295, 2013, 1–15.

[40] E.T. Saka, Synthesis, characterization and photocatalytic properties of non-peripherally 3-(pyridin-4-yl) propane-1-oxy groups substituted Cu(II) Phthalocyanine and water soluble derivative, Sakarya Unv J Scien, 24, 2020, 1029–1039

[41] R. Zhou, F. Josse, W. Göpel, Z.Z. Öztürk, Ö. Bekaroğlu, Review: Phthalocyanines as sensitive materials for chemicals sensors, Appl Organomet Chem, 10, 1990, 557–577.

[42] R.J. Mortimer, A.L. Dyer, J.R. Reynolds, Electrochromoc organic and polymeric materials for display applications, Displays, 27, 2006, 2–18.

[43] D. Atilla, N. Kılınç, F. Yüksel, A.G. Gürek, Z.Z. Öztürk, V. Ahsen, Synthesis, characterization, mesomorphic and electrical properties of tetrakis(alkylthio) substituted Lutetium(III) bisphthalocyanines, Synthetic Metals, 159, 2009, 13–21.

[44] S.Z. Mohammadi, D. Afzali, Y.M. Baghelani, Ligandless-dispersive liquid-liquid microextraction of trace amount of copper ions, Anal Chim Acta, 653, 2009, 173–177.

[45] R. Khani, F. Shemirani, B. Majidi, Combination of dispersive liquid-liquid microextraction and flame atomic absorption spectrometry for preconcentration and determination of copper in water samples, Desalination, 266, 2011, 238–243.

[46] C. Wu, B. Zhao, Y. Li, Q. Wu, C. Wang, Z. Wang, Development of dispersive liquid-liquid microextraction based on solidification of floating organic drop for the sensitive determination of in water and beverage samples by flame atomic absorption spectrometry, Bull Korean Chem Soc, 32(3), 2011, 829–834.

[47] K. Shrivas, N.K. Jaiswal, Dispersive liquid-liquid microextraction for the determination of copper in cereals and vegetable food samples using flame atomic absorption spectrometry, Food Chem, 141, 2013, 2263–2268.

[48] X. Wen, Q. Yang, Z. Yan, Q. Deng, Determination of caadmium and copper in water and food samples by dispersive liquid-liquid microextraction combined with UV-vis spectrophotometry, Microchem J, 97, 2011, 249–254.

[49] M.M. Sanagi, H.H. Abbas, W.A.W. Ibrahim, H.Y. Aboul-Enien, Dispersive liquid–liquid microextraction method based on solidification of floating organic droplet for the determination of triazine herbicides in water and sugarcane samples, Food Chem, 133, 2012, 557–562.

[50] A. Asghari, M. Ghazaghi, M. Rajabi, M. Behzad, M. Ghaedi, Ionic liquid-based dispersive liquid-liquid microextraction combined with high performance liquid chromatography-UV detection for simultaneous preconcentration and determination of Ni, Co, Cu and Zn in water samples. J Serbian Chem Soc, 79, 2014, 63–76.

[51] D.A. Lambropoulou, T.A. Albanis, Application of solvent microextraction in a single drop for the determination of new antifouling agent in waters, J Chromatogr A, 1049, 2004, 17–23.

Promising antimicrobial and antifungal activities of free peppermint (*Mentha piperita* L.) essential oil and its conjugated form with chitosan

Pinar Sen* iD , Parisa Bolouri iD , Fikrettin Sahin iD

Yeditepe University, Department of Genetics and Bioengineering, Faculty of Engineering, İstanbul, 34755, Türkiye

Abstract

The emergence of antimicrobial resistance has necessitated the new approaches. The peppermint (*Mentha piperita* L.) essential oil (PEO) is known for its antimicrobial and antifungal activities. However, the employing of it in workable applications is troublesome because of the sensitivity to the environmental conditions. Thus, it was encapsulated into chitosan to eliminate the difficulties in its use and increase its activity. It was observed that the immobilization of the PEO into the chitosan (PEO-Chitosan) influenced the biological activities resulting in observing less Minimum Inhibitory Concentration (MIC) values in addition to protecting the essential oil by the chitosan as environment-friendly biomaterial. The determined MIC values of the target product (PEO-Chitosan) are between 0.001–0.95 mg/mL for the studied bacterial strains and 0.006–0.36 mg/mL for the studied fungi isolates, which led us to consider them as new therapeutic alternative. *In vitro* antiviral studies gave us that even the encapsulation of the essential oil into the chitosan made the prepared product still promising candidate for the antiviral therapy.

Keywords: *Mentha piperita* L., encapsulation, chitosan, antibacterial, antifungal and antiviral activity

1. Introduction

Infectious diseases have been an important health problem for years. Since the discovery and administration of penicillin in the 1940s, antibiotics have played unique roles as invaluable weapons to combat infectious for humans and animals [1]. It is used to cure the diseases caused by microorganisms and has the ability to kill bacteria or inhibit their development by inhibiting the formation of cell membranes, protein synthesis, cytoplasmic membranes or nucleic acid synthesis [2]. In line with this importance, newer drugs as antibiotics have been introduced into clinical practice such as β-lactams, sulphonamides, polypeptides to prevent or treat the infectious disease over the decades [3].

Before the advent of antibiotics, these diseases were the leading cause of morbidity and death in human populations. But later, the facing with the crisis of antimicrobial resistance among pathogenic bacteria is dynamic increasing problem. This might be the because of the overuse and abuse of antimicrobial drugs posing a major threat to both human and animal health [4].

In the same way, another threat for the humanity is that the increasing resistance to antifungal compounds,

originating from drug target alteration or overexpression [5]. In a consequence of this, a number of scientific investigations have driven to the new therapeutic alternatives by the scientist to combat fungal infectious disease. Today, plant-based natural products carried out by different disciplines on the production of antibacterial and antifungal substances are increasing day by day.

Viral infections are a serious and increasing health problem and cause high morbidity, mortality and economic burden [6]. The limited availability of current therapy methods has prompted researchers to obtain new products of biotechnological importance.

The extracted essential oils from the plants have been reported as antibacterial [7], antiviral [8], antifungal [9]. Among them, peppermint (*Mentha piperita* L.) is cultivated all over the world for its use in medicinal and pharmaceutical applications in addition to using in food, herbal tea preparations due to its flavor and fragrance [10]. Because of the antimicrobial, antifungal and antiviral activities, the peppermint essential oil have been subjected in some studies [11–13]. Although the high activity of essential oils in different applications,

some environmental conditions hinder them to use in their pure form. The conjugation to the nano-carriers or encapsulation into nano materials have been the focus of considerable interest in developing new alternatives to overcome this drawback. These strategies allow essential oils not only to preserve their bioactive components, but also to prepare new materials aimed at increasing the effectiveness of essential oils [14].

In accordance with this purpose, the studied peppermint essential oil (PEO) was encapsulated into chitosan. Chitosan as biocompatible biomaterial is known for its antibacterial and antifungal feature against bacterial and fungal pathogens that infect human hosts [15,16]. The antibacterial and antifungal activities of the obtained chitosan conjugate of oil were investigated against selected bacteria and fungus strains as compared with the pure form of peppermint essential oil. In addition to this, the prepared samples were tested *in vitro* cytotoxicity and antiviral activity, against virus's representative of herpes simplex virus-1 and Human poliovirus Type 1.

2. Experimental

2.1. Chemicals and Instruments
The *Mentha piperita* L. (peppermint) sample used in this study was collected from the north of Iran (Gorgan City, Golestan Province, Iran) before flowering. Chitosan, acetic acid, acetone, diethyleter, dimethylsulfoxide (DMSO), ampicillin and fluconazole were purchased from Sigma–Aldrich. Ultra-pure water was from MilliQ water. Nutrient agar and agar bacteriological BBL Muller Hinton broth were purchased from Merck. Dulbecco's phosphate-buffered saline (DPBS) was purchased from Sigma Aldrich All the bacteria species were provided by the Department of Genetics and Bioengineering, Faculty of Engineering, Yeditepe University (Istanbul, Turkey) such as *Staphylococcus aureus* (*S. Aureus)* (ATCC 6538), *Escherichia coli* (*E. Coli*) (ATCC 10536), *Pseudomonas aeruginosa* (ATCC 15442), *Staphylococcus epidermidis* (*S. epidermidis*) (ATCC 15442), *Candida albicans* (*C. Albicans)* (ATCC 10231), *Aspergillus niger* (ATCC 16404), *Penicillium* spp and *Methicillin-resistant Staphylococcus aureus* (*MRSA*) were isolated and characterized by MALDI-TOF (Bruker Microflex LT/SH).

Immortalized human keratinocytes (HaCaT) cell line, Herpes Simplex Type 1 (MacIntyre, #0810005CF, Zeptometrix), and Human poliovirus Type 1 (LSc-2ab, RVB 1260, FLI) viruses were used (cell line and viruses were obtained from the Genetic and Bioengineering Department of Yeditepe University). GC Agilent 6890N; MS: Agilent 5973 with an HP5-MS column (30 m × 0.25 mm fused silica capillary column, film thickness 0.25 μm) was used for GC/ MS analysis. FTIR spectra were recorded on an attenuated total reflectance (ATR) apparatus on a Thermo Scientific Nicolet IS10-IZ10. SEM images were taken by a Zeiss evo 40 instrument following gold sputtering (EM ACE200, Leica). Zeta Potential of chitosan conjugate was determined using Zetasizer Nano-ZS90 (Malvern Instruments). Electronic spectra were recorded on a PerkinElmer LAMBDA 25 Series UV−vis spectrophotometer with a quartz cell of 1 cm.

2.2. Method of Extraction Essential oil *Mentha piperita* L.
The essential oil of peppermint (*Mentha piperita* L.) was collected from the region (Gorgan province in Iran), then the aerial parts were dried, and finally the essential oil was obtained by hydro distillation technique. The essential oil was analyzed by GC/MS method in Dr. Soltani Akhula's factory in East Azarbaijan Province, Iran. Distillation details are given in reference [17].

2.3. Immobilization of peppermint essential oil to Chitosan
Preparation of the encapsulation of the PEO into chitosan was carried out using a procedure reported in the literature with slight modification, namely, without precipitation with NaOH to obtain charged solution [18]. Briefly, for the preparation of PEO-chitosan, chitosan (0.2 g) was stirred in water/2% acetic acid (10 mL) until obtaining homogeneous mixture. Then 1 ml of PEO by dissolving in DMSO was added into this solution and stirred continuously for 24 h. After complete mixing, washed several times with distilled water until the pH of water was neutral. The new product was collected by centrifuging and dried by freeze-drying.

2.4. *In vitro* antibacterial and antifungal activities
Activity studies of PEO and its encapsulated derivative were carried out by micro-well dilution assays [19]. Briefly, the microorganisms (tested for activity were transferred from stock culture to suspend in PBS and adjusted to approx. 1×10^6 cfu/ml per ml with the help of MacFarland turbidity curve. MIC values were determined according to the broth dilution method and performed in 96 flat-bottomed microliter plates. Each of the bacterium and the fungi suspensions was added to the first test well and mixed. Serial two-fold dilutions of the extractions were prepared in broth with a final volume of 100 μL in 96-well microplates. Then, 100 μL of bacterial suspension was inoculated in each well. The microplates were incubated at 37 °C for 24 h. The last wells including nutrient broth only and nutrient broth containing bacterium or fungi without compound was considered as negative and positive control, respectively. MIC was idendified as the lowest concentration of the samples that kills 99.9% or more of the initial inoculum.

2.5. *In vitro* antiviral activities

The cytotoxicity and the virus-inhibitory effect of each sample was determined *in vitro* by employing MTS (3-(4,5-dimethylthiazol-2-yl)-5-(3-arboxymethoxyphenyl)-2-(4-sulfophenyl)-2H-tetrazolium) method on human immortalized keratinocyte (HaCaT) cell line along with the cytotoxic concentration (CC$_{50}$) by determining first the non-toxic concentration of the samples against HaCaT cell line [20]. All experiments were carried out three times. The data were given as logarithmic form.

3. Result Discussion

3.1. Structure characterization

This study was started with the extraction of the essential oil from the *Mentha piperita* L. by hydro distillation technique. The determined main components of *Mentha piperita* L. essential oil that was analyzed by GC/MS method are: menthol (43.25%), menthone (15.1%), menthofuran (9.33%), ciscarane (6.7%), 1,8-cineole (5.37%), neomenthol (5.37%), 4.1% and limonene (1.95%). The goal of our work was the encapsulation of essential oil of *Mentha piperita* L. through conjugation into chitosan in order to enhance their antimicrobial activity by the procedure as stated in the experimental part under the "Immobilization of peppermint essential oil to Chitosan" section (Scheme 1). The obtained conjugate (PEO-chitosan) was characterized by using analytical techniques such as Fourier transform infrared spectroscopy (FT-IR), SEM, UV/Vis by comparing the PEO alone and zeta potential measurement of the conjugate. The results confirmed the presence of target compounds.

FT-IR spectrums of the studied samples show the existence of the functional groups. In the FT-IR spectrum of PEO, the band at 3398 cm^{-1} is attributed to the OH groups coming from the alcohol derivatives which are the some of the components of the PEO. The other characteristic peaks at 2958–2869 cm^{-1}, 1712 cm^{-1}, 1459 and 1370 cm^{-1}, 1246 cm^{-1} and 1046 cm^{-1}, belonging to the aliph. -CH stretchings, C=O stretching, aliph. C-C stretching, -C-O asym. and –C-O sym. stretching, respectively, were seen in the FT-IR spectrum of PEO (Fig. 1B).

In the FT-IR spectrum of chitosan powder, the peaks at 3357 and 3290 cm^{-1} are attributed to the NH$_2$ and OH groups as overlapped with each other. The aliph. -CH stretchings and -N–H bending vibration of primary amine (−NH$_2$) were observed at 2924, 2871 cm^{-1} and 1649 cm^{-1}. The peak originating from the saccharide structure of chitosan arised at 1062 cm^{-1} for –C-O sym. stretching (Fig. 1A).

Upon conjugation of PEO to the chitosan, In the FT-IR spectrum of PEO-chitosan, the peaks at 3380 cm^{-1} reflect the –OH and –NH stretchings that are superimposed by contributions from all the components present in the mixture. The C=O stretching which is the one of the main characteristic peaks coming from the PEO components shifted to 1702 cm^{-1}, implying the complex formation via electrostatic interaction between NH$_3^+$ groups of chitosan and carbonyl group of PEO. Also, the shifting of the C-C stretching and –C-O sym. stretching to the 1457,1378 cm^{-1} and 1066 cm^{-1}, respectively, prove the complexation between chitosan and PEO [21] (Fig. 1C).

The UV-vis absorption spectra of PEO and its chitosan conjugate were recorded in DMSO. In the UV/Vis spectrum of PEO, considerably intense band at λ_{max} = 311 nm, which can be attributed to the high contents of terpenes, terpenoids and phenolic compounds and might be the characteristic liquid state of aggregation [22]. Upon the non-covalent immobilization of PEO into chitosan, the absorption
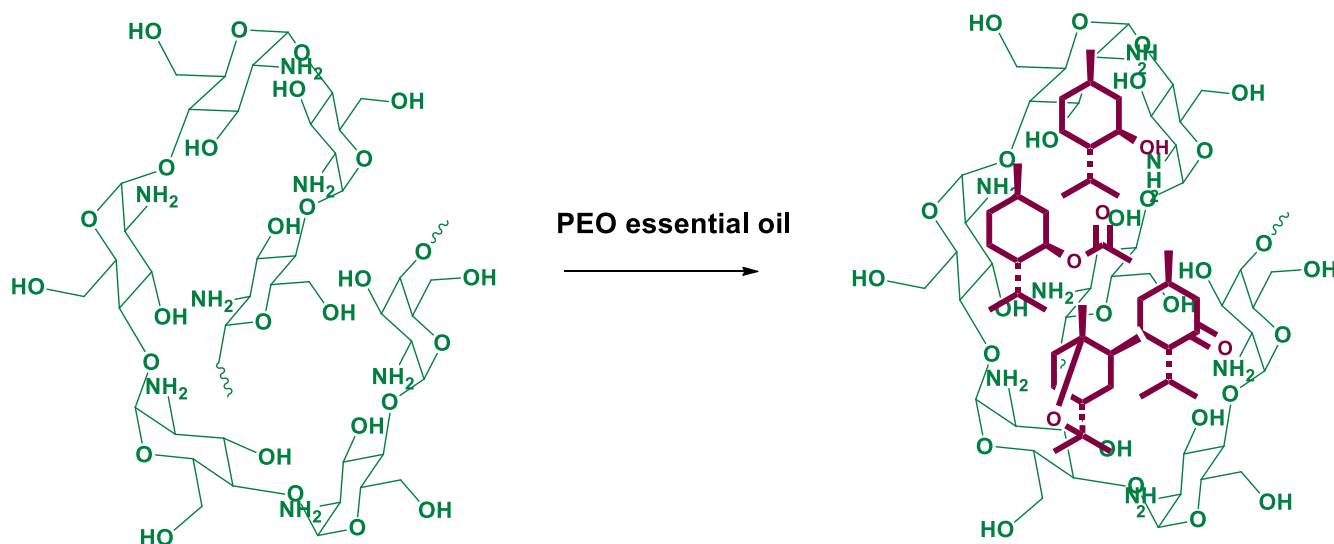
Scheme 1. Schematic illustration of conjugation PEO to chitosan (only four of ingredient was used for illustration) (PEO: peppermint essential oil)

band was observed at 290 nm with blue shift compared to the PEO alone, which can be explained by decreasing the intermolecular electronic coupling of the PEO in the conjugate (Fig. 2) [23].

Scanning electron microscopy (SEM) has been used to study the surface morphology and the image of the conjugate is shown in Fig. 3. In the SEM images, PEO-chitosan have smooth, flat and homogeneous surfaces at its morphology. The irregularities like air bubbles or oil droplets meaning to macroscopic phase separation were not observed, showing that the PEO is well distributed in the chitosan.

Surface charge (zeta potential) (ζ) determination is a measure of charges that is carried by conjugates suspended in a liquid. It could considerably affect the stability of conjugates in suspension and *in vitro* efficiency of the prepared samples with the cell membrane of bacteria, through the electrostatic repulsion between particles [24]. The measurement of the chitosan conjugate (PEO-Chitosan) showed that the surfaces of sample have a positive charge about 4 mV, resulting from the dissociation of acidic groups that are on the chitosan units [25].

3.2. Determination of the antimicrobial activity

The antimicrobial activities of PEO alone and its conjugation with chitosan (PEO-chitosan) against *S. aureus, S. epidermidis, MRSA* as gram-(+), *Pseudomonas aeruginosa, and E. coli* as gram-(−) bacterial strains, *C. albicans, Aspergillus niger* and *Penicillium* spp. as fungi isolates were compared to investigate the effect of the conjugation of PEO with the biorganic molecule. The initial concentration of the PEO used in the study was assumed to be 100% corresponding to the 80 mg/mL while the conjugate dissolved in DMSO were first prepared at the highest concentration to be tested (7.6 mg/mL). The minimum inhibitory concentration results are presented in Table 1.

Both PEO alone and PEO-chitosan exhibited antibacterial activities against microorganisms. Pure PEO showed antibacterial activity against bacteria strains with MIC value of 2.64 mg/mL for *Pseudomonas aeruginosa*, 1.32 mg/mL for *S. aureus and MRSA*, 0.66 mg/mL for *S. epidermidis* and 2.64 mg/mL for *E. Coli.* The encapsulated PEO exhibited enhancement of bactericidal activity against all the studied microorganisms with MIC value of 0.95 mg/mL for *S. aureus, Pseudomonas aeruginosa* and *MRSA* and 0.001 mg/mL for *E. coli* as compared to PEO alone. The reason why the lowest MIC value was observed for *E. coli* may be behind the better penetration of immobilized PEO molecules through the lipophilic cell wall of gram-negative bacteria [26].
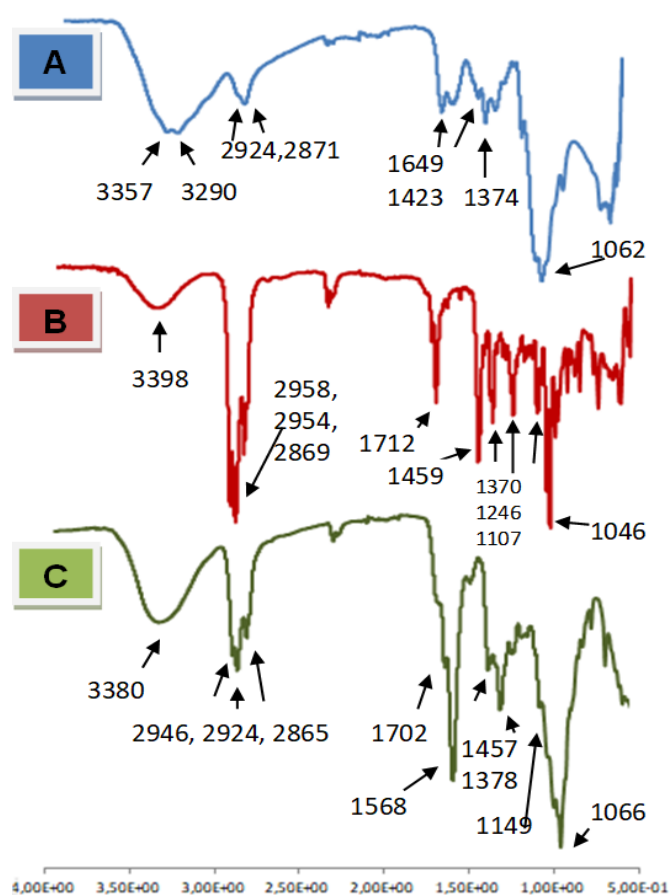

Figure 1. FTIR spectra of A: Chitosan, B: Peppermint oil alone C: PEO-Chitosan (wavenumber cm⁻¹) (PEO: peppermint essential oil)
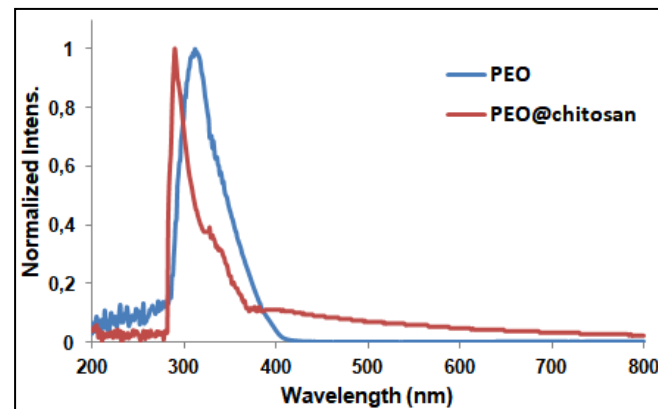

Figure 2. Normalized absorption spectra of PEO and its chitosan conjugate (PEO-chitosan) (PEO: peppermint essential oil)
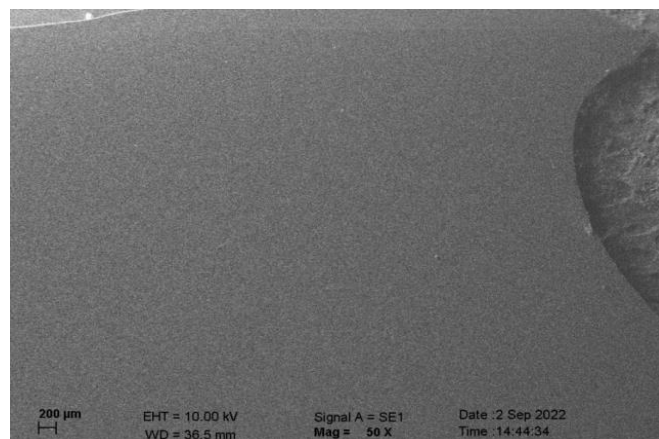

Figure 3. SEM of the surface image of PEO-chitosan film viewed at a magnification of 1000x. (PEO: peppermint essential oil)

Table 1. *In vitro* antimicrobial and antifungal activity of the studied samples (MIC in mg/mL)

Microorganisms	MIC			
	PEO	PEO-chitosan	Amp.	Fluc.
Staphylococcus aureus	1.32	0.95	0.01 [31]	—
Pseudomonas aeruginosa	2.64	0.95	0.05 [31]	—
Staphylococcus epidermidis	0.66	0.03	0.05 [32]	—
Methicillin-resistant Staphylococcus aureus	1.32	0.95	0.05 [33]	—
Escherichia coli	2.64	0.001	0.025 [31]	—
Candida albicans	0.33	0.36	—	0.0023 [34]
Aspergillus niger	0.33	0.022	—	> 0.58 [34]
Penicillium spp	0.09	0.006	—	0.00025 [35]

PEO: peppermint essential oil,
MIC: Minimum Inhibitory Concentration
Amp.: Ampicillin, Fluc.: Fluconazole

Also, this could be attributed to the contribution of the chitosan units due to already known antibacterial properties [27,28].

The studied samples (PEO alone and PEO-Chitosan) exhibited also antifungal activity. When compared to the PEO alone, the results showed that the PEO-Chitosan has more potent antifungal activity against *Aspergillus niger* with the MIC value of 0.022 mg/mL and *Penicillium* spp with the MIC value of 0.006 mg/mL than that of PEO alone (Table 1). This could be attributed that the bioactivity of PEO-Chitosan enhanced through the activation of passive mechanisms of cell absorption [29]. However, the antifungal activity of PEO-Chitosan is not as potent as that of PEO alone with the MIC value of 0.36 mg/mL against *C. albicans.* The resistance of PEO-Chitosan to *C. albicans* may be the result of the weak interaction between cell membrane components (phospholipids) leading to the fungal plasma membrane impermeability [30]. The results coming from the currently used an antibiotic (applied concentration:0.124 mg/mL) and antifungal drug (applied concentration:1,4 mg/mL) were shown in Table 1 to compare with the studied samples [31–35].

3.3. Determination of the antiviral activity

The antiviral activities of the studied samples (PEO alone and PEO-Chitosan) against Herpes Simplex Type 1 and Human poliovirus Type 1were compared to investigate the effect of the encapsulation of the essential oil and the results are summarized in Table 2. As can be seen from Table 2, it was found that the samples showed antiviral activities. PEO alone was found the more active than PEO-Chitosan with log reduction values of 3.75 for Human poliovirus Type 1 and 4.5 for Herpes Simplex Type 1. The same experiments exhibit the antiviral activity for the encapsulated PEO (PEO-Chitosan) as 3.25 log for Human poliovirus Type 1 and 3 log for Herpes Simplex Type 1. We might conclude that the PEO alone activated the immune system of host to some extent and induced the releases of immune factors [36].

Table 2. Antiviral activity of the studied samples

Microorganisms	Log reduction	
	PEO	PEO-chitosan
Herpes Simplex Type 1	4.5	3
Polio	3.75	3.25

PEO: peppermint essential oil

4. Conclusions

In the present study, a successful preparation of the conjugate of PEO into the chitosan via the immolization method was carried out to improve the antibacterial and antifungal activity of PEO against bacterial and fungal pathogens. The biological actions of the PEO alone and its conjugate were determined separately. Results displayed the encapsulation process promoted an increase in antibacterial and antifungal activity *in vitro* by disrupting membrane integrity.

This research proved that combining biologically active components resulted in better efficacy. In summary, this conjugate is biologically active macromolecules that might be used as for new antimicrobial and antifungal agent and could be considered potential options instead of the currently available synthetic drugs. We observed that the employed essential oil had better activity against the studied viruses compared to the encapsulated derivative.

Acknowledgements

References

[1] P.I. Lerner, Producing penicillin, N Engl J Med, 351, 2004, 524.

[2] G. Cheng, M. Dai, S. Ahmed, H. Hao, X. Wang, Z. Yuan, Antimicrobial Drugs in Fighting against Antimicrobial Resistance, Front Microbiol, 7, 2016, 470.

[3] R. Aminov, History of antimicrobial drug discovery: Major classes and health impact. Biochem Pharmacol, 133, 2017, 4–19.

[4] B. Aslam, W. Wang, M.I. Arshad, M. Khurshid, S. Muzammil, M.H. Rasool, M.A. Nisar, R.F. Alvi, M.A. Aslam, M.U. Qamar, M.K.F. Salamat, Z. Baloch, Antibiotic resistance: a rundown of a global crisis. Infection and Drug Resistance, 11, 2018, 1645–1658.

[5] L.E. Cowen, Predicting the emergence of resistance to antifungal drugs, FEMS Microbiol Lett, 204, 2001, 1–7.

[6] R.E. Baker, A.S. Mahmud, I.F. Miller, M. Rajeev, F. Rasambainarivo, B.L. Rice, S. Takahashi, A.J. Tatem, C.E. Wagner, L.F. Wang, A. Wesolowski, C.J.E. Metcalf, Infectious disease in an era of global change, Nat Rev Microbiol, 20, 2022, 193.

[7] S. Prabuseenivasan, M. Jayakumar, S. Ignacimuthu, *In vitro* antibacterial activity of some plant essential oils. BMC Complement Altern Med, 6, 2006, 39.

[8] L. Ma, L. Yao, Antiviral Effects of Plant-Derived Essential Oils and Their Components: An Updated Review, Molecules, 25, 2020, 2627.

[9] F. Nazzaro, F. Fratianni, R. Coppola, V.D. Feo, Essential Oils and Antifungal Activity. Pharmaceuticals 10, 2017, 86.

[10] D. Brown, Encyclopaedia of Herbs and Their Uses, 1995, London, Dorling Kindersley

[11] L. Jirovetz, G. Buchbauer, S. Bail, Z. Denkova, A. Slavchev, A. Stoyanova, E. Schmidt, M. Geissler, Antimicrobial Activities of Essential Oils of Mint and Peppermint as Well as Some of Their Main Compounds, J Essent Oil Res, 21, 2009, 363–366.

[12] A. Schuhmacher, J. Reichling, P. Schnitzler, Virucidal effect of peppermint oil on the enveloped viruses herpes simplex virus type 1 and type 2 *in vitro*, Phytomedicine 10, 2003, 504–510.

[13] M. Mahboubi, N. Kazempour, Chemical composition and antimicrobial activity of peppermint (*Mentha piperita* L.) Essential oil Songklanakarin. J Sci Technol, 36, 2014, 83–87.

[14] M. Radünza, M.L.M. Trindade, T.M. Camargo, A.L. Radünz, C.D. Borges, E.A. Gandra, E. Helbig, Antimicrobial and antioxidant activity of unencapsulated and encapsulated clove (Syzygium aromaticum, L.) essential oil, Food Chemistry, 276, 2019, 180–186.

[15] E.I. Rabea, M.E.T. Badawy, C.V. Stevens, G. Smagghe, W. Steurbaut, Chitosan as antimicrobial agent: applications and mode of action, Biomacromolecules, 4, 2003, 1457–65.

[16] L.Y. Ing, N.M. Zin, A. Sarwar, H. Katas, Antifungal Activity of Chitosan Nanoparticles and Correlation with Their Physical Properties, Int J Biomater, 2012, 2012, 1–9.

[17] A.A. Taherpour, S. Khaef, A. Yari, S. Nikeafshar, M. Fathi, S. Ghambari, Chemical composition analysis of the essential oil of *Mentha piperita* L. from Kermanshah, Iran by hydrodistillation and HS/SPME methods, J, Anal, Sci, Technol, 8, 2017, 11.

[18] P. Khoza, T. Nyokong, Photocatalytic behaviour of zinc tetraaminophthalocyanine silver nanoparticles immobilized on chitosan beads, J Mol Catal Chem, 399, 2015, 25–32.

[19] K.T Altin, N. Topcuoglu, G. Duman, M. Unsal, A. Celik, S.S. Kuvvetli, E. Kasikci, F. Sahin, G. Kulekci, Antibacterial effects of saliva substitutes containing lysozyme or lactoferrin against Streptococcus mutans, Arch Oral Biol, 129, 2021, 105183.

[20] S. Demir, A.T. Atayoglu, F. Galeotti, E.U. Garzarella, V. Zaccaria, N. Volpi, A. Karagoz, F. Sahin. Antiviral Therapy, 25, 2020, 353–363.

[21] P.Y. Zhuang, Y.L. Li, L. Fan, J. Lin, Q.L. Hu, Modification of chitosan membrane with poly(vinyl alcohol) and biocompatibility evaluation, Int J Biol Macromol 50, 2012, 658–663.

[22] M. Masłowski, A. Aleksieiev, J. Miedzianowska, K. Strzelec, Potential Application of Peppermint (*Mentha piperita* L.), German Chamomile (Matricaria chamomilla L.) and Yarrow (Achillea millefolium L.) as Active Fillers in Natural Rubber Biocomposites, Int J Mol Sci, 22, 2021, 7530.

[23] R. Bonnetta, M.A. Krystevab, I.G. Lalovb, S.V. Artarsky, Water disinfection using photosensitizers immobilized on chitosan, Water Res, 40, 2006, 1269–1275.

[24] S. Kamble, S. Agrawal, S. Cherumukkil, V. Sharma, R.V. Jasra, P. Munshi, Revisiting Zeta Potential, the Key Feature of Interfacial Phenomena, with Applications and Recent Advancements, ChemistrySelect 7, 2022, 2–4.

[25] N. Saïed, M. Aïder, Zeta Potential and Turbidimetry Analyzes for the Evaluation of Chitosan/Phytic Acid Complex Formation, J Food Res, 3, 2014, 2.

[26] R. Singh, M.A. Shushni, A. Belkheir, Antibacterial and antioxidant activities of *Mentha piperita* L, Arab J Chem, 8, 2015, 322–328.

[27] M.G. Ghahfarokhi, M. Barzegar, M.A. Sahari, M.H. Azizi, Enhancement of thermal stability and antioxidant activity of thyme essential oil by encapsulation in chitosan nanoparticles, J Agric Sci Technol, 18, 2016, 1781–1792.

[28] H.F. Huang, C.F. Peng, Antibacterial and antifungal activity of alkylsulfonated chitosan, Biomark Genom Med, 7, 2015, 83–86.

[29] F. Hossain, P. Follett, S. Salmieri, V.K. Dang, C. Fraschini, L. Monique, Antifungal activities of combined treatments of irradiation and essential oils (EOs) encapsulated chitosan nanocomposite films in *in vitro* and in situ conditions, Int J Food Microbiol, 295, 2019, 33–40.

[30] M. Eweis, S.S. Elkholy, M.Z. Elsabee, Antifungal efficacy of chitosan and its thiourea derivatives upon the growth of some sugar-beet pathogens, Int J Biol Macromol, 38, 2006, 1–8.

[31] Z. Iyigundogdu, S. Kalayci, A.B. Asutay, F. Sahin, Determination of antimicrobial and antiviral properties of IR3535, Molecular Biology Reports, 46, 2019, 1819–1824.

[32] X. Zhou, F. Jia, X. Liu, J. Yang, Y. Zhang, Y. Wang, *In Vitro* Synergistic Interaction of 5-O-Methylglovanon and Ampicillin against Ampicillin Resistant Staphylococcus aureus and Staphylococcus epidermidis Isolates, Arch. Pharm. Res. 34, 2011, 1751–1757.

[33] C. Santiago, E.L. Pang, K. Lim, H. Loh, K.N. Ting, Inhibition of penicillin-binding protein 2a (PBP2a) in methicillin resistant Staphylococcus aureus (MRSA) by combination of ampicillin and a bioactive fraction from Duabanga grandiflora, BMC Complementary and Alternative Medicine, 15, 2015, 178.

[34] N. Nam, S. Sardari, M. Selecky, K. Parang, Carboxylic acid and phosphate ester derivatives of fluconazole: synthesis and antifungal activities, Bioorganic & Medicinal Chemistry, 12, 2004, 6255–6269.

[35] M.A. Pfaller, S.A. Messer, P.R. Rhomberg, R.N. Jones, M. Castanheira, *In Vitro* Activities of Isavuconazole and Comparator Antifungal Agents Tested against a Global Collection of Opportunistic Yeasts and Molds, Journal of Clinical Microbiology, 51, 2013, 2608.

[36] X. He, R. Xing, S. Liu, Y. Qin, K. Li, H. Yu, P. Li, The improved antiviral activities of amino-modified chitosan derivatives on Newcastle virus, Drug Chem Toxicol, 44, 2021, 335–340.

Turkish Journal of Analytical Chemistry